Cellular response to compartmentalized redox alterations

Doctoral Thesis

for the award of the degree

"Doctor of Philosophy"

Division of Mathematics and Natural Sciences

of the Georg-August-Universität Göttingen

in the Molecular Medicine Study Program

of the Georg-August University School of Science (GAUSS)

Submitted by

Aram Revazian

Born in

Khabarovsk, Russia

Göttingen, 2022

Thesis Committee

Prof. Dr. Ivan Bogeski (supervisor)

Department of Cardiovascular Physiology,
University Medical Center, Göttingen

Prof. Dr. Blanche Schwappach

Department of Molecular Biology,
University Medical Center, Göttingen

Prof. Dr. med. Wolfram-Hubertus Zimmermann

Department of Pharmacology and Toxicology,
University Medical Center, Göttingen

Examination Board

Prof. Dr. med. Dörthe M. Katschinski

Department of Cardiovascular Physiology,
University Medical Center, Göttingen

Prof. Dr. Silvio Rizzoli

Department of Neuro- and Sensory Physiology,
University Medical Center, Göttingen

PD Dr. Antje Ebert

Department of Cardiology and Pneumology,
University Medical Center, Göttingen

Date of oral examination: 05.07.2022

Table of content

List of publications

1. Gibhardt, D.S., Cappello, S., Bhardwaj, R., Schober, R., Kirsch, S.A., Bonilla del Rio, Z., Gahbauer, S., Bochiccio, A., Shumanska, M., Ickes, C., Stejerean-Todoran, I., Mitkovski, M., Alansary, D., Zhang, X., **Revazian, A.**, Fahrner, M., Lunz, V., Frischauf, I., Luo, T., Ezerina, D., Messens, J., Belousov, V.V., Hoth, M., Böckmann, R.A., Hediger, M.A., Schindl, R., Bogeski, I. Oxidative Stress-Induced STIM2 Cysteine Modifications Suppress Store-Operated Calcium Entry. *Cell Rep.* 2020 Oct 20;33(3):108292. doi: 10.1016/j.celrep.2020.108292.

2. Beretta, M., Santos, C.X.C., Molenaar, C., Hafstad, A.D., Miller, C.C., **Revazian, A.**, Betteridge, K., Schröder, K., Streckfuß-Bömeke, K., Doroshow, J.H., Fleck, R.A., Su, T.-P., Belousov, V.V., Parsons, M., Shah, A.M. Nox4 regulates $InsP_3$ receptor-dependent Ca^{2+} release into mitochondria to promote cell survival. *EMBO J* 2020 Oct 1;39(19):e103530. doi: 10.15252/embj.2019103530. Epub 2020 Aug 10.

List of figures

List of tables

Abbreviations

2D-TPP	two-dimensional thermal proteome profiling
AFG3L2	AFG3-like protein 2
AKAP1	A-kinase anchor protein 1
ALDH18A1	delta-1-pyrroline-5-carboxylate synthase
ALDH5A1	aldehyde dehydrogenase 5 family, member A1
Amp	ampicillin sodium salt
AMPK	AMP-activated protein kinase
AP-1	activator protein 1
AP-MS	affinity-purification mass spectrometry
APEX1/Ref1	apurinic/apyrimidinic (abasic) endonuclease/ redox factor-1
APS	ammonium persulfate
AQP	aquaporin
AQUA	advanced quick assembly
ASK1	apoptosis signal-regulating kinase 1
Atg4	autophagin 4
ATM	ataxia-telangiectasia mutated
BCA	bicinchoninic acid
BCAT2	branched Chain Amino Acid Transaminase 2
BP	biological process
BSC	biosafety cabinet
CALR	calreticulin
CC	cellular component
CDK1, 4	cyclin-dependent kinase 1 , 4
CHORDC1	cysteine and histidine-rich domain-containing protein 1
CM	culture medium
COX8A	cytochrome c oxidase subunit 8A
Co-IP	co-immunoprecipitation
cpYFP	circularly permuted yellow fluorescent protein
CysPAT	cysteine-specific phosphonate adaptable tag
DAAD	D-amino-acid dehydrogenase
DD	destabilization domain
DAO	D-amino acid oxidase
DAPD	meso-diaminopimelate dehydrogenase
DDO	D-aspartate oxidase

DJ-1/PARK7	protein deglycase DJ-1/parkinson disease protein 7
DMSO	dimethyl sulfoxide
DPBS	Dulbecco's phosphate-buffered saline
DUOX	dual oxidase
Dvl	dishevelled
D-Ala	D-Alanine
EDTA	ethylenediaminetetraacetic acid
EGF	epidermal growth factor
EM	experiment medium
ER	endoplasmic reticulum
ER-lumen	lumen of endoplasmic reticulum
ERP44	Endoplasmic reticulum resident protein 44
ETF: QO	electron transfer flavoprotein: ubiquinol oxidore-ductase
FAD	flavin adenine dinucleotide
FASN	fatty acid synthase
FITExP	Functional Identification of Target by Expression Proteomics
FMN	flavin mononucleotide
FOXO3	forkhead box O3
FP	fluorescent protein
FS	farnesylation signal
GAPDH	glyceraldehyde-3-phosphate dehydrogenase
GEFI	genetically-encoded fluorescent indicator
GO	gene ontology
GOEA	gene ontology enrichment analysis
Gpx	glutathione peroxidase
GR	glutathione reductase
Grx	glutaredoxin
GSH	glutathione
GSSG	oxidized glutathione
GST	glutathione S-transferase
HCT116	human colorectal carcinoma
HEK293(T)	human embryonic kidney 293 (T) cells
HEPES	hydroxyethyl piperazineethanesulfonic acid
HRP	horse radish peroxidase
HSP	heat shock protein
HSPA4	heat shock 70-related protein APG-2
IAM	iodoacetamide

IMAC	immobilized metal affinity chromatography
IMM	inner mitochondrial membrane
IMS	mitochondrial intermembrane space
IP3R	inositol trisphosphate receptor
IPM	2-iodo-N-(prop-2-yn-1-yl)acetamide)
IRE1	Inositol-requiring enzyme 1
JAK2	janus kinase 2
Keap1	kelch-like ECH-associated protein 1
KEGG	Kyoto Encyclopedia of Genes and Genomes
KSR1	kinase suppressor of Ras-1
LB	Luria-Bertani
LC-MS/MS	liquid chromatography with tandem mass spectrometry
MAO	monoamine oxidase
MCM	mini-chromosome maintenance
MEK1/MAP2K1	mitogen-activated protein kinase kinase
MEM	minimum essential medium
MERC	mitochondria-ER contact
mETC	mitochondrial electron transport chain
MF	molecular function
MMO	microsomal monooxygenase
MPP	mitochondrial processing peptidase
MLS	mitochondrial localization signal
MS	mass spectrometry
MTAP	S-methyl-5'-thioadenosine phosphorylase
MTS	mitochondrial targeting sequence
NADPH	nicotinamide adenine dinucleotide phosphate
NEM	N-ethylmaleimide
NES	nuclear export signal
NF-κB	nuclear factor kappa B
NFKB2	nuclear factor NF-kappa-B p100 subunit
NLS	nuclear localization signal or sequence
NMDA	N-methyl D-aspartate
NOS2	nitric oxide synthase 2
NOX	NADPH-oxidase
Nrf2	nuclear factor erythroid 2-related factor 2
NSD	non-stop decay
OMM	outer mitochondrial membrane
OSER	organized smooth ER

OxICAT	oxidative isotope-coded affinity tag
OxiPTM	oxidative post translational modification
P4HB	protein disulfide-isomerase
PCR	polymerase chain reaction
PDGF	platelet-derived growth factor
PDI	protein disulfide isomerase
PDI/Ero1	protein disulfide isomerase, ER oxidoreductin 1
PDIA	protein disulfide-isomerase A
PEI	polyethylenimine
PEX	peroxin
PI3K	phosphatidylinositol 3-kinase
PKM2	pyruvate kinase M1/2
PLA2G4A	cytosolic phospholipase A2
POI	protein of interest
Pol II	RNA polymerase II
POR	NADPH-cytochrome P450 oxidoreductase
PP2A	protein phosphatase 2A
PRDX	peroxiredoxin
Prx	peroxiredoxin
PTEN	phosphatase and tensin homolog
PTM	post-translational modification
PTP	protein tyrosine phosphatases
PTS1	peroxisomal targeting signal 1
Puro	puromycin dihydrochloride
QSOX	quiescin sulfhydryl oxidase
QTRP	quantitative thiol reactivity profiling
RAC	resin-assisted capture
RAF	rapidly cccelerated fibrosarcoma
redox	reduction-oxidation
RgDAO	rhodotorula gracilis d-amino acid oxidase
RNS	reactive nitrogen species
ROI	region of interest
ROS	reactive oxygen species
RPL	60S ribosomal protein
RPS	40S ribosomal proteins
RSS	reactive sulfur species
RT	room temperature
RTK	receptor tyrosine kinase
RyRs	ryanodine receptors

SDS	sodium dodecyl sulfate
SDS-PAGE	Sodium Dodecyl Sulfate–Polyacrylamide Gel Electrophoresis
Sec61B	SEC61 Translocon Subunit Beta
SENPs	sentrin-specific protease
SERCA	sarco/endoplasmic reticulum calcium-ATPase
SICyLIA	stable isotope cysteine labelling with iodoacetamide
SKIV2L	helicase SKI2W
SOD	superoxide dismutase
SPG7	paraplegin
STIMs	Ca^{2+}-sensor stromal interaction molecules
SUMO	small ubiquitin-like modifier
SV40	simian virus 40
TEMED	tetramethylethylenediamine
TF	transcription factor
TMT	tandem mass tag
TPP	thermal proteome profiling
TRAP1	tumor necrosis factor receptor-associated protein 1
TREX	TRanscription and Export
TR-TPP	temperature range - thermal proteome profiling
Trx	thioredoxin
Trx-fold	thioredoxin-like domain
TrxR	thioredoxin reductase
TTC37	tetratricopeptide repeat protein 37
TXNDC5	thioredoxin domain-containing protein
TXNRD	thioredoxin reductase
UBA2	(SAE1)/ubiquitin like modifier activating enzyme 2
UV	ultraviolet
VDAC	voltage dependent anion channel
VEGFR2	vascular endothelial growth factor receptor 2
WB	Western Blot
WDR61	WD repeat-containing protein 61
wt	wild type
XDH	xanthine dehydrogenase/oxidase
YFP	yellow fluorescent protein
ZC3H14	zinc finger CCCH-type containing 14

Abstract

Reactive oxygen species (ROS) were considered only as toxic and unavoidable by-products of aerobic cell life in the past. Nevertheless, their significance for cellular signalling is currently widely accepted and extensively investigated. The most well-studied and perhaps most important specie among all ROS, in terms of redox signalling, is hydrogen peroxide (H_2O_2). Cellular response to H_2O_2 is largely determined by its capability to affect protein activity via oxidative post-translational modifications (PTMs) of certain amino acid residues (mostly cysteines) and depends on many factors, including among others the subcellular i.e. compartmental control of H_2O_2 production. Level of H_2O_2 is tightly connected to another cellular redox-active compound, NADPH, which is involved in both H_2O_2 generation and disposal due to the operation as an electron donor to NAPDH oxidases and to antioxidant systems, respectively. Since redox signalling is important for cell functioning not only under physiological, but also under pathological conditions, in the current study we focused on the investigation of compartmentalized alterations of redox homeostasis in HEK293 and melanoma cells. To this end, we assembled plasmids encoding HyPer-DAO (D-amino acid oxidase) and iNap-DAAD (D-amino acid dehydrogenase) proteins fused to sequences for targeting to various cellular compartments. These protein systems provide an opportunity to simultaneously induce and monitor H_2O_2 or NADPH level alterations in a specific cellular compartment. The assembled plasmids were utilized for production of lentiviruses, which were in turn applied for making stable melanoma and HEK293 cell lines. To identify proteins involved in the cellular response to compartmentalized H_2O_2 generation, we established HEK293 cell lines expressing HyPer/TagBFP-DAO in the cytosol, the nucleus and the lumen of endoplasmic reticulum (ER-lumen). With these cells we performed Thermal Proteome Profiling (TPP) – quantitative proteomics method that allows identification of proteins, which alter their thermostability in response to various stimuli, such as protein-protein interaction, ligand binding, PTMs, etc. Unlike redox proteomic methods that allow identification of only those proteins that directly change their reduction/oxidation state, TPP is able to give more general and broader picture of cellular response to compartmentalized oxidative challenge. As a result, we identified several hundred proteins that were involved in the cellular response to H_2O_2 generation in at least one of abovementioned cellular compartments. The largest number of these proteins were identified upon H_2O_2 production in the cytosol, followed by the nucleus and the ER-lumen. Furthermore, we found that many proteins responded similarly to H_2O_2 generated

in the nucleus and the cytosol, while their response to H_2O_2 produced in the ER-lumen differed. Using bioinformatics, we found that the identified proteins participate in various cellular processes, ranging from oxidative stress counteraction to transcription, translation and replication. To better understand how H_2O_2 affects protein thermostability, we selected several bait-proteins and performed co-immunoprecipitation (Co-IP/MS). We found that under oxidative challenge some proteins alter binding partners, while others may change stability due to other reasons, e.g., due to emergence of PTMs. Many proteins identified in our study as novel molecular players of redox signalling are poorly studied that points towards new directions for future investigations.

1 Introduction

1.1 ROS

Reactive oxygen species (ROS) is a common name widely used to refer to various partially reduced oxygen derivatives. Initially, ROS were considered only as unavoidable by-products of aerobic life to be get rid of at all costs (Winterbourn, 2012). Indeed, ROS can damage a broad spectrum of different biological molecules such as DNA, lipids, proteins, etc., (Sies, 2017) and, therefore, are connected to various disorders like aging, cancer, neurodegenerative and cardiovascular diseases (Brieger et al., 2012). However, during the last several decades this paradigm has substantially changed with the recognition of at least some ROS as signalling molecules for inter- (Niethammer et al., 2009) and intracellular communication (Woolley et al., 2013). ROS can have radical, non-radical, electrically charged, or uncharged nature, various thermodynamic reduction-oxidation (redox) potentials and kinetic properties (Winterbourn, 2012). As a result, biologically relevant ROS differ in their ability to diffuse from source of generation, pass lipid membranes and react with diverse biological molecules. Among all ROS, in the biological context, hydrogen peroxide (H_2O_2) is the most well-studied and perhaps has the most well-suited set of properties for execution of a signalling function.

1.1.1 Hydrogen Peroxide (H_2O_2)

Hydrogen peroxide is a strong two-electron oxidant (standard reduction potential is equal to 1.32 V at pH 7.0). Nevertheless, H_2O_2 reacts poorly with most of biomolecules along with low molecular weight antioxidants and most protein thiols (Winterbourn, 2013). The reason is that reactions with H_2O_2 are characterized with high activation energy (kinetic barrier), which has to be surmounted to set free its oxidizing power (Winterbourn, 2013). With several exceptions thiols react with hydrogen peroxide quite slow and solely in a form of thiolate anion (deprotonated SH-group). Thus, thiols with a low pK_a (surrounded by positively charged amino acids in proteins or in solutions with high pH values) react more willingly. However, some thiol proteins such as glutathione peroxidases (GPxs) and peroxiredoxins (Prxs) have extremely high reactivity towards H_2O_2, which cannot be explained only by low pK_a of their respective thiol groups. For instance, active sites of Prxs not only stabilize the thiolate form of Cys, but also align the -O–O- bond, polarize it with additional hydrogen bonds in transition state and thus guide the -O–O- breakdown (Poole et al., 2011). Limited spectrum of biological targets renders H_2O_2-mediated redox signalling the

selectivity, which is an essential feature of a second messenger. Transition metal centres, including heme peroxidases, iron-suflur centre proteins, low-molecular weight chelates are other important targets of hydrogen peroxide. Transition metals like iron and copper are able to cleave -O–O- bond in H_2O_2 that leads to the production of hydroxyl radical – extremely reactive and thus indiscriminate strong oxidant, which is considered to be responsible for a substantial portion of oxidative damages evoked by hydrogen peroxide in the cell (Imlay, 2008).

Due to low intrinsic reactivity H_2O_2 can potentially diffuse over relatively long distances (in comparison to other ROS) in aquatic environments (Winterbourn, 2012). However, the cell abundantly expresses different peroxidases, such as mentioned above Prxs and GPxs, which function as a sink for H_2O_2 and thus attenuate (terminate) H_2O_2-mediated redox signalling via H_2O_2 removal (Mishina et al., 2011). Furthermore, the cell can regulate H_2O_2 transport across biological membranes via their lipid composition (Bienert et al., 2006) and membrane channels – aquaporins (Bestetti et al., 2020). Thereby the cell has mechanisms to control redox signalling propagation in a spatiotemporal way.

Selectivity of a second messenger, the ability of the cell to terminate signalling and regulate its propagation are necessary, but not sufficient properties of cellular signalling systems. Another requirement – is to be able to control mechanisms of the signal generation upon a stimulus. The most well-known sources of cellular ROS generation are NADPH-oxidases (NOXs) – membrane-localized enzymes, which are able to produce significant amount of ROS (superoxide anion and H_2O_2) in response to various stimuli (Lambeth, 2004). Due to the presence of special enzymes, such as superoxide dismutases (SODs), the cell can easily convert produced superoxide anion ($O_2^{-\cdot}$) to hydrogen peroxide and thus initiate redox signalling in a close proximity to NOXs.

H_2O_2-mediated redox signalling is carried out via oxidative post-translational modifications (OxiPTMs) of cysteine thiols in target proteins and thus to terminate signalling the cell should be able not only to dispose of H_2O_2, but also to reduce back H_2O_2-induced OxiPTMs. For this purpose, the cell has two antioxidant systems: thioredoxin (Trx) and glutathione (GSH) systems, which reduce oxidized cysteines and terminate redox signalling.

1.2 Cysteine thiol modifications

As mentioned above, redox signalling is mostly mediated by oxidative cysteine modifications in proteins, which affect protein activity, conformation, function, etc. There are multiple different redox modifications, which cysteines in proteins can undergo (Figure 1.1).

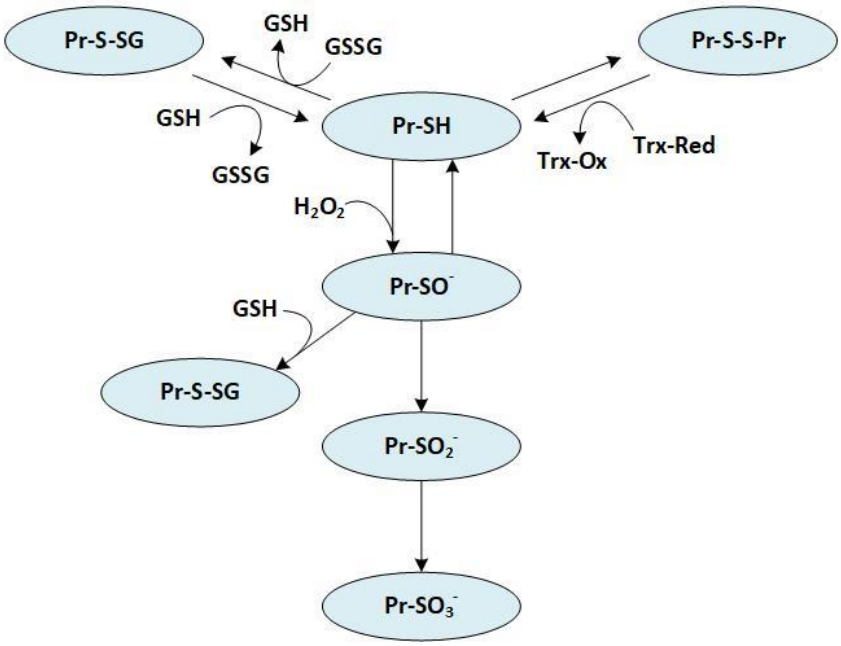

Figure 1.1: *Some of oxidative cysteine thiol modifications and their interconversions. Pr-SH – cysteine thiol, Pr-S-SG – glutathionylated protein, Pr-SO$^-$ - sulfenic acid, Pr-SO$_2^-$ - sulfinic acid, Pr-SO$_3^-$ - sulfonic acid, Pr-S-S-Pr – intra- or intermolecular disulfide bond, GSH – reduced glutathione, GSSG – oxidized glutathione, Trx – thioredoxin.*

An active thiol form, a thiolate anion (Pr-S$^-$), can directly react with H_2O_2 to form sulfenic acid (Pr-SO$^-$), which can further oxidize to form sulfinic (Pr-SO$_2^-$) and sulfonic (Pr-SO$_3^-$) acids (van Bergen et al., 2014). Sulfinic and sulfonic acids are generally considered to be irreversible. Meanwhile, for at least some proteins, such as typical 2 Cys Prxs, sulfinic acid was shown to be able to be reduced back to sulfenic acid in ATP-dependent manner by sulfiredoxin, nevertheless, quite slow (Mishra et al., 2015). In contrary, sulfenic acid is a reversible cysteine modification and can react with reduced glutathione (GSH) or Trx to reduce back to thiol form (Gupta & Carroll, 2014).

In addition, protein thiol (thiolate) can form an inter- or intramolecular disulfide bond (Pr-S-S-Pr) with a cysteine of another disulfide bond in the same or another protein via classical thiol-disulfide exchange mechanism (Nagy, 2013). This reaction is slow, but it can be accelerated with oxidoreductases of Trx superfamily. Furthermore, there are other mechanisms of new disulfide bond formation, such as a reaction of sulfenic acid with a thiol group. A cysteine thiol was also shown to react with an oxidized glutathione (GSSG) to produce mixed disulfides. Presence of a glutathione residue on a cysteine thiol represents another PTM termed glutathionylation. Similar to sulfenic acid, protein glutathionylation and disulfide bond formation are reversible and can be reduced back to a thiol

form with participation of GSH and glutaredoxins (Grxs) or Trx systems, respectively (Nagy, 2013).

The considered above modifications do not represent all possible alterations that cysteine thiols in proteins can undergo in the cell. Besides these ones, there are also other redox modifications, such as S-nitrosylation (Pr-S-NO) and S-sulfhydration (Pr-S-SH), which are evoked by reactive nitrogen (RNS) and sulfur (RSS) species, respectively (Chung et al., 2013).

1.3 Mechanisms of redox signalling

There are several possible mechanisms of cellular redox signal transmission (Winterbourn, 2013). First and the simplest is direct oxidation of (a) cysteine thiol(s) in the target protein (Figure 1.2). However, since H_2O_2 has low reactivity towards protein thiols in general, only a small amount of highly abundant target proteins, including Prxs and GPxs, are considered to be oxidized directly. Another mechanism is based on extremely reactive redox-sensitive sensor proteins, e.g. Prxs, which upon oxidation by H_2O_2 transmit oxidative equivalents to less reactive target proteins (Sobotta et al., 2015). The next (3rd) mechanism describes a protein interaction between a sensor and a target protein, when the redox-sensitive sensor protein is oxidized and dissociates (partially) from the target protein, which becomes activated. As an example of this model, NRF2/KEAP1 (Nuclear factor erythroid 2-related factor 2/Kelch-like ECH-associated protein 1) system can be mentioned (see below) (Yamamoto et al., 2018). The 4th mechanism implies the agent, such as Trx, which is capable of sensor protein recycling, transmits the redox signal to a target protein via thiol-disulfide exchange mechanism or due to changed binding with the latter. This model was shown for apoptosis signal-regulating kinase 1 (ASK1) (Sakauchi et al., 2017). ASK1 is inactive in the complex with reduced Trx, however, upon oxidation, Trx dissociates from ASK1 that leads to ASK1 autophosphorylation and activation. The 5th model termed «Floodgate» hypothesis. According to this model, the initial increase in H_2O_2 concentration leads to overoxidation and inactivation of sensor proteins, such as Prxs, involved in cellular antioxidant defence, and thus to further rapid H_2O_2 accumulation that is necessary for oxidation of less-reactive target proteins. In the variation of this model, transient local H_2O_2 accumulation was shown in response to inactivation of the membrane-localized Prx1, mediated via phosphorylation instead of overoxidation (Woo et al., 2010). The last model implies an association of a H_2O_2-generator and a target protein and facilitated delivery of oxidative equivalents in directed manner to low reactive target proteins, such as protein tyrosine phosphatases (PTPs) (Winterbourn, 2013).

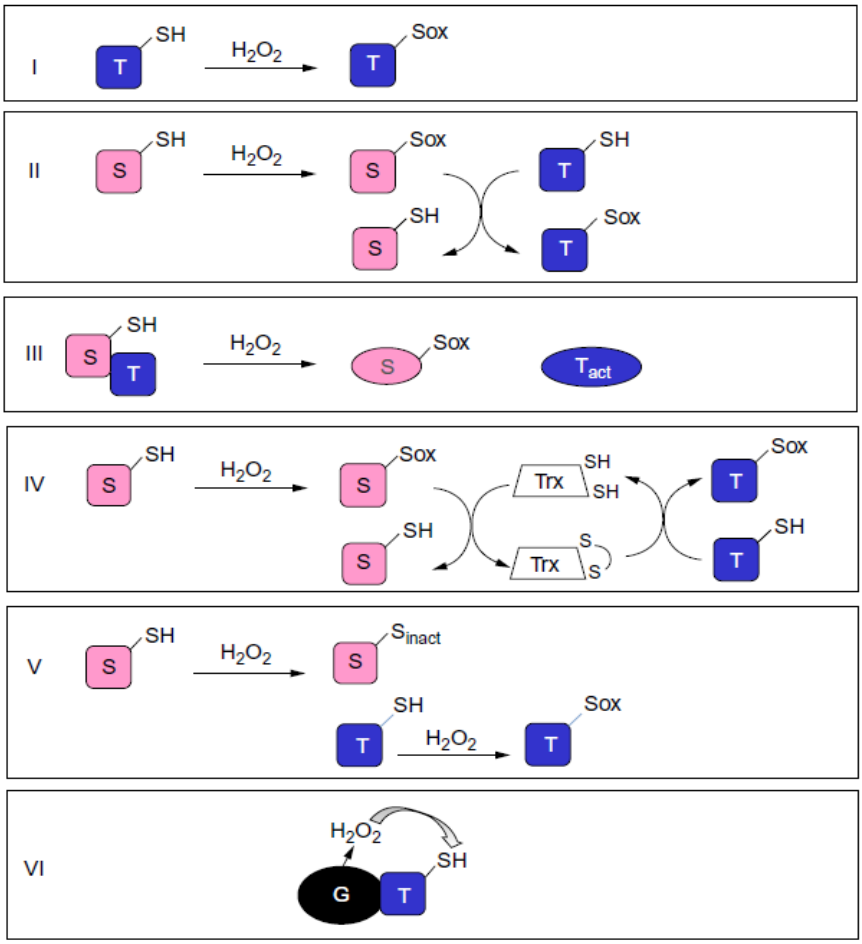

Figure 1.2: *Mechanisms of H_2O_2-mediated redox signalling. T – target protein, S – sensor protein, G – generator, Sox – oxidized sensor protein, (in)act – (in)activated. The figure is adapted from (Winterbourn, 2013).*

1.4 Major protein systems involved in redox homeostasis

In this section we shortly discuss major systems involved in H_2O_2 removal and generation in various cellular compartments.

1.4.1 Peroxiredoxins

Peroxiredoxins (Prxs) represent a broadly distributed (Table 1.1) family of enzymes with peroxidase activity capable of elimination of hydro- and lipid peroxides (Heo et al., 2020). They mostly utilize Trxs as a source of electrons for hydrogen peroxide reduction, however, some isoforms can also use Grx (glutaredoxin) (Peskin et al., 2016). There are six Prx isoforms identified in mammalian cells, which are classified into three groups based on the number of cysteine residues in the active site and the type of the disulfide bond formed upon oxidation: typical 2-Cys Prxs (intermolecular disulfide bond between cysteines of

2 Prx monomers), atypical 2-Cys Prxs (intramolecular bond between 2 cysteine residues within one protein molecule) and 1-Cys Prx (Heo et al., 2020). As mentioned above, Prxs are very abundant and extremely reactive towards peroxides (Rhee & Kil, 2017), however, their functions are not limited to only removal of oxidants. Prxs are enzymes of significant impact in various cellular processes (Park et al., 2014). As already discussed above, Prxs play an extremely important role in redox signalling. Furthermore, it was shown that upon overoxidation some Prxs multimerize and prevent protein aggregation by operating as chaperones (Rhee et al., 2012).

Table 1.1: *Summary table of some characteristics of peroxiredoxin isoforms. Table is adapted from (Heo et al., 2020).*

Prx Isoform	Subfamily	Subcellular Localization
PrxI	2-Cys Prx	Cytosol, nucleus, centrosome, plasma membrane
PrxII	2-Cys Prx	Cytosol, nucleus, plasma membrane
PrxIII	2-Cys Prx	Mitochondria
PrxIV	2-Cys Prx	Cytosol, ER, lysosome, extracellular localization
PrxV	Atypical 2-Cys Prx	Cytosol, mitochondria, peroxisome, nucleus
PrxVI	1-Cys Prx	Cytosol, lysosome, extracellular localization

1.4.2 Thioredoxin system

Prxs mostly obtain electrons from thioredoxin (Trx) system. Trx system consists of Trx, thioredoxin reductase (TrxR) and nicotinamide adenine dinucleotide phosphate (NADPH) and along with glutathione system represents one of two major cellular antioxidant systems, which maintain cellular redox status (Figure 1.3) (Lu & Holmgren, 2014a). Trxs together with other proteins, such as glutarderoxins (Grxs), glutathione S-transferases (GSTs), glutathione peroxidases (GPxs), Prxs, quiescin sulfhydryl oxidases (QSOXs), etc., have a common characteristic feature – the Trx-fold structure based on which they are united into the Trx-supefamily (Lu & Holmgren, 2014a, 2014b). Trxs are able to transfer electrons to a wide range of proteins involved in various cellular processes, including transcription factors (TFs) and antioxidant defence enzymes, such as Prxs, among others. There are two Trx isoforms in mammalian cells: nuclear/cytosolic Trx1 and mitochondrial Trx2, which receive electrons upon oxidation from nuclear/cytosolic and mitochondrial isoforms of TrxR – TrxR1 and 2, respectively (Jones & Go, 2010; Lu & Holmgren, 2009). TrxRs are NADPH-oxidizing, selenium-dependent flavoproteins with a broad substrate specificity (Xavier et al., 2018). Among TrxR substrates are: Trx, protein disulfide

isomerase (PDI), Grx2, etc. Due to the presence of a redox-sensitive selenocysteine in the active site, TrxRs are also prone to oxidation and inactivation upon oxidative stress (Nauser et al., 2014).

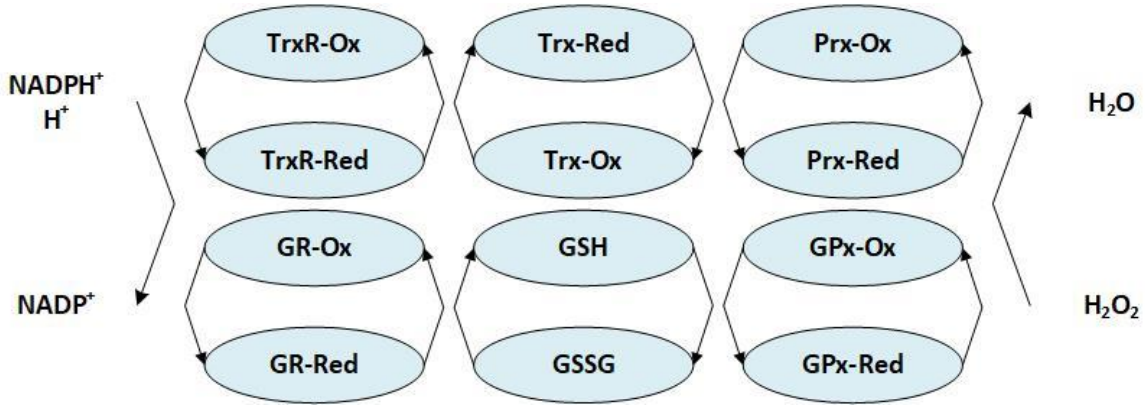

Figure 1.3: *Scheme representing Trx and GSH systems operation upon elimination of H_2O_2. GSH – glutathione, GR – glutathione reductase, Trx –thioredoxin, TrxR – thioredoxin reductase, Prx – peroxiredoxin, GPx – glutathione peroxidase.*

1.4.3 Glutathione system

Cellular glutathione (GSH) antioxidant system functions similarly to Trx system and consists of following elements: GSH, glutathione reductases (GRs) and NADPH (Figure 1.3). GSH is the most abundant cellular low molecular weight thiol, which concentration is estimated to be in a low millimolar range (Forman et al., 2009). In the eukaryotic cell, GSH localizes in all organelles (Ushioda & Nagata, 2019) and synthesizes in two sequential steps in the cytosol containing the majority of all cellular GSH (Lu, 2009).

GSH and oxidized glutathione (GSSG) are involved in protein glutathionylation. Protein glutathionylation is currently considered as a protective mechanism against irreversible overoxidation of protein cysteine residues under oxidative stress as well as a mechanism of redox-signal transmission under oxidative conditions (Forman et al., 2009; Matsui et al., 2020). Dynamic process of protein glutathionylation/deglutathionylation is regulated by key enzymes – glutaredoxins (Grxs) (Ogata et al., 2021). Human organism has four Grxs: Grx1, 2, 3 and 5 with different cellular localization and structure, which, in addition to glutathionylation, were found to be involved in protein cysteines denitrosylation, iron-sulfur cluster formation, etc.

GSSG, which is generated as a product of protein deglutathionylation or antioxidant activity of GPxs (see below), is reduced back to GSH by the mean of cellular GRs in order to maintain GSH system activity. The structure of mammalian GRs, which employ NADPH for GSSG reduction, is similar to TrxR,

however, with a lack of selenocysteine-containing motif on the C-terminus (Ren et al., 2017).

Besides mentioned above, there are also other important enzymes utilizing GSH – glutathione S-transferases (GSTs), which catalyse the reaction of conjugation of GSH to reactive electrophiles. Human organism has several GST family members with cytoplasmic, mitochondrial or membrane-bound localization. GSTs are involved in multiple cellular processes playing a cytoprotective role and a role in cell signalling (Singh & Reindl, 2021).

GSH functions as a cellular antioxidant via providing reducing equivalents to GPxs. There are eight GPxs in the human organism, which perform antioxidant function in various cellular compartments and extracellular environment. GPxs enzymes can be divided into two groups based on the amino acid residue in the active site of the enzyme, which reacts with (oxidizes by) peroxides: selenocysteine (Sec) containing GPxs – GPx1-4, 6 and cysteine (Cys) containing – GPx5, 7, 8. Sec-containing GPxs utilize GSH as a reductant, while 2 Cys-containing GPxs similarly to atypical 2 Cys Prxs, preferentially use Trxs (Brigelius-Flohé & Maiorino, 2013). Furthermore, GPxs also as Prxs are extremely reactive enzymes towards hydro- and lipid peroxides that makes them very efficient in peroxide elimination. Nevertheless, similar to Prxs they cannot be just viewed only as antioxidants (Brigelius-Flohé & Maiorino, 2013).

Despite GSH and Trx systems were thought to work in parallel, there are data suggesting that they can function as backup systems for each other (Lu & Holmgren, 2014a).

1.4.4 NADPH oxidases

In contrary to the discussed proteins, which function as antioxidants, NOXs (NADPH oxidases) act as oxidant-generating enzymes. NOXs and structurally/functionally similar dual oxidases (DUOXs) are membrane localized enzymes, which produce ROS in a wide variety of cell types in response to different signals, including growth factors, cytokines, calcium and thus represent controllable cellular system for ROS production (Lambeth, 2004). NOXs, based on the transmembrane topology and domain structure, can be divided into three groups: NOX1-4 (basic structure, no additional domains), NOX5 (additional calcium-binding domain), DUOX1-2 (additional calcium-binding and peroxidase domains) (Figure 1.4). NOXs catalyse oxidation of NADPH molecules and transfer electrons across the membrane to molecular oxygen via FAD and heme domain and finally produce superoxide anion and H_2O_2 (Lambeth, 2004).

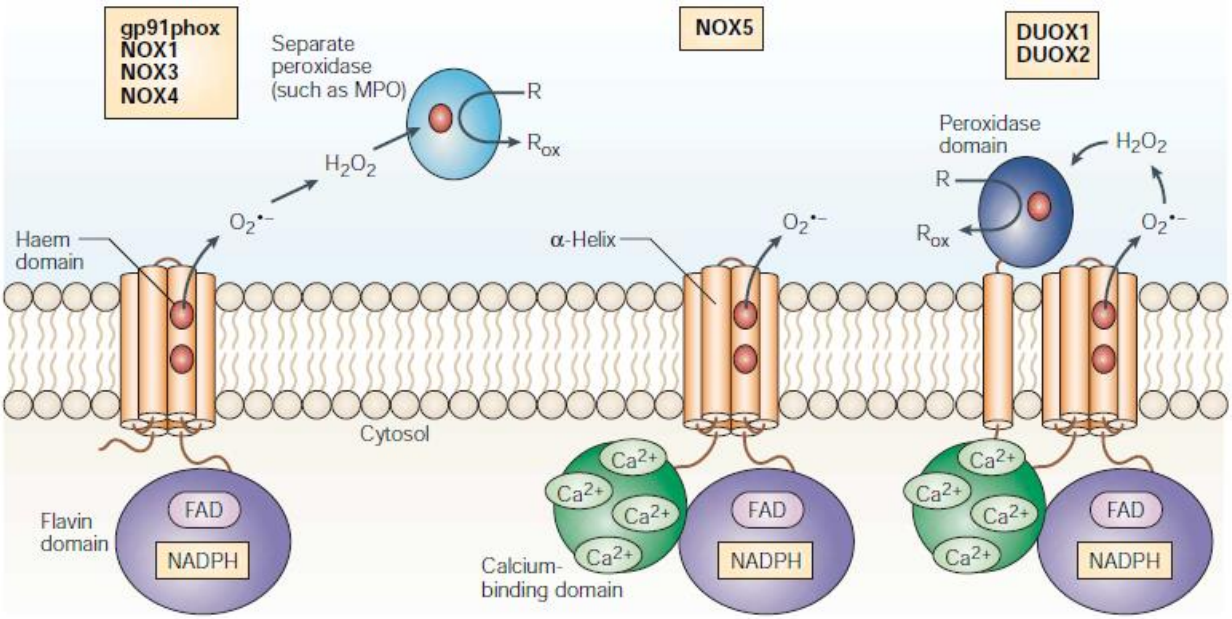

Figure 1.4: *Topology and structure of NOXs and DUOXs. The figure is adapted from* (*Lambeth*, 2004).

1.5 Redox processes in cellular compartments

As eukaryotic cells are compartmentalized into organelles, they can spatially separate different cellular processes from each other and to create suitable conditions within each compartment for a particular process. These conditions also imply appropriate redox environment, which is greatly dependent on the action of the enzymes described above and additional, compartment-specific protein systems. In the next sections, particular enzymes and proteins of great importance for each cellular compartment and related redox processes are highlighted.

1.5.1 Mitochondria

Mitochondria are usually considered as the main or at least one of major cellular organelles generating ROS (Murphy, 2009). The majority of ROS generated by mitochondria is believed to originate from mitochondrial electron transport chain (mETC). Mammalian mETC can produce ROS at various sites, whose relative contribution to total ROS-production markedly depends on a substrate type being consumed by mETC as a fuel molecule and other factors (operating mode, oxygen and caloric availability, etc.) (Wong et al., 2017). Among these sites, Complex I (NADH: ubiquinone oxidoreductase) and III (ubiquinol-cytochrome c reductase) are thought to be responsible for the production of the majority of ROS amount (Zhao et al., 2019). Four protein

complexes, quinol pool reducers, localized in or nearby to the inner mitochondrial membrane (IMM), namely succinate dehydrogenase (Complex II, Sdh), electron transfer flavoprotein: ubiquinol oxidoreductase (ETF: QO), dihydroorotate dehydrogenase and mitochondrial glycerol-3-phosphate dehydrogenase, can also generate different amount of ROS under certain metabolic conditions (Bak & Weerapana, 2015).

Besides mETC, mitochondria are capable of producing ROS with other means. Protein 2-oxo dehydrogenase complexes, such as pyruvate dehydrogenase, 2-oxoglutarate dehydrogenase as well as branched-chain keto-acid dehydrogenase and 2-oxoadipate dehydrogenase complex, are also able to substantially impact on mitochondrial ROS production (Bak & Weerapana, 2015).

It should also be noted that a substantial part of mitochondrial H_2O_2 is derived via superoxide anion radical (superoxide) dismutation (Miriyala et al., 2011). Superoxide is a very unstable molecule, which fast dismutates either spontaneously or enzymatically via superoxide dismutases (SODs) with H_2O_2 production. Two SOD isoforms are found in mitochondria: Cu/Zn-containing SOD1, which besides the cytosol and the nucleus also resides in the IMM, and Mn-containing SOD2, which localizes within mitochondrial matrix (Miriyala et al., 2011; Okado-Matsumoto & Fridovich, 2001).

Mia40/Erv1 is a protein system localized in IMM and responsible for disulfide bond formation in nascent proteins destined for operation in IMM (Pfanner et al., 2019). Similar to analogous system (PDI/Ero1), which operates within endoplasmic reticulum (ER), disulfide bond formation catalysed by Mia40/Erv1 is accompanied by molecular oxygen reduction and H_2O_2 generation (Dickson-Murray et al., 2021).

Among other well-known mitochondrial sources of H_2O_2 is monoamine oxidases (MAO) A and B catalysing oxidative deamination of biogenic amines and localizing on the outer mitochondrial membrane (OMM). These enzymes were shown to produce significant amount of H_2O_2 under certain conditions and can be responsible for H_2O_2-mediated oxidative damage to mitochondria and degenerative processes in neuronal and heart tissues (Edmondson, 2014; Hauptmann et al., 1996).

Despite mitochondria are often considered as a major source of ROS in the cell, mitochondrial matrix maintains highly reducing redox-environment (Lu & Holmgren, 2014b). This seems possible, given mitochondria are endowed with abundant H_2O_2-scavenging enzymes (Konno et al., 2021). There are representatives of both antioxidant systems within mitochondria: Prxs and GPxs.

Mitochondria enclose two Prx isoforms: Prx3 and Prx5, which efficiently reduce H_2O_2 and organic hydroperoxides, respectively (Cox et al., 2009). Oxidized Prxs are reduced by mitochondrial Trx system composed of Trx2 and TrxR2. Mitochondrial GPx isoforms, GPx1 and 4, like their Prx counterparts specialize for reduction of soluble (H_2O_2) and lipid hydroperoxides, respectively, however, utilize mitochondrial GSH pool as a reductant (Imai & Nakagawa, 2003). Apart from enzymatic systems, mitochondria contain low molecular weight compounds, such as lipoate and α-ketoacids, which may contribute to mitochondrial ROS elimination as well (Bak & Weerapana, 2015).

Presence of multiple H_2O_2-generating and scavenging systems suggests that mitochondria are organelles, wherein redox processes are of a great significance. Indeed, there are numerous evidences that many proteins and related mitochondrial activities are redox-regulated. Among them: subunits of mETC complexes (Chouchani et al., 2016), metabolic enzymes (Nulton-Persson et al., 2003); proteins involved in mitochondrial quality control (Bohovych et al., 2019; Ježek et al., 2018; Kim et al., 2018), calcium homeostasis (Joseph et al., 2019), thermogenesis (heat production) (Ježek et al., 2019), etc.

1.5.2 Peroxisomes

As suggested by name, peroxisomes play critical role in cellular H_2O_2 metabolism. Peroxisomes have impressive number of enzymes producing H_2O_2 involved in various metabolic processes like ß-oxidation of fatty acids (acyl-CoA oxidases), catabolism of amino acids (D-amino acid (DAO), D-aspartate (DDO), pipecolic acid and sarcosine oxidases), purines (urate oxidase), oxidation of polyamines (polyamine oxidase) and 2-hydroxy acids (hydroxyacid oxidases) (Fransen & Lismont, 2018). They also contain xanthine dehydrogenase/oxidase (XDH) and inducible nitric oxide synthase 2 (NOS2) – potential sources of superoxide and NO radicals (Fransen & Lismont, 2019). Furthermore, peroxisomes have SOD1, which converts superoxide anion into H_2O_2 (Antonenkov et al., 2010).

Regarding the list of H_2O_2-generating enzymes, it is not surprising that these organelles are well-equipped with antioxidant enzymes specialized for elimination of ROS and hydrogen peroxide particularly (Fransen & Lismont, 2018). Catalase is a principally peroxisomal, heme-containing enzyme, which is capable of extremely fast H_2O_2 degradation (Okumoto et al., 2020). Prx5 (PMP20) has the widest cellular distribution among Prxs (Fransen & Lismont, 2018), in addition to mitochondrial, it also has peroxisomal, nuclear and cytosolic localizations, and is involved in the removal of alkyl hydroperoxides and to a

lesser extent H_2O_2 (Knoops et al., 2011). At the same time, since no thioredoxin has been detected in mammalian peroxisomes so far, it is not clear, how Prx5 is reduced back (Fransen & Lismont, 2019). Furthermore, despite the presence of GPx activity in peroxisomes, its identity is yet to be determined. In addition, it is also obscure whether mammalian peroxisomes possess a functional GSH system and how GSH is transported across the membrane (Fransen & Lismont, 2019).

A long-standing question in the redox field, whether peroxisomes act as cellular sources of or sinks for H_2O_2. It seems like peroxisomes are not confined to strictly implement one of the functions, instead, they can significantly vary their contribution to cellular H_2O_2 metabolism based on many factors, including tissue and cell type, cellular physiological state or microenvironment (Fransen & Lismont, 2019). Currently, it is not fully understood how H_2O_2 passes through peroxisomal membranes (H_2O_2-transporting proteins have not been identified), however, there are evidences that this process is bidirectional (Boveris et al., 1972; Ho et al., 2004).

Peroxisome-derived ROS can regulate not only peroxisomal, but other cellular proteins: ataxia-telangiectasia mutated (ATM) involved in pexophagy (autophagy) (Zhang et al., 2015); cycling import receptor, peroxin (PEX) 5, necessary for peroxisome biogenesis; p50 (NFκB1) and p65 (RelA) representatives of nuclear factor kappa B (NF-κB) protein family; phosphatase and tensin homolog (PTEN); forkhead box O3 (FOXO3) (Lismont et al., 2019).

1.5.3 ER

Endoplasmic reticulum (ER) is a compartment, which plays the important role in cellular Ca^{2+} homeostasis, lipid biosynthesis and protein folding. Correct folding of different membrane and secretory proteins within ER requires proper disulfide bond formation. This function is fulfilled by PDI/Ero1 (protein disulfide isomerase, ER oxidoreductin 1) system (Konno et al., 2021). More than 20 different oxidoreductase-chaperone enzymes of PDI family interact with their multiple protein substrates via thioredoxin-like domain (Trx-fold) and are involved in disulfide bond formation, isomerization and reduction (Lu & Holmgren, 2014b; Ushioda & Nagata, 2019). Upon reduction PDI donate electrons to Ero1, highly conserved FAD-dependent oxidoreductase, which in turn passes electrons to molecular oxygen to produce H_2O_2. Activity of PDI/Ero1 system is thought to significantly contribute to hydrogen peroxide generation in ER (Roscoe & Sevier, 2020). This fact apparently explains significantly higher in comparison to other cellular compartments redox potential within the ER-lumen (Birk et al., 2013; Malinouski et al., 2011).

Another source of H_2O_2 in the ER is representatives of the quiescin-sulfhydryl oxidases (QSOX) protein family. Similar to Ero1, activity of these FAD-dependent enzymes of Trx superfamily is accompanied by disulfide bond formation in target proteins with concomitant reduction of oxygen and H_2O_2 generation. These proteins collaborate with PDI/Ero1 system, in a complex process of protein disulfide bond formation (Kodali & Thorpe, 2010). In addition to ER, QSOX enzymes can be found throughout the cellular secretory pathway and extracellular fluids, wherein they are plausible to be able to contribute to H_2O_2-production (Kakihana et al., 2012; Kodali & Thorpe, 2010).

Besides luminal H_2O_2 sources, there are also ER membrane located ROS sources, such as NOX4. In comparison to other representatives of NOX-family, predominantly ER-localized NOX4 constitutively generates H_2O_2 (instead of superoxide) as a main product towards the ER-lumen (Guo & Chen, 2015; Roscoe & Sevier, 2020). In addition to the ER-membrane, NOX4 was also found in the mitochondria, nucleus and focal adhesions depending on the particular cell type (Guo & Chen, 2015). Other NOX isoforms were also identified in the ER-membrane, however, whether they have transient (on the way to other cellular membranes, e.g., plasma membrane) or constant ER localization awaits clarification (Roscoe & Sevier, 2020).

ER membrane-located multienzyme system – microsomal monooxygenase (MMO) is thought to be among principal ROS sources in the ER (Zeeshan et al., 2016). This system is involved in multiple biochemical processes via oxygenation of broad spectrum of different exo- and endogenous substrates. A central role in this system is occupied by NADPH-cytochrome P450 oxidoreductase (POR), which functions as an electron donor to various partners, including cytochrome P450 (Riddick et al., 2013). Electron transfer between NADPH and cytochrome P450, which is catalysed by POR, is quite inefficient process and leads to electron leakage and production of significant amounts of ROS (such as superoxide and H_2O_2) (Zeeshan et al., 2016).

Furthermore, due to numerous contact sites, which ER forms with other cellular compartments, perturbations of H_2O_2 level inside or closely to ER can originate from non-ER-related sources, such as mitochondria or peroxisomes (Yoboue et al., 2018).

In the ER-lumen there are several enzymes involved in H_2O_2 removal. Among them are peroxidases, such as Prx4 and GPx7 and 8 (Ushioda & Nagata, 2019), which utilize H_2O_2 to mediate oxidation of PDI-family member proteins and thus further fuel oxidative protein folding (Konno et al., 2021; Lu & Holmgren, 2014b). GPx7 and 8 and Prx4 are Cys-dependent peroxidases and in

addition to oxidoreductases of Trx superfamily, such as PDI, can also utilize GSH as a reductant, however, less efficiently (Buday & Conrad, 2020; Kakihana et al., 2012).

The ER-lumen also contains GSH at significant amounts. Nevertheless, since GSH-synthesizing enzymes reside exclusively in the cytosol, and there is only limited information regarding GSH and (or) GSSG transporters in the ER-membrane, thus, it is unclear how GSH system operates in the ER (Ushioda & Nagata, 2019).

Data indicate that generated H_2O_2 can diffuse from the ER-lumen (Ramming et al., 2014). H_2O_2 diffusion across membranes is controlled by certain members of aquaporin (AQP) family proteins, peroxiporins. Among peroxiporins, several ones have been detected in the ER membrane. For instance, in HeLa cells AQP11 was figured out to be a typical resident protein and the key H_2O_2 channel in the ER, while ER-localization of AQP8 is more likely transient on the way towards the plasma membrane (Bestetti et al., 2020). Despite that, AQP8 folds and thus is functional in the ER (Bertolotti et al., 2013). Furthermore, it is known that conductance of AQP8 for H_2O_2 can be redox regulated (Bestetti et al., 2018). These data suggest that H_2O_2 crosses the ER-membrane and further underline the importance of H_2O_2 for the ER and cell physiology in general.

Truly redox regulation was shown to be important for the ER-related processes. Activity of Ero1 and master regulator of ER functions, chaperone BiP (Grp78), are known to be redox regulated (Roscoe & Sevier, 2020). In addition, redox processes affect ER Ca^{2+} homeostasis (outward and inward ion fluxes) through several ER membrane proteins. Among these proteins are inositol trisphosphate receptor (IP3R) channels (Joseph et al., 2019), ryanodine receptors (RyRs) (Zissimopoulos & Lai, 2006), sarco/endoplasmic reticulum calcium-ATPase (SERCA) pumps (Roscoe & Sevier, 2020), Ca^{2+}-sensor stromal interaction molecules (STIMs) 1, 2 (Bhardwaj et al., 2016; Gibhardt et al., 2020), etc.

1.5.4 Nucleus

The primary task of the nucleus is to store DNA and to maintain its integrity and safety, therefore, it is reasonable to keep agents, which have a potential to damage DNA, away from entering this compartment. This logic is in accordance with the fact that nuclei are among the most reducing cellular compartments, with the redox potential similar to that of another DNA-containing organelle – mitochondria (Lu & Holmgren, 2014b). Nevertheless, NOX4 is shown to be able to significantly contribute to increase of nuclear ROS level and related DNA

damage (de Mochel et al., 2010; Guida et al., 2014). Furthermore, ROS from the ER-lumen can enter nuclei and lead to DNA damage as well (Peng et al., 2012).

To maintain reducing environment, nuclei contain both major antioxidant systems – Trx and GSH as wells as other thiol reductants and redox regulators (Lukosz et al., 2010). Via reduction of oxidized cysteines in DNA-binding domains and thereby enhancement of DNA-binding, nuclear Trx1 can activate certain transcription factors (TFs), including NF-κB (p50 and p65/RelA) (Hirota et al., 1999), Nrf-2 (Lukosz et al., 2010), glucocorticoid and estrogen receptors (Makino et al., 1999) among others and thus promote expression of target genes.

Independently or in concert with Trx1, APEX1/Ref1 (redox factor-1), a redox-regulated chaperone with DNA-repair and endonuclease activity, was also shown to reduce and activate various TFs in the nucleus, including AP-1, NF-κB, p53 (Lukosz et al., 2010).

Prx1 was found to differentially regulate NF-kB activity in the nucleus and the cytosol apparently via modulation of peroxide tone in the respective organelle (Hansen et al., 2007). Several other Prx isoforms were also reported to localize in the nucleus (Table 1.1) (Heo et al., 2020). The presence of multiple Prx isoforms suggests that Prxs may perform important and most likely distinct functions in this organelle.

Low-molecular weight compounds, such as GSH and GSSG, were reported to diffuse between the nucleus and the cytosol due to relatively large nuclear pore size, and concentration of GSH in both compartments is equal (Watson & Jones, 2003). However, there are data suggesting the semiautonomous control of thiol/disulfide systems in these compartments (Go et al., 2007).

Besides above considered TFs, redox environment in the nucleus affects other nuclear proteins as well, including histones (García-Giménez et al., 2013), histone methylases and deacetylases (Niu et al., 2015; Nott et al., 2008), among others, and therefore is extremely important for cell functioning.

1.5.5 Cytosol

Similar to the nucleus, the cytosolic redox potential is low, although higher than the nuclear one (Jones & Go, 2010) that probably may be explained by higher metabolic activity and ROS production in the cytosol. Cytosolic ROS and H_2O_2 can have various sources. One of these sources is the plasma membrane localized NADPH oxidases (NOXs). Upon binding to a specific receptor tyrosine kinase (RTK), an extracellular stimulus can lead to the activation of NOXs and ROS production, necessary for the signal amplification and its further propagation. Cellular response to various stimuli operates in this mode, including growth

factors (e.g., EGF, PDGF), some hormones (insulin), interleukins, etc. (Woolley et al., 2013). Besides NOXs, enzymes involved in metabolism of arachidonic acid (lipoxygenase and cyclooxygenase) generate H_2O_2, e.g., required for G2-M transition in the cell cycle (Cho et al., 2011; Heo et al., 2020). Furthermore, peroxisomes (Lismont et al., 2019), mitochondria (Lennicke et al., 2015) and ER (Ramming et al., 2014) affect cytosolic ROS level.

Many cellular proteins, which reside in the cytosol are known to be redox regulated. Since it is not possible to discuss all of them here, we mention only some of them. For instance, signal transmission from RTKs is based on phosphorylation of target proteins due to inactivation of protein tyrosine phosphatases (PTPs) (Woolley et al., 2013). Inactivation of phosphatases is mediated via oxidation of cysteine residues in their active sites that is mediated by stimulated NOXs. The group of redox-sensitive phosphatases includes PTP1B (Salmeen et al., 2003), protein phosphatase 2A (PP2A) (Raman & Pervaiz, 2019), phosphatase and tensin homolog (PTEN) (Schwertassek et al., 2014), among others. In addition to phosphatases, redox regulation is peculiar to protein kinases, e.g., non-receptor tyrosine kinases of Src family (Giannoni et al., 2010), JAK2 (Smith et al., 2012) and RTKs, e.g., VEGFR2 (Kang et al., 2011).

Small GTPases of Ras superfamily, known participants of various cellular processes and regulating cell proliferation, motility and gene expression, are also redox-sensitive due to the conserved cysteine-containing sequence, whose redox-state influences the GTPase-nucleotide interaction and the protein activity (Heo, 2011).

Among other cytosolic redox-regulated proteins are cysteine-based thiol proteases, including ones involved in autophagy: autophagin-4 (Atg4), caspases; deSUMOylation (SENPs) and deubiquitination (carboxy-terminal hydrolase L1) of proteins; calpains (Guttmann & Ghoshal, 2011).

In comparison to cysteine-based thiol proteases, proteasome, a multi-subunit protein complex with protease activity participating in elimination of cellular proteins (including oxidatively modified), does not have catalytic cysteines. Nevertheless, its activity was also shown to be affected by redox agents, including GSSG and peroxide (Guttmann & Ghoshal, 2011; Lefaki et al., 2017).

Furthermore, many proteins of translation machinery are susceptible to redox modifications, including aminoacyl-tRNA-synthetases, initiation, elongation and termination factors, ribosomal proteins, etc., (Shcherbik & Pestov, 2019; Shenton et al., 2006; Topf et al., 2018).

In addition to abovementioned redox regulation in the nucleus, redox-dependent activation of TFs also takes place in the cytosol. Often, the stimulus

for such an activation is an oxidation of TF itself or its regulatory protein (Marinho et al., 2014; Sobotta et al., 2015). For example, under normal conditions cytosolic NRF2 is stably forwarded for the degradation by KEAP1, its negative, cysteine-rich regulator. However, when reducing environments are disturbed by oxidants, cysteine thiols in KEAP1 undergo modifications that leads to KEAP1 inactivation and NRF2 translocation into the nucleus, with its following heterodimerization with small musculo-aponeurotic fibrosarcoma family protein members and, consequently, antioxidant genes upregulation (Yamamoto et al., 2018).

1.6 Importance of ROS for melanoma cells

1.6.1 ROS and cancer

Besides cellular processes, which occur in norm, ROS, and hydrogen peroxide particularly, are also known to play important role in the establishment of wide range of pathophysiological conditions and diseases, ranging from cardiovascular diseases to neurodegenerative processes and cancer (Kudryavtseva et al., 2016; Zarkovic, 2020). ROS are directly involved in the initiation step of cancer development due to oxidative modification of DNA molecules and therefore emergence of mutations in genes connected to tumour formation (Srinivas et al., 2019). In addition, cellular redox imbalance is known to be significant for cancer progression, metastasis and chemotherapy resistance (Kim et al., 2019; Perillo et al., 2020). There are evidence indicating that tumour cells and tissues have higher level of ROS in comparison to normal cells (Meyskens et al., 2001; Moloney & Cotter, 2018). Cancer cells achieve enhanced ROS production via several mechanisms, namely activation of certain oncogenes, loss of tumour suppressors, metabolic rewiring, etc. (Pizzimenti et al., 2021).

1.6.2 Melanoma and current therapies

Melanoma in this complex scenario is not an exception. Melanoma is a malignant tumour with increasing incidence and is responsible for the majority of skin cancer deaths mostly due to high metastatic potential (Damsky et al., 2010; Schadendorf et al., 2015). Melanoma arises from melanocytes, cells, which produce melanin, pigment that protects cells against UV irradiation (Miller & Mihm, 2006). Depending on the stage melanoma is treated differently. In the early stages, surgical excision alone is sufficient as a treatment, and survival rate of patients is high, however, on the last, metastatic stage, survival rate decreases dramatically (Davis, 2019). There are several types of strategies that are currently used for advanced melanoma treatment (Luke et al., 2017). One of them is targeted therapies based on the combination of BRAF (vemurafenib, dabrafenib) and MEK (trametinib, cobimetinib) inhibitors. $BRAF^{V600E}$ activating mutation is

observed in 50% of cutaneous melanomas and thus its presence is a predictive biomarker for the use of BRAF inhibitors (Schadendorf et al., 2015). Since the usage of BRAF inhibitors alone leads to quite rapidly developing resistance to the therapy, often due to reactivation of MAPK/ERK signalling, inhibitors of MEK, a downstream kinase of RAF in the pathway, are currently used in combination with inhibitors of BRAF (Su et al., 2012). Nevertheless, melanoma patients develop resistance even to the combined treatment (Flaherty et al., 2012). Melanoma has the highest somatic mutation prevalence among tumours, and hence it is very immunogenic, thus, another treatment strategy is to recruit the immune system to eliminate tumour cells (Alexandrov et al., 2013). However, owing to its known mutagenic nature, melanoma is able to escape the immune response e.g., via downregulation of MHC class I molecules on the cell surface or upregulation of immune checkpoints (Passarelli et al., 2017). Understanding of underlying mechanisms of immune resistance and immunosuppression led to the development of effective therapies for melanoma patients, such as immune checkpoint inhibitors – antibodies against PD1, PD-L1/2, CTLA-4 molecules (Davis 2019; Passarelli et al., 2017). Notwithstanding, even this approach has drawbacks, such as possible severe side-effects, lack of response and secondary resistance.

Elaborated remedies significantly ameliorated the prognosis of patients with metastatic melanoma, yet the response to these treatments does not last long. Thus, new therapies and the improvement of existing ones are highly demanding for melanoma treatment. One of possible directions for solving this task is to exploit altered redox status of melanoma cells.

1.6.3 Sources of ROS and their importance for melanoma development

It is long known that melanoma cells, similarly to other cancer cells, produce significant amounts of ROS, such as hydrogen peroxide and superoxide anion (Meyskens et al., 2001; Szatrowski & Nathan, 1991). ROS affect different stages in melanoma development, such as melanocyte transformation, metabolism, invasiveness and metastasis, immune surveillance and response, chemoresistance, etc. (Mishra & Patel, 2018).

There are two unique ROS sources, which are possibly responsible for the elevated ROS level observed in melanoma: exposure to UV light and melanin synthesis (Wittgen & van Kempen, 2007). Besides known mutagenic effect of UV irradiation on DNA molecules due to formation of cyclobutane pyrimidine dimers, UV induces ROS generation through cellular photosensitizers (Cadet et al., 2015). Melanin production in turn is accompanied with superoxide anion and H_2O_2 generation as a result of several oxidative reactions in melanin biosynthetic pathway (Pizzimenti et al., 2021). In addition, yellow-red melanin form,

pheomelanin, itself contributes to ROS formation irrespective of UV irradiation (Nasti & Timares, 2015).

Among other primary sources of ROS in melanoma are NOX enzymes. There is evidence suggesting expression of at least three members of this family in melanocytic lineage: NOX1, NOX4 and NOX5 (Liu-Smith et al., 2014). NOX1 was reported to be overexpressed in melanoma cell lines compared to melanocytes and enhance melanoma cell invasion via induced epithelial–mesenchymal transition *in vitro* (Liu et al., 2012). Nevertheless, neither mRNA nor protein levels of NOX1 were found to differ between primary and metastatic melanoma that suggests NOX1 expression is not connected to melanoma progression (Liu-Smith et al., 2014). Meanwhile, another NOX enzyme, NOX4 was found to be expressed only in some metastatic melanoma cell lines, implying its role in cell invasion (Liu-Smith et al., 2014). In melanoma cells NOX4 was reported to be important for ROS generation and for cell growth and tumorigenesis by promoting G2-M cell cycle progression (Yamaura et al., 2009). Furthermore, AKT, a protein kinase in PI3K signalling pathway, responsible for melanoma growth transformation from radial to vertical phase and thus melanoma invasiveness and metastasis, is also associated with aggressive melanoma behaviour partly via induction of NOX4 (Govindarajan et al., 2007). NOX4 via production of ROS is also able to support melanoma cell survival through the FAK (focal adhesion kinase) pathway and sustain cell viability and adhesion (Ribeiro-Pereira et al., 2014).

In addition to NOX family members, NOS (nitric oxide synthase) enzymes are also able to contribute to increase of cellular ROS level. All three NOS isoforms: endothelial (eNOS), inducible (iNOS) and neuronal (nNOS) are known to be involved in melanoma progression (Pizzimenti et al., 2021). One of the isoforms, eNOS, under certain conditions, such as in the absence of the cofactor tetrahydrobiopterin, catalyses production of superoxide anion instead of NO, owing to the phenomenon known as uncoupling (Gebhart et al., 2019). Superoxide production by uncoupled eNOS was reported to be able to drive anoikis resistance and malignant melanoma transformation (Melo, 2011).

Collectively, elevated ROS level contributes to melanomagenesis in genotoxic and nongenotoxic ways. In the nucleus ROS can evoke direct DNA damage that may lead to oncogene activation, inactivation of tumour suppressor genes, genomic instability and altered pattern of epigenetic modifications (Xian et al., 2019). Nongenotoxic effect of ROS on tumour development manifests in activation of a number of cellular signalling pathways, including MAPK/ERK, PI3K/AKT/mTOR, NRF2, NF-κB, each of which makes a significant contribution to cancer and melanoma progression through stimulation of proliferation, angiogenesis, metastasis and etc. (Xian et al., 2019).

Besides cancer cells themselves, ROS can also modulate activity and behaviour of normal cells residing in tumour microenvironment. Elevated ROS level in M1 macrophages increases their number as well as tumouricidal activity (Farhood et al., 2019). Amplified ROS level in highly sensitive to oxidative conditions immunosuppressive regulatory T cells decreases their number (Farhood et al., 2019). Oxidative stress also plays a role in reprogramming of fibroblasts, which inhibit early stage melanoma development, into a cancer associated fibroblasts, which create an optimal niche for tumour development (Avagliano et al., 2020; Zhou et al., 2016). Furthermore, it is known that ROS, e.g., H_2O_2, produced within tumour microenvironment have immunosuppressive role via inhibition of T and NK cell functions (Mimura et al., 2017)

1.6.4 Role of antioxidants in melanoma development

Since elevated ROS level is important for initiation and progression of melanoma, antioxidants seemed to be the promising therapeutic option against the disease. However, current results of single antioxidant based therapies failed in clinical trials due to inability to stop the disease progression and even further promotion of cancer development (Mishra & Patel, 2018). Elevated ROS level stimulates tumour growth, however, high level of ROS has detrimental effect on cells via either premature senescence or apoptosis (Schimmel et al., 2002; Toussaint et al., 2000). To counteract excessive accumulation of ROS and to protect cells from oxidative damage and at the same time to sustain survival and enhanced cell proliferation, melanoma relies on amplified antioxidant supply. Major cellular antioxidants are under control of NRF2 transcription factor, which is known as the master regulator of cellular response to oxidative stress and is responsible for expression of multiple antioxidant genes (Rojo de la Vega et al., 2018). The role of NRF2 in melanoma development is quite intricate. On the one hand, evidence suggests the ability of NRF2 to protect cells against oxidative stress and therefore to suppress tumorigenesis, especially in the early stage (Wu et al., 2019). On the other hand, due to upregulation of NRF2 signalling pathway tumour cells obtain advantages such as unlimited growth and proliferation, an ability to evade apoptosis and induce angiogenesis, intensified chemo- and radioresistance as well as an opportunity to metastasize (Rojo de la Vega et al., 2018; Wu et al., 2019). NRF2 knockdown was reported to suppress viability, invasion and migration as well as increase apoptosis of murine B16-F10 melanoma cells (Gao et al., 2018). Similarly, authors of another study showed that NRF2 is required for melanoma cell growth and that its downregulation leads to a significantly diminished cell proliferation as well as increased ROS level and enhanced sensitivity to oxidative stress (Jessen et al., 2020).

Particular antioxidant enzymes were shown to be connected to melanoma malignancy as well. Peroxiredoxins (Prx) 2 and 6 were reported to be expressed in melanoma cell lines, and expression level of Prx6 correlated with metastatic potential (Lokaj et al., 2009). Activity of mitochondrial SOD (MnSOD/SOD2) was also found to correlate with melanoma progression with highest activity detected in melanoma patients of the terminal, stage IV (metastatic disease) (Bisevac et al., 2018). In another study, however, it was found out the opposite, melanoma cells transfected with MnSOD displayed altered phenotype, inability to form colonies in soft agar as well as tumours in nude mice (Church et al., 1993). Compared to MnSOD, extracellular SOD (EcSOD/SOD3) has an unambiguous anti-proliferative and anti-tumour role in melanoma progression (Griess et al., 2017). Another antioxidant enzyme, glutathione peroxidase 3 (Gpx3), was found to be downregulated in both melanoma cell lines and melanoma tissue samples (like in many other tumours), and Gpx3 depletion was discovered to stimulate proliferation, motility and melanoma cell invasiveness (Chen et al., 2016). Additionally, controversial data are available for the role of catalase in melanoma progression (Bisevac et al., 2018; Bracalente et al., 2016).

Controversial data were also reported using non-enzymatic antioxidants. It was shown that oxidative stress prevents melanoma cells metastasis *in vivo*, and to successfully counteract this challenge cells adapt their metabolism to produce more NADPH partly via the folate pathway (Piskounova et al., 2015). Authors discovered that NAC (N-acetyl cysteine) treatment significantly increased metastatic potential of melanoma cells suggesting that antioxidants stimulate melanoma progression. Meanwhile, the mitochondria-targeted superoxide scavengers MitoTEMPO and MitoQ suppressed melanoma cell migration, implicating the role of mitochondrial ROS in promotion of melanoma metastasis (Porporato et al., 2014).

Taken together, one can conclude that using antioxidants to decrease ROS level in melanoma cells is controversial and may even be deleterious under certain conditions. Meanwhile, production of high ROS levels in lethal doses inside melanoma cells seems to be a promising approach for the treatment and do not have any apparent contradictions. Nevertheless, a more complete comprehension of interconnection of melanoma and ROS, and thus further researches in this field are required for the elaboration of more effective remedies for the disease treatment.

1.7 Methods review

Despite knowledge in the field of redox biology is accumulating increasingly, current understanding of cellular redox processes is far away from desired level. To figure out more details of cellular redox signalling, more

investigations are required. Following sections focus on methods allowing investigation of cellular redox processes.

1.7.1 H_2O_2 detection techniques

The study of H_2O_2-mediated redox processes requires in one way or another measurement of H_2O_2 level. Currently, several different kinds of approaches are used for H_2O_2 detection, among them: horse radish peroxidase (HRP) dependent assays, boronate-based probes, genetically-encoded fluorescent indicators (GEFIs), etc., (Rezende et al., 2018). All of these methods have their own advantages and drawbacks. Below in this section we will only focus on GEFIs, due to their extremely useful properties.

A significant milestone in the biology was the discovery of fluorescent proteins (FPs) and the development, of GEFIs, capable of detection of various small agents including different ions and molecules (Kostyuk et al., 2019). GEFIs have several important advantages in comparison to other detection methods and foremost they allow for the measurement of an intracellular level of a specific agent without disturbance of cell integrity.

Among this kind of probes is HyPer – GEFI for intracellular hydrogen peroxide detection (Belousov et al., 2006). HyPer probe consists of a cpYFP (circularly permuted yellow fluorescent protein) inserted into the sensor domain of *E. coli* OxyR. OxyR is a redox-sensitive transcription factor with two cysteines involved in the catalytic cycle, one of which is oxidized upon H_2O_2 treatment and forms a disulfide bond with the second one. Similar to OxyR, a disulfide bond formation in HyPer has transient nature, due to reduction by the cell and as a result, HyPer's oxidation is reversible. Disulfide bond formation leads to conformational changes in OxyR. These changes via linkers are transmitted to cpYFP and finally modulate fluorescent signal of the HyPer probe. HyPer, as a fluorescent protein, has excitation and emission spectra with maxima at 420, 500 and 516 nm, respectively. HyPer signal (ratio) is calculated as a ratio of emission intensity at 516 nm upon excitation with 500 nm light to emission intensity at the same 516 nm, but upon excitation with 420 nm light. HyPer’s ratio reflects its oxidation state. Upon oxidation or reduction, HyPer’s ratio increases and decreases, respectively. Ratiometric signal is extremely useful readout, since it is not affected by sensor expression level, sample density, etc. Despite many advantages, HyPer also has several drawbacks. The first and probably the most critical one is its pH-sensitivity. Thus, additional, control experiment with H_2O_2-insensitive derivative of HyPer, SypHer, is highly recommended. The second

HyPer's drawback is low brightness, which significantly limits *in vivo* application.

By now, new versions of HyPer sensor have been created, which differ from the original version by minor changes, and therefore have quite similar functional properties (Markvicheva et al., 2011; Bilan et al., 2013). In addition, red HyPer probe (HyPerRed) based on another cpFP (cpmApple) and HyPer7, pH-insensitive and far more H_2O_2-sensitive sensor, were developed (Ermakova et al., 2014; Pak et al., 2020). HyPer family sensors have been successfully used in various cells, cellular compartments and organisms that significantly expanded our knowledge of the role of H_2O_2 in living systems (Bilan & Belousov, 2016). In addition to HyPer family probes, other GEFIs for H_2O_2 detection were developed, such as roGFP2-Orp1 (Gutscher et al., 2009), roGFP2-Tsa2$\triangle C_R$ (Morgan et al., 2016) and roGFP2-Tpx1.C169S (Carmona et al., 2019).

1.7.2 Methods for H_2O_2 level modulation inside living cells

To study H_2O_2-related redox signalling, methods for H_2O_2 level modulation inside living cells are particularly useful. There are several ways of how to alter H_2O_2 level, and definitely the simplest one among them is the addition of H_2O_2 bolus to cell medium. Due to its simplicity it is widely used in many studies. Nevertheless, this mean does not allow affecting H_2O_2 level in an organelle-specific manner. To achieve such a specificity, methods and tools for a localized modulation of H_2O_2 level within a target cellular compartment are necessary.

There are several strategies, which can be used for this kind of task. For instance, depending on a particular organelle, ROS level can be modulated via regulation of a copy number of a specific organelle; regulation of an activity of a metabolic process within an organelle of interest, which is coupled to H_2O_2 generation; regulation of an endogenous pro- or antioxidant enzyme activity and etc., (Fransen & Lismont, 2019).

Furthermore, there are methods, which do not rely on the inner features of a particular organelle and thus are universal. This kind of approaches imply expression of a pro- or an antioxidant protein in a particular cellular compartment, wherein, ideally, the probe fast enough can transit between on and off states at the request of a researcher (in response to an external stimulus). This strategy can be implemented by usage of photosensitizers: KillerRed (Bulina et al., 2006) and KillerOrange (Sarkisyan et al., 2015), which in response to light stimulation generate ROS. Another approach is to use DAO enzymes (D-amino acid oxidases), which produce H_2O_2 in response to the addition of suitable D-amino acid substrates (Pollegioni et al., 2007).

1.7.3 D-amino acid oxidases

D-amino acid oxidases (DAOs) are FAD-dependent enzymes, which catalyse oxidative deamination of D-amino acids with the production of ammonium, respective ketoacids and H_2O_2 (Figure 1.5).

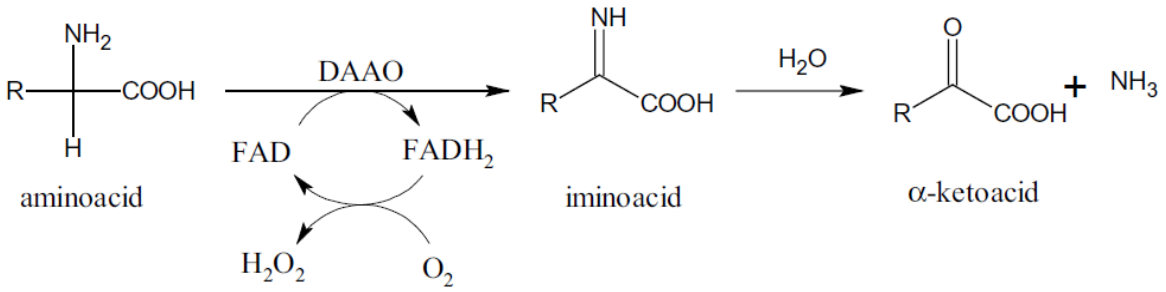

Figure 1.5: *Reaction catalysed by a D-amino acid oxidase (DAO). The figure is adapted from (Genchi, 2017).*

DAOs have absolute stereoselectivity towards D-amino acids and do not utilize L-amino acids as substrates. DAOs are quite ubiquitous enzymes in nature and found in different living beings: bacteria, fungi, invertebrates and vertebrates, including mammals (Pollegioni et al., 2007). Human organism is able to acquire D-amino acids by several ways: from intestinal microbiome, via ingestion of food and from decomposition of the polypeptides undergoing racemization. Besides mentioned sources, D-amino acids, mostly D-serine and D-aspartate, are also found to originate endogenously in brain and (neuro)endocrine tissues, respectively, as products of D-serine racemase via biosynthesis from respective L-amino acids (Genchi, 2017). Despite multiple origins, endogenous concentrations of D-amino acids in most of cells and derived cell lines are assumed negligible.

In addition to D-serine racemase participating in production of D-amino acids, there are two enzymes in human organism, which are involved in D-amino acids degradation: DAO and DDO (D-aspartate oxidase). DDO is a flavoenzyme with quite similar to DAO amino acid sequence and which catalyses the same reaction of oxidative deamination of D-amino acids. However, in comparison to DAO, which has wide spectrum of possible substrates and prefer neutral and basic D-amino acids to acidic ones (Pollegioni et al., 2007), DDO principally specializes for acidic D-amino acids, such as D-Asp, NMDA and D-Glu (Takahashi, 2020). Human DDO is highly specific for deamination of D-Asp and N-methyl D-aspartate (NMDA), shows much less activity for D-Glu (Katane et

al., 2010) and no activity for most of other D-amino acids (Katane et al., 2015). The highest activity of DDO was found in kidney, liver and brain, and, relatively low, in other tissues (Takahashi, 2020).

In several experiments, wherein the strategy of DAO-mediated H_2O_2 generation was employed, DAO from the yeast *Rhodotorula gracilis* (RgDAO) was utilized in combination with D-Alanine (D-Ala) as a substrate (Haskew-Layton et al., 2010; Matlashov et al., 2014). Among D-amino acids, D-Ala – is one of the best substrates for RgDAO, which turns into pyruvate upon deamination and thus can be fuelled into the Krebs cycle. RgDAO has notable kinetic properties and is one of the most efficient DAO characterized *in vitro*, significantly more efficient than human DAO (Pollegioni et al., 2007). Despite RgDAO has recommended itself as a suitable tool for the manipulation of H_2O_2-level in human cells, other DAOs (e.g., human DAO) were also successfully utilized as inducible, organelle-specific H_2O_2-generators (Lismont et al., 2019).

1.7.4 Proteomic techniques

1.7.4.1 Redox proteomics

In the previous sections, methods for intracellular H_2O_2-generation and monitoring were discussed, however, to shed light on cellular redox signalling, it is necessary to be able to identify respective protein participants. Proteins can be involved in adaptive response directly (reacting with H_2O_2) or indirectly (downstream protein effectors). Since cellular response to redox perturbations is extremely complex and multifaceted and simultaneously engages a vast number of proteins, proteomic methods (mostly based on mass spectrometry (MS) as a detection technique) allowing contemporaneous identification and interrogation of many proteins became an indispensable tool for the exploration of cellular redox signalling.

To detect direct protein targets, a group of redox proteomic methods was developed (Day et al., 2021; Shi & Carroll, 2020). Despite differences in experimental procedure, these methods are focused on the trapping of certain types of oxidative post-translational modifications (OxiPTMs) in proteins, mainly modifications of cysteine residues, emerging within cellular proteome in response to (a) particular oxidant(s) (Mermelekas et al., 2013). There are two kinds of approaches usually utilized for analysis of protein cysteine oxidation (Shi & Carroll, 2020). The first one, indirect, can be described shortly as a following workflow: blocking reduced, non-modified thiol groups, further reduction of reversible cysteine OxiPTMs into thiol form and labelling of derived (nascent) thiols with detectable tags. The second one, direct, implies investigation of

particular kinds of OxiPTM using selective compounds (Shi & Carroll, 2020). Since cysteine content in proteins is quite low (Miseta & Csutora, 2000), most of redox proteomic methods involve enrichment of cysteine-containing peptides prior to sample analysis.

Several approaches provide an opportunity for quantitative estimation of cysteine oxidation in protein samples (Day et al., 2021). In OxICAT (oxidative isotope-coded affinity tag) method, free thiol groups in proteins are labelled with the light ICAT probe, followed by the reduction of reversibly oxidized cysteines and labelling of the nascent thiols with the heavy ICAT reagent. Following the digestion and the enrichment, samples are analysed by MS. Oxidation of a particular cysteine is determined as a ratio of signal intensities of the peptide labelled with heavy and light ICAT probe (Leichert et al., 2008).

Since the coverage of cysteine sites in the proteome is a known challenge for redox proteomic methods, improved cysteine-modifying compounds, Cysteine-specific Phosphonate Adaptable Tags (CysPATs), were elaborated to increase efficiency of enrichment step due to utilizing immobilized metal affinity chromatography (IMAC) (Huang et al., 2016). This approach was applied for determination of cysteine oxidation profiles in ten organs of young and old mice (Xiao et al., 2020). Authors quantified more than 34,000 unique cysteine sites across over 9,400 proteins (oxidation status of 98% sites were not previously quantified) and thus demonstrated significantly improved throughput of the approach in comparison to other methods.

Compared to previously discussed techniques, which imply protein digestion and only then enrichment of thiol-containing peptides, in an alternative method, resin-assisted capture (RAC), first, thiol-containing proteins are enriched using thiol-reactive resin for capturing nascent (reversibly oxidized) thiols, and only then proteins undergo further processing (Guo et al., 2014). Such an order enables to reduce sample complexity and improve efficiency of further processing steps.

In another technique, quantitative thiol reactivity profiling (QTRP), free thiols in proteins are modified with thiol-reactive compound, 2-iodo-N-(prop-2-yn-1-yl)acetamide) (IPM), and then proteins in samples are digested (Fu et al., 2017; Fu et al., 2020). Next, IPM-modified peptides react with isotopically light or heavy azido-UV-biotin tag, undergo enrichment using streptavidin beads, elution by UV light (due to presence of the photo-cleavable linker in the azido-UV-biotin tag) and analysis by MS. Reactivity of an individual free thiol in this method is quantified as a ratio of signal intensities of the thiol-containing peptide labelled with heavy and light azido-probes in experimental and control samples,

respectively. All abovementioned techniques involve enrichment step that is a potential source of sample loss and contamination and can introduce bias, e.g., due to insufficient enrichment. Stable Isotope Cysteine Labelling with IodoAcetamide (SICyLIA) workflow provides an alternative option for proteome-scale cysteine profiling (van der Reest et al., 2018). Briefly, light and heavy isotopically-labelled variants of iodoacetamide (IAM) are used for modification of free thiols in two samples (e.g., experimental and control). Next, equal amounts of protein samples are combined, reversibly oxidized thiols are reduced and blocked with N-ethylmaleimide (NEM), and samples are digested and analysed by MS. A ratio of signal intensities, corresponding to peptides labelled with heavy and light probes is used for thiol oxidation status comparison between samples.

Despite abovementioned approaches have been established themselves as a useful group of methods for investigation of redox-related biological processes, these techniques do not enable to identify key proteins involved in the cell response to redox perturbation via non-redox mechanisms.

1.7.4.2 Thermal Proteome Profiling

The most widely used group of methods for detection of proteins, which are involved in cellular response to H_2O_2 treatment is redox proteomics. Nevertheless, these methods are able to identify proteins only directly modified by redox relays via oxidative cysteine modifications, while indirect, downstream protein targets remain elusive. In comparison to redox proteomics, Thermal Proteome Profiling (TPP) represents another quantitative proteomics method, which is based on protein feature to denature, aggregate and precipitate in response to heat-treatment (Savitski et al., 2014). Compared to redox proteomics, potential of TPP is not limited to identification of direct redox targets that allows to use TPP as a powerful alternative or better as a complementary approach to redox proteomics for investigation of cellular redox processes (Saei et al., 2020). Proteins are highly dynamic molecules, which can change their conformation in response to various stimuli, including heat treatment. Temperature increase leads to unfolding (denaturation), hydrophobic core exposure, which under normal condition hidden from surrounding molecules, and finally protein aggregation. Upon heat treatment, thousands of cellular proteins undergo simultaneous denaturation and aggregation. Protein aggregation and further precipitation (elimination of aggregates from soluble fraction) leads to the decrease of protein amount in the sample. This decrease, upon temperature increase, is reflected on a protein melting curve (Figure 1.6). Alterations of protein-protein interaction, ligand binding, emergence of PTMs, etc., can affect protein thermostability that

is evaluated to conclude whether protein is involved in cellular response to a particular stimulus (Mateus, Kurzawa, et al., 2020).

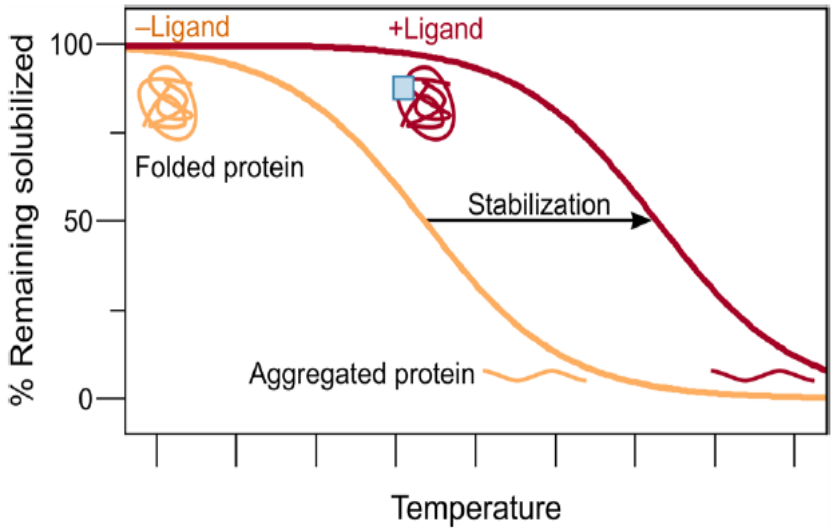

Figure 1.6: *Melting curves of free and stabilized (via ligand binding) protein. The figure is adapted from (Mateus et al., 2017).*

In addition to the detection of individual proteins, which change thermostability in response to a stimulus, TPP provides an opportunity to monitor responding dynamics of whole protein complexes. Upon heat denaturation physically interacting proteins demonstrate higher melting curve similarities than non-interacting proteins due to cooperative aggregation. This feature can be helpful for identification of new protein interactions establishing upon stimulus exposure (Figure 1.7) (Tan et al., 2018).

TPP can be performed in several formats, including temperature range TPP (TR-TPP) and two-dimensional TPP (2D-TPP), depending on the labelling scheme of peptide samples (multiplexing) (Mateus et al., 2017). In TR-TPP format, peptide samples (corresponding to one condition) treated at different temperatures are labelled using unique isobaric tandem mass tags (TMT), combined together and analysed in the same MS run. In comparison to TR-TPP, in 2D-TPP format, in addition to temperature, there is another variable (second dimension), e.g., drug concentration, that is being studied (Becher et al., 2016). In the latter TPP mode, peptide samples corresponding to condition/concentration-temperature combinations are labelled with different tags of the same TMT set, mixed and analysed together (see respective section in the methods part). Both formats have pros and cons and the correct choice depends on a goal of a particular research.

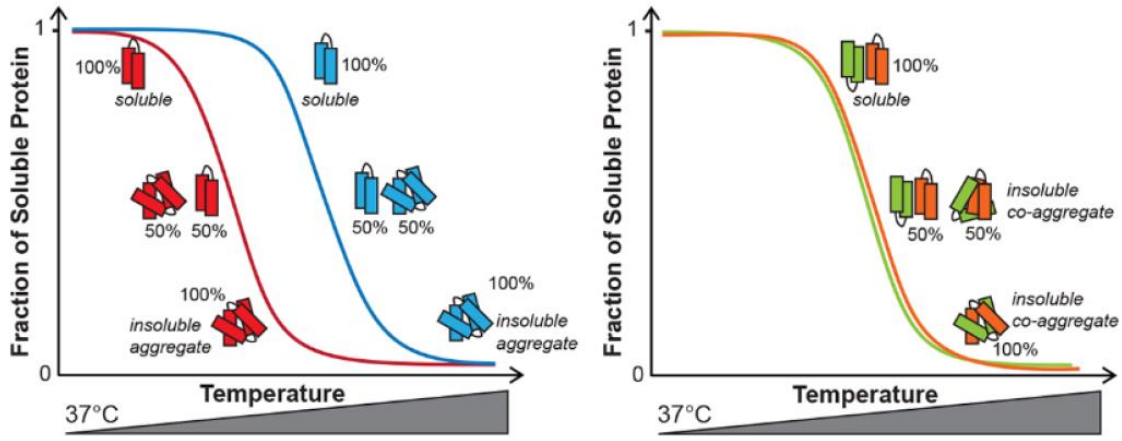

Figure 1.7: *Melting curves of non-interacting (left) or physically interacting proteins (right). The figure is adapted from (Tan et al., 2018).*

1.7.5 Methods for study of cellular NADPH

As it was discussed above, cellular H_2O_2 metabolism is tightly connected to another cellular compound NADPH. On the one hand, NADPH is a potential source for H_2O_2 generation via operation of membrane located NOX enzymes (NADPH oxidases). On the other hand, NADPH provides reducing equivalents for two major cellular antioxidant systems based on glutathione and thioredoxin. These facts highlight the importance of NADPH for cellular H_2O_2-mediated redox signalling. Similar to H_2O_2, to investigate effects of NADPH on cellular redox processes special molecular instruments are required.

There are several methods of how to monitor cellular NADPH level, however, they are either invasive, and thus can lead to sample oxidation and results corruption, or require special instrumentation that are not always available. This challenge was partially faced with the development of the set of genetically-encoded fluorescent indicators (GEFIs) for NADPH detection – iNaps (Tao et al., 2017). These sensors were engineered based on GEFI for NADH detection, SoNar, via switching of the binding specificity from NADH to NADPH (Zhao et al., 2015). SoNar and thus iNaps consist of NAD(H) binding domain of Rex (redox-sensing transcriptional repressor) from *Thermus aquaticus* as well as circularly permuted YFP (cpYFP). Presence of cpYFP defines spectral characteristics of iNaps that are quite similar to the ones of other cpYFP-based GEFIs, such as HyPer. As HyPer, iNaps are also ratiometric probes and have two excitation and one emission peaks at 400, 500 and 515 nm, respectively. All four developed iNaps have similar spectral properties, but differ in affinities to NADPH. Apparent K_d values for two of these sensors, iNap1 and iNap3, are around ~2.0 μM and ~25 μM, respectively. Different K_d values of iNaps enable to measure NADPH pool in various cellular compartments. For instance, iNap1 and 3 were successfully used by the authors of original paper to estimate NADPH

concentration in the cytosol (3.1 ± 0.3 μM) and the mitochondrial matrix (37 ± 2 μM) of HeLa cells, respectively.

There were successful attempts to alter intracellular NADPH level (Cracan et al., 2017). Authors of the study managed to change the selectivity of a *Lactobacillus brevis* H_2O-forming NADH oxidase from NADH to NADPH by site directed mutagenesis and to create a molecular tool named triphosphopyridine nucleotide oxidase (TPNOX). TPNOX catalyses the following reaction: $2NADPH + 2H^+ + O_2 \rightarrow 2NADP^+ + 2H_2O$. Despite obvious utility of the tool, its activity was not inducible (only expression), which restricts its application for fast and controllable alterations of NADPH level. This limitation can be overcome by utilizing the tool analogous to the DAO described above for the manipulation of intracellular H_2O_2 level. One promising candidate for this role is $NADP^+$-dependent D-amino acid dehydrogenase (DAAD) derived from meso-diaminopimelate dehydrogenase of *Ureibacillus thermosphaericus* strain A1 by site-directed mutagenesis (Akita et al., 2012). The addition of certain D-amino acids to DAAD (e.g., D-Lysine) leads to reduction of $NADP^+$ and thus NADPH level increase. DAAD catalyses the following reaction: D-amino acid + $NADP^+$ + $H_2O \rightarrow$ α-keto acid + NADPH + H^+. Considering limited availability of D-amino acids for most of eukaryotic cells, addition of suitable exogenous D-amino acid to cells makes production of NADPH inducible. On the whole, combining of DAAD with iNaps would allow to create the system analogous to HyPer-DAO, but instead capable of manipulation and monitoring of NADPH level.

2 Aims of thesis

Hydrogen peroxide and associated redox compounds, such as NADPH, play an important role in cellular redox signalling in physiology and pathology. Nevertheless, our knowledge of influence of these molecules on cell processes and respective proteins are quite limited. In this doctoral thesis, we attempted to investigate the response of malignant and non-malignant cells to alterations of H_2O_2 and NADPH level in various cellular compartments, through implementation of following tasks:

1) Assemble plasmids encoding HyPer-DAO and iNap-DAAD proteins fused to sequences for subcellular localization.

2) Produce lentiviruses and stable melanoma (malignant) and HEK293 (non-malignant) cell lines expressing HyPer-DAO and iNap-DAAD fusion proteins targeted to various cellular compartments.

3) Characterize the response of melanoma cells to alterations of H_2O_2 and NADPH level *in vitro*.

4) Study the influence of compartmentalized H_2O_2 generation on the cell proteome by Thermal Proteome Profiling (TPP).

5) Based on processed TPP data, build a database of proteins, which respond to endogenous compartmentalized oxidative stress.

6) Examine H_2O_2 influence on interactome of several proteins involved in cellular redox signalling (according to our TPP results) by the mean of co-immunoprecipitation (validate TPP data).

3 Materials and methods

3.1 Materials

3.1.1 Plasmids

All plasmids, which were used (but not made) in the current study, are listed in the Table 3.1.

Table 3.1: *Plasmids.*

purpose	plasmid	origin/manufacturer
Cloning	AAV-HyPer-DAO-3NLS	V. Belousov's lab
	pC1-TagBFP-DAO-KDEL	V. Belousov's lab
	pHyPer-dMito	Evrogen
	pLVX-Puro-DAAD	V. Belousov's lab
	pRDNA3.1-hydro-cyto-iNap1	Y. Yang's lab
	pRDNA3.1-hydro-cyto-iNapc	Y. Yang's lab
	pRDNA3.1-hydro-tdCox8-iNap3	Y. Yang's lab
	pRDNA3.1-hydro-tdCox8-iNapc	Y. Yang's lab
	SypHer3s-IMS	V. Belousov's lab
	TagBFP-DAO-Sec61B	V. Belousov's lab
Lentivirus production	pMD2.G	Addgene, #12259
	pCMV-dR8.91	Creative Biogene, OVT2971
Co-IP	pASIET-EGFP	J. Messens's lab
	pcDNA3.1(+)-PARK7-FLAG	GenScript, NM_007262.5
	pcDNA3.1(+)-TRAP1-FLAG	GenScript, NM_016292.3
	pcDNA3.1(+)-MAP2K1-FLAG	GenScript, NM_002755.4
	pcDNA3.1(+)-UBA2-FLAG	GenScript, NM_005499.3
	pcDNA3.1(+)	Invitrogen, V79020

3.1.2 Primers

All primers used in the current work were designed using OligoAnalyzer™ Tool, which is provided as an online service by Integrated DNA Technologies (IDT), purchased from Sigma company and are listed in the Table 3.2.

Table 3.2: *Primers.*

primer	sequence (5' – 3')
1	CGCTGTTTTGACCTCCATAGAAGACACCGACTCCGTCAGATCCGCTAGCATG
2	AGTCGGTGTCTTCTATGGAGGTCAAAAC
3	AACCGCCTGTTTTAAAACTTTATCGAAATGGC
4	GCCATTTCGATAAAGTTTTAAAACAGGCGGTTG
5	CAGAGCTGTGAGGGCAGAATTGGTGGAAATCATTAGCTCTCCCTAGCTGCGC

6	TGATTTCCACCAATTCTGCCCTCACAGCTCT
7	CTATTAACTGGCGAACTACTTACTCTAGCTTCCC
8	GGGAAGCTAGAGTAAGTAGTTCGCCAGTTAATAG
9	CGCTGTTTTGACCTCCATAGAAGACACCGACTGCCACCATGGAGATGGCAAGC
10	CAGAGCTGTGAGGGCAGAATTGGTGGAAATCAGCGCTGCTCGAGGCAAGC
11	CATTACAGGGTCAGCCGCTCCAGGGGGGGCAGGCTCTCCCTAGCTGCGCC
12	GCTGATGCTGGAAGATGGTCACAGCTTGCGCGATCAGGCAATGTC
13	GACATTGCCTGATCGCGCAAGCTGTGACCATCTTCCAGCATCAGC
15	AGAGCTGTGAGGGCAGAATTG
16	GCAAGGGCGAGGAGCTG
17	CAGACGGACCCAGACAAGC
38	CGTATCACGAGGCCCTTTCGAAGACACCGACTCTGGCTAGCATGTCCGTC
40	CGTATCACGAGGCCCTTTCGAAGACACCGACTGCCACCATGCCAAAAAAGAAGAGAAAGGTAGATCCAAAAAAGAAGAGAAAGGTAGATGATCCGATGAACCGGAAGTGGG
41	CGTATCACGAGGCCCTTTCGAAGACACCGACTGCCACCATGCTTCAACTTCCTCCTCTTGAACGTCTTACTCTCTCTGATCCGATGAACCGGAAGTGGG
46	AATAATCCTAGGGTGGAGGCTGAAAGAATCGTC
49	AATAATCTCGAGTTACAATTTACTTCCACTGCTCTCCCTAGCTGCGC
50	CTGGTCCACTCTCATCAGGAGGGTTCAGCTTAGATCTGAGTCCACTGCTCTCCCTAGCTGCGC
51	AATAATCTCGAGTTAGGAGAGCACACACTTGCAGCTCATGCATCCTGGTCCACTCTCATCAGGAGGG
52	CGCAGTCGCAGGACCAGTAGCAACAGAGATGGCAAGCCAGCAGG
54	AATAATCTCGAGTTACAGCTCGTCCTTTCCAGATCTACCTCCTCCACCGCTCTCCCTAGCTGCGC
57	GCCCTTTCGAAGACACCGACT
58	TTTAATGAATTCTTGCGTGTGTGTCAAAGCTG
59	GCTACTAACTTCAGCCTGC
60	CCAGCCTGCTTCAGCAGGCTGAAGTTAGTAGCTCCGGATCCGCCCATCATCTCCTCCCG
73	AAAAAAAGAAGACACCGACTATGCTCCTATCCGTGCCGTTGCTGTTAGGTCTACTAGGACTCGCAGTCGCAGGACCAG
74	AAAAAAGCTAGCATGGCAATCCAGTTGCGTTCGCTCTTCCCCTTGGCGTTGCCCGGAATGCTGGCCCTCCTTGGCTGGTGGTGGTTTTTCTCTCGTAAAAAAGACCTGGAGCTGAAGCTG
75	TTTTTTGGATCCCCGGTTGCCACAGGAGGGTCCCTGGCCCTAGGCACGGTGCTCTGCAGTATTCTCAGCTTCAGCTCCAGGTCTTTTTTACGAG
76	AAAAAACTCGAGCTACGAACGAGTGTACTTGCCCCAAATG
77	AATAATCTCGAGTTACAATTTACTTTTCAGACTTCCTATGACAGGGCTCTCCCTAGCTGCGC
86	AAAAAATCTAGAGCCACCATGAGCGAGCTGATTAAGGAGAACATG
87	AAAATTGGATCCTTATAGCTCGTCTTTGCTCTCCC

3.1.3 Enzymes

Enzymes and buffers used in the current study are listed in Table 3.3.

Table 3.3: *Enzymes and respective buffers.*

enzyme/buffer	Manufacturer, catalogue number
AvrI	NEB, R0174
BamHI	NEB, R0136
BbsI	NEB, R0539
Benzonase	Merck, 71206-3
CutSmart® Buffer	NEB, B7204
EcoRI	NEB, R0101
NEBuffer™ 1.1	NEB, B7201
NEBuffer™ 2.1	NEB, B7202
NEBuffer™ 3.1	NEB, B7203
NheI	NEB, R0131
OneTaq® Quick-Load® 2X Master Mix with Standard Buffer	NEB, M0486
Q5® High-Fidelity DNA Polymerase	NEB, M0491
Q5 Reaction Buffer (5X)	NEB, B9027
T4 DNA-Ligase	NEB, M0202
T4 DNA Ligase Reaction Buffer	NEB, B0202
XbaI	NEB, R0145
XhoI	NEB, R0146

3.1.4 Kits

Purchased kits used in the current study are listed in Table 3.4.

Table 3.4: *Commercially available kits.*

kit	manufacturer, catalogue number
ANTI-FLAG M2 Magnetic Beads	Sigma, M8823-5ML
HiSpeed Plasmid Maxi Kit	Qiagen, 12663
PCR Mycoplasma Test Kit I/C	PromoKine, PK-CA91
Pierce™ BCA Protein Assay Kit	Thermo Scientific, 23225
Pierce™ ECL Western Blotting Substrate	Thermo Scientific, 32109
Pierce Rapid Gold BCA Protein Assay Kit	Thermo Scientific, A53225
QIAquick PCR Purification Kit	Qiagen, 28104
QIAquick Gel Extraction Kit	Qiagen, 28704
QIAprep Spin Miniprep Kit	Qiagen, 27104
QIAGEN Plasmid Maxi Kit	Qiagen, 12163

3.1.5 Bacterial strains and eukaryotic cell lines

Bacterial strains and eukaryotic cell lines used in the current study are listed in Table 3.5.

Table 3.5: *Bacterial strains and eukaryotic cell lines.*

cells		application
Bacterial strains	*E.coli* XL1Blue chemically competent cells	plasmids production
Eukaryotic cell lines	HEK293	stable HEK293 cell lines production, control cell line in experiments
	HEK293TN	lentivirus production
	HeLa	validation of protein localization
	Melanoma 1205Lu	stable melanoma cell lines production, control cell line in experiments
	Melanoma WM3734	
	Melanoma WM88	

3.1.6 Media and solutions for eukaryotic cells

Constituents and recipes of complete media and solutions used for bacterial and eukaryotic cell culture in the current study are listed in Table 3.6 and Table 3.7, respectively.

Table 3.6: *Constituents used for preparation of complete media and solutions.*

medium/solution	Manufacturer/catalogue number
DMEM, high glucose, pyruvate	Thermo Scientific/Gibco, 41966-029
DPBS (Dulbecco's Phosphate-Buffered Salines), calcium, magnesium	Thermo Scientific/Gibco, 14040
DPBS (Dulbecco's Phosphate-Buffered Salines) no calcium no magnesium	Thermo Scientific/Gibco, 14190-094
Fetal Calf Serum (FCS)	Sigma-Aldrich, F7524
Insulin, human	Sigma-Aldrich, H-7523
L15 Leibovitz liquid medium	Merck/Biochrom, F 1315
L-Glutamine	Life Technologies, 67513
MCDB153 basal medium	Merck/Biochrom, F 8105
Minimum Essential Medium Eagle	Sigma, M3024
Opti-MEM™ (Reduced Serum Medium)	Thermo Scientific/Gibco, 31985062
Penicillin/Streptomycin (Pen/Strep)	Sigma-Aldrich, P0781
Trypsin-EDTA (0.25%), phenol red	Thermo Scientific/Gibco, 25200056

Table 3.7: *Recipes of complete media and solutions.*

medium/solution	recipe	purpose
LB (Luria-Bertani) liquid medium	tryptone – 10 g, NaCl – 10 g, yeast extract – 5 g, H_2O – up to 1 L	bacterial cell culture

solid agar medium	agar – 15 g, tryptone – 10 g, NaCl – 10 g, yeast extract – 5 g, H_2O – up to 1 L	agar plates for growing bacterial colonies
CM (culture medium)	DMEM, high glucose, pyruvate, FCS – 10%, (Pen/Strep – 1%)	eukaryotic cell culture (HEK293, HeLa)
EM (Experiment Medium)	DPBS calcium, magnesium, 1x, Glucose – 5.56 mM	experiments, imaging (HEK293 cell lines)
IM (Imaging Medium)	Minimum Essential Medium Eagle (Sigma, M3024), HEPES – 20 mM, L-Glutamine – 2 mM, H_2O – up to 1 L, pH = 7.4	experiments, imaging (melanoma cell lines)
Tu 2%	L15 Leibovitz liquid medium – 0.1 L, MCDB153 basal medium – 0.4 L, FCS – 10 ml, $CaCl_2$ (1M) – 840 µl, Insulin (10 µg/ml) – 250 µl (sterile, filtered)	eukaryotic cell culture (melanoma cell lines)

Wild type HEK293 cells and derived stable HEK293 cell lines were cultured on DMEM without Pen/Strep. Only prior to and during Co-IP experiment, they were cultured on DMEM containing Pen/Strep. HEK293TN cell line was cultured on DMEM without Pen/Strep.

3.1.7 Other solutions and buffers

Other solutions and buffers used in the current study are listed in Table 3.8.

Table 3.8: *Other solutions and buffers.*

solution/buffer/gel	recipe
agarose gel, 1%	TBE, 1x – up to 50 ml agarose – 0.5 g, GelRed® Nucleic Acid Gel Stain – 4 µl
ampicillin (1000x stock solution)	sodium ampicillin – 1 g, H_2O – 10 ml
Blocking solution (membrane, WB)	dry unfatted-milk – 1 g, 1x TBST – 20 ml
cOmplete Roche protease inhibitor (50x stock)	cOmplete protease inhibitor – 1 tablet, DPBS, 1x – 1 ml
Crystal violet staining solution	Crystal Violet – 0.5g, Formaldehyde, 37% – 27 ml, PBS, 10x – 100 ml,

	Methanol – 10 ml (1%), H_2O – up to 1 L
D-alanine (1M stock solution)	dissolve in H_2O
FLAG-peptide elution buffer (5 mg/ml, 10x stock)	FLAG-peptide – 4 mg, 1x TBS – 0.8 ml
Glucose, stock solution (30%)	Glucose – 6 g, H_2O – 20 ml
kanamycin (1000x stock solution)	Kanamycin – 0.5 g, H_2O – 10 ml
Loading (Laemmli) Buffer, 4x	1 M Tris-HCl pH 6.8 – 2.0 ml, SDS – 0.8 g, 100% glycerol – 4.0 ml, 14.7 M β-mercaptoethanol – 0.4 ml, 0.5 M EDTA – 1.0 ml, bromophenol Blue, 8 mg, H_2O – up to 10 ml
Lysis buffer (for TPP)	DPBS, 1x, NP-40, 1.33%, $MgCl_2$, 2.5 mM, cOmplete, 1.6x, PhosStop, 1.6x, Benzonase, 0.417 U/µl
Lysis Buffer 1	DPBS,1x, NP-40, 0.8%, $MgCl_2$, 1.5 mM, cOmplete, 1x, PhosStop 1x, Benzonase, 0.250 U/µl
Lysis Buffer 3	DPBS, 1x, NP-40, 0.8%, $MgCl_2$, 1.5 mM
Lysis Buffer 4	DPBS, 1x, NP-40, 0.8%, $MgCl_2$, 1.5 mM, cOmplete, 1x, PhosStop 1x
PhosStop (phosphatase inhibitor, Roche), (50x stock)	PhosStop – 1 tablet, DPBS, 1x – 0.5 ml
Polybrene (stock solution)	Polybrene – 50 mg, 0.9% NaCl in H_2O – 50 ml
Puromycin dihydrochloride (stock solution)	Puromycin dihydrochloride – 0.5 g, H_2O – 10 ml
Running Buffer (SDS-PAGE), (10x stock solution)	Tris base – 250 mM, glycine – 1.92 M, SDS – 1%, H_2O, pH = 8.3
Separating polyacrylamide gel, 12%	30% acryl/bis-acrylamide – 2.4 ml,

(6 ml/gel)	1.5 M Tris, pH 8.8 – 1.5 ml, H_2O – 1.975ml, 10% SDS – 60 µl, 10% APS – 60 µl, TEMED – 6 µl
Stacking polyacrylamide gel (3 ml/gel)	30% acryl/bis-acrylamide – 0.5 ml, 1 M Tris, pH 6.8 – 0.38 ml, H_2O – 2.06 ml, 10% SDS – 30 µl, 10% APS – 30 µl, TEMED – 3 µl
TBE (Tris/Borate/EDTA), 10x	Tris – 108 g, boric acid – 55 g, 0.5 M EDTA (pH 8.0) – 40 ml, H_2O – up to 1L
TBS (10x stock)	Tris – 24 g, NaCl – 88 g, H_2O – 1L, pH = 7.6
TBST, 1x	10x TBS – 100 ml, Tween® 20 – 0.1%, H_2O – 1 L
Towbin transfer buffer	Tris – 25 mM, Glycine – 192 mM, MeOH – 20%, H_2O, pH 8.3

3.1.8 Chemicals and reagents

Chemicals and reagents used in the research are listed in Table 3.9.

Table 3.9: *Chemicals and reagents.*

chemical	manufacturer	catalogue number
Acetic acid	Carl Roth	KK62.1
Acrylamide/Bis-acrylamide, 30% solution	Sigma	A3574
Agar Bacteriology grade	PanReac AppliChem	A0949
Agarose Broad Range	Carl Roth	T846.3
Ampicillin sodium salt (Amp)	Carl Roth	K029.2
Ammonium persulfate (APS)	Carl Roth	9592
β-Mercaptoethanol	Carl Roth	4277.1
Bromophenol blue sodium salt	Carl Roth	A512.1
Boric acid	Carl Roth	6943.1
Calcium chloride 2-hydrate ($CaCl_2 * 2H_2O$)	Carl Roth	5239.1
cOmplete™ Protease Inhibitor Cocktail	Sigma	11697498001
Crystal violet, Cation-based violet dye	Abcam	ab143095
D-alanine	Sigma	A7377
Dimethyl sulfoxide (DMSO)	Sigma	D2650

EDTA	Carl Roth	8043.2
Formaldehyde, 37 %, p.a., ACS	Carl Roth	4979.1
Glucose	Merck	108337
Glycerol	Carl Roth	3783.2
Glycine	Carl Roth	3908.2
HEPES	Sigma	H7523
Hydrogen Peroxide (H_2O_2) solution	Sigma	H1009
Isopropanol	Sigma	W292907
Kanamycin	Carl Roth	T832.1
Magnesium chloride 6-hydrate ($MgCl_2 * 6H_2O$)	PanReac AppliChem	141396
Methanol	Carl Roth	4627.5
NP-40, 20%	Sigma	I8896
Polybrene (Hexadimethrine bromide)	Sigma	H9268
Polyethylenimine, Linear, MW 25000, Transfection Grade (PEI 25K™)	Polysciences	23966
PhosStop (phosphatase inhibitor)	Sigma	4906845001
Puromycin dihydrochloride (Puro)	VWR	540222-25
Sodium chloride (NaCl)	Sigma	S7653
Sodium dodecyl sulfate (SDS)	Carl Roth	4360.2
Tetramethylethylenediamine (TEMED)	Carl Roth	2367.3
Tris	Carl Roth	5429.3
Trypton	PanReac AppliChem	403682
Tween® 20	Carl Roth	91271
Yeast extract	Carl Roth	2363.1

3.1.9 Other commercially available products

***Table 3.10**: Other commercially available products.*

product	application	manufacturer	catalogue number
Deoxynucleotide (dNTP) Solution Mix	Molecular cloning	NEB	N0447S
Carboxy-terminal FLAG-BAP™ Fusion Protein	Co-IP	Sigma	P7457
FLAG-peptide	Co-IP	Sigma	F3290
FuGENE® HD Transfection Reagent	Eukaryotic cells transfection	Promega	E2312
Gel Loading Dye, Purple (6X)	Molecular cloning	NEB	B7024S
GelRed® Nucleic Acid Gel Stain	Molecular cloning	biotium	41002
GeneRuler 1kb DNA Ladder	Molecular cloning	Thermo Scientific	SM0311
InstantBlue® Coomassie Protein Stain	Gel staining	Abcam	ab119211
PageRuler™ Prestained Protein Ladder, 10 to 180 kDa	Co-IP (SDS-PAGE)	Thermo Scientific	26617

TMTpro™ 16plex Label Reagent Set	Peptides labeling (Mass Spectrometry)	Thermo Scientific	A44522

3.1.10 Consumables

Consumables used in the current study are listed in Table 3.11.

***Table 3.11**: Consumables.*

consumable	manufacturer	catalogue number
Cell culture dishes, 35mm	Sarstedt	83.3900.300
Cell culture dishes, 100mm	Sarstedt	83.3902.300
Cell culture dish, Cellstar® TC	Greiner	639160
Cell culture flasks, T25	Sarstedt	83.3910.002
Cell culture flasks, T75	Sarstedt	83.3911.002
Cell culture plates, 6-well	Sarstedt	83.3920.300
Cell culture plates, 24-well	Sarstedt	83.3922
Cell culture plates, 96-well	Sarstedt	82.1581.001
Coverslips (Ø=25 mm)	O.Kindler	02R1215-D
CryoPure 2.0ml tubes	Sarstedt	72.379
Falcon® 15 mL Polystyrene Centrifuge Tube	Corning Life Sciences	352099
Falcon® 50 mL High Clarity PP Centrifuge Tube	Corning Life Sciences	352098
Glass Pasteur Pipettes	Brand	ISO 7712
MultiScreenHTS HV Filter Plate, 0.45 µm	Millipore	MSHVN4550
Omnifix® disposable syringes, 5ml	B. Braun	4616057V
Petri dishes	Sarstedt	82.1473.001
PVDF Transfer Membrane, 0.45 µm, 26.5 cm x 3.75 m	Thermo Scientific	88518
Pyrex® cloning cylinder	Merck	CLS31666
Reaction tubes, 0.5ml	Sarstedt	72.699
Reaction tubes, 1.5 ml	Sarstedt	72.690.001
Reaction tubes, 2.0 ml	Sarstedt	72.691
Sapphire pcr 8-tube strips, 0.2 ml	Greiner	673210
Sapphire 8-cap strips	Greiner	373250
Serological pipettes, 1 ml	Sarstedt	86.1251.001
Serological pipettes, 2 ml	Sarstedt	86.1252.001
Serological pipettes, 5 ml	Sarstedt	86.1253.001
Serological pipettes, 10 ml	Sarstedt	86.1254.001
Serological pipettes, 25 ml	Sarstedt	86.1685.001
Syringe filter 0.20 µm pore size	Sartorius	16541-q
Syringe filter 0.45 µm pore size	Sartorius	16533-guk
TPP® tissue culture dishes, 15cm	Merck	Z707694
twin.tec® PCR Plate 96	Eppendorf	0030133390

All pipette tips were purchased from VWR company.

3.1.11 Antibodies

Antibodies used in the current study are listed in Table 3.12.

Table 3.12: *Antibodies.*

antibody	working dilution	manufacturer	catalogue number
Monoclonal ANTI-FLAG® M2 antibody, mouse (primary)	1:1000	Sigma	F3165
Goat anti-Mouse IgG (H+L) Secondary Antibody, HRP	1:5000	Thermo Scientific, Invitrogen	62-6520

3.1.12 Devices

Devices used in the current study are listed in Table 3.13.

Table 3.13: *Devices.*

Device	Manufacturer	Application
AxioObserver Z1	Zeiss	Fluorescence microscopy
AxioObserver D1	Zeiss	Fluorescence microscopy
BioWizard Silver Line Biosafety cabinet	Kojair	Sterile work
B15 convection incubator	Heraeus	Bacteria cultivation on agar plates, eukaryotic cells incubation without CO_2
CB53	Binder	eukaryotic cells cultivation
CoolCell™ LX Cell Freezing Container	Corning	Freezing cells
Centrifuge, MiniSpin	Eppendorf	Centrifugation
Centrifuge, 5415R	Eppendorf	
Centrifuge, Biofuge fresco	Heraeus	
Centrifuge, Labofuge 400R	Heraeus	
Centrifuge, Megafuge 40R	Heraeus	
Centrifuge, Fresco17	Thermo Scientific	
Countess II FL Automated Cell Counter	Life technologies	Cells counting
C1000 Touch Thermal Cycler	Bio-Rad	DNA-amplification
ChemiDoc XRS+ System	Bio-Rad	WB membrane imaging
Gel Doc EZ Imager	Bio-Rad	Gel imaging
Herasafe™ KS (NSF) Class II, Type A2 Biological Safety Cabinets	Thermo Scientific	Sterile work
Liquidator 96 From Rainin	Biocompare	Pipetting 96-well plates (TPP)
Magnetic rack	Sansure Biotech Inc.	Magnetic beads separator
Micro tube holder for 40 x 10-11.5mm tubes for SB2 and SB3	Appleton woods	Orbital rotator

Mini-PROTEAN® Tetra System	Bio-Rad	SDS-PAGE
Mini-Sub Cell GT Systems	Bio-Rad	DNA-electrophoresis
MS1 S1 Vortex Shaker	IKA	Tubes shaking
Mithras LB 940 Multimode Microplate Reader	Berthold Technologies	Plate reader
NanoDrop™ 2000/2000c Spectrophotometer	Thermo Scientific	Determination of DNA concentration
Optical microscope telaval 31	Zeiss	Cell observation
PMR-30 Platform 2D Rocker – Fixed Tilt	Grant Instruments	Western Blot
PowerPac Basic Power Supply	Bio-Rad	SDS-PAGE, DNA-electrophoresis
Q Exactive™ Plus Hybrid Quadrupole-Orbitrap™ Mass Spectrometer	Thermo Scientific	Mass Spectrometry
SureCycler 8800 Thermal Cycler	Agilent	TPP, heating
TC20 Automated Cell Counter	Bio-Rad	Cell counting
ThermoMixer F2.0	Eppendorf	heating/cooling/shaking
Trans-Blot® Turbo™	Bio-Rad	Western Blot
UV Transilluminator (MD-25/HD-25)	Wealtec	Detection of stained dna bands in agarose gels
Wide Mini-Sub Cell GT Cell	Bio-Rad	DNA-electrophoresis
WTW InoLab ph Level 1 ph Meter with WTW SenTix81 Probe	InoLab	pH measurement/ adjustment

3.1.13 Software

Table 3.14: *Software packages.*

software/distributive/tool	provider	application
Python packages		
jupyter/ipython	conda/pypi	Python coding IDE
numpy/scipy/pandas	conda/pypi	core data processing packages
matplotlib/seaborn	conda/pypi	Plot creation
scikit-learn	conda/pypi	Machine Learning package (Pedregosa et al., 2011)
statsmodels	conda/pypi	Statistical package (Seabold & Perktold, 2010)
beautifulsoup4	conda/pypi	XML processing
goatools	GitHub	GOEA (Klopfenstein et al., 2018)
R packages		
IRdisplay/IRkernel	conda/CRAN	R conding IDE
tidyverse/dplyr/stringr/rlang/data.table/purrr	conda/CRAN	Core data processing packages
DEP	bioconductor	Analysis of differences in quantitative proteomics (Zhang et al., 2018)

lme4/afex	conda/CRAN	Mixed-effects models and their statistical analysis (Bates et al., 2015)
vsn	bioconductor	Variance-stabilizing normalization (Huber et al., 2002)
LIMMA	bioconductor	Empyrical bayess statistical test (Ritchie et al., 2015)
fdrtool	conda/CRAN	Multiply-hypothesis adjustment (Strimmer, 2008)
ggplot2	conda/CRAN	Plot creation
Co-IP/MS data processing		
ThermoRawFileParser	github/dockerhub	Converter of raw spectra of THERMO format (Hulstaert et al., 2020)
MSFragger	Nevislab.org/github	Proteomics search engine (Kong et al., 2017)
Philosopher	Nevislab.org/github	Proteomics toolkit (da Veiga Leprevost et al., 2020)
IonQuant	Nevislab.org/github	Tool for LFQ (Yu et al., 2021)
TPP data processing		
Mascot	MatrixScience	Commercial proteomics search engine
isobarQuant	Github	Quantification of isobaric labelled experiment (Franken et al., 2015)
Other software		
FIJI (ImageJ)	Wayne Rasband, Curtis Rueden	Fluorescence microscopy images processing (Schneider et al., 2012)
Mendeley Desktop v1.19.8	Mendeley	Bibliography generation
OligoAnalyzer™ Tool	IDT	Primers design
Inkscape	Inkscape project	Figures-panels creation
SnapGene Viewer	SnapGene	Plasmids design

3.2 Methods

3.2.1 Molecular cloning methods

3.2.1.1 Amplification of DNA fragments (PCR)

DNA fragments for assembly of plasmids were amplified by PCR (polymerase chain reaction). PCR was performed in accordance to the protocol of Q5 polymerase provided by the manufacturer with minor modifications. PCR mix consisted of 0.5 µl of Q5 polymerase, 1 µl of dNTP mix, 1 µl of plasmid DNA (5 ng/µl), 1µl of primer mix (10 µM of each, forward and reverse ones), 2.5 µl of DMSO (100%), 10 µl of 5x Q5-polymerase buffer and 34 µl of ddH_2O (up to 50 µl). PCR-program slightly varied depending on the sequences of primers, DNA

plasmid and the length of desired PCR product and can be summarized as following:

Table 3.15: *PCR-program for amplification of DNA fragments.*

Step	Temperature, ^{o}C	Duration, s	Process
1	95	180	DNA denaturation
2	95	20	
3	58-62	30-45	Primers annealing
4	72	30-300	Fragment amplification
5	72	60-120	

Steps 2-4 were repeated 25 times before reaching step 5. Primers used for DNA amplification are listed in Table 3.2.

3.2.1.2 DNA electrophoresis

Validation of PCR results, separation of DNA fragments upon restriction of plasmid DNA and assertion of purity of DNA samples was performed by DNA electrophoresis. Each DNA sample was premixed with 6x Gel Loading Dye (NEB) and loaded in a particular well of prepared 1x TBE-based 1% agarose gel. Separation of DNA samples was performed in 1x TBE, 4–10 V/cm within 15-40 min depending on a particular task. For determination of the length of DNA fragment, 0.1 kb or 1 kb DNA ladder was used. In case of purification of a target DNA fragment from a mix of multiple DNA fragments, entire volume of a PCR-mix was loaded in a well. Gels were observed using UV Transilluminator. The same device in the low light intensity mode was used for monitoring of DNA bands excision from gel.

3.2.1.3 DNA purification from reaction mix

DNA molecules were purified from reaction (PCR/restriction/ligation) mix with QIAquick PCR Purification kit according to the manufacturer recommendations.

3.2.1.4 AQUA-cloning

AQUA (advanced quick assembly) cloning – is an enzyme-free cloning method, which requires only amplification of target sequences (fragments), mixing them in ddH_2O and transformation of competent bacterial cells with the derived mix (Beyer et al., 2015). Method was performed in accordance to the protocol described by authors in the original study with minor modifications.

Assembly of plasmids by *E. coli* was based on 32 bp short homology regions created at ends of each fragment during amplification step.

3.2.1.5 Overlap Extension PCR

Chimeric gene products before insertion into a plasmid backbone were assembled by Overlap Extension PCR (OE-PCR) according to the protocol with modifications (Heckman & Pease, 2007), (Figure 4.2). DNA fragments were amplified from G-blocks (purchased from IDT company) and plasmids encoding required genes using described above PCR program (Table 3.15). Then, derived PCR products were extracted from reaction mixes and were used for OE-PCR. The composition of the reaction mix for OE-PCR was following: of 0.5 µl of Q5 polymerase, 1 µl of dNTP mix, 50 ng of each of two PCR product, 2.5 µl of DMSO (100%), 10 µl of 5x Q5-polymerase buffer and ddH_2O (up to 50 µl). PCR was performed according to the scheme (Table 3.16):

Table 3.16: *PCR-program for amplification of DNA fragments by Overlap Extension PCR.*

Step	Temperature, ^oC	Duration, sec	Process
1	95	180	DNA denaturation
2	95	20	
3	62	20	Primers annealing
4	72	90	Fragment amplification
5	72	120	

Steps 2-4 were repeated 10 times before reaching step 5. Next, 1µl of primer mix (10 µM of each forward and reverse ones) was added to the PCR mix and PCR was continued according to the same program (Table 3.16). Steps 2-4 were repeated additional 15 times before reaching step 5.

3.2.1.6 Transformation of chemically competent bacterial cells

Chemically competent XL1 Blue *E. coli* cells were stored in the freezer at -80 ^oC and before transformation were thawed on ice for 5-10 min. Then 10-100 ng of DNA were added to cells and resulting suspension was mixed by tapping. The tube containing DNA-cell mixture was incubated for 60-90 sec at 42 ^oC (“heat-shock”). After heating the tube was transferred on ice for a short time. Suspension of transformed cells was relocated to a pre-warmed (at 37 ^oC) tube with 500 µl of LB medium and incubated at 37 ^oC, 350 rpm for 40-60 min. Next, bacterial suspension from the tube was transferred on a Petri dish with respective antibiotic (ampicillin or kanamycin), spread over the dish with a sterilized spatula and grown at 37 ^oC for 16-18 h (overnight). On the next day bacterial clones were

screened (see bacterial colony screening) or used for plasmid DNA production.

3.2.1.7 Bacterial colony screening

In order to validate, whether an individual bacterial clone on agar plate contains properly assembled molecular construct, colonies were screened for the presence of a specific DNA sequence by PCR. A part of an individual bacterial clone was transferred into a tube with a mix (10µl) of OneTaq® Quick-Load® 2X Master Mix diluted twice with ddH_2O and containing 200 nM of each of both forward and reverse primers (final concentration). A PCR-program used for colony screening was following:

Table 3.17: *PCR-program used for bacterial colony screening.*

Step	Temperature, ^oC	Duration, sec	Process
1	95	180	DNA denaturation
2	95	15	
3	58-62	30	Primers annealing
4	68	30-180	Fragment amplification
5	68	60-120	

Steps 2-4 were repeated 21 times before reaching step 5. Four µl of each PCR-reaction mix were loaded on an agarose gel for PCR-product size analysis. Bacterial clones with length of PCR-product similar to the expected one were grown overnight for further plasmid DNA isolation and sequencing.

3.2.1.8 Plasmid DNA isolation from bacterial suspension

Single colony on a Petri dish was transferred to 4 ml (QIAprep Spin Miniprep Kit) or 100-150 ml (depending on the plasmid copy number, QIAGEN Plasmid Maxi Kit) LB-medium containing respective antibiotic (ampicillin – 100 µg/ml or kanamycin – 50 µg/ml), and were grown overnight (16-18 h) at 37 ^oC, 180 rpm. On the next day plasmid DNA was extracted from *E. coli* suspension using respective DNA extraction kit according to the manufacture's recommendations.

3.2.1.9 DNA digestion

PCR products and plasmids were cut using a pair of endonucleases in a suitable buffer. The reaction mix contained 1 µg DNA, 1 µl of each enzyme, 5 µl of 10x reaction buffer and ddH_2O up to 50 µl. Reaction was incubated for 1 h at 37 ^oC. Resulting DNA fragments were purified either using PCR purification kit

or DNA electrophoresis with following fragment excision from the gel and gel extraction kit, respectively.

3.2.1.10 DNA extraction from agarose gel

After DNA electrophoresis, in case of the presence of multiple DNA fragments in a sample, target fragments were excised from agarose gel. The excision process was monitored with UV Transilluminator in the low light intensity mode. DNA fragments were recovered from the gel segment with DNA-extraction kit in accordance to manufacture's recommendations. Concentration of extracted DNA fragments was determined with spectrophotometer.

3.2.1.11 DNA ligation

Ligation of preliminary digested DNA fragments was performed using T4 phage ligase. Insert and plasmid backbone were mixed using a molar ratio of 3:1. Reaction mix consisted of 2 μl of 10x DNA ligase buffer, 100 ng of plasmid backbone, respective amount of insert DNA, 1 μl of DNA ligase and ddH_2O up to 20 μl. Reaction mix was incubated for 16-18 h at 16 ^oC (overnight). On the next day DNA was purified from the reaction mix and used for transformation of bacterial cells.

3.2.1.12 DNA sequencing

In order to validate correctness of plasmids assembly purified plasmids were outsourced to Microsynth Seqlab GmbH for sequence determination.

3.2.2 Working with eukaryotic cells

All procedures with eukaryotic cell lines were fulfilled in sterile conditions of biosafety cabinet (BSC).

3.2.2.1 Thawing cells

A cryovial with 1 ml of frozen eukaryotic cells were thawed at 37 ^oC for several min, and suspension of cells was transferred to a 15 ml tube containing 10 ml of pre-warmed medium. The tube with cells was centrifuged for 5 min, 180 g (rcf), RT. Supernatant was discarded and a cell pellet was resuspended in 10 ml of fresh, pre-warmed medium. Suspension was transferred to a T-75 flask and then, to incubator for long-term cultivation. Thawed cells were passaged several times before starting any experiments.

3.2.2.2 HEK293 and HeLa cells cultivation

HEK293 cell line, its genetically modified derivatives and HeLa cells were grown in DMEM-medium with FBS 10% at 37 °C with 5% CO_2. Original HEK293, derived HEK293 cell lines stably expressing DAO (produced in the current study), HEK293TN and HeLa cells were regularly split 1:3, 1:2-3, 1:10 and 1:4 every 3-4 days using trypsin solution for cell detachment, respectively. All cell lines were regularly checked for mycoplasma contamination according to the manufacturer's protocol.

3.2.2.3 Melanoma cell lines cultivation

Melanoma cell lines (1205Lu, WM3734 and WM88) and their genetically modified derivatives were grown in Tu 2% medium at 37 °C with 5% CO_2. WM3734, 1205Lu and WM88 and corresponding derived stable cell lines were split every 3-4 days 1:3-4, 1:4-5 and 1:3-4, respectively. All cell lines were regularly checked for mycoplasma contamination according to the manufacturer's protocol.

3.2.2.4 Transfection of eukaryotic cells

Transfection of eukaryotic cells with plasmids was performed using FuGENE-HD in accordance to the manufacture's recommendations.

Day 1. Cells in 2 ml of medium were seeded in a well of 6-well plate.

Day 2. To 100 µl of Opti-MEM medium were added 1 µg of plasmid DNA and 3 µl of FuGENE-HD. Derived solution was thoroughly mixed and added to cells. Transfected cells were cultivated in an incubator for 6 h with the transfection mix and then medium was changed for fresh one.

3.2.2.5 Determination of puromycin concentration

Puromycin concentration required for killing of all non-infected HEK293 and melanoma cells in 48 h was empirically determined. One day before addition of puromycin, original HEK293 and melanoma cells were seeded in six wells of a 6-well plate. On the next day, cells in each well were treated with puromycin of different concentrations: 0.5, 1.0, 1.5, 2.0, 2.5 and 3.0 µg/ml. Cells were observed for 2 days and the minimal puromycin concentration required for killing all cells in a well was determined as 1 and 2 µg/ml for HEK293 and melanoma cell lines (1205Lu, WM3734 and WM88), respectively.

3.2.2.6 Production of lentiviruses and stable cell lines

Day 1. 10^6 HEK293TN cells in 3 ml of DMEM-medium containing 10% FCS were seeded in wells of a 6-well plate. Cells were transferred to an incubator and cultivated for several hours. Next, the plate was transported to S2 lab and all further steps of the procedure were done there.

Day 2. To 300 μl of Opti-MEM medium were added 3 plasmids required for lentiviral production – 2 μg of packaging plasmid (pCMV-dR8.91), 0.6 μg of envelope plasmid (pMD2.G) and 2.5 μg of transfer plasmid (pLVX-Puro with gene of interest). Required amounts of plasmids were calculated based on 1:1:1 molar ratio. Then, 15 μl of FuGENE-HD were also added to the mixture and the derived solution was added to HEK293TN cells.

Day 3 (24h after transfection). Cell medium, containing viruses was changed for 3 ml of fresh one. Meanwhile, HEK293/melanoma cells were seeded in wells of a 6-well plate for upcoming infection. An additional (control) well was seeded with the same amount of cells in order to estimate completeness of puromycin selection.

Day 4 (48h after transfection). Medium from each well with HEK293TN cells was collected and filtered through 0.45 μm pore size filter attached to a 5 ml syringe. The plate with HEK293TN cells was discarded. Polybrene was added to 1 ml of collected medium containing virus in a concentration of 16 μg/ml. Medium of HEK293/melanoma cells was replaced with the virus-polybrene containing medium, which was overlaid with 1 ml of fresh cell medium to dilute virus-polybrene twice (final concentration of polybrene – 8 μg/ml). In the control well medium was also changed for fresh one. Remaining volume of virus-containing medium was frozen at -80 ^{o}C.

Day 5. Virus-containing medium was removed and new fresh medium was added.

Day 6. Medium from all wells (including control) was removed and fresh medium containing 1 or 2 μg/ml puromycin was added to select cells successfully infected with the virus. Cells were incubated with puromycin (antibiotic was in cell medium) until there were no cells in a control well (2-3 days). Before transferring cells out of the S2 lab, cells were washed 3 times with PBS to remove all remaining virus.

Fluorescence of survived (selected) cells was examined with AxioObserver D1. Successfully selected cells were further expanded and frozen.

3.2.2.7 Monoclonal selection of stable cell lines

Stable HEK293 cell lines (expressing HyPer-DAO-NES and HyPer-DAO-3NLS) after production were further selected in order to produce monoclonal cell lines. Monoclonal selection was performed using cloning cylinders.

HEK293 cells were detached with trypsin solution, counted, diluted with DMEM medium to around 50 cells in 10 ml and were seeded on a 10 cm Petri dish. For each stable cell line several dishes with the same amount of cells were seeded. Cells were grown in an incubator for several days. In 2-3 days, dishes were examined for single cells located far enough from other cells on the same dish. Those cells were marked as potential candidates, and dishes were incubated for additional several weeks. During incubation medium in dishes was regularly checked for contamination and replaced (once in several days) for fresh one. Marked colonies were also examined for fluorescence intensity with AxioObserver D1.

When colonies reached hundreds of cells, medium from the dish was removed thoroughly, and cloning cylinders were set around selected colonies using sterilized glue. To each chamber formed by a cylinder 0.2 ml of trypsin solution was added. Detached cells from an individual colony were transferred to a well of 48/24-well plate, expanded for several weeks, constantly transferring sufficiently confluent cells to a tissue culture plastic with a larger surface, and finally frozen.

3.2.2.8 Freezing cells

Cells in culture T75-flasks at 70-80% confluency were trypsinized, counted and centrifuged for 5 min at 180 g, RT. Obtained cell pellet was resuspended in a proper volume of FBS supplemented with 10% DMSO to get 10^6 cells/ml. Derived cell suspension was aliquoted into cryovials and frozen at -80 ^{o}C in cell freezing container. Within 2 months, cryovials with frozen cells were relocated to liquid nitrogen for a long-term storage.

3.2.3 Crystal Violet Assay (CVA)

3.2.3.1 CVA procedure

Day 1. Cells were seeded in wells of a 24-well plate in the amount of $4 \cdot 10^4$ cells/well in the volume of 0.5 ml.

Day 2. To each well 0.5 ml of pre-warmed medium (with or without 2x D/L-Ala of selected concentrations) were added, and plates were thoroughly mixed. Zero time point plates were stained immediately afterwards.

Staining. From each well medium was removed and cells were washed with 1x PBS. Ice-cold methanol was added to each well of the plate in the amount of 0.3 ml/well and the plate was incubated at RT for 15 min with constant shaking for fixation of cells. Methanol was removed and cells were washed two times with 1x PBS. Crystal violet solution in the amount of 0.4 ml was added to each well of the plate and the plate was incubated at RT for 0.5 h with constant shaking. Staining solution was removed thoroughly and cells were washed twice with ddH_2O. The plate was dried overnight.

Day 3. Staining of 24 h time point plates as described above.

De-staining. Acetic acid (40%), 0.4 ml, was added to each well of dried zero time point plates, and plates were incubated at RT for 25 min with constant shaking. Derived solution (20 µl from a well) was mixed with 180 µl of ddH_2O in a well of a 96-well plate. For further background subtraction four wells were filled with 20 µl of acetic acid mixed with of 180 µl ddH_2O. Absorbance of derived mixtures was measured using a plate reader at 590 nm wavelength.

Day 4 and later. The procedure described above was performed analogously for plates corresponding to other time points.

3.2.3.2 CVA data analysis

Data analysis was performed using appropriate Python packages. Initially, background was subtracted and all values were normalized to the ones corresponding to zero time point. Shapiro-Wilk test was performed to validate the hypothesis that the data were normally distributed. Samples were compared in a pairwise manner using two-sided Mann-Whitney U test. The Bonferroni test was used for a multiple-comparison correction.

3.2.4 Fluorescence microscopy

3.2.4.1 Tracing the kinetic of HyPer's oxidation

Day 1. HEK293/melanoma cells expressing HyPer-DAO protein were seeded in 2 ml of culture medium (CM, DMEM supplemented with 10% FCS) on a glass coverslip in a well of a 6-well plate.

Day 2. *Incubation*. CM was thoroughly removed and cells were washed with 1x DPBS. Each coverslip with cells was set in a plastic ring-chamber, which was refilled with 0.9 ml of Experiment (HEK293 cells) or Imaging (melanoma cells) Medium. Next, cells were incubated for 45 min at 37 ^oC without CO_2.

Tracing of kinetic. Following incubation, baseline fluorescence of HyPer was recorded for 5 min, and then, D-Ala (0.1 ml, 10x solution) was added to cells. Imaging was performed using Zeiss AxioObserver Z1 microscope equipped with Zeiss «Fluar» 40×/1.3 Oil M27 objective, Zeiss Axiocam 702 mono camera and

Colibri LED light source. Images were obtained every 15 (melanoma) or 30 (HEK293) sec by sequential excitation of HyPer with light of two wavelengths – 420 and 505 nm via 420/40 and 500/15 band-pass excitation filters, respectively, and collection of emission light from HyPer via 538/40 barrier (emission) filter. A custom filter cube with installed dichroic mirror (beamsplitter) 509 was used.

3.2.4.2 Image Acquisition

Images of eukaryotic cells expressing fluorescent proteins were acquired using the same Zeiss AxioObserver Z1 setup mentioned in the previous section. In addition to 40×/1.3 Oil, other objectives: Zeiss "Fluar" 10x/0.50 and α Plan-Fluar 100x/1.45 Oil M27 were used for image acquisition. Images of HEK293 cell line expressing TagBFP-DAO-KDEL were obtained by excitation of cells with 400 nm wavelength light and usage of another filter cube (band-pass excitation filter: 400/40, dichroic mirror 458, band-pass emission filter: 483/32). Images of cells expressing HyPer and iNaps were acquired with the same filter cube used for tracing HyPer's kinetic oxidation and described in the previous section. Coloured images of cells represent the result of applying pseudocolours to black and white original images.

3.2.4.3 Data analysis

Analysis of HyPer's oxidation kinetic was performed using Fiji (ImageJ). Files were opened with «split channels» option. Type of images in both stacks of images (corresponding to emission of HyPer upon excitation with the light of 420 and 505 nm wavelength) were changed from 8-bit to 32-bit. Background of images was subtracted using rolling ball algorithm and threshold was adjusted. A stack of images that were acquired by excitation of cells with the light of 505 nm wavelength was divided frame-by-frame by respective images of the 2nd stack acquired by the excitation of cells with the light of 400 nm wavelength. Cells were selected manually on images of the derived «ratio» stack as regions of interest (ROIs). Mean intensities of pixel within each ROI were exported as .xlsx files.

Further analysis of derived .xlsx files was fulfilled in Python 3.8 (Jupyter Notebook, anaconda 3) with respective packages. Mean of ratio values corresponding to first 5 min in a time series (baseline fluorescence of HyPer before addition of D-Ala) (R_0) was calculated. Then ratio values at each time point in the derived time series were divided by respective baseline mean value (R_0) in order to normalize HyPer's ratio (R/R_0).

3.2.5 Thermal Proteome Profiling (TPP)

3.2.5.1 TPP experiment procedure

(Performed with the help of Isabelle Becher, Savitski Team, EMBL, Heidelberg, Germany)

Thermal Proteome Profiling (TPP) is high-throughput method based on Mass-Spectrometry (MS) for detection of protein stability changes in response to various alterations, such as post-translational modifications, protein complex formation/dissociation, (un)binding of low-molecular weight compounds etc., (Becher et al., 2016; Savitski et al., 2014).

In the present study TPP was performed with the original, wild type (wt) HEK293 cells and stable HEK293 cell lines expressing TagBFP-DAO-KDEL (ER), HyPer-DAO-3NLS (nuclei) and HyPer-DAO-NES (cyto).

Day 1. *Seeding of cells*. 15 cm dishes were seeded with HEK293 cells in 30 ml of culture medium (CM, DMEM supplemented with 10% FCS) to have dishes with 60-70% confluency on the day of experiment (Day 2). In total eight dishes were seeded (four cell lines, two dishes/cell line) for each biological replicate.

Table 3.18: *Scheme of HEK293 cells treatment with D-Ala in TPP experiment.*

Dish	Cell line	D-Ala, mM
1	wt	2 mM (+)
2	wt	–
3	ER	8 mM (+)
4	ER	–
5	nuclei	2 mM (+)
6	nuclei	–
7	cyto	2 mM (+)
8	cyto	–

Day 2. *Treatment of cells*. Cell medium was changed for 15 ml of experiment medium (EM, 1x DPBS with Mg^{2+}/Ca^{2+}/glucose) and dishes were incubated for 45 min at 37 ºC without CO_2. Next, medium from one dish of each cell line was changed for 15 ml EM supplemented with 2 mM (wt/nuclei/cyto) or 8 mM (ER) D-Alanine. Medium of remaining four dishes was replaced with EM without D-Ala. In these media cells were incubated for 10 min at 37 ºC without CO_2. From each dish EM was collected to an individual 50 ml tube, and cells were treated with 3 ml trypsin solution (+/– D-Ala) for 3 min at 37 ºC. Trypsinization was stopped with 7 ml of CM (+/– D-Ala), and cells were transferred to the same 50 ml tubes. Dishes were rinsed with additional 10 ml of EM (+/– D-Ala), and remaining cells in EM were collected to the same 50 ml tubes. Cells were counted

with TC20 automated cell counter and following centrifugation were resuspended in a volume of EM (+/– D-Ala) to have $5 \cdot 10^6$ cells/ml.

Heat treatment. Ten aliquots of each cell suspension (0.1 ml) were transferred into 0.25 ml 96-well PCR-plate (Eppendorf). Plates were centrifuged for 2 min at 390 g, RT. A fraction of supernatant volume (80 µl) from each well of PCR-plate was removed with liquidator 96 and, and cell pellets were resuspended in remaining volume of supernatant using multi-channel pipette. Plates were sealed with aluminium foil and treated with temperature gradient (ten temperature points) using thermal cycler for 3 min. Plates were incubated for additional 3 min at RT.

	1	2	3	4	5	6	7	8	9	10
T, ºC	37.0	40.4	44.0	46.9	49.8	52.9	56.5	58.6	62.0	66.3

Cell lysis and filtration. All steps were performed on ice or at low temperature. To each well of a plate 30 µl of cold lysis buffer were added, and content of wells were resuspended using a multi-channel pipette. The plate was sealed and incubated on a shaker for 1 h at 4 ºC and 500 rpm. Wells of a 0.45 µm 96-well filter plate were pre-wet with 50 µl of lysis buffer (Table 3.8). The filter plate was centrifuged for 2 min at 1200 rpm to dry filters. The plate with samples was also centrifuged for 3 min at 2000 rpm at 4 ºC. Supernatant from samples (40 µl) was transferred to wells of the filter plate, the filter plate was centrifuged for 5 min at 500 g and 4 ºC and filtered supernatant was collected in standard 96-well plate.

Mass Spectrometry (MS) preparation. Protein concentration of samples treated with the two lowest temperatures (37.0 and 40.4) was measured with BCA assay kit, and the sample volumes containing 10 µg of protein were used for MS analysis. Samples treated with higher temperatures were used for MS analysis in the same volume (mean volume of the two samples treated with two lowest temperatures).

3.2.5.2 Sample preparation and LC-MS/MS measurement

(Performed by Isabelle Becher, Savitski Team, EMBL, Heidelberg, Germany)

The procedure was performed according to the «LC-MS/MS measurement» section described in (Becher et al., 2018) with minor modifications. Protein samples were treated similarly to the described procedure using modified SP3 protocol (Hughes et al., 2014; Mateus, Kurzawa, et al., 2020). Peptides were labelled with TMTpro (Thermo Scientific) according to the scheme below (Table

3.19). Labelled samples (four cell lines treated with or without D-Ala) corresponding to one pair of temperatures (16 samples in total) were mixed and fractioned, resulting twelve fractions (Hughes et al., 2014).

Peptides were separated using the same LC system and settings as described in the respective method section (Becher et al., 2018). The LC system was connected to the same Q Exactive™ Plus mass spectrometer (Thermo Scientific) and mass spectrometry was performed according to the described procedure with the normalized collision energy equal to 30.

Table 3.19: *Scheme of TMT-multiplexing for the described 2D-TPP procedure.*

	1	2	3	4	5	6	7	8	9	10	11	12	13	14	15	16
TMT	126	127L	127H	128L	128H	129L	129H	130L	130H	131L	131H	132L	132H	133L	133H	134L
cell line	wt		cyto		nuclei		ER		wt		cyto		nuclei		ER	
D-Ala	–	+	–	+	–	+	–	+	–	+	–	+	–	+	–	+
T, °C	37.0								40.4							
	44.0								46.9							
	49.8								52.9							
	56.5								58.6							
	62.0								66.3							

3.2.5.3 Analysis of TPP data

(Performed by Frank Stein, Savitski Team, EMBL, Heidelberg, Germany)

TPP data analysis, such as processing of raw MS data and cluster analysis, was performed by Frank Stein, Savitski's lab, Heidelberg, Germany. Protein identification and quantification was performed using both the IsobarQuant (Franken et al., 2015) and Mascot search engine. TrEMBL human proteome was used as a reference database. Only proteins, which were quantified with two unique peptide matches and in at least 2/3 of the replicates, were kept for the analysis. Batch effect was removed by corresponding function of LIMMA package (Ritchie et al., 2015). Finally, vsn normalization (Huber et al., 2002) was applied to $\log_2$ of raw quantity values. Normalization coefficients were estimated for each temperature separately.

Stability and abundance scores were calculated as previously described (Mateus, Hevler, et al., 2020). Stability change (score) for a protein in a cell line was calculated by the equation:

$$S = \sum_{T_1}^{T_{10}} \left(\log_2 \frac{E_T}{C_T} - A \right), \qquad (1)$$

where E_T and C_T – raw protein quantities in +D-Ala (E) and -D-Ala (C) conditions measured for temperature T; A – abundance change (score) for the protein in the cell line. A was calculated by the equation:

$$A = \frac{1}{2} \left(\log_2 \frac{E_{T_1}}{C_{T_1}} + \log_2 \frac{E_{T_2}}{C_{T_2}} \right), \qquad (2)$$

where T_1 and T_2 represent first two temperatures of the range – 37.0 and 40.4 °C, respectively. After calculation these values were normalized to *Z(0,1)* and feed to lmFit. LIMMA test was performed for statistical estimation of stability and abundance Z-scores reflecting difference between +D-Ala and –D-Ala conditions for every cell line. Estimated *t* values were further evaluated with fdrtool to obtain false discovery rates (q-values) (Strimmer, 2008).

According to performed statistical analysis proteins were classified as 'hits' (q-value < 1% and |Z-score| > 3), 'candidates' (q-value < 5% and |Z-score| > 2), and 'no hits' (others).

Hits and candidates were then clustered according to their behaviour under oxidative conditions. For every protein the following vector was built:

$$[{}^{c}S,\ {}^{n}S,\ {}^{e}S,\ {}^{w}S,\ {}^{c}A,\ {}^{n}A,\ {}^{e}A,\ {}^{w}A],$$

where superscript indicate cell line (c – cyto, n – nuclei, w – wt, e – ER), S – stability change Z-score, A – abundance change Z-score. We then performed clustering of these vectors with K-means method using Euclidean distance. Optimal number of clusters (9) was determined with the elbow method.

Figures in the TPP section (4.9) were prepared by the author of the thesis if not stated otherwise.

3.2.5.4 Gene ontology enrichment analysis

(Performed with Alexey Nesterenko, FCBRN, Moscow, Russia)

Gene ontology enrichment analysis (GOEA) was performed using python *goatools* instrument (Klopfenstein et al., 2018). Basic ontology (*go-basic.obo*) from https://geneontology.org (Ashburner et al., 2000; Carbon et al., 2021) was used as an ontology graph, and *goa_human.gaf* was used for mapping, respectively. *goatools* utilizes Fischer exact test for estimating p-value of term

enrichment and uses Benjamini-Hochberg correction to deal with multiple hypothesis. Total protein list identified in TPP proteomics was used as a background list. Overrepresentation and q-values calculated with *goatools* were used for plotting Figures 4.23 and 4.25. Redundancy of overrepresented GO terms was removed using Revigo (Supek et al., 2011).

GOEA was performed by AN, while GO redunduncy removal and figures preparation by the author of the thesis.

3.2.6 Co-immunoprecipitation experiment

3.2.6.1 PEI transfection

Day 1. HEK293 cells were seeded in 15 cm tissue culture dishes at 60% confluency in 29 ml of DMEM medium with 10% FCS and Pen/Strep.

Day 2. To 1 ml of OptiMEM 4.26 pmol of plasmid DNA (15-20 μg) and 5x μg PEI (DNA (μg): PEI (μg) – 1:5) were added sequentially. Derived solution was mixed by tapping and incubated for 10 min at RT and then was added to a dish with cells. Medium was replaced with 20 ml of fresh one in 4 h. Cells were incubated for 24 h after transfection before starting further experiments.

Optimization of PEI transfection was performed similarly. For the optimization wt HEK293 were seeded in 2 ml of medium in wells of a 6-well plate. For the transfection certain amounts of pASIET-EGFP plasmid and respective amounts of PEI were mixed in OptiMEM and the mixture was added to cells. Transfection efficiency and toxicity were estimated in 24 h after transfection.

3.2.6.2 Co-immunoprecipitation procedure

Day 1. Five 15 cm dishes were seeded with HEK293 cells (2 × wt, 3 × cyto) according to the details stated in PEI transfection section.

Day 2. Four dishes (2 × wt and 2 × cyto) were transfected with pcDNA3.1 plasmid encoding one of FLAG-tagged proteins of interest (POIs) and one (cyto) with empty plasmid (control) using PEI (Table 3.20).

Day 4. *Treatment of cells with D-Ala*. Medium from dishes was removed, cells were washed with 10 ml of 1x DPBS, and 15 ml of prewarmed EM (no D-Ala) were added to cells. Dishes were incubated for 45 min at 37 ^{o}C without CO_2. EM was replaced with 15 ml of EM with 2 mM (dishes 1, 3 and 4) or without D-Ala (dishes 2 and 5). Dishes were incubated for 10 min at 37 ^{o}C without CO_2. Further similarly, if cells were treated differently with D-Ala, medium for dishes

1, 3 and 4 contained 2 mM D-Ala, while for 2, 5 dishes – did not. Medium from each dish was transferred to an individual 50 ml empty tube. Still attached cells were trypsinized with 3 ml of trypsin with/without D-Ala for 3 min at 37 ºC and trypsinization was stopped by addition of 7 ml of CM (culture medium) with/without D-Ala. Medium with cells was transferred to the same 50 ml tubes containing EM. 1× DPBS (10 ml, with/without D-ala) was added to dishes to collect cells completely and was transferred to the same 50 ml tubes containing detached cells. 50 ml tubes were centrifuged for 15 min at 100 g and 4 ºC, and supernatant was thoroughly removed.

Cell lysis. Lysis Buffer 1 (0.5 ml) was added to each of collected cell pellets. Cells were resuspended by pipetting. Suspensions were incubated on an orbital rotator for 1 h at 4 °C. Resin for Co-IP was prepared during incubation. Lysates were centrifuged for 15 min at 4 ºC and 15000 g.

Table 3.20: *Treatment scheme of cell dishes prior to co-immunoprecipitation experiment.*

dish	Cell line	POI expressed	D-alanine added
1	cyto	+	+
2	cyto	+	–
3	cyto	–	+
4	wt	+	+
5	wt	+	–

Resin Preparation. Resin was thoroughly resuspended by gentle inversion. Resin (100 µl of suspension/reaction) was aliquoted into 7 (5 dishes and positive/negative Co-IP controls) tubes (2.0 ml). Magnetic beads were collected and storage buffer was discarded. Beads were washed twice with 0.25 ml of Lysis Buffer 3.

Co-IP. Cell lysates from previous step were added to washed beads. Lysis buffer 4 (0.5 ml) and 3 µl of 2 µg/µl of BAP-FLAG fusion protein (6 µg) were added to resin (positive Co-IP control). Lysis Buffer 4 (0.5 ml) with no protein was added to another tube (negative Co-IP control). Tubes were incubated for 1 h at 4 ºC using orbital rotator. Beads were collected with magnetic separator and supernatant was thoroughly removed. Beads were washed three times by addition of Lysis Buffer 4 (0.35 ml). After addition of the 3rd volume of Lysis Buffer 4 beads were transferred to a new 2 ml tube and collected by magnet. Washing solution was thoroughly removed. Proteins bound to beads were eluted with FLAG-peptide solution (0.1 ml). Samples were incubated by gently shaking for 0.5 h at 4 ºC. Then, beads were discarded and eluates were collected and stored for a long-term storage at -20 °C.

3.2.6.3 SDS-PAGE

SDS-PAGE (Sodium dodecyl sulphate polyacrylamide gel electrophoresis) is a method capable of separating protein mixtures in polyacrylamide gel by molecular weight in an electric field.

Gels consisted of two parts: top – stacking and low – separation gels. Eluates (16.5 µl each) derived from Co-IP experiment were mixed with 4x loading buffer (5.5 µl), heated for 5 min at 95 ^{o}C and loaded into individual wells of the stacking gel. Gel was set in an inner electrophoresis chamber, which as well as an external chamber was filled with running buffer. SDS-PAGE was performed for around 1 h at 100-150 V.

3.2.6.4 Western Blot

Transfer. Six pieces of thick (0.8 mm) Whatman paper and PVDF-membrane of the same size as separating gel were prepared. PVDF-membrane was pretreated by soaking in 100% MeOH for 1-2 min. Then, pieces of paper, membrane and separating part of gel were transferred into ice-cold transfer buffer for 3-5 min. Sandwich was assembled in the centre of the bottom side of the Trans-Blot Turbo system cassette (anode) in the following order (from the bottom to the top): 1) bottom ion reservoir stack (3 paper pieces), 2) membrane, 3) gel and 4) top ion reservoir stack (3 paper pieces). Any air bubbles between layers should be removed. Cassette was closed with the lid (cathode) and inserted into Trans-Blot Turbo system. Transfer was performed in semi-dry conditions. The following program settings were used: -25 V, 1.3 A, 7 or 10-12 min for transferring of FLAG-tagged proteins < and > 70kDa, respectively.

Staining. Following transfer the sandwich was disassembled, the gel was stained (see staining of polyacrylamide gel section), the membrane was rinsed with ddH_2O and immersed in blocking solution (5 ml) for 1 h or overnight on a shaking platform. Blocking solution was changed for a new one (5 ml) and primary antibody (5 µl, anti-FLAG) were directly added to the solution. Membrane was stained with antibodies for 1 h on a shaking platform. Membrane was washed out of non-bound antibodies in TBST (5 ml) three times for 2 min each. Membrane was immersed into the new potion of blocking solution (5 ml) containing secondary antibodies (1 µl, anti-mouse) and incubated for additional 1 h on a shaking platform. The membrane was again incubated in TBST (5 ml) three times for 2 min each.

Protein detection. Reagent 1 (peroxide solution, 0.5 ml) and reagent 2 (luminol enhancer solution, 0.5 ml) of Pierce™ ECL Western Blotting Substrate kit were mixed and added to the membrane (secondary antibodies were HRP-

conjugated). The membrane was incubated for 1 min before imaging at RT, and images were acquired using ChemiDoc XRS+ System (BioRad).

3.2.6.5 Staining of polyacrylamide gel

Following the transfer of proteins from a polyacrylamide gel to a membrane, gel with remaining proteins (due to incompleteness of transfer) was incubated in Instant Blue for 20-40 min on a shaking platform. When protein bands became visible, the gel was destained in water until background became transparent.

3.2.6.6 Sample preparation and LC-MS/MS measurement

(Performed by Didier Vertommen in UC Louvain, Brussels)

Protein samples (eluates from Co-IP step) were precipitated with acetone, resuspended in 50 mM NH_4HCO_3 by sonication and digested overnight with trypsin/Lys-C at 37 °C (Promega, MS grade). The reaction was stopped with 0.1% (v/v) TFA (Trifluoroacetic acid).

The following steps were performed according to the procedure described previously in the section «2.18. Mass spectrometry and statistic analysis» with minor modifications (Luo et al., 2021). Peptide peaks above threshold in MS survey were dynamically excluded for 40.0 s. MS scans were in m/z range from 350 to 1800. Top N peptide precursors were subjected for MS/MS and fragmented in HCD using normalized collision energy (NCE) at 30%. Automatic gain control (AGC) was set at $4x10^5$ and a maximum injection time (MaxIT) at 100 ms.

3.2.6.7 Processing of raw Co-IP data

(Performed by Alexey Nesterenko, FCBRN, Moscow, Russia)

Raw instrument data (*.raw) was converted into open *mzML* format using ThermoRawFileParser (Hulstaert et al., 2020) accessed through docker image: caetera/thermorawfileparser. TrEMBL (unreviewed) human proteome (UP000005640) was used for database construction. Using Philosopher (da Veiga Leprevost et al., 2020) we also added standard contaminants to the database. HyPer-DAO and all four FLAG-tagged proteins were added to the database as well. Proteomics search was performed with MSFragger-3.3 (Kong et al., 2017) using precursor mass tolerance of 12 ppm and fragment mass tolerance of 0.3 Da allowing maximum 3 missed cleavages with additional mass calibration and deisotoping turned on. Three variable modifications were allowed: N-terminus acetylation, methionine oxidation and cysteine oxidation (to sulfenic acid).

Initial statistical refinement and target-decoy analysis of peptide matches was performed with peptideProphet-5.2.1 (as a part of Philosopher toolbox) for every MS run (with following parameters: "--expectscore --accmass --ppm --decoyprobs –nonparam"). Statistical validation of protein identification was performed with proteinProphet-5.2.1 (as a part of Philosopher toolbox) for all spectra at once (with parameter: "--maxppmdiff 2000000"). Finally, we used Philosopher's filter for multi-level FDR estimation for every MS run (with following par-s: "--sequential –-razor --mapmods"). At the last step we performed ionQuant-1.5.5 (Yu et al., 2021) for all the data with match-between-runs option turned on ("--mbr 1 --minexps 1"). As a result, we obtain quantification results at every level (psm, ion, peptide, protein).

3.2.6.8 Analysis of Co-IP/MS data

(Performed with Alexey Nesterenko, FCBRN, Moscow, Russia)

Protein "razor" intensities were extracted for further work. After log-transformation we normalized datasets to zero mean and equal dispersion using preprocessing StandardScaler of scikit-learn library. Then dataset was filtered for proteins having less than 4 missing values in a row; the rest missed values were imputed with normally distributed (σ=0.2) random numbers. By this way we implemented "missing not at random" (MNAR) strategy (Karpievitch et al., 2012).

Mixed-effects regression was performed to analyse an influence of two factors on the protein level: the presence of FLAG-tagged protein (protein of interest, POI) in the sample and exposure of cells to oxidative stress. We used the following model:

$$V_{ox,poi,id} = \beta + \alpha_{id} + p \cdot R^{id}_{poi} + o \cdot R^{id}_{ox} + \varepsilon,$$

where *id* – protein identifier, *p* – logical factor of POI presence, *o* – logical factor of oxidative stress presence, V – $\log_2$-quantity of the protein, β – intercept depending on conditions ("batch" intercept), R^{id}_{poi} – regression coefficients reflecting whether the protein co-precipitate with POI, R^{id}_{ox} – regression coefficient reflecting protein's binding to beads under oxidative stress, α_{id} – random intercept distributed normally among all proteins, ε – random noise with zero mean and diagonal covariance matrix (standard for linear models).

We applied this model to every Co-IP experiment using lme4 package (Bates et al., 2015). From obtained T-statistic values of every regression coefficient, we calculated adjusted p-value using fdrtool package. We considered the value confident if its regression coefficient was positive and q-value < 0.05.

We used another model to find proteins changing their (non-specific) binding to anti-FLAG beads under oxidative conditions. In this case, we used the united dataset including all four Co-IP experiments and filtered proteins having more than 6 missed values in all conditions in all experiments. A simpler model was used:

$$V_{ox,exp,id} = \beta + \alpha_{id,exp} + o \cdot R_{ox}^{id} + \varepsilon,$$

where V, id, β, ε, o – have the same meanings; R_{ox}^{id} – regression coefficient for the protein reflecting its binding to beads under oxidative stress; $\alpha_{id,exp}$ – random intercept distributed normally over proteins and POI experiments. Proteins, which demonstrated confident link to oxidative conditions in the last model were considered as non-specific hits in Co-IP experiment.

Data postprocessing required for figures plotting and the preparation of figures were performed by the author of the thesis if not stated otherwise.

4 Results

4.1 Cloning of plasmids encoding HyPer-DAO and iNap-DAAD

Importance of redox signalling for the cell and particular cellular organelles prompted us to establish cell lines expressing protein systems, which would allow to locally manipulate H_2O_2 and NADPH levels in various cellular compartments and to simultaneously monitor evoked alterations. For this purpose, we constructed several plasmids encoding HyPer-DAO and iNap-DAAD proteins, respectively (Figures 4.1 and 4.2).

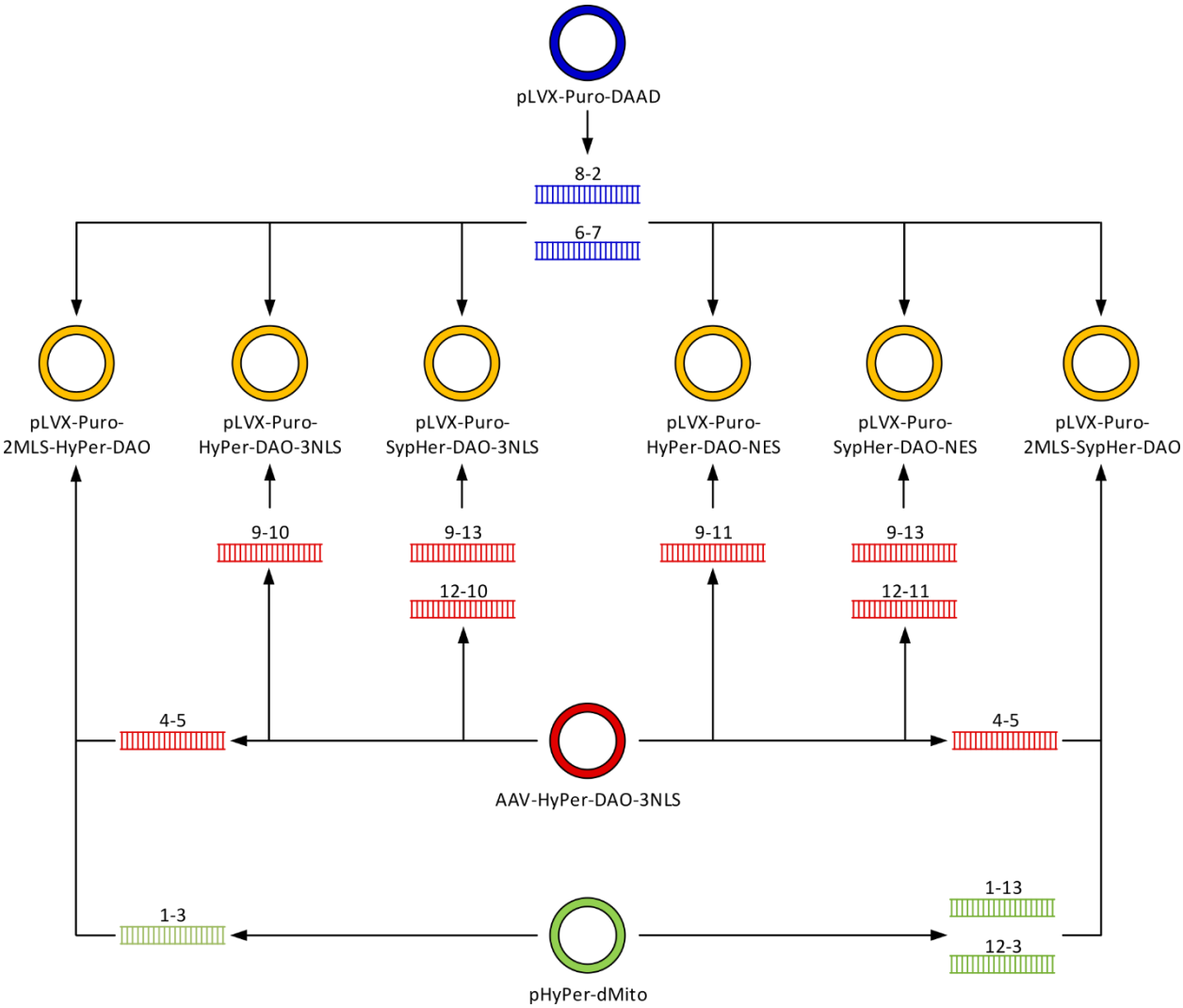

Figure 4.1: *The scheme for cloning of plasmids encoding HyPer/SypHer-DAO proteins fused to signals for localization in the mitochondrial matrix, the nucleus and the cytosol. Coloured circles represent plasmids, where blue, green and red circles display original plasmids and yellow – derived ones. Rectangles indicate PCR-products amplified from a respective plasmid (of the same colour). Numbers above rectangles denote pairs of forward and reverse primers (delimited with «-»), which were utilized for the amplification of PCR-products. Plasmids from required PCR-products were assembled according to the AQUA-cloning method. MLS –*

mitochondrial localization signal (from Homo sapiens cytochrome c oxidase subunit 8A, COX8A), NES – nuclear export signal, NLS – nuclear localization signal of SV40.

HyPer-DAO fusion protein has been successfully used previously and thus we did not change the arrangement of this system (Matlashov et al., 2014). Meanwhile, since iNap-DAAD system was not established before, and considering that iNaps and DAAD are dimer proteins, we decided to separate iNap and DAAD sequences in plasmids by a sequence encoding self-cleaving P2A peptide (Akita et al., 2012; Akita et al., 2015; Tao et al., 2017). In addition, due to the C-terminal tail of meso-diaminopimelate dehydrogenase (DAPD) from *Ureibacillus thermosphaericus*, which DAAD was derived from by site-directed mutagenesis, extends towards the corresponding region of the other subunit of the homodimer, we placed all auxiliary protein tags on the N-terminus of the DAAD (Akita at al., 2012; Akita et al., 2015). These tags were required for protein targeting to a specific cellular compartment (localization signals) or were intended for the validation of proper cellular localization of DAAD (FLAG-tag). FLAG-tag was not required for DAO, since compared to DAAD, DAO was fused with HyPer and hence its localization was possible to verify using fluorescence microscope. Despite proteins of iNap-DAAD system were separate, nevertheless, they were co-expressed within the same cellular compartment due to the presence of the same localization signals on both proteins.

In total, six plasmids encoding HyPer/SypHer-DAO proteins fused to sequences for targeting of proteins to the mitochondrial matrix, the nucleus and the cytosol were assembled to study effects of local alterations of H_2O_2 level in these cellular compartments on melanoma cells (Figure 4.1). We focused on these three compartments, since ROS production in them is known to notably contribute to progression of cancer and melanoma particularly. The respective plasmids encoding SypHer-DAO were assembled to be able to distinguish if response of HyPer is induced by alterations of H_2O_2 or pH level upon DAO stimulation, when it was necessary. HyPer/SypHer-DAO plasmids, which we assembled are: 1) pLVX-Puro-2MLS-HyPer-DAO, 2) pLVX-Puro-2MLS-SypHer-DAO, 3) pLVX-Puro-HyPer-DAO-3NLS, 4) pLVX-Puro-SypHer-DAO-3NLS, 5) pLVX-Puro-HyPer-DAO-NES and 6) pLVX-Puro-SypHer-DAO-NES. pLVX-Puro represents a lentivirus transfer vector and was chosen as a plasmid backbone for our constructs in order to directly produce lentiviruses and then stable melanoma cell lines with the generated plasmids. All plasmids were assembled via enzyme-free AQUA-cloning method according to the respective section in the method part (Beyer et al., 2015). Initially all required DNA-fragments for each of the six plasmids were amplified from three matrices: pLVX-Puro-DAAD, AAV-HyPer-DAO-3NLS and pHyPer-dMito (Figure 4.1). Plasmid backbone of pLVX-Puro-DAAD, the same for all six plasmids, was too long to amplify as one PCR-

product, therefore its sequence was derived using two pairs of primers: 8-2 and 6-7, and hence as two DNA fragments. Other DNA fragments encoding two mitochondrial localization signals (2MLS) and initial part of HyPer/SypHer and required for assembly of first two plasmids (mitochondrial versions of HyPer/SypHer-DAO) were derived from pHyPer-dMito plasmid using 1-3 for HyPer and 1-13, 12-3 for SypHer (two DNA fragments were needed for introduction of the inactivation mutation C121S in HyPer and its conversion into SypHer) pairs of primers, respectively. The last matrix plasmid, AAV-HyPer-DAO-3NLS, was amplified with 4-5 pairs of primers for mitochondrial, 9-10 and 9-13, 12-10 for nuclear, and 9-11 and 9-13, 12-11 for cytosolic versions of HyPer-DAO and SypHer-DAO, respectively. Derived DNA fragments required for an assembly of a plasmid were mixed and used for bacteria transformation. Number of different fragments required for plasmid assembly depended on a particular plasmid and varied from 3 to 5.

Next we assembled plasmids encoding iNap-DAAD system (Figure 4.2). Analogous to HyPer-DAO constructs, we assembled six iNap-DAAD plasmids in total, three of which contained iNap1 or iNap3 sequences and the remaining three – pH-control, iNapc (iNap probes are also pH-sensitive). iNap-DAAD proteins encoded by these plasmids were targeted to the same three cellular compartments, namely: the mitochondrial matrix, the nucleus and the cytosol. Since it was shown that in HeLa cells NADPH level in these three compartments significantly differs, we targeted iNap1 sensor version with higher affinity to NADPH to the nucleus and the cytosol and iNap3 version characterized with less affinity to NADPH to the mitochondrial matrix, wherein NADPH level was estimated to be an order of magnitude higher than in the nucleus or the cytosol (Tao et al., 2017). The strategy of separate expression of proteins entailed a more complex structure of iNap-DAAD plasmids compared to HyPer-DAO plasmids, due to the necessity for additional tags in front of DAAD sequences, thus we used commercially synthesized DNA fragments, G-blocks, in order to assemble these plasmids.

Six iNap-DAAD constructs: 1) pLVX-Puro-2MLS-iNap3-P2A-3MLS-FLAG-DAAD, 2) pLVX-Puro-2MLS-iNapc-P2A-3MLS-FLAG-DAAD, 3) pLVX-Puro-2NLS-iNap1-P2A-3NLS-FLAG-DAAD, 4) pLVX-Puro-2NLS-iNapc-P2A-3NLS-FLAG-DAAD, 5) pLVX-Puro-NES-iNap1-P2A-NES-FLAG-DAAD and 6) pLVX-Puro-NES-iNapc-P2A-NES-FLAG-DAAD were assembled according to the scheme (Figure 4.2). Required DNA fragments for mitochondrial versions of plasmids (1 and 2) were derived by PCR from pRDNA3.1-hygro-tdCox8-iNap3 and pRDNA3.1-hygro-tdCox8-iNapc with the 38-60, and from the G-Block, P2A-3MLS-FLAG-DAAD, with 59-58 pairs of primers, respectively. Fragments for the nuclear versions – from pRDNA3.1-

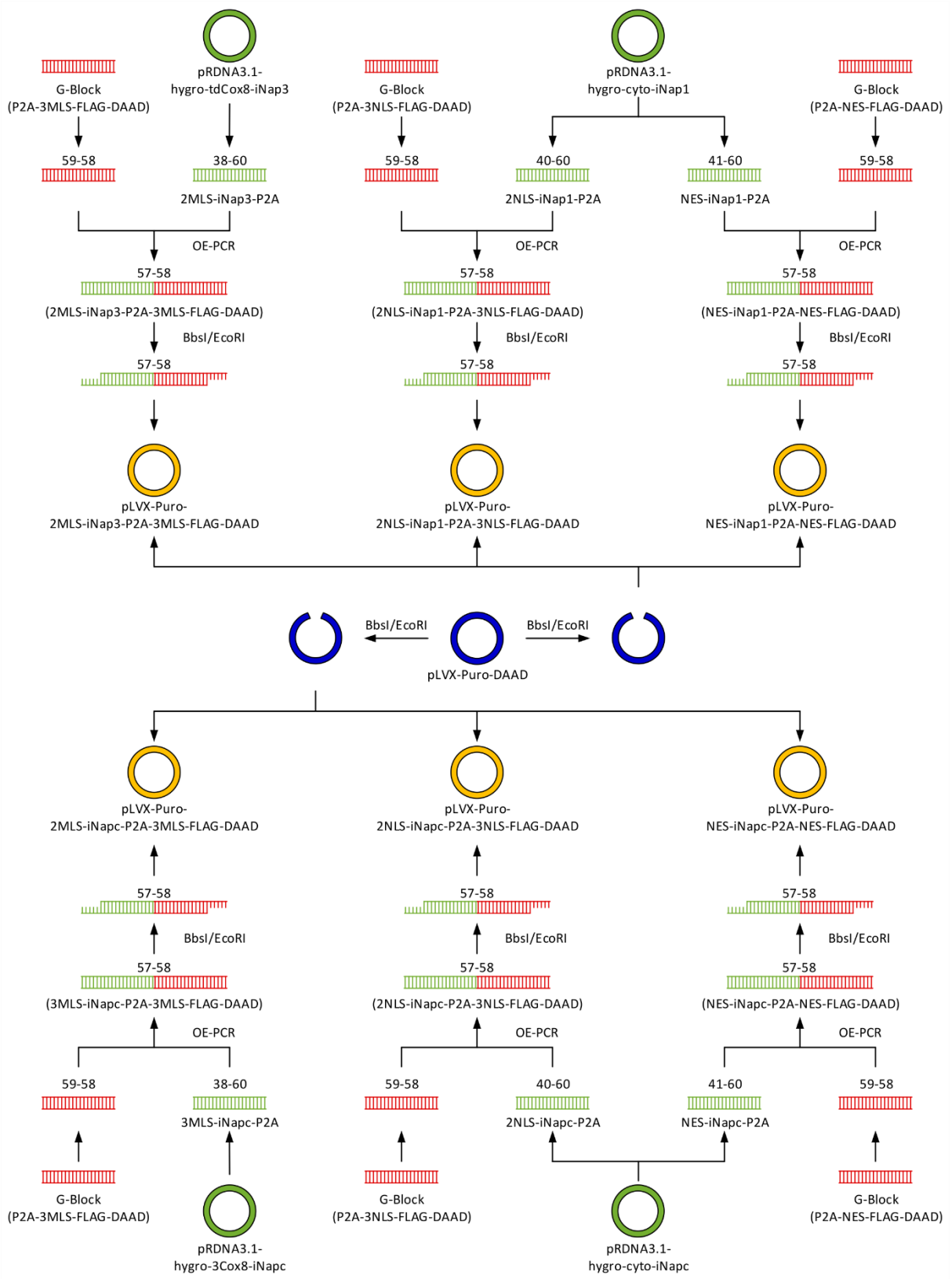

Figure 4.2: *The scheme for cloning of plasmids encoding iNap and DAAD proteins fused to signals for localization in the mitochondrial matrix, the nucleus and the cytosol. Coloured circles represent plasmids, where blue and green circles display original plasmids and yellow – derived ones. Along with plasmids, commercially synthesized DNA-sequences (G-blocks, denoted in red rectangles) were also utilized for amplification of PCR-products. Other rectangles indicate PCR-products amplified from a respective plasmid or a G-block (of the*

same colour). Numbers above rectangles denote pairs of forward and reverse primers (delimited with «-»), which were utilized for the amplification of PCR-products. Hygro – hygromycin resistance, MLS – mitochondrial localization signal (from Homo sapiens cytochrome c oxidase subunit 8A, COX8A), NES – nuclear export signal, NLS – nuclear localization signal of SV40, OE-PCR – Overlap Extension PCR, P2A – self-cleaving peptide, Puro – resistance to puromycin.

hygro-cyto-iNap1 and pRDNA3.1-hygro-cyto-iNapc using 40-60 and from the G-Block, P2A-3NLS-FLAG-DAAD, with 59-58 pairs of primers, respectively. The plasmids encoding cytosolic versions of probes were derived from the same pRDNA3.1-hygro-cyto-iNap1 and pRDNA3.1-hygro-cyto-iNapc plasmids, however, with another, 41-60 pair of primers and from G-Block, P2A-NES-FLAG-DAAD using 59-58 primers, respectively. Next, for each plasmid two obtained fragments were combined by Overlap Extension PCR using 57-58 pair of primers, and the combined sequences were cut with BbsI/EcoRI restriction enzymes and ligated with the pLVX-Puro-DAAD, pre-treated with the same pair of enzymes.

All plasmids constructed for study of alterations of intracellular H_2O_2 and NADPH levels in melanoma cells are represented in Table 4.1. The derived plasmids were used for the production of lentiviruses, which in turn were used for making stable melanoma cell lines expressing HyPer-DAO and iNap-DAAD proteins.

Table 4.1: *Assembled pLVX-Puro plasmids encoding protein sequences for manipulation of H_2O_2 and NADPH levels in the mitochondrial matrix, the nucleus and the cytosol of melanoma cells.*

compound	compartment	encoding sequence	pH-controls
H_2O_2	Mitochondrial matrix	2MLS-HyPer-DAO	2MLS-SypHer-DAO
	Nucleus	HyPer-DAO-3NLS	SypHer-DAO-3NLS
	Cytosol	HyPer-DAO-NES	SypHer-DAO-NES
NADPH	Mitochondrial matrix	2MLS-iNap3-P2A-3MLS-FLAG-DAAD	3MLS-iNapc-P2A-3MLS-FLAG-DAAD
	Nucleus	2NLS-iNap1-P2A-3NLS-FLAG-DAAD	2NLS-iNapc-P2A-3NLS-FLAG-DAAD
	Cytosol	NES-iNap1-P2A-NES-FLAG-DAAD	NES-iNapc-P2A-NES-FLAG-DAAD

4.2 Production of stable melanoma cell lines

Different melanoma cell lines have different origin and genetic background and thus their response to the alterations of levels of key cellular redox compounds may also be distinct. To make sure that the response of melanoma cells to the

redox alterations is not specific to one selected cell line, we chose three melanoma cell lines for the production of stable cell lines expressing HyPer-DAO and iNap-DAAD systems in the mitochondrial matrix, the nucleus and the cytosol, namely, WM3734, 1205Lu and WM88.

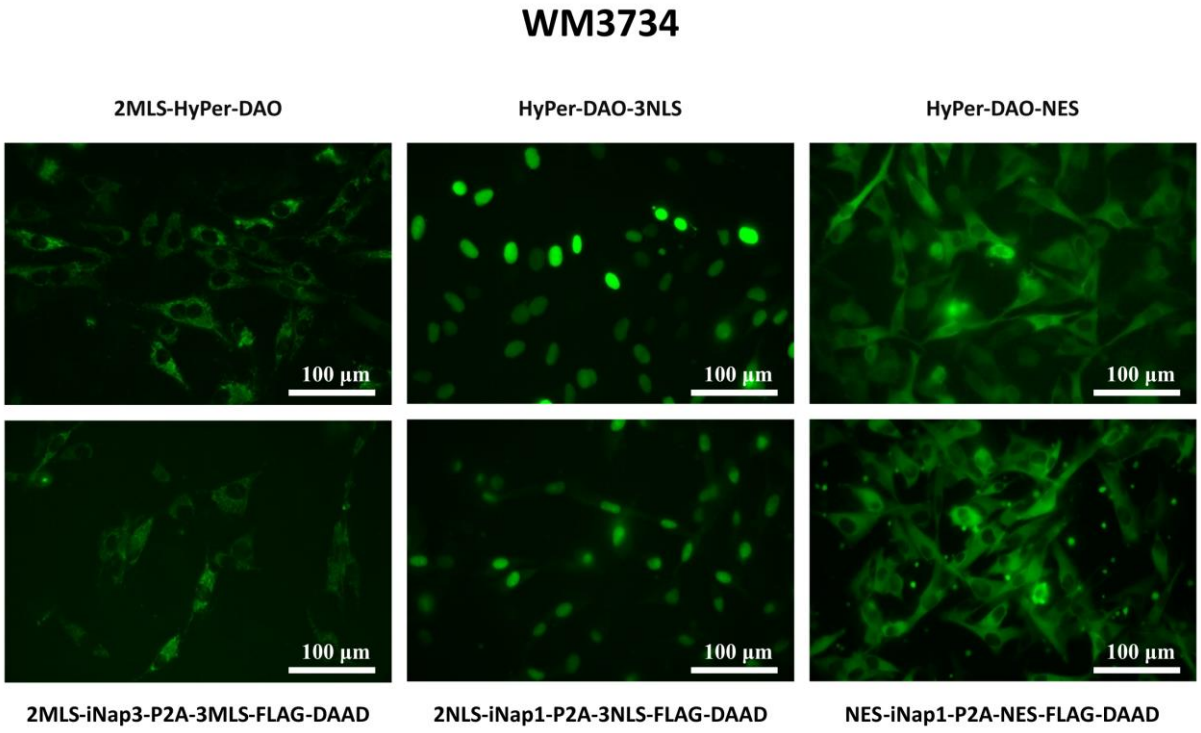

Figure 4.3: *Images of engineered stable WM3734 melanoma cell lines. Cell lines express chimeric HyPer-DAO (top row) or separate iNap and DAAD proteins in three compartments: the mitochondrial matrix (left column), the nucleus (middle column) and the cytosol (right column). Images were obtained using fluorescence microscopy. MLS – mitochondrial localization signal (from Homo sapiens cytochrome c oxidase subunit 8A, COX8A), NES – nuclear export signal, NLS – nuclear localization signal of SV40, P2A – self-cleaving peptide.*

One reason for choosing these cell lines was that all of them were derived from patients with the metastatic stage of the disease. Such patients have substantially decreased chances of curing and thus new therapies and improvements of existing ones are highly demanding. Selected cell lines were established from various metastatic sites, including brain (WM3734) and lung (1205Lu), and also have different genetic background. In addition to $BRAF^{V600E}$ mutation that is common for all three cell lines, 1205Lu line also has hemizygous deletion of phosphatase and tensin homolog (PTEN), a phosphatase negatively regulating the PI3K/AKT/mTOR signalling pathway and thus functioning as a tumour suppressor. This cell line also bears K22Q point mutation in cyclin-dependent kinase 4 (CDK4), a protein associated with the development of a variety of tumours (https://web.expasy.org/cellosaurus/CVCL_5239). Besides $BRAF^{V600E}$, WM3734 cell line carries homozygous deletion of CDKN2A gene

encoding p16 (INK4A) and p14 (ARF) proteins, both of which function as tumour suppressors (https://web.expasy.org/cellosaurus/CVCL_6800), while WM88 cells has wild type copies of PTEN, N-RAS, c-KIT and CDK4 (https://www.rockland.com/categories/cell-lines-and-lysates/wm88-viable-cells-1-million-cells-WM88-01-0001/), which are often found mutated in melanoma (Davis et al., 2019). Another reason for the selection of these cell lines is that all of them have an ability to form tumours after injection into immunocompromised mice that can be useful for experimental validation of the *in vitro* results *in vivo*, on murine models in the future.

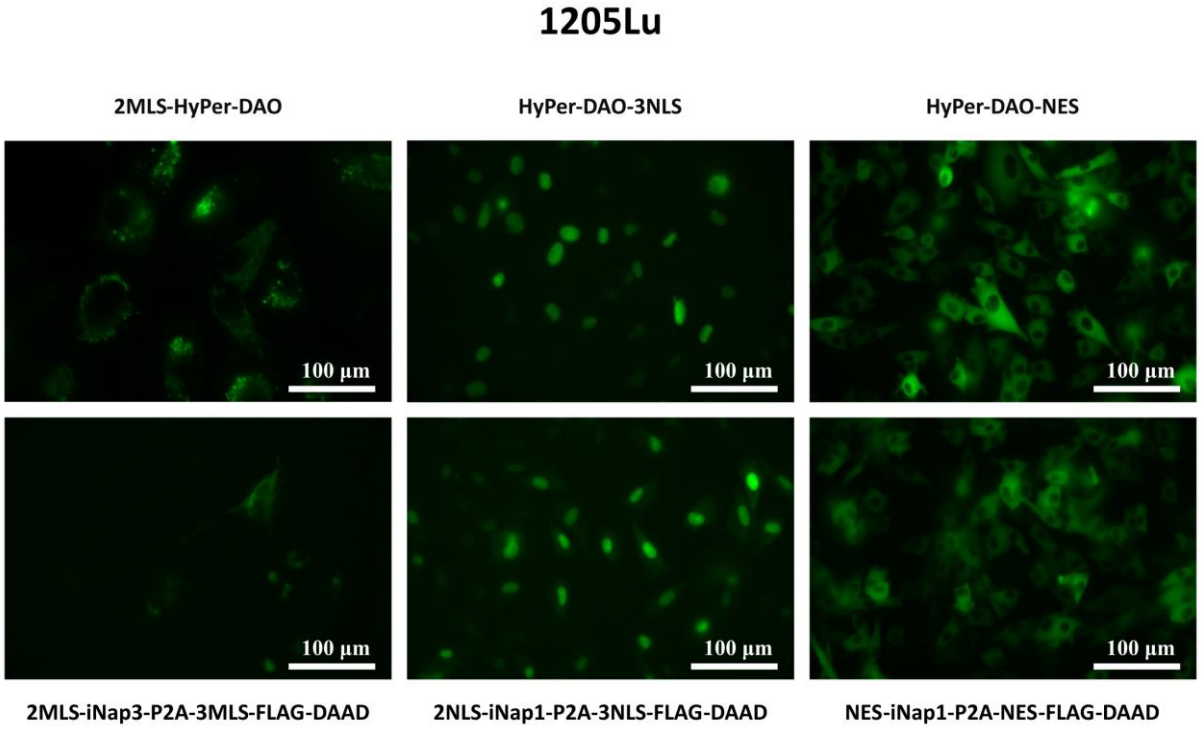

Figure 4.4: *Images of engineered stable 1205Lu melanoma cell lines. Cell lines express chimeric HyPer-DAO (top row) or separate iNap and DAAD proteins in three compartments: the mitochondrial matrix (left column), the nucleus (middle column) and the cytosol (right column). Images were obtained using fluorescence microscopy. MLS – mitochondrial localization signal (from Homo sapiens cytochrome c oxidase subunit 8A, COX8A), NES – nuclear export signal, NLS – nuclear localization signal of SV40, P2A – self-cleaving peptide.*

These melanoma cell lines were used for the production of stable cell lines (Figures 4.3-4.5). One can clearly see that expressed HyPer-DAO and iNap-DAAD proteins were properly localized in cellular compartments of all three cell lines. Nevertheless, one can also notice the relatively high (compared to HyPer-DAO-3NLS) fluorescent background in the cytosol of cell lines derived by infection with lentiviruses bearing 2NLS-iNap1-P2A-3NLS-FLAG-DAAD coding sequence.

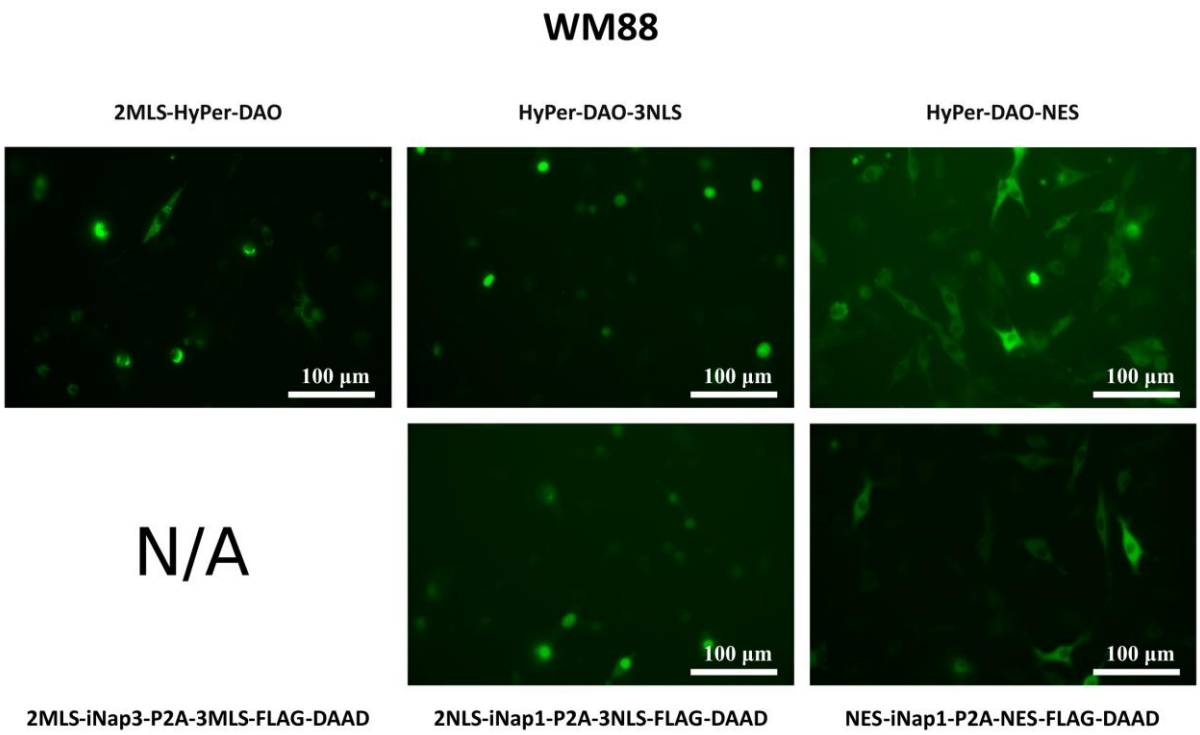

Figure 4.5: *Images of engineered stable WM88 melanoma cell lines. Cell lines express chimeric HyPer-DAO (top row) or separate iNap and DAAD proteins in three compartments: the mitochondrial matrix (left column), the nucleus (middle column) and the cytosol (right column). Images were obtained using fluorescence microscopy. MLS – mitochondrial localization signal (from Homo sapiens cytochrome c oxidase subunit 8A, COX8A), N/A – not available, NES – nuclear export signal, NLS – nuclear localization signal of SV40, P2A – self-cleaving peptide.*

4.3 H_2O_2 generation in the engineered melanoma cell lines

Before starting any experiments with the engineered melanoma cell lines stably expressing HyPer-DAO, we needed to make sure that the produced cell lines operate properly as well as to find the optimal concentration of D-Alanine (D-Ala) for DAO stimulation. For this reason, we attempted to induce H_2O_2 generation in WM3734 and 1205Lu cell lines stably expressing HyPer-DAO in the cytosol using a range of D-Ala concentrations: 1, 2, 4 and 8 mM (Figure 4.6 and 4.7). We selected these concentrations, since they were utilized for DAO stimulation within its chimera with HyPer, in HeLa-Kyoto and NIH-3T3 cells, previously (Matlashov et al., 2014).

Cell response to D-Ala can be described by two values: 1) maximal ratio [$\max(R/R_0)$], which HyPer reaches during experiment, and 2) time required HyPer reaching the half of this maximal ratio ($T_{0.5}$). Both cell lines expressing HyPer-DAO-NES reacted to 2mM and all higher tested concentrations of D-Ala.

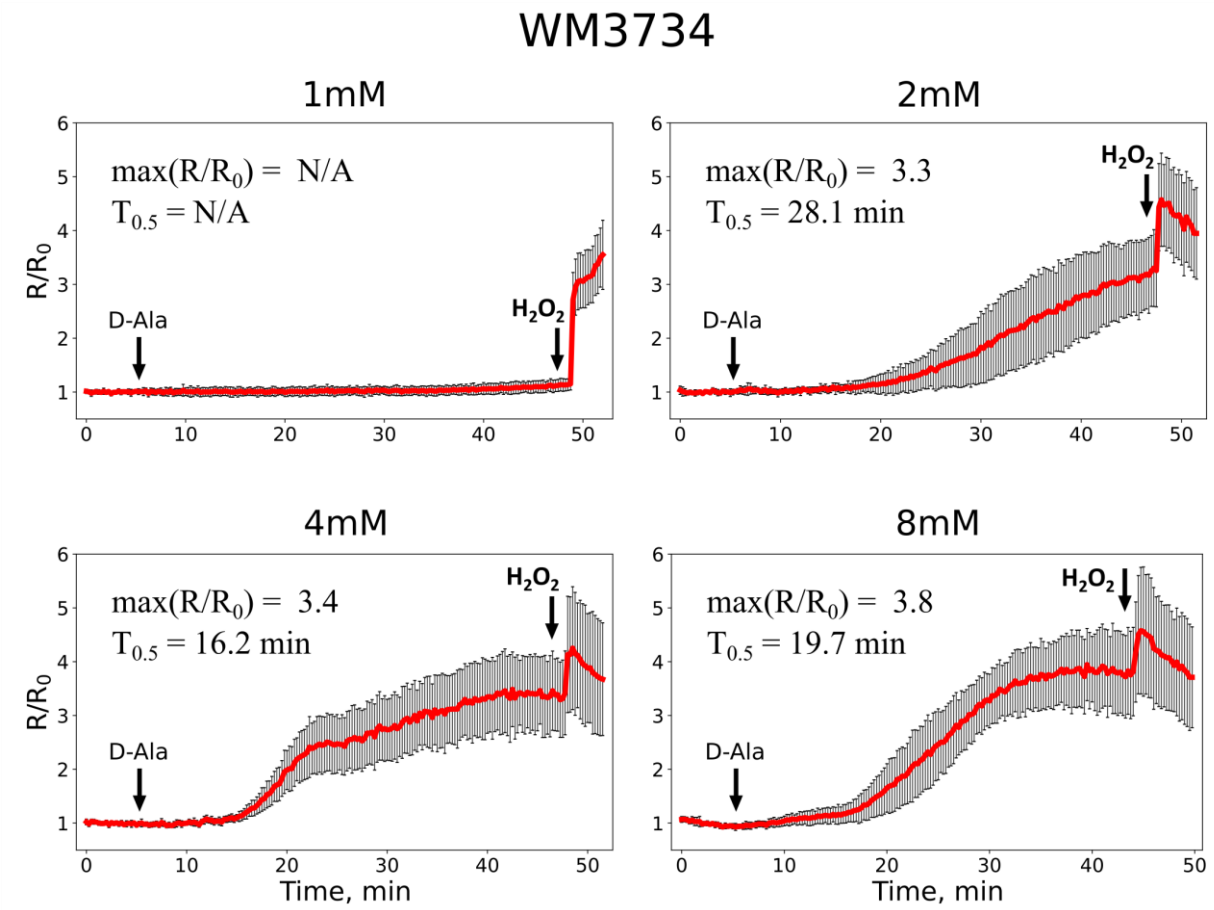

Figure 4.6: *Kinetics of HyPer's oxidation in response to the addition of different D-Alanine concentrations to the stable WM3734 melanoma cell line expressing HyPer-DAO-NES (in the cytosol). R/R_0 – normalized HyPer's ratio, max(R/R_0) – maximal ratio that HyPer reaches upon addition of D-Ala during experiment, $T_{0.5}$ – time required HyPer reaching the half of the maximal ratio. Each curve represents mean response of 10-20 cells from the same dish, bars represent standard deviation (std). NES – nuclear export signal. Arrows indicate time points when D-Alanine and H_2O_2 (150 μM) were added.*

Nevertheless, the response of these cell lines to D-Ala slightly differed. Maximal ratios that HyPer reached in response to D-Ala in general were higher for WM3734 melanoma cell line (3.3, 3.4 and 3.8) than for 1205Lu (1.8, 3.5 and 2.6). In response to addition of 2 mM of D-Ala to 1205Lu cells, HyPer was oxidized to around half of the maximum level. Higher concentrations of D-Ala, 4 and 8 mM, led to almost full and full oxidation of HyPer in 1205Lu cells, respectively. Unlike 1205Lu, addition of 2 mM of D-Ala to WM3734 cell line evoked HyPer's oxidation of around two-thirds of the maximum level, while 4 and 8 mM of D-Ala induced higher oxidation of HyPer, which, however, was not complete. Two cell lines also demonstrated different $T_{0.5}$ values in pairwise comparison at every single concentration of D-Ala, most pronounced at 2 and 4 mM. Nevertheless, since each experiment was performed only once, more replicates and statistical analysis are required to make more robust conclusions.

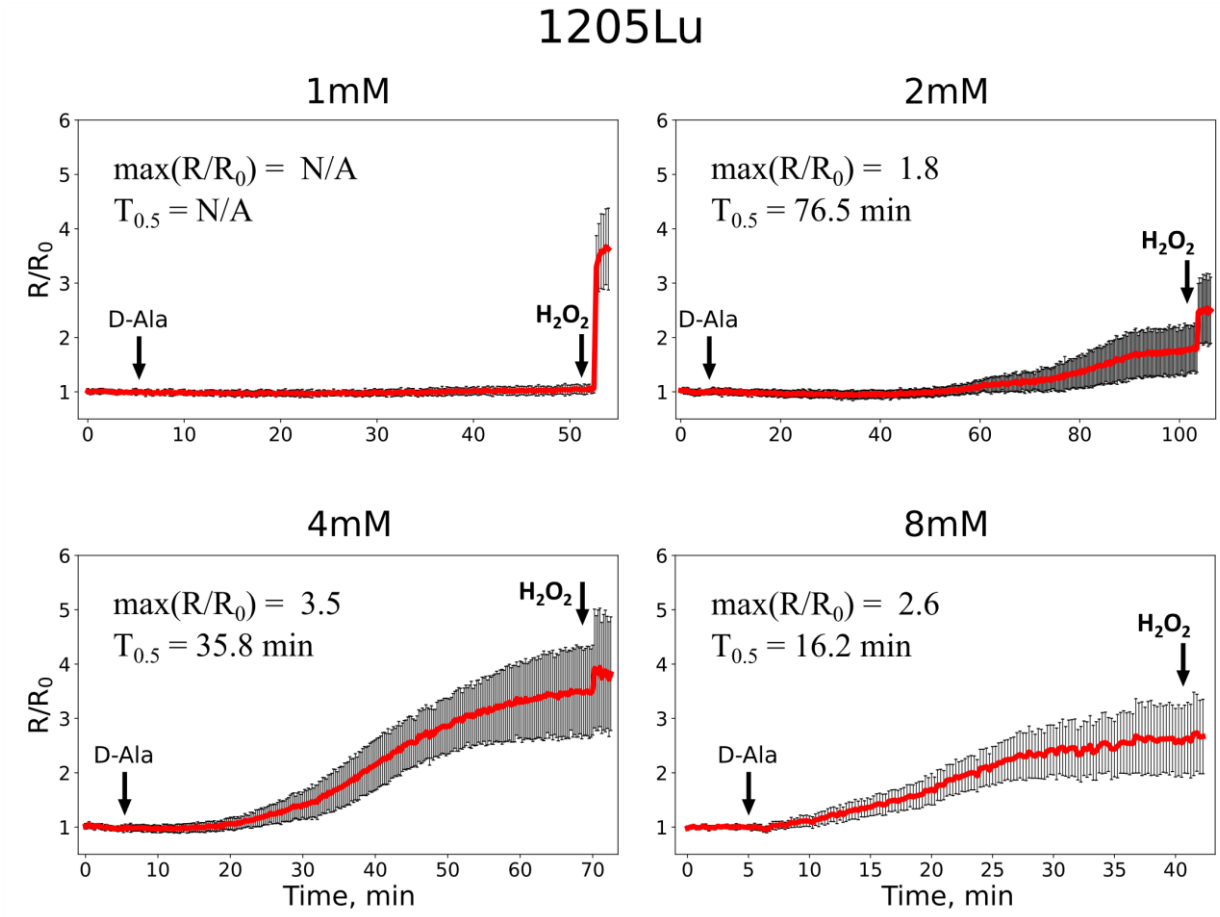

Figure 4.7: *Kinetics of HyPer's oxidation in response to the addition of different D-Alanine concentrations to the stable 1205Lu melanoma cell line expressing HyPer-DAO-NES (in the cytosol). R/R_0 – normalized HyPer's ratio, max(R/R_0) – maximal ratio that HyPer reaches upon addition of D-Ala during experiment, $T_{0.5}$ – time required HyPer reaching the half of the maximal ratio. Each curve represents mean response of 15-30 cells from the same dish, bars represent standard deviation (std). NES – nuclear export signal. Arrows indicate time points when D-Alanine and H_2O_2 (150 μM) were added.*

4.4 Influence of D-Alanine on melanoma cells proliferation

To understand how these concentrations affect proliferation and viability of derived stable melanoma cell lines, we performed crystal violet assay (CVA) with some of these lines, namely WM3734 and 1205Lu expressing HyPer-DAO in the cytosol and the nucleus (Figure 4.8). Primarily, we focused on the highest tested concentration of D-Ala – 8 mM. To rule out the influence of alanine on melanoma cell growth, we also tested L-Ala of the same concentration. We found that D-Ala substantially and significantly affected proliferation and viability of cell lines, which express DAO in both the cytosol and the nucleus due to proliferation arrest and cell death. We also found that D-Ala at this concentration was able to decrease growth rate of original (wt) melanoma cell lines. D-Ala had more considerable effects on WM3734 (wt) line, than on 1205Lu (wt), nevertheless, its effect on the

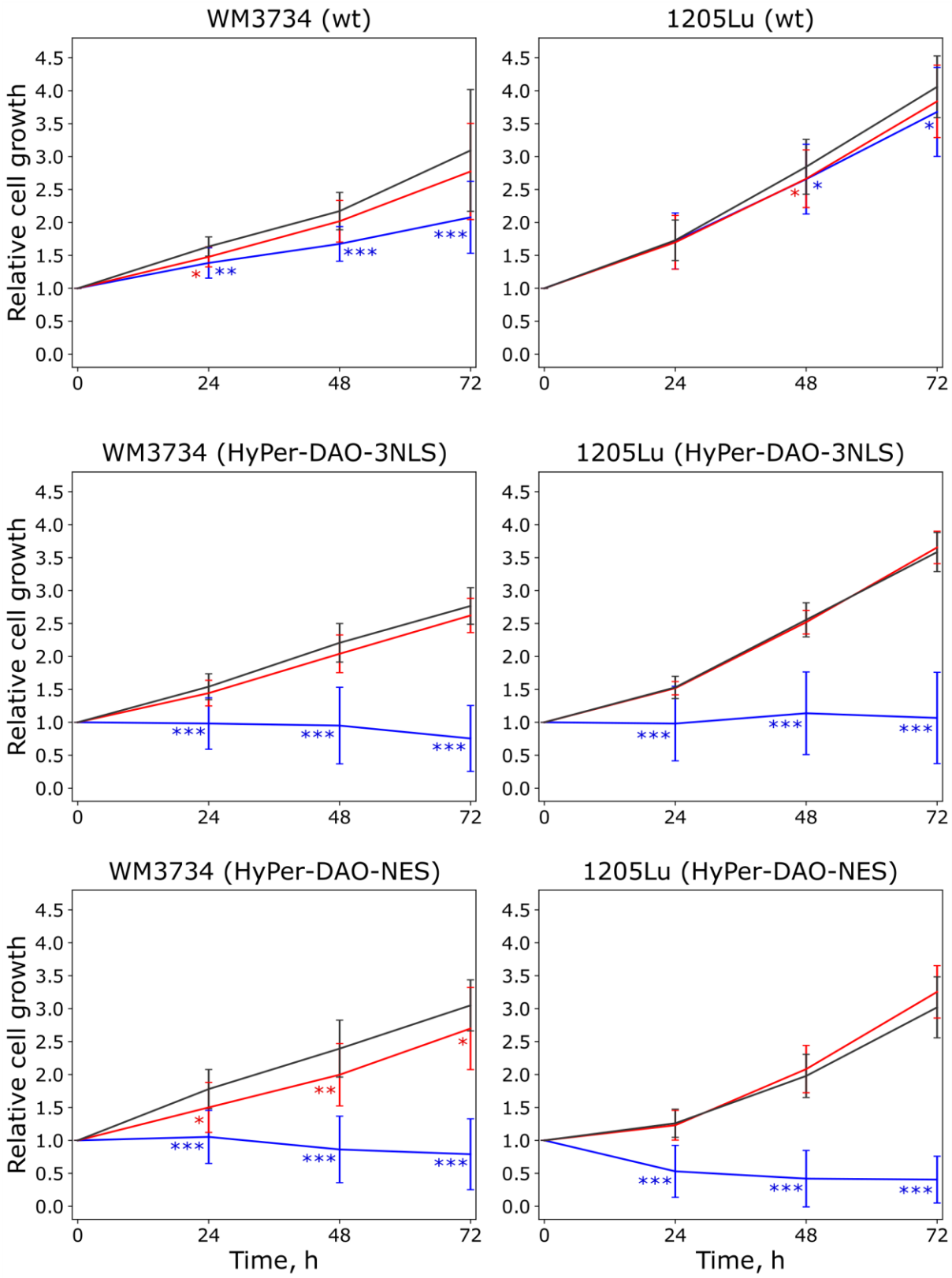

Figure 4.8: *Melanoma cell proliferation and viability estimated by crystal violet assay. Cells were incubated with 8 mM of D-Alanine (blue curves), 8 mM of L-Alanine (red curves) or without supplements (control, black curves). Experiment was performed five times with four measurements for each combination of cell line/time point/treatment type per replicate. Error bars represent standard error means. Treatment conditions (L- and D-Alanine) were compared*

with control. Statistical significance designation: one asterisk (*) denotes p-value ≤ 0.05, two asterisks (**) – p-value ≤ 0.01, three asterisks (***) – p-value ≤ 0.001.

latter one was also detected to be statistically significant. While D-Ala had pronounced impact on melanoma cell proliferation and viability, even on wt lines, L-Ala was not found to considerably affect growth of most of validated melanoma cell lines.

4.5 Cloning of additional HyPer-DAO plasmids

Since another task of the current research was to study the influence of alterations of H_2O_2 level on non-malignant cells, we used HEK293 cells for making stable cell lines expressing HyPer-DAO system in various cellular compartments. To accomplish this task, in addition to mentioned above HyPer-DAO plasmids, which we assembled for engineering of stable melanoma cell lines, we made several other plasmids encoding HyPer-DAO fused to signals for protein targeting to peroxisomes, the plasma membrane, as well as the ER- and other mitochondria-related compartments (Figure 4.9).

In total four plasmids were assembled for localization of HyPer/SypHer-DAO to cellular peroxisomes. For assembly of pLVX-Puro-HyPer/SypHer-DAO-PTS1 and pLVX-Puro-HyPer/SypHer-DAO-PTS1 (longer linker) required DNA fragments were amplified from previously produced pLVX-Puro-HyPer/SypHer -DAO-3NLS plasmids using 46-49 and 46-77 pairs of primers, respectively. Produced fragments and pLVX-Puro-HyPer/SypHer-DAO-3NLS plasmids were then cut with AvrII/XhoI restriction enzymes and ligated.

Four additional plasmids were produced for targeting HyPer-DAO to other mitochondria-related compartments, such as the mitochondrial intermembrane space (IMS) and the outer mitochondrial membrane (OMM). To perform this task, we fused HyPer/SypHer-DAO to a part of A-kinase anchor protein 1 (AKAP1) and Smac/DIABLO protein, respectively. The necessary part of AKAP1 protein was synthesized by PCR without DNA matrix using the 74-75 pair of primers, which form self-annealing dimers. The IMS fragment (DNA sequence of Smac/DIABLO) was cut out from the SypHer3s-IMS plasmid using NheI/BamHI restriction enzymes. The same pair of enzymes were employed to cut the amplified AKAP1 fragment and pLVX-Puro-2MLS-HyPer/SypHer-DAO plasmids. Prepared DNA fragments and plasmid backbones were then mixed and ligated to produce pLVX-Puro-AKAP1-HyPer/SypHer-DAO and pLVX-Puro-IMS-HyPer/SypHer-DAO plasmids.

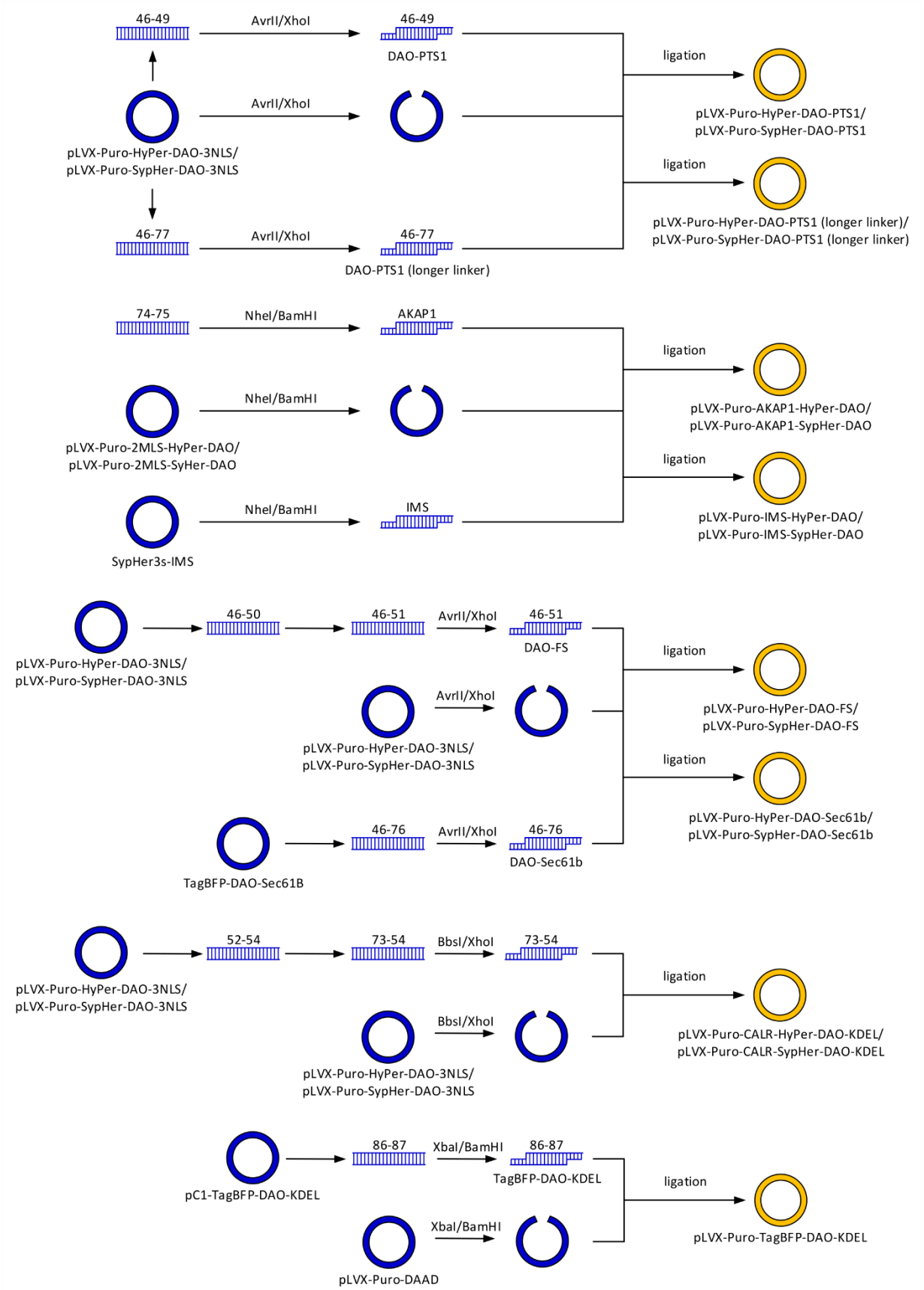

Figure 4.9: *The scheme for cloning of plasmids encoding HyPer/SypHer-DAO proteins with signals for localization in peroxisomes, mitochondria and ER-related compartments as well as on the plasma membrane. Coloured circles represent plasmids, where blue circles display*

original plasmids and yellow – derived ones. Rectangles indicate PCR-products. Numbers above rectangles denote pairs of forward and reverse primers (delimited with «-»), which were utilized for the amplification of PCR-products. AKAP1 – part of A-kinase anchor protein 1 coding sequence, CALR – N-terminal hydrophobic targeting sequence of calreticulin for the localization in the ER-lumen, FS - farnesylation signal, IMS – sequence of Smac/DIABLO for the localization in mitochondrial intermembrane space, KDEL – C-terminal ER retention sequence, MLS – mitochondrial localization signal (from Homo sapiens cytochrome c oxidase subunit 8A, COX8A), NLS – nuclear localization signal of SV40, PTS – peroxisomal targeting signal, Sec61B – Sec61 translocon subunit beta.

To target HyPer/SypHer-DAO to the cytosolic side of the plasma membrane we fused these proteins with farnesylation signal (FS). Initially, pLVX-Puro-HyPer/SypHer-DAO-3NLS plasmids were amplified using 46-50 and the derived PCR product with 46-51 pairs of primers. Next, the derived inserts and vectors (pLVX-Puro-HyPer/SypHer-DAO-3NLS) were cut with AvrII/XhoI enzymes and ligated to produce pLVX-Puro-HyPer/SypHer-DAO-FS plasmids.

ER-related cellular compartments that we selected for targeting were the ER-membrane (the cytosolic side) and the ER-lumen. To localize HyPer/SypHer-DAO on the ER-membrane we amplified TagBFP-DAO-Sec61B plasmid using the 46-76 pair of primers (to obtain Sec61 translocon subunit beta (Sec61B) sequence), cut the derived PCR-product and the pLVX-Puro-HyPer/SypHer-DAO-3NLS with AvrII/XhoI enzymes, and then ligated derived insert and vectors to produce pLVX-Puro-HyPer/SypHer-DAO-Sec61B plasmids.

For targeting DAO to the ER-lumen we constructed three plasmids: pLVX-Puro-CALR-HyPer/SypHer-DAO-KDEL and pLVX-Puro-TagBFP-DAO-KDEL. To produce pLVX-Puro-CALR-HyPer/SypHer-DAO-KDEL, pLVX-Puro-HyPer/SypHer-DAO-3NLS plasmids and 52-54 pair of primers were used for PCR, and the derived DNA fragments were further elongated using another, 73-54, pair of primers. Obtained fragments and pLVX-Puro-HyPer/SypHer-DAO-3NLS plasmids were then cut with BbsI/XhoI restriction enzymes and ligated. pLVX-Puro-TagBFP-DAO-KDEL was assembled by ligation of TagBFP-DAO-KDEL insert, which was amplified from pC1-TagBFP-DAO-KDEL plasmid, with pLVX-Puro-HyPer/SypHer-DAO-3NLS vectors. Insert and vectors were digested with XbaI/BamHI enzymes before ligation.

Plasmids constructed for study of intracellular H_2O_2 level alterations in various compartments of HEK293 cells are represented in Table 4.2.

Table 4.2: *Assembled pLVX-Puro plasmids encoding protein sequences for manipulation of H_2O_2 level in various compartments of HEK293 cells.*

Compartment	Encoding sequence	pH-controls
Outer Mitochondrial Membrane	AKAP1-HyPer-DAO	AKAP1-SypHer-DAO
Mitochondrial Intermembrane Space	IMS-HyPer-DAO	IMS-SypHer-DAO
Peroxisomes	HyPer-DAO-PTS1	SypHer-DAO-PTS1
	HyPer-DAO-PTS1 (longer linker)	SypHer-DAO-PTS1 (longer linker)
Plasma membrane	HyPer-DAO-FS	SypHer-DAAO-FS
ER-membrane (cytosolic side)	HyPer-DAO-Sec61B	SypHer-DAAO-Sec61B
ER-lumen	CALR-HyPer-DAO-KDEL	CALR-SypHer-DAO-KDEL
	TagBFP-DAO-KDEL	N/A

4.6 Production of stable HEK293 cell lines

To verify constructed plasmids encoding HyPer/SypHer-DAO fused to the peroxisomal targeting signal (PTS1), we transiently transfected cells with pLVX-Puro-HyPer-DAO-PTS1 (Figure 4.10, left). One can see that besides presence of small green dots, which strongly resemble peroxisomes, cells had a strong background fluorescence, most likely due to the presence of HyPer in the cytosol. The strong presence of HyPer-DAO-PTS1 in the cytosol perhaps reflected inefficient import of nascent cytosolic HyPer-DAO-PTS1 into peroxisomes and is in accordance to the fact that peroxisomal proteins are synthesized on cytosolic ribosomes and transported into peroxisomes after synthesis (Platta & Erdmann, 2007). Since high amount of DAO in the cytosol would substantially compromise following experiments, we attempted to reduce this cytosolic fraction of DAO to a minimum. For this purpose, we assembled new plasmids encoding HyPer/SypHer-DAO-PTS1, however, with a longer linker between DAO and PTS1, since a longer linker could potentially increase the accessibility of PTS to the peroxisomal protein import machinery. One can clearly see that cells transiently transfected with HyPer-DAO-PTS1 (longer linker) (Figure 4.10 middle) displayed significantly reduced amount of HyPer-DAO-PTS1 in the cytosol (compared to the previous HyPer-DAO-PTS1 version) with the retention of the fusion protein in peroxisomes. Therefore, we used the corresponding plasmid for the production of stable HEK293 cell line (Figure 4.10, right). Despite HyPer-DAO protein was visibly expressed in peroxisomes of the derived stable cell line, cells also demonstrated explicit cytosolic localization of the protein. For this reason, none of the designed plasmids encoding peroxisomal versions of

HyPer-DAO and respective stable cell lines were not used for further experiments in the current study.

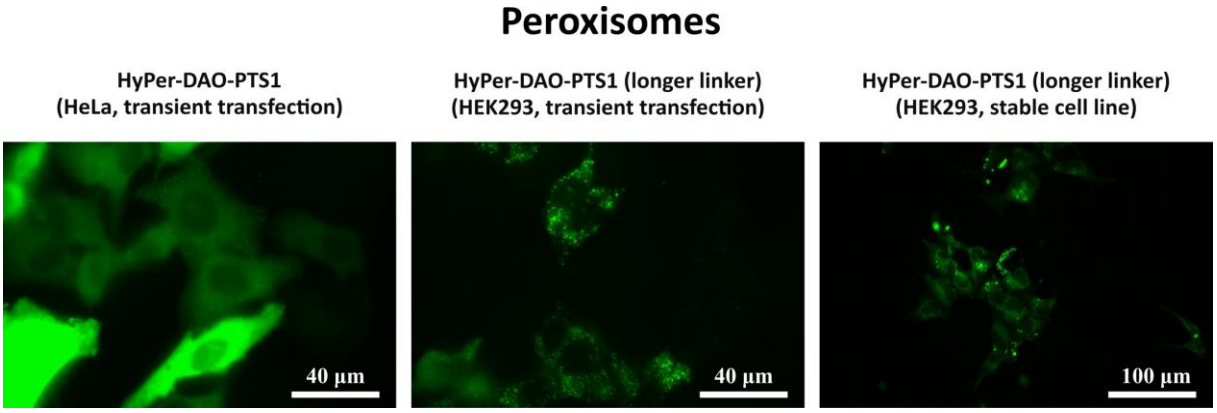

Figure 4.10: *Images of HEK293 and HeLa cells expressing HyPer-DAO protein in peroxisomes. Left – HeLa cells transiently transfected with HyPer-DAO-PTS1. Middle and right – transiently transfected and stable HEK293 cells expressing HyPer-DAO-PTS1 (with longer linker between DAO and PTS1), respectively. Images were obtained using fluorescence microscopy. PTS – peroxisomal targeting signal.*

Next, we examined plasmids encoding HyPer/SypHer-DAO fused to signals for localization in the ER-lumen. Despite presence of both the targeting and the retention signals within CALR-HyPer/SypHer-DAO-KDEL proteins, they did not show ER localization (Figure 4.11, left). Instead, expressed proteins displayed cytosolic localization.

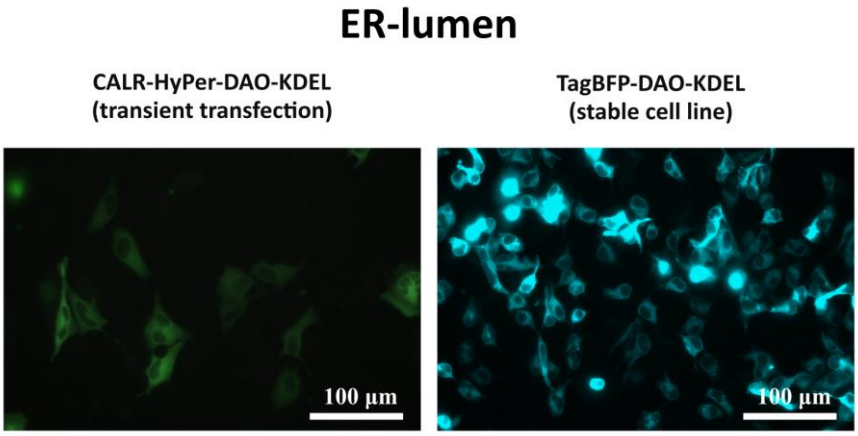

Figure 4.11: *Images of HEK293 cells expressing HyPer-DAO and TagBFP-DAO proteins for localization in the ER-lumen. Images were obtained using fluorescence microscopy. CALR – N-terminal hydrophobic targeting sequence of calreticulin for the localization in the ER-lumen, KDEL – C-terminal ER retention sequence.*

Since previous reports indicated almost full oxidation of HyPer in the ER-lumen (Malinouski et al., 2011; Mehmeti et al., 2012) and thus not a great utility of

HyPer in this cellular compartment, we assembled another plasmid – pLVX-Puro-TagBFP-DAO-KDEL. The coding region of this plasmid was borrowed from pC1-TagBFP-DAO-KDEL plasmid, which was successfully used previously for the expression of TagBFP-DAO in the ER-lumen. Cells transiently transfected with assembled pLVX-Puro-TagBFP-DAO-KDEL plasmid did not show any visible mistargeting and thus we used this plasmid for the stable HEK293 cell line production. Derived stable cell line also did not demonstrate discernible fluorescent signal in other than ER compartments (Figure 4.11, right) and therefore was utilized in further experiments.

To localize HyPer/SypHer-DAO on the cytosolic side of the ER-membrane we made pLVX-Puro-HyPer/SypHer-DAO-Sec61B plasmids. Cells transiently transfected with these plasmids revealed ER-localized fluorescent signal (Figure 4.12, left). Notwithstanding, stable HEK293 cell line produced using pLVX-Puro-HyPer-DAO-Sec61B demonstrated explicit abnormal distribution of the expressed protein (Figure 4.12, right) that prevented its usage in following experiments.

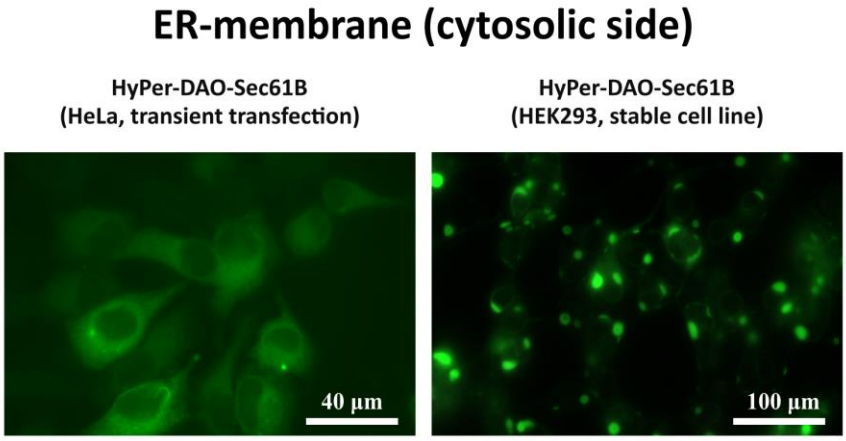

Figure 4.12: *Images of HEK293 and HeLa cells expressing chimeric HyPer-DAO protein on the ER-membrane (cytosolic side). Images were obtained using fluorescence microscopy. Sec61B – Sec61 translocon subunit beta.*

We also attempted to target HyPer-DAO to three mitochondria-related compartments of HEK293 cells: the mitochondrial matrix, the cytosolic side of the outer mitochondrial membrane (OMM) and mitochondrial intermembrane space (IMS). For the production of stable HEK293 cell line expressing HyPer-DAO in the mitochondrial matrix we used previously derived pLVX-Puro-2MLS-HyPer-DAO plasmid. Stable HEK293 cell lines expressing HyPer-DAO on the OMM and in the IMS were generated using pLVX-Puro-AKAP1-HyPer-DAO and pLVX-Puro-IMS-HyPer-DAO, respectively (Figure 4.13). All stable cell lines derived using abovementioned plasmids had fluorescent signal in mitochondria. Nevertheless, besides mitochondria, within each of these stable cell

lines were cells, which had HyPer-DAO in the cytosol most likely in addition to mitochondria (Figure 4.13, right). For this reason, none of stable cell lines expressing HyPer-DAO in mitochondria-related compartments, were used in the current study.

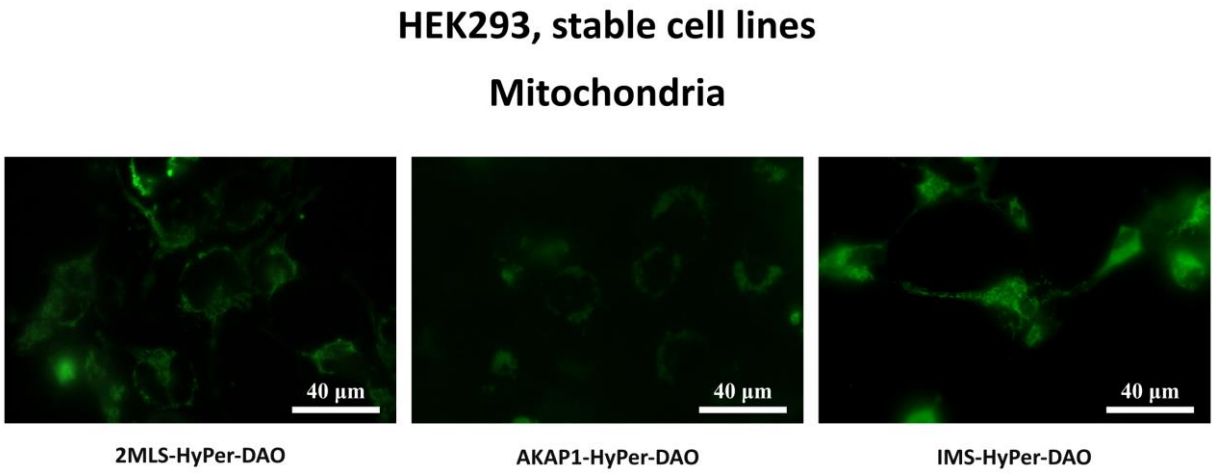

Figure 4.13: *Images of engineered stable HEK293 cell lines expressing chimeric HyPer-DAO protein in mitochondria-related compartments. Left – cells expressing HyPer-DAO in the mitochondrial matrix, middle – on the outer mitochondrial membrane and right – in the mitochondrial intermembrane space. AKAP1 – part of A-kinase anchor protein 1, IMS – localization signal for mitochondrial intermembrane space (part of Smac/DIABLO protein), MLS – mitochondrial localization signal (from Homo sapiens cytochrome c oxidase subunit 8A, COX8A).*

In addition to the cell lines discussed previously we produced other HEK293 cell lines expressing HyPer-DAO in the cytosol, the nucleus and on the cytosolic side of the plasma membrane (Figure 4.14). All of these stable cell lines expressed the HyPer-DAO protein properly in a required compartment and did not display any visible mistargeting.

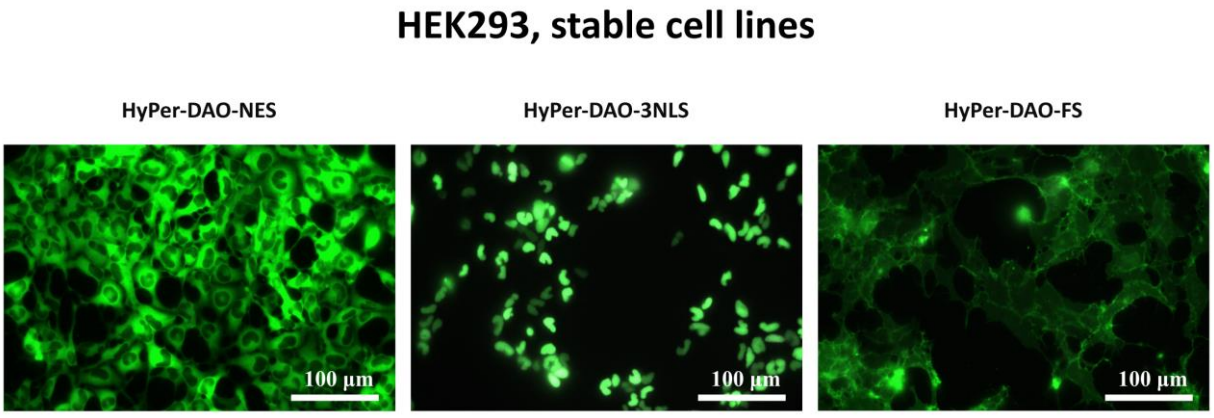

Figure 4.14: *Images of engineered stable HEK293 cell lines expressing HyPer-DAO protein in the cytosol, the nucleus and on the plasma membrane (cytosolic side). Images were obtained*

using fluorescence microscopy. FS - farnesylation signal, NES – nuclear export signal, NLS – nuclear localization signal of SV40.

4.7 Monoclonal selection of produced stable HEK293 cell lines

In further experiments we focused only on three produced HEK293 cell lines stably expressing chimeric proteins in three cellular compartments: the cytosol (HyPer-DAO-NES, Figure 4.14), the nucleus (HyPer-DAO-3NLS, Figure 4.14) and the ER-lumen (TagBFP-DAO-KDEL, Figure 4.11). To obtain similar behaviour of cells within the same cell line, cell lines expressing HyPer-DAO in the nucleus and the cytosol were subjected to monoclonal selection (Figure 4.15). Based on fluorescent properties, clone 1 and 2 derived from stable HEK293 cell lines expressing HyPer-DAO-3NLS and HyPer-DAO-NES, respectively, were used in further experiments.

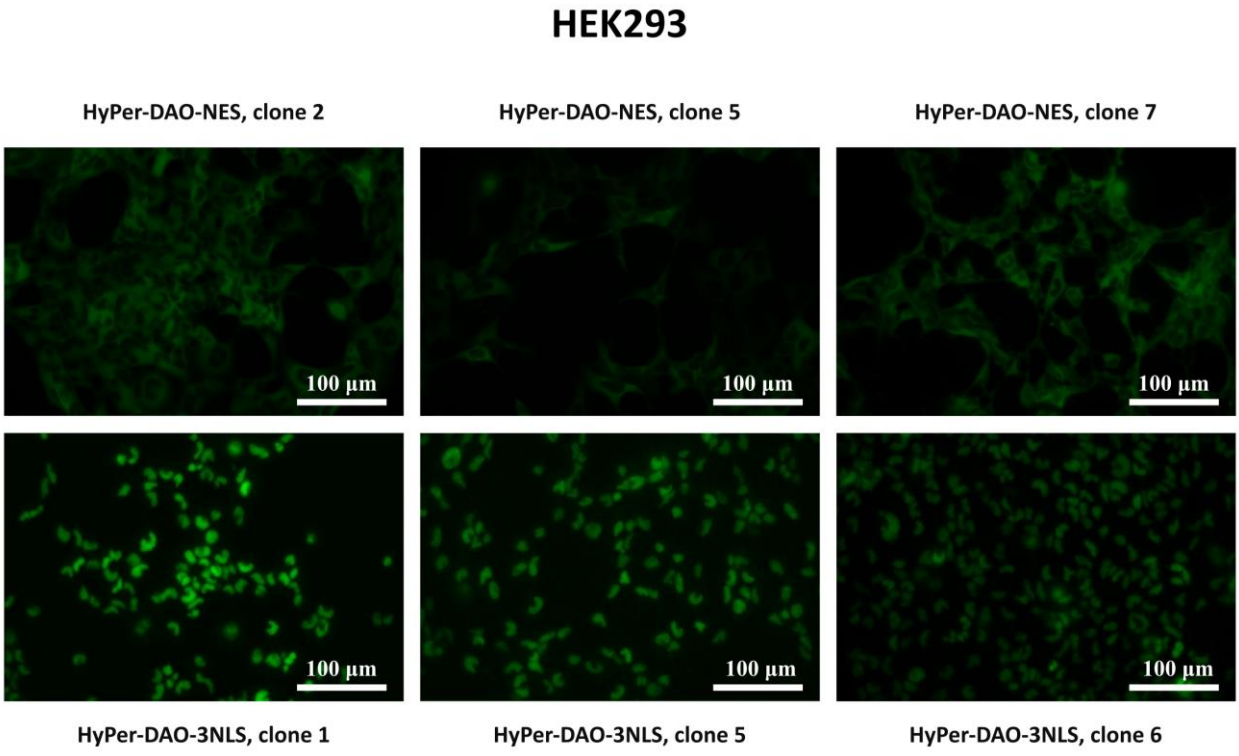

Figure 4.15: *Images of monoclonal HEK293 cell lines stably expressing HyPer-DAO in the nucleus and the cytosol. Images were obtained using fluorescence microscopy. For comparison exposure settings used for imaging of clones derived from the same parental cell line were the same. NES – nuclear export signal, NLS – nuclear localization signal of SV40.*

4.8 Optimization of stable HEK293 cell lines stimulation

To find the optimal D-Ala concentration required for H_2O_2 generation in produced stable HEK293 cell lines, we tested a range of D-Ala concentrations:

0.15 (0.25), 1, 2 and 4 mM. Using fluorescence microscopy, we found that HyPer expressed in the cell cytosol showed substantial response to 0.25 mM of D-Ala, while HyPer expressed in the nucleus did not respond to 0.15 mM of D-Ala (Figures 4.16 and 4.17). Meanwhile, 1mM of D-Ala induced maximal oxidation of HyPer localized in both the cytosol and the nucleus. Since HyPer was fused to DAO, H_2O_2 level in the immediate vicinity of HyPer is assumed to be higher, than in more distant sites even within the same organelle, therefore, to ensure more robust elevation of H_2O_2 within the organelle of interest we used 2 mM of D-Ala for stimulation of both cell lines expressing HyPer-DAO. It is also noteworthy that maximal HyPer ratios were higher and $T_{0.5}$ values were substantially lower upon addition of D-Ala to both cyto and nuclei cell lines than in to any of melanoma cell lines (Figures 4.6 and 4.7).

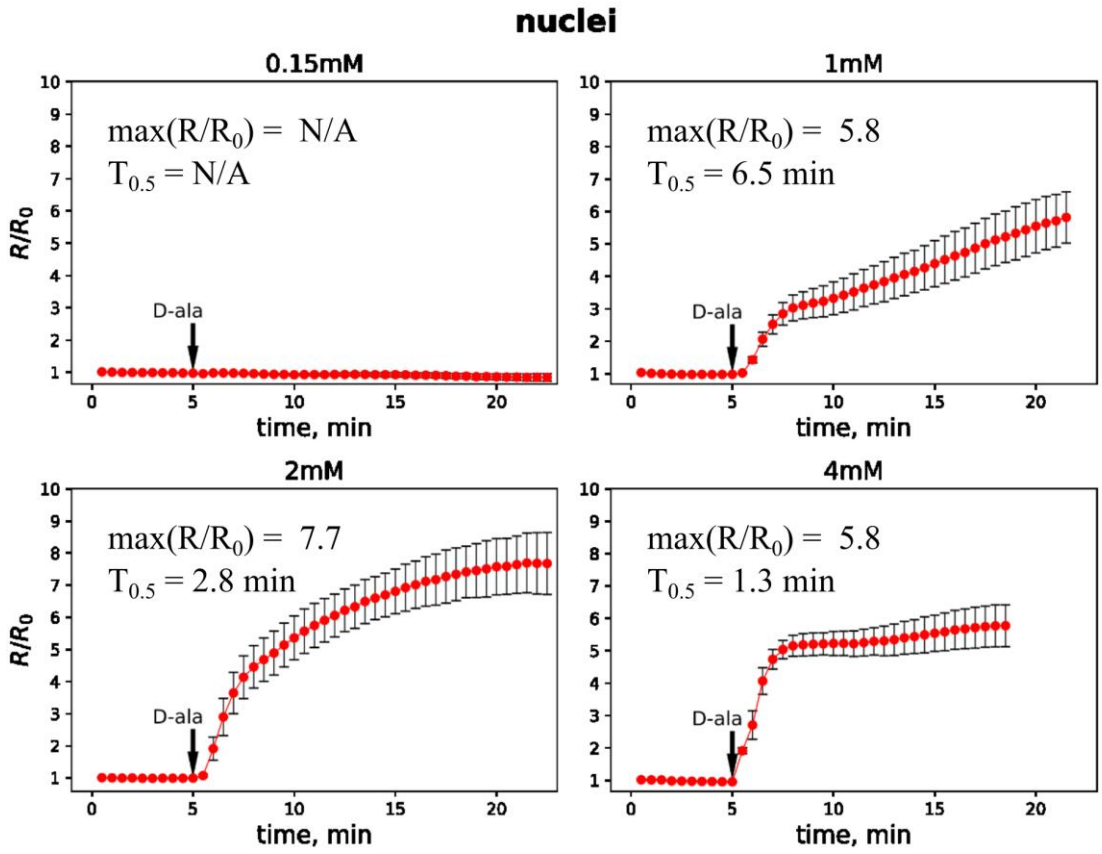

Figure 4.16: *Kinetics of HyPer's oxidation in response to the addition of different D-Alanine concentrations to the stable HEK293 cell line expressing HyPer-DAO-3NLS (nuclei). R/R_0 – normalized HyPer's ratio, max(R/R_0) – maximal ratio that HyPer reaches upon addition of D-Ala during experiment, $T_{0.5}$ – time required HyPer reaching the half of the maximal ratio. Each curve represents mean response of least 10 cells from the same dish, bars represent standard deviation (std).*

Whereas HyPer is a H_2O_2 sensor and can be used as a reporter in experiments with the cyto (HyPer-DAO-NES) and nuclei (HyPer-DAO-3NLS) cell lines, TagBFP does not to provide such an opportunity for the ER cell line (TagBFP-DAO-KDEL). Since we could not estimate amount of H_2O_2 generated by DAO in the ER-lumen in response to D-Ala addition, and taken into account multiple reports suggesting that ER produces and handles elevated H_2O_2 concentrations in comparison to other cellular compartments, we used higher concentration of D-Ala (8 mM) for DAO stimulation in ER cell line in further experiments.

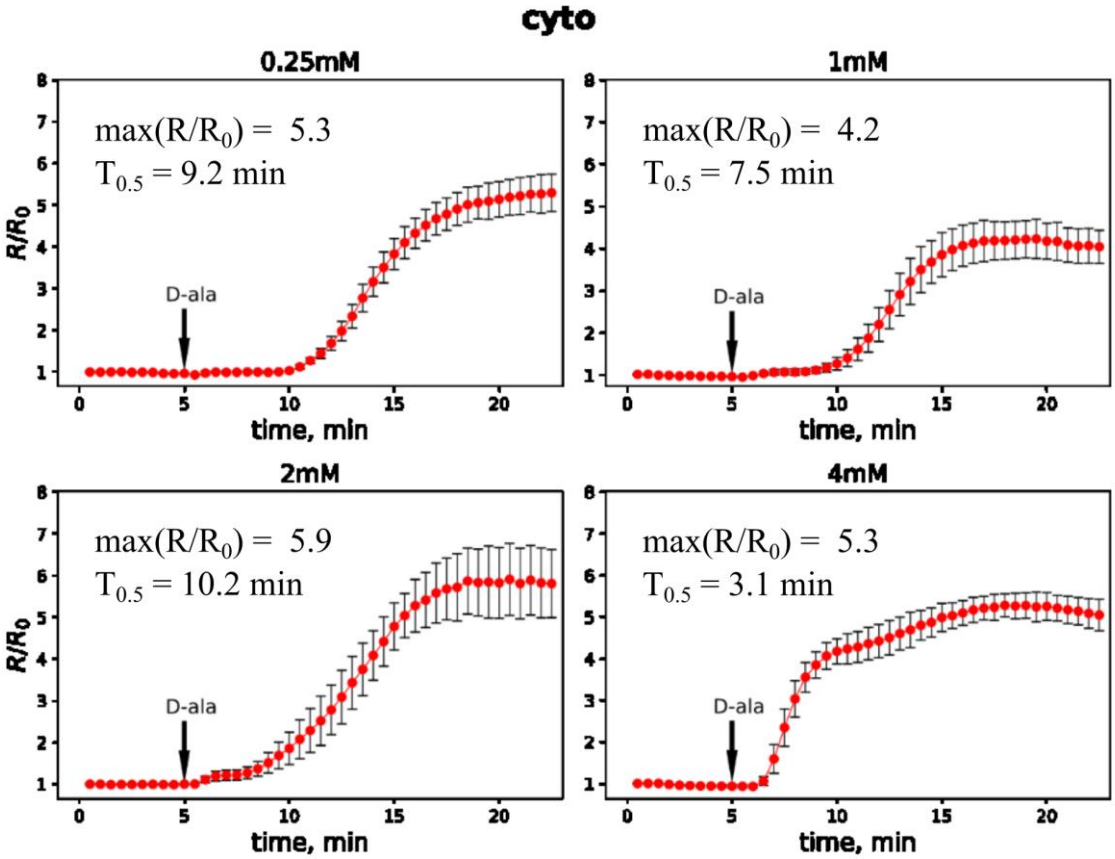

Figure 4.17: *Kinetics of HyPer's oxidation in response to the addition of different D-Alanine concentrations to the stable HEK293 cell line expressing HyPer-DAO-NES (cyto). R/R_0 – normalized HyPer's ratio, max(R/R_0) – maximal ratio that HyPer reaches upon addition of D-Ala during experiment, $T_{0.5}$ – time required HyPer reaching the half of the maximal ratio. Each curve represents mean response of at least 10 cells from the same dish, bars represent standard deviation (std).*

4.9 Thermal Proteome Profiling

Considering the complexity of cancer cells proteome due to various and multiple genomic aberrations, and the fact that melanoma cells are much less

studied compared to HEK293, we decided to postpone proteomic experiments with melanoma cells and instead study the influence of redox alterations on proteome of established HEK293 cell lines.

4.9.1 Thermal Proteome Profiling experiment

To find out which proteins are involved in cellular response to H_2O_2 regardless of the presence of redox-sensitive cysteines in amino-acid sequence, we performed a high throughput proteomics method – Thermal Proteome Profiling (TPP). TPP experiment was executed according to the procedure described in the method section. The experimental procedure of TPP was performed with the help of Isabelle Becher, Savitski's lab, EMBL, Heidelberg, Germany. In brief, four HEK293 cell lines: wild type (wt), ER, nuclei and cyto, were incubated with or without D-Ala of selected concentrations. Next, cells were aliquoted and subjected to the thermal denaturation under a range of temperatures (ten temperature points) and then lysed. The lysates were centrifuged and proteins from the soluble fraction (supernatant) were extracted and digested. Samples containing digested proteins were labelled according to the 2D-TPP scheme of multiplexing with 16plex label reagent set TMTpro^{TM} (Table 3.19). A combination of sixteen labelled samples (four cell lines * two conditions * two temperatures) were mixed and analysed using liquid chromatography with tandem mass spectrometry (LC-MS/MS) in each single MS run. Derived raw MS data were then processed according to the procedure described in the respective section of the method part. As a result, more than five thousand (5252) different proteins with at least two peptides were identified in our study.

4.9.2 Quality estimation of performed procedure

In order to compare the composition of the obtained protein data set and to estimate the quality of the performed TPP procedure, we employed results of TPP experiments reported previously by several other groups. For this purpose, several publications, wherein authors performed TPP using intact cells, were selected (Figure 4.18). The first study (Saei et al., 2020) was selected because in this study the authors performed TPP on intact cells following redox disturbance (HCT116 cell treatment with a thioredoxin reductase inhibitor auranofin). The second study (Tan et al., 2018) was chosen because it was performed using HEK293T cell line, which is derived from HEK293 line that was used in our study. The last study selected (Becher et al., 2018) was fulfilled using the experimental workflow (proteomic procedure, equipment, reagents) and data processing pipeline similar to our study. Total numbers of proteins in data sets from the compared studies

were: 5010 (Saei et al., 2020), 7199 (Tan et al., 2018), 5391 (Becher et al., 2018) and 5252 (our study) (Figure 4.18). Among them, 3042 proteins were found to be common for all four data sets, which constitutes 57.9% of all proteins detected in our study. Furthermore, our data set shared 3761 (71.6%), 4400 (83.8%) and 3794 (72.7%) common proteins with (Saei et al., 2020), (Tan et al., 2018) and (Becher et al., 2018), respectively. The total number of proteins in our data set and the significant share of common proteins between our set and the ones selected for comparison indicate that TPP procedure was performed correctly.

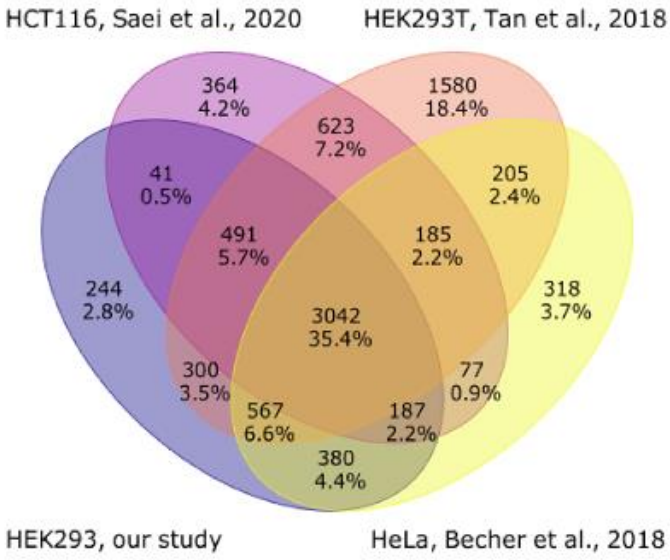

Figure 4.18*: Venn diagram showing similarity of sets of proteins (with at least two detected peptides each) identified in four indicated studies, wherein authors performed Thermal Proteome Profiling on intact cells. Supplementary tables 4, 21 and 2 were used as data sets for comparison from (Saei et al., 2020), (Tan et al., 2018), and (Becher et al., 2018), respectively. Prior to comparison, supplementary table 21 (Tan et al., 2018) was filtered to remove proteins with less than two detected peptides.*

To get a better grasp of how individual proteins as well as the cellular proteome in general responded to a temperature increase, melting curves of individual proteins and an average (mean) melting curve of all proteins in the data set were plotted (Figure 4.19, left). For comparison we also plotted analogous curves for proteins from the study of (Tan et al., 2018) (Figure 4.19, right). Since we used the abovementioned 2D-TPP scheme of multiplexing, samples corresponding to only two different temperatures were analysed in one MS run and thus five different MS runs were required for the analysis of protein composition of samples corresponding to all ten temperatures.

Separate analysis of samples in different MS runs can lead to the situation, when a particular protein is not detected in one or more MS runs. In our case, it means that a melting curve of an individual protein will have two or more (multiple of two) missing values (gaps on the curve) depending on the number of runs, where the protein was not identified. This can be clearly seen in the bottom part of the plot (Figure 4.19, left), where melting curves of several proteins are suddenly interrupted. Furthermore, it is obvious that protein melting curves plotted based on our study have greater variance, than respective ones plotted using the study of (Tan et al., 2018). This also can be explained by the separate analysis of samples that introduces technical variation between injections. In contrary to our study, in the study of (Tan et al., 2018) authors used another scheme of multiplexing – TR-TPP, which allows simultaneous analysis of all ten temperatures in one MS run. This scheme guarantees that if a protein is identified, then there will not be any missing values on the melting curve (Figure 4.19, right). Regardless of differences in multiplexing between two studies, it is obvious that melting profiles of both proteomes were similar.

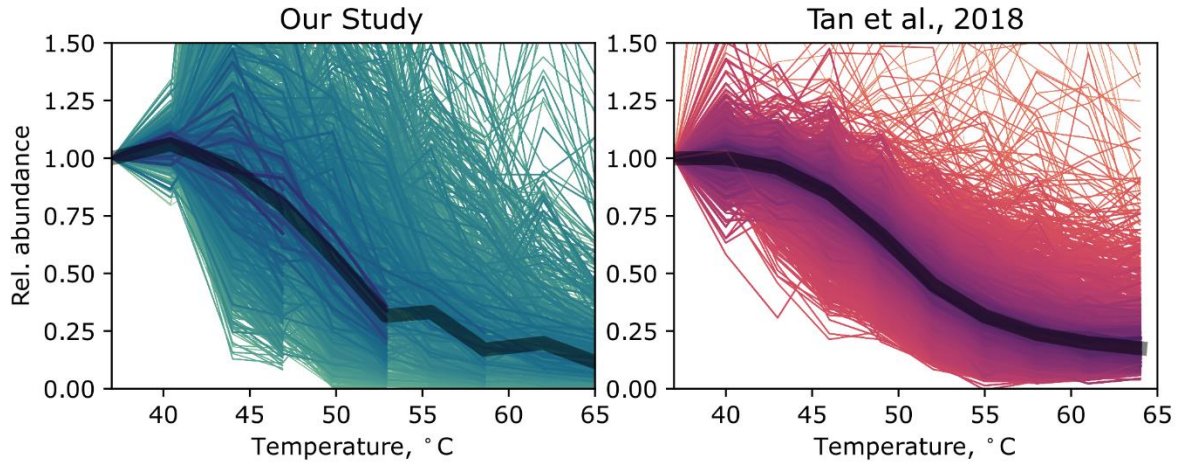

Figure 4.19: *Melting curves of proteins identified in our study (wt HEK293 cell line) and (Tan et al., 2018). Supplementary table 21 (HEK293T) from (Tan et al., 2018) was used as a data set. Solid lines represent mean melting curves of all proteins of the respective data sets, other lines – melting curves of individual proteins. For the convenience only melting curves of two thousand randomly chosen proteins are represented for each data set. The picture was prepared by Alexey Nesterenko.*

4.9.3 Classification of proteins into hits, candidates and no hits

Despite its drawbacks, 2D-TPP was a more appropriate option for our study than TR-TPP, since our main goal was to compare responses of different cell lines to H_2O_2. In 2D-TPP, cell lines and conditions are multiplexed and analysed in one MS run (alike temperatures in TR-TPP) that ensures identification (or no

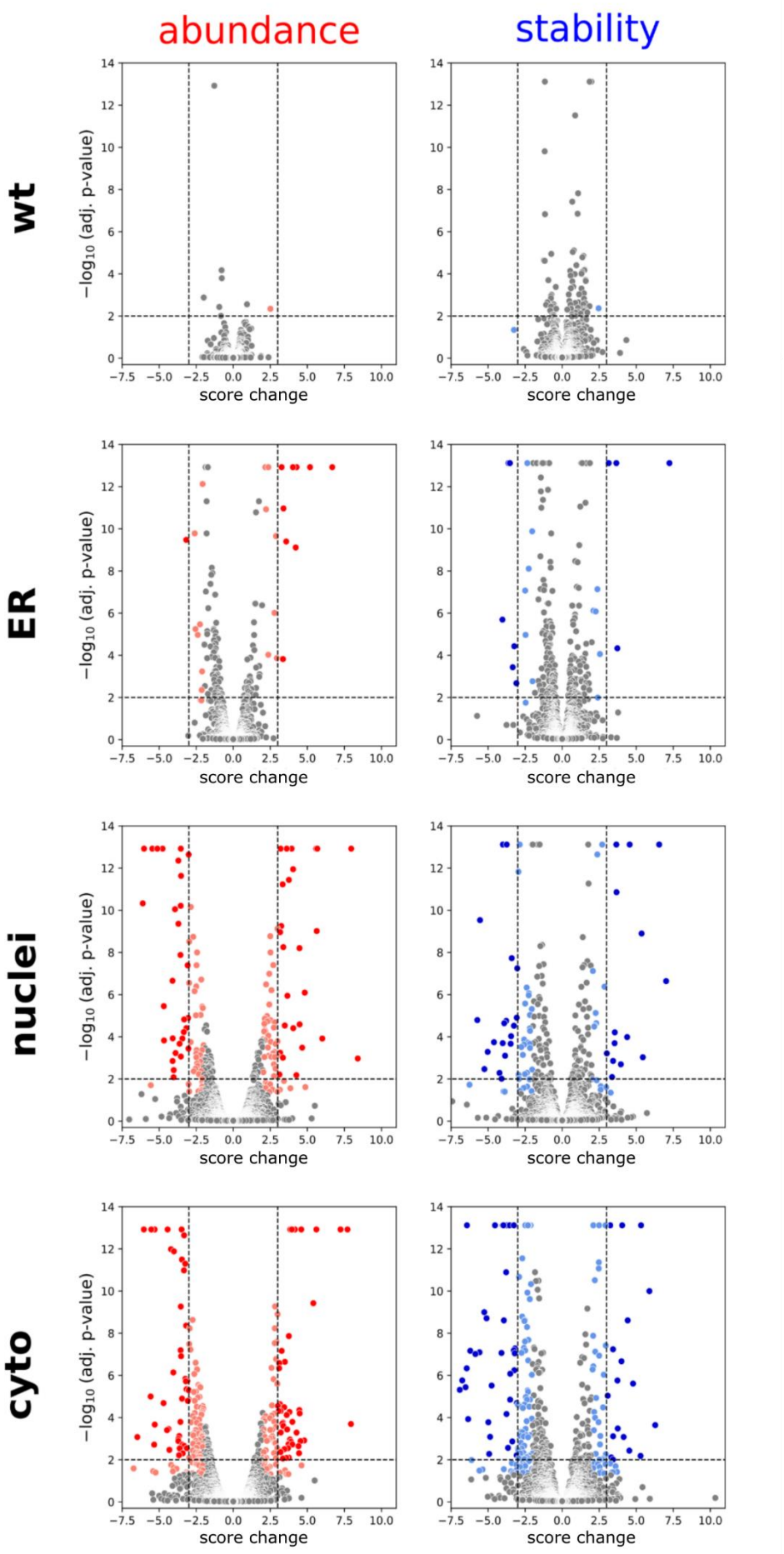
abundance
stability
wt
ER
nuclei
cyto
−log10 (adj. p-value)
score change

Figure 4.20: *Volcano plots representing proteins identified in Thermal Proteome Profiling experiment. Abundance colour palette: hit – «red», candidate – «salmon», no hit – «grey». Stability colour palette: hit – «medium blue», candidate – «cornflower blue», no hit – «grey». Annotation of proteins: hit – adj. p-value < 0.01 and score > 3, candidate – adj. p-value < 0.05 and score > 2, no hit – adj. p-value > 0.05 or score < 2. Horizontal and vertical dashes show thresholds for hit proteins.*

identification) of an individual protein in all multiplexed cell lines and conditions, and that cannot be done using TR-TPP. This feature of 2D-TPP allowed to calculate ratios of protein amounts identified in samples corresponding to experimental and control conditions at particular temperatures, and based on them major TPP characteristics: *abundance* and *stability* scores for an individual protein in all cell lines. *Abundance* score reflects an alteration of a protein amount in soluble fraction extracted from samples treated with two lowest temperatures (see formula 2). *Stability* score in turn was calculated according to the formula 1, given in the respective section of the method part. Based on the magnitude of protein stability and abundance scores and respective statistical significance values (adj. p-value), all proteins were classified into three groups: hits – adj. p-value < 0.01 and score > 3, candidates – adj. p-value < 0.05 and score > 2 and no hits – adj. p-value > 0.05 or score < 2. Numbers of proteins identified as hits and candidates are represented in Table 4.3. For a better understanding of the distribution of hit and candidate proteins for each cell lines, all proteins were also represented on volcano plots (Figure 4.20).

Table 4.3: *Number of proteins identified as hits and candidates based on abundance and stability scores and respective adj. p-values upon D-Ala addition to four cell lines.*

Score		Abundance		Stability	
Protein		Candidate	Hit	Candidate	Hit
cell line	wt	1	0	2	0
	ER	18	11	12	11
	nuclei	91	56	47	33
	cyto	145	88	119	54

As expected, the number of hits and candidates for wt cell line (incapable of H_2O_2 generation in response to D-Ala) was close to zero. More hits and candidates were identified upon H_2O_2 generation in the ER, however, much less than in the nuclei and the cyto cell lines. The nuclei and the cyto cell lines had much more proteins with high abundance/stability score, in comparison to both

the wt and ER cell lines. The number of hits and candidates identified in the cyto cell line was the largest among all cell lines.

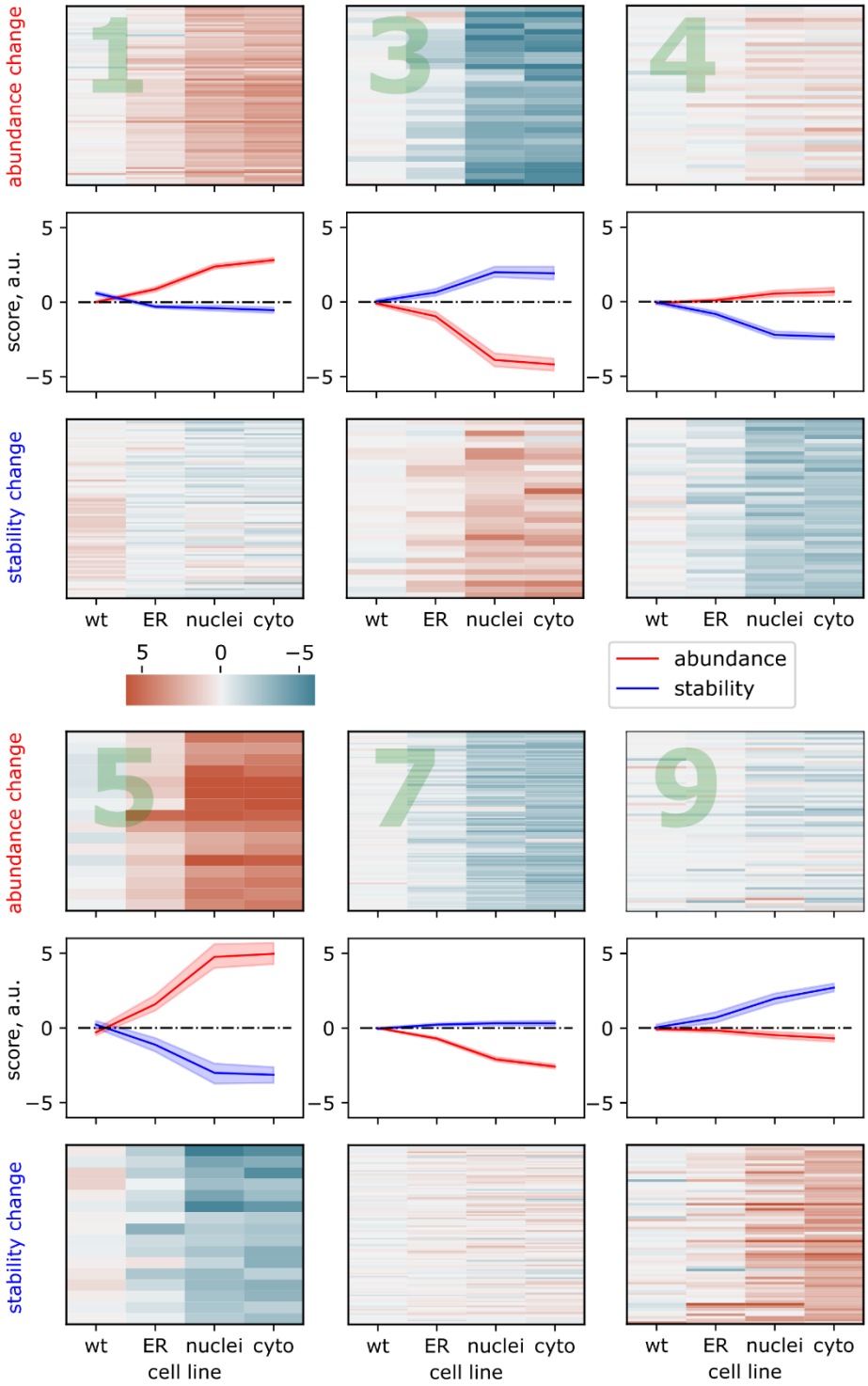

Figure 4.21: *Results of k-means cluster analysis (1). Six clusters uniting hit and candidate proteins with comparatively similar abundance/stability changes in response to elevation of H_2O_2 level in the cytosol and the nucleus (in the cyto and the nuclei cell lines). Clusters are represented by vertical panels consisting of three figures each. Three figures: top – heatmap of*

protein abundance changes; middle – line plots depicting mean abundance and stability changes of all proteins of the cluster, shades around lines depicting std; bottom - heatmap of protein stability changes. wt – wild type HEK293 cell line (original), ER – HEK293 TagBFP-DAO-KDEL, nuclei – HEK293 HyPer-DAO-3NLS, cyto – HEK293 HyPer-DAO-NES.

4.9.4 Cluster analysis

To group hit and candidate proteins identified in our study based on the magnitude of abundance and stability changes in response to D-Ala addition to cell lines, we performed cluster analysis. Cluster analysis of hit and candidate proteins characterized with abundance and stability changes in each of four cell lines was performed in eight-dimensional space (each protein was represented with eight values). Figures 4.21 and 4.22 represent each cluster as a vertical panel of three graphs. Derived nine clusters were further united into three groups based on mean abundance and stability changes of proteins forming a cluster (middle graph in each cluster panel).

The first group included six clusters (Figure 4.21), which united proteins characterized with similar abundance/stability changes in response to elevation of H_2O_2 level in the cytosol and the nucleus. The response of proteins of these clusters to H_2O_2 generated in the cytosol and in the nucleus was much stronger than respective response to H_2O_2 generated in the ER-lumen.

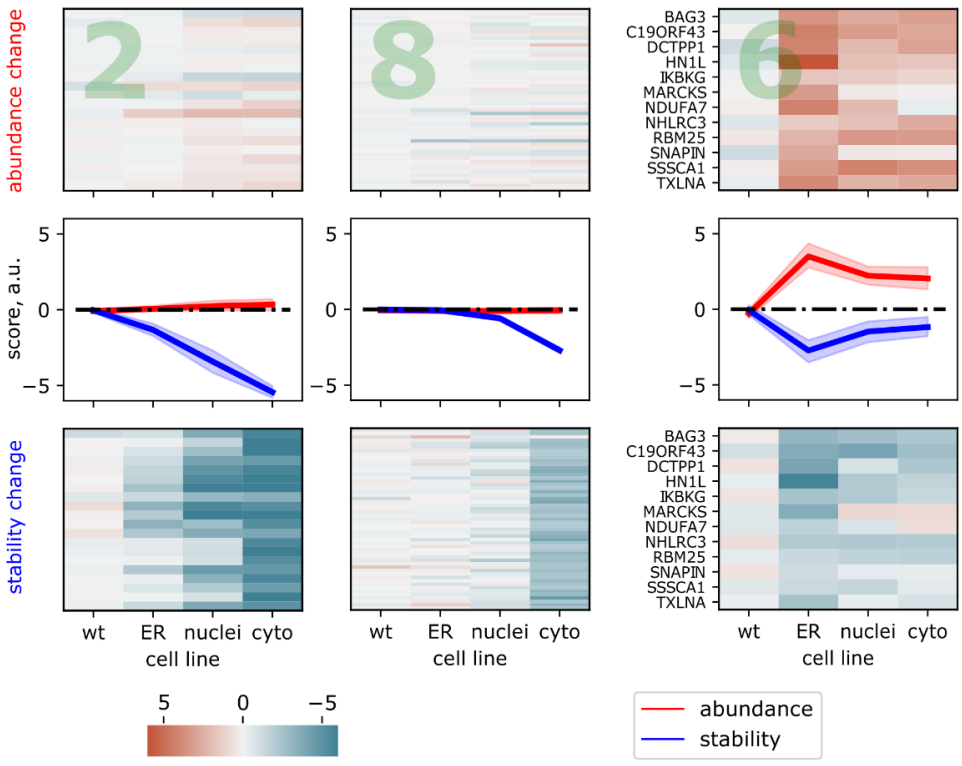

Figure 4.22: *Results of k-means cluster analysis (2). Two clusters (2 and 8) uniting hit and candidate proteins with highest stability changes in response to elevation of H_2O_2 level in the*

cytosol (cyto) and one cluster (6) – proteins with the highest abundance and stability changes in response to H_2O_2 generated in the ER-lumen. Clusters are represented by vertical panels consisting of three figures each. Three figures: top – heatmap of protein abundance changes; middle – line plots depicting mean abundance and stability changes of all proteins of the cluster, with shades around lines depicting std; bottom - heatmap of protein stability changes. wt – wild type HEK293 cell line (original), ER – HEK293 TagBFP-DAO-KDEL, nuclei – HEK293 HyPer-DAO-3NLS, cyto – HEK293 HyPer-DAO-NES.

The second group consisted of two clusters – 2 and 8 (Figure 4.22). These clusters combined proteins, which changed only stability. Proteins of cluster 2 changed stability in response to H_2O_2 generated in all three cellular compartments, with highest changes in response to elevation of cytosolic H_2O_2, then nuclear and finally H_2O_2 generated in the ER-lumen. Meanwhile, proteins of cluster 8 responded only to H_2O_2 produced in the cytosol. Proteins of these two clusters did not change abundance regardless of a cellular compartment, which generated H_2O_2.

The third group included only cluster 6, which united 12 proteins in total (Figure 4.22). These proteins were characterized with strong abundance and stability changes in response to elevation of H_2O_2 level in the ER-lumen and relatively small changes in response to H_2O_2 accumulation in the nucleus or in the cytosol.

4.9.5 Gene ontology enrichment analysis

To retrieve functional profiles of derived clusters and to get more information about cellular components (CC) the proteins are constituent of, molecular functions (MF), which proteins execute, and biological processes (BP) proteins are involved in, gene ontology enrichment analysis (GOEA) was performed for each of the obtained clusters (Figure 4.23).

Terms of all three gene ontology domains (CC, BP and MF) associated with protein synthesis, RNA-binding and ribosome formation were found to be significantly overrepresented in cluster 1 (Figure 4.23). The reason is that cluster 1 comprised many ribosomal proteins (> 40), including 60S ribosomal proteins: L6 (RPL6), L7a (RPL7A), L13 (RPL13) etc.; as well as 40S ribosomal proteins: S3a (RPS3A), S6 (RPS6), S23 (RPS23) etc., which increased abundance (presence in soluble fraction) upon H_2O_2 generation (Figure 4.21).

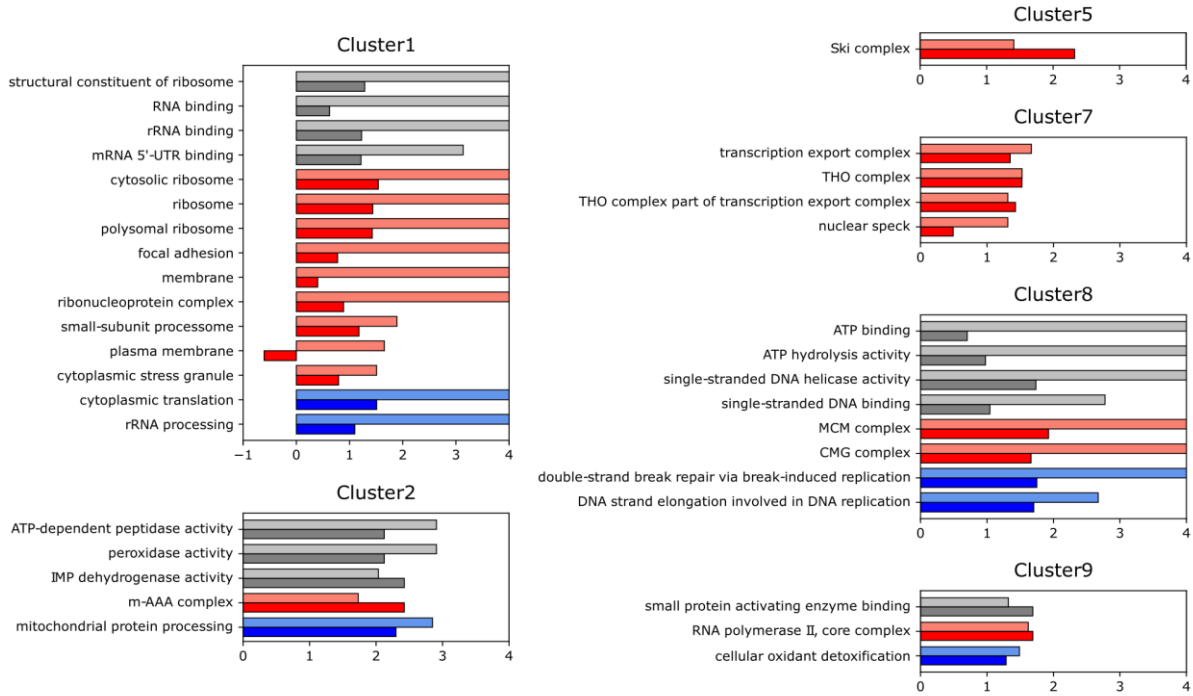

Figure 4.23: *Results of gene ontology enrichment analysis performed for derived clusters. Grey colour palette (grey and silver) represents Molecular Function terms, red (red and salmon) – Cellular Component terms and blue (blue and cornflowerblue) – Biological Process terms. Lighter colours (silver, salmon and cornflowerblue) represent negative log_{10}(adj. p-value), while darker ones (grey, red and blue) denote log_{10}(overrep-n). Overrep-n – overrepresentation, adj. p-value – adjusted p-value. Gene ontology terms were used from the following resource: (Ashburner et al., 2000; Carbon et al., 2021). After analysis redundant GO terms were removed using Revigo (Supek et al., 2011).*

The next cluster of interest in the first group is cluster 5. Cluster 5 was found to be enriched only in SKI complex, which was represented with two proteins in this cluster: helicase SKI2W (SKIV2L) and tetratricopeptide repeat protein 37 (TTC37) and with one protein, WD repeat-containing protein 61 (WDR61, also constituting PAF1 complex) in cluster 1. The SKI protein complex represents a tetramer of SKIV2L, TTC37, and WDR61 with 1:1:2 stoichiometry, has helicase activity (SKIV2L), and is necessary for operation of the exosome in the cell cytoplasm (Halbach et al., 2013; Zinder & Lima, 2017). Exosome complex has 3'-to-5' mRNA digestion activity and particularly participates in non-stop decay (NSD), a process of recognition and elimination of mRNA molecules with attached ribosomes stalled at 3'-end of mRNAs due to poly(A)-tail readthrough (van Hoof et al., 2002). Interestingly, SKI complex changed solubility only at low temperatures under oxidative stress (Figure 4.24, A). Evidently, under higher temperature this complex rapidly aggregated and precipitated without any connection to stress conditions.

Cluster 7 was found to be enriched in proteins constituting conserved multi-subunit nuclear THO complex, which consists of six proteins (THOC1-3, 5-7), three of which, THO complex subunit 1, 2 and 5 (THOC1, THOC2, THOC5), were represented in the cluster. THO complex as a core part of a larger and dynamic TREX (TRanscription and EXport) complex links together gene transcription, mRNA processing and export of derived mRNA from the nucleus into the cytosol (Heath et al., 2016; Jimeno & Aguilera, 2010). Processing of at least some mRNA molecules in the nucleus was found to be coordinated by THO complex via physical interaction with ZC3H14 (zinc finger CCCH-type containing 14) protein (Morris & Corbett, 2018). ZC3H14 is an RNA binding protein, which binds to a poly(A)-tail of mRNA molecules, and is involved in several post-transcriptional processes, such as regulation of length of mRNA poly(A)-tail (Kelly et al., 2014), mRNA splicing (Soucek et al., 2016) and nuclear export (Marfatia et al., 2003). Similar melting curves of ZC3H14 and components of THO complex also suggests interaction of these proteins (Figure 4.24, B).

The last cluster of the first group, cluster 9, was enriched in proteins forming core of the RNA polymerase II (Pol II), which takes part in the generation of several RNA species, and mRNA particularly (Sims et al., 2004). Pol II is a protein complex, which consists of multiple subunits, three the largest ones of which: RPB1, RPB2, RPB3 (POLR2A, POLR2B, POLR2C) were found to increase thermostability in our study upon intracellular H_2O_2 generation (Figure 4.24, C).

The second group of clusters contained proteins, which changed only stability in response to H_2O_2 production, most prominently (cluster 2) or only (cluster 8) in the cytosol. Cluster 2 was enriched in proteins with metalloendopeptidase activity: matrix ATPases associated with diverse cellular activities AAA (m-AAA) protease: paraplegin (SPG7), AFG3-like protein 2 (AFG3L2); and intermembrane AAA (iAAA) protease composed of an ATP-dependent zinc metalloprotease YME1L1 (YME1L1). These proteins are involved in mitochondrial protein quality control (Quirós et al., 2015). In addition, several peroxidases: glutathione peroxidase 1, phospholipid hydroperoxide glutathione peroxidase and peroxiredoxin-5, (GPX1, GPX4 and PRDX5), well-known for participation in cellular response to oxidative stress and related redox processes were also significantly overrepresented in cluster 2.

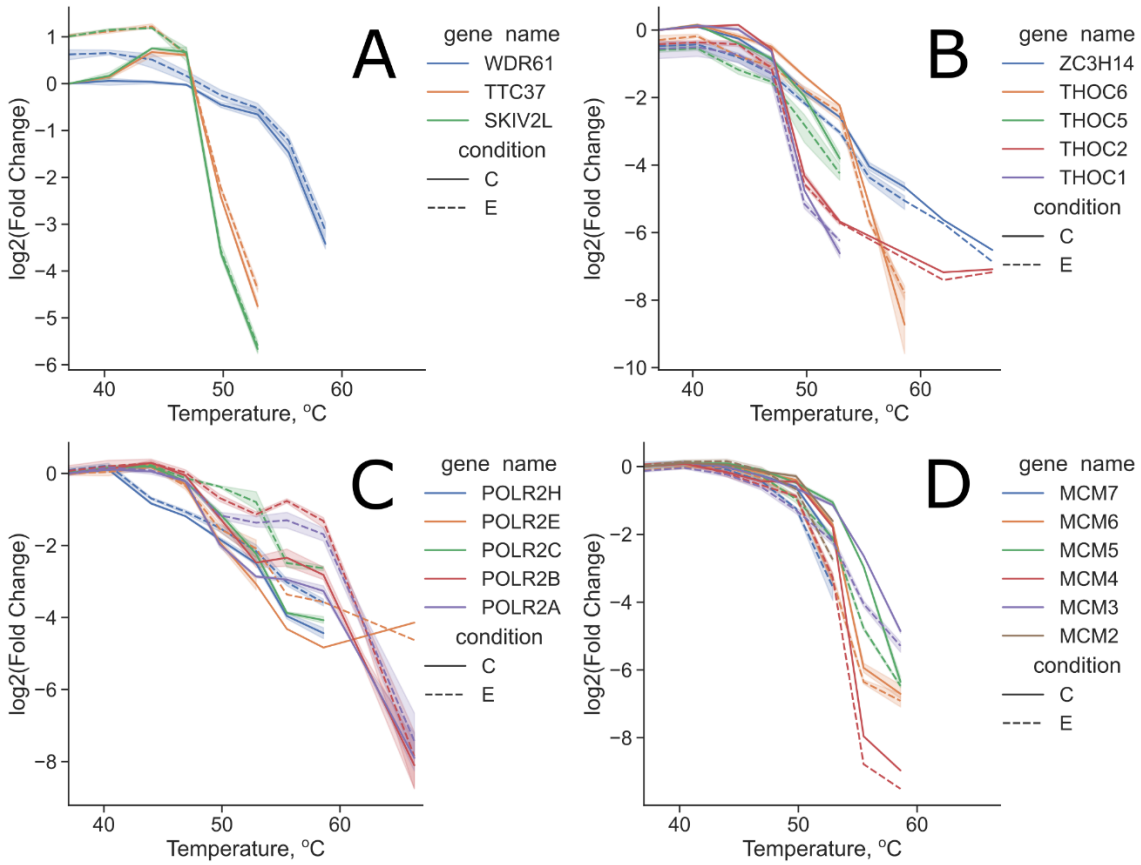

Figure 4.24: *Melting curves of proteins forming following protein complexes: (A) SKI complex, (B) THO complex, (C) RNA polymerase II, (D) MCM complex. Solid and dashed lines represent melting curves of proteins extracted from the cyto cell line treated with (experiment, E) or without (control, C) D-Alanine. Amount of a protein at each temperature was normalized to the amount of the protein in control at 37 °C (Fold Change). Shades around curves represent std. The picture was prepared by Alexey Nesterenko.*

Finally, cluster 8 was enriched in proteins implicated in organization of mini-chromosome maintenance protein (MCM) complex, which functions as a heterohexameric helicase in DNA replication (Parker et al., 2017). MCM complex consists of six replication licensing factors MCM2-7 assembled into a ring-like structure, five of which, namely MCM3-7, were identified in our study as significantly changing stability in response to H_2O_2 generated in the cytosol (Figure 4.24, D).

Other clusters were not significantly enriched in any of GO terms.

To get a better understanding of which GO terms were overrepresented in each of three cell lines stably expressing DAO, we performed another gene ontology enrichment analysis (Figure 4.25). The nuclei and the cyto cell lines emerged to be quite similar and had many common GO terms with more terms overrepresented in the cyto cell line.

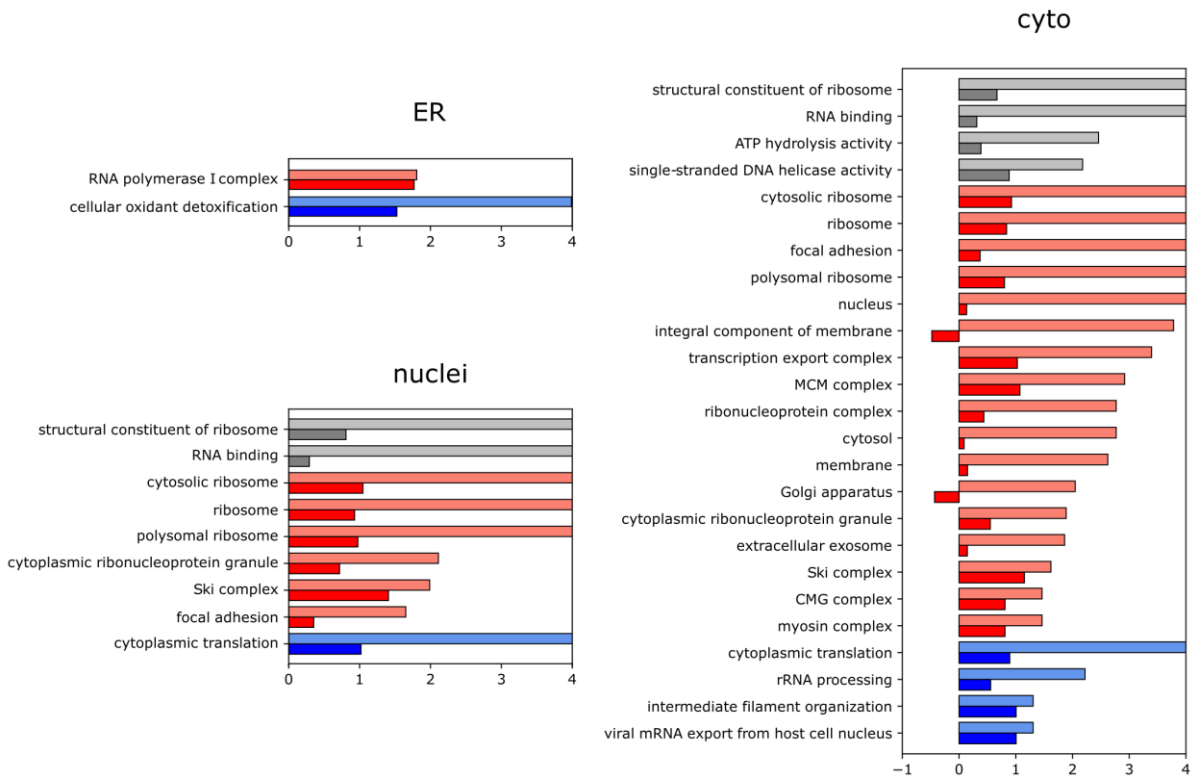

Figure 4.25: *Results of gene ontology enrichment analysis performed for three cell lines stably expressing DAO. Grey colour palette (grey and silver) represents Molecular Function terms, red (red and salmon) – Cellular Component terms and blue (blue and cornflowerblue) – Biological Process terms. Lighter colours (silver, salmon and cornflowerblue) represent negative* log_{10}*(adj. p-value), while darker ones (grey, red and blue) denote* log_{10}*(overrep-n). Overrep-n – overrepresentation, adj. p-value – adjusted p-value. Gene ontology terms were used from the following resource: (Ashburner et al., 2000; Carbon et al., 2021). After analysis redundant GO terms were removed using Revigo (Supek et al., 2011).*

These results were expected, since as shown in Figure 4.21 many proteins forming six clusters similarly responded to H_2O_2 generated in the nuclei and the cyto cell lines. For instance, one can clearly see that both cell lines were essentially enriched in GO terms related to protein synthesis, RNA-binding and ribosome formation – all of which, as mentioned previously, were overrepresented in cluster 1. Meanwhile, the ER cell line remarkably differed from the nuclei and the cyto cell lines (Figure 4.25). Despite the proteins, which significantly changed abundance or stability in response to H_2O_2 generated in the nucleus and the cytosol, responded less pronouncedly to H_2O_2 generated in the ER-lumen, proteins of the RNA polymerase I: RNA polymerase I subunits RPA1, RPA2 and RPA49 (POLR1A, POLR1B and POLR1E) appeared to be significantly overrepresented only in the ER cell line.

4.9.6 TPP database

To make TPP results available to researchers in redox biology and related fields of study, we organized the data in a database that will be soon publicly available in an online form. Currently, data are available in succinct form of tables via following link: https://drive.google.com/drive/folders/17SfrN5_9lU-XVdnOYQhpw3E4QWdWYcoX. Small parts of these tables displaying values corresponding to several proteins, namely CDIPT, Prx5 (PRDX5), and TXNRD1, are exemplified in Table 4.4-4.5.

4.10 Validation of Thermal Proteome Profiling results

To validate our TPP results and to demonstrate how the derived database can be utilized in future studies, we selected several hits and candidates as bait-proteins and performed co-immunoprecipitation (AP-MS – affinity-purification mass spectrometry) experiment with them.

Table 4.4: *Representation of TPP results database (1). Score value denotes calculated value of abundance/stability score. Significance represents negative log10(adj. p-value). Cells of the table based on which a protein was classified as «candidate» or «hit» are highlighted in yellow and orange, respectively.*

Gene name	Protein ID	Description	abundance								stability							
			wt		ER		nuclei		cyto		wt		ER		nuclei		cyto	
			score value	significance	score value	significance	score value	significance	score value	significance	score value	significance	score value	significance	score value	significance	score value	significance
CDIPT	B3KY94…	CDP-diacyl-glycerol-inositol 3-phosphatidyl transferase	-0.04	0.02	0.97	0.37	4.86	1.62	4.46	4.35	0.31	0.05	-1.96	1.14	-6.43	0.78	-4.93	2.28
PRDX5	P30044	Peroxiredoxin-5, mitochondrial	0.16	0.05	-0.05	0.03	0.22	0.04	0.02	0.02	-0.14	0.08	-2.20	0.83	-4.60	3.74	-4.98	3.78
TXNRD1	A0A087WSW…	Thioredoxin reduc-tase 1, cytoplasmic	0.03	0.03	0.06	0.03	0.41	0.08	0.39	0.06	-1.07	0.91	7.24	13.12	7.02	6.64	2.17	1.83

Table 4.5: *Representation of TPP results database (2). Found in MS runs – number of MS runs, where a protein was identified (max=15). FC (fold change) – mean ratio of protein amount in samples derived from cells treated with and without D-Ala and heated at a particular temperature (displayed after FC).*

Gene name	Protein ID	Description	Found in MS runs	cell line	FC 37.0	FC 40.4	FC 44.0	FC 46.9	FC 49.8	FC 52.9	FC 55.5	FC 58.6	FC 62.0	FC 66.3
CDIPT	B3KY94…	CDP-diacylglycerol-inositol 3-phosphatidyl transferase	15	wt	1.033	0.962	0.994	1.008	0.965	0.993	1.115	0.975	1.126	1.271
				ER	1.129	1.194	1.059	0.995	0.969	0.981	0.915	0.923	0.961	0.948
				nuclei	2.180	2.146	1.201	1.221	1.166	1.185	1.034	1.190	1.164	0.887
				cyto	2.035	1.933	1.283	1.437	1.186	1.188	0.950	1.393	1.368	0.990
PRDX5	P30044	Peroxiredoxin-5, mitochondrial	15	wt	1.008	1.041	1.027	1.012	0.989	1.040	1.028	0.945	0.952	1.108
				ER	1.010	0.975	0.982	0.995	0.924	0.834	0.856	0.737	0.730	0.698
				nuclei	1.012	1.056	1.025	0.977	0.869	0.754	0.617	0.449	0.319	0.971
				cyto	1.018	0.987	1.025	0.975	0.876	0.611	0.615	0.353	0.380	0.506
TXNRD1	A0A087WSW…	Thioredoxin reductase 1, cytoplasmic	15	wt	0.991	1.019	0.975	0.979	0.961	0.974	0.897	0.787	0.861	0.814
				ER	1.011	1.008	1.032	0.989	1.042	1.241	2.544	3.679	3.599	5.806
				nuclei	1.070	1.056	1.080	1.077	1.114	1.115	1.472	2.987	5.537	9.765
				cyto	1.059	1.061	1.102	1.117	1.048	0.869	0.900	1.065	1.826	4.589

4.10.1 Co-immunoprecipitation experiment

To investigate whether proteins identified as hits and candidates in TPP change stability due to altering binding partners, four proteins with C-terminal FLAG-tag: PARK7 (candidate, cluster 9), TRAP1 (hit, cluster 8), MAP2K1 (hit, cluster 8) and UBA2 (candidate, cluster 9) were utilized as bait-proteins for co-immunoprecipitation (Co-IP). PARK7 is a multifunctional protein with a great variety of reported activities, including deglycase (Richarme et al., 2015), protease (Chen et al., 2010), chaperone, etc., which are of a particular importance under oxidative stress (Mencke et al., 2021). TRAP1 (tumour necrosis factor receptor associated protein 1) is a mitochondrial HSP90-like chaperone (HSP75), which among other functions was reported to participate in the regulation of protein synthesis and the protection from the ER stress (Swann Matassa et al., 2014) as well as the prevention of mitochondrial permeability transition pore opening and the regulation of mitochondrial respiration (Masgras et al., 2017). We also selected MAP2K1 (MEK1), a well-known participant of a RAF/MEK/ERK (MAPK) signalling pathway, and UBA2, a subunit of an E1 activating enzyme involved in a process of protein SUMOylation (Stankovic-Valentin & Melchior, 2018).

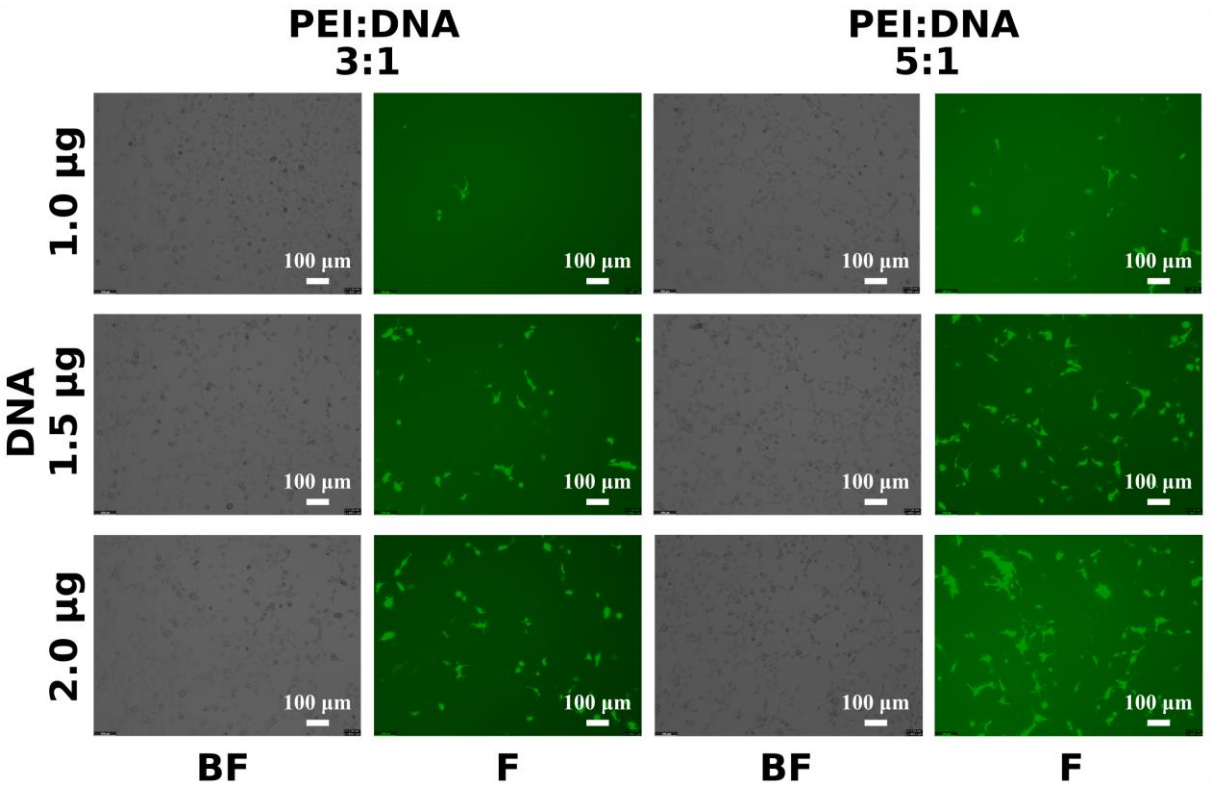

Figure 4.26: *Results of PEI transfection optimization of wt HEK293 cells. HEK293 were transfected with pASIET-EGFP plasmid in wells of a 6-well plate. BF – bright-field, F – fluorescence microscopy.*

Since efficiency along with toxicity are cornerstones of every transfection-based protein overexpression experiment, prior to implementation of co-immunoprecipitation we optimized polyethylenimine (PEI) transfection of HEK293 cells. We examined effects of various combinations of PEI to DNA amounts ratio and total DNA amount (and PEI accordingly) on transfection efficiency and toxicity using wt HEK293 cells (Figure 4.26). Upon cell transfection with EGFP encoding plasmid, efficiency was estimated visually based on fluorescence (green) channel, while toxicity – mostly via bright-field channel. Obtained results indicate that the best transfection efficiency was achieved using 5:1 PEI to DNA amounts ratio and 2.0 μg of DNA (10.0 μg of PEI). Due to both efficiency and toxicity of transfection were admissible, we used this combination for the co-immunoprecipitation experiment. This amount of EGFP encoding plasmid (2.0 μg) corresponds to 0.280 pmol of DNA. Since transfection optimization was performed in wells of a 6-well plate, this amount needed to be recalculated for transfection of cells in 15-cm dishes, which were used for co-immunoprecipitation experiment. Considering that surface area of a 15-cm dish is around 15 times larger, than that of a 6-well plate well (surface areas are 145 and 9.6 cm^2, respectively) 4.26 pmol of a plasmid encoding one of FLAG-tagged bait protein was used for transfection of cells in a 15-cm dish.

Since all four proteins most significantly changed stability in response to H_2O_2 generated in the cytosol, only the cyto and wt (control) HEK293 cell lines were transiently transfected with plasmids encoding FLAG-tagged proteins of interest (POIs) and treated with or without 2mM of D-Ala according to the scheme (Table 4.6).

Table 4.6: *Utilized conditions for co-immunoprecipitation experiment.*

condition	cell line	POI	D-Alanine
CPD	cyto	+	+
CP	cyto	+	–
CD	cyto	–	+
WPD	wt	+	+
WP	wt	+	–

Co-IP experiment was fulfilled according to the procedure described in the respective section of the method part. After experiment derived samples were analysed for the amount of POI with SDS-PAGE and Western Blot (WB) (Figure 4.27).

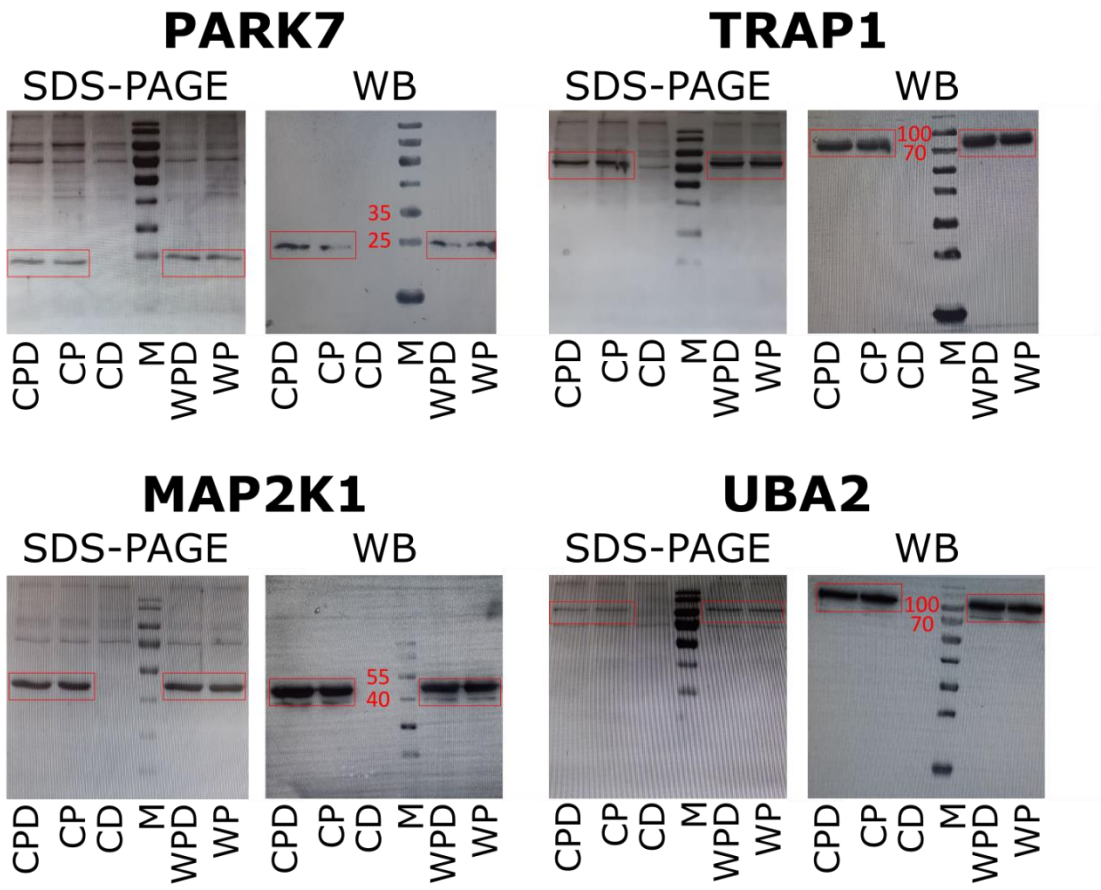

Figure 4.27: *Validation of protein expression after HEK293 cells transfection with plasmids encoding one of four FLAG-tagged proteins of interest (POIs) or empty plasmid by SDS-PAGE and Western Blot (WB). After each SDS-PAGE proteins were transferred on a membrane, and a polyacrylamide gel with remaining proteins was stained with Coomassie Blue (SDS-PAGE). The membrane with transferred proteins was treated sequentially with primary (anti-FLAG) and secondary antibodies (WB). Molecular weights (observed) of target proteins: PARK7 – 20 (25) kDa, TRAP1 – 75 kDa, MAP2K1 – 49.2 kDa, UBA2 – 75 (~100) kDa. Red frames display bands corresponding to POIs, red numbers – close molecular weights (kDa) of protein markers. Each experimental condition is denoted as an abbreviation of several symbols, wherein C denotes HEK293 HyPer-DAO-NES (cyto) cell line, D – presence of D-Ala (2mM), P – expression of POI in cells, W – wild type HEK293 cells. M – PageRuler™ Prestained Protein Ladder, 10 to 180 kDa (Thermo Scientific, 26617).*

4.10.2 Quality estimation of performed co-immunoprecipitation

Samples (three replicates/condition, five conditions/protein) were processed according to the protocol described in the respective section of the method part and analysed by MS. MS results were analysed and numbers of spectral counts, peptides and proteins were calculated (Tables 4.7-4.8). The sample of MAP2K1 protein corresponding to the first replicate of WP condition was discarded and not taken into account due to a low number of identified proteins in the sample.

All values for UBA2 samples had higher standard deviation (displayed in red) than respective values for other proteins. This difference is due to higher amount of protein in UBA2 samples of the first replicate, which in turn can be explained with apparently not sufficient removal of non-specific proteins during washing step. In average, samples contained more than a thousand proteins each, most of which, despite presence of a washing step, were non-specifically bound proteins.

Table 4.7: *Proteomics data characteristics of POI-containing samples. Quantities (mean ± std) of spectral counts (razor), proteins (razor peptide ions > 1 and razor intensity > 0) and respective peptides calculated for Co-IP samples based on MS results are represented. Only samples derived from cells overexpressing a protein of interest (corresponding to four conditions: CPD, CP, WPD and WP) were taken into account. For each protein, except MAP2K1, first replicate of which WP was discarded, twelve samples in total were used for calculation.*

Protein	Spectral Counts	Peptides	Proteins
PARK7	11534 ± 2216	10923 ± 1441	1141 ± 144
TRAP1	9837 ± 3097	8226 ± 2199	1067 ± 240
MAP2K1	10433 ± 2405	8240 ± 1645	1053 ± 221
UBA2	10588 ± 4077	9187 ± 3247	1148 ± 393

Table 4.8: *Proteomics data characteristics of POI-free samples. Quantities (mean ± std) of spectral counts (razor), proteins (razor peptide ions > 1 and razor intensity > 0) and respective peptides calculated for Co-IP samples based on MS results are represented. Only samples derived from cells transfected with an empty plasmid (corresponding to the CD condition) were taken into account. For each protein, three samples (replicates) were used for calculation.*

Protein	Spectral Counts	Peptides	Proteins
PARK7	10709 ± 1642	10552 ± 1135	1353 ± 155
TRAP1	12466 ± 3903	10992 ± 2044	1381 ± 284
MAP2K1	11952 ± 2805	10031 ± 1685	1264 ± 220
UBA2	11025 ± 4807	9506 ± 3135	1185 ± 394

Further, we estimated quantities of POI and HyPer-DAO in each sample (Figure 4.28). Since FLAG-tagged POIs were not expressed in CD condition, these proteins (their endogenous counterparts), as expected, were found in substantially lower amount in CD conditions than in conditions, where POIs were expressed. In addition, the difference in POI amounts between conditions with and without POI were found to vary depending on a particular POI and reflecting the amount of POI overexpressed and/or quality of magnetic bead washing and of protein elution steps during co-immunoprecipitation. For UBA2 this difference

was the least pronounced perhaps due to the amount of expressed UBA2-FLAG was less than of other POIs (Figure 4.27). HyPer-DAO protein was expressed only in HEK293 cyto cell line, but not in wt cells, thus, it was expected to be identified only in CPD, CP and CD, but not in WPD and WP conditions. Nevertheless, though in smaller amounts, HyPer-DAO protein was identified in all samples, including those ones derived from wt cells. Perhaps HPLC column of LC-MS/MS setup was not washed thoroughly between separation of samples and some remaining peptides from previous samples derived from the cyto cell lines were eluted together with the samples derived from wt cells.

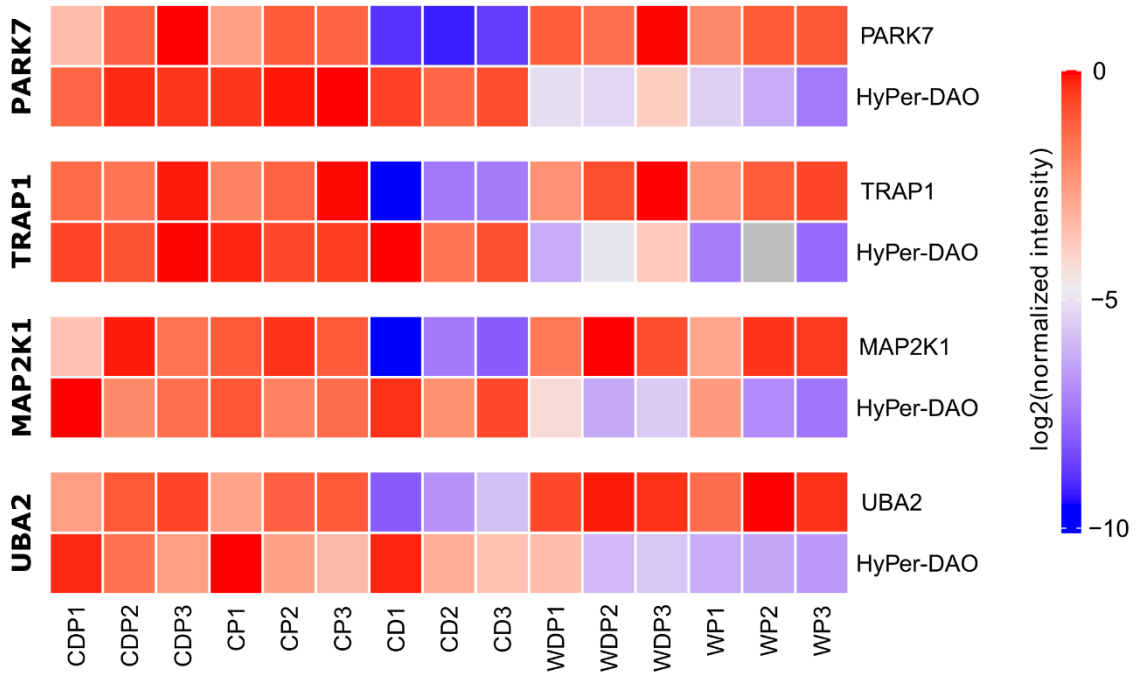

Figure 4.28: *Quantities of two proteins (overexpressed FLAG-tagged protein of interest + endogenous counterpart and HyPer-DAO) identified in Co-IP samples. Protein quantity in each sample is represented as a logarithm of protein amount previously normalized to the maximum protein amount in the raw of samples. Designations of conditions are explained earlier (Table 4.6). Numbers behind designations of conditions indicate number of a replicate. The picture was prepared together with Vasilina Tereshchuk.*

To get a better grasp of protein composition of derived samples and of the extent of their similarity, Venn diagrams were plotted (Figure 4.29). Each experimental condition (coloured ellipse) of protein diagrams represents a protein set identified in all three biological replicates (the same POI and condition). One can clearly see that different conditions of the experiment with the same target protein (POI) have significant degree of similarity, and numbers in the centre of each diagram, which represent a number of proteins identified in all compared

conditions, have largest values and constitute more than a half or, in three of four cases, more than 65% of all proteins.

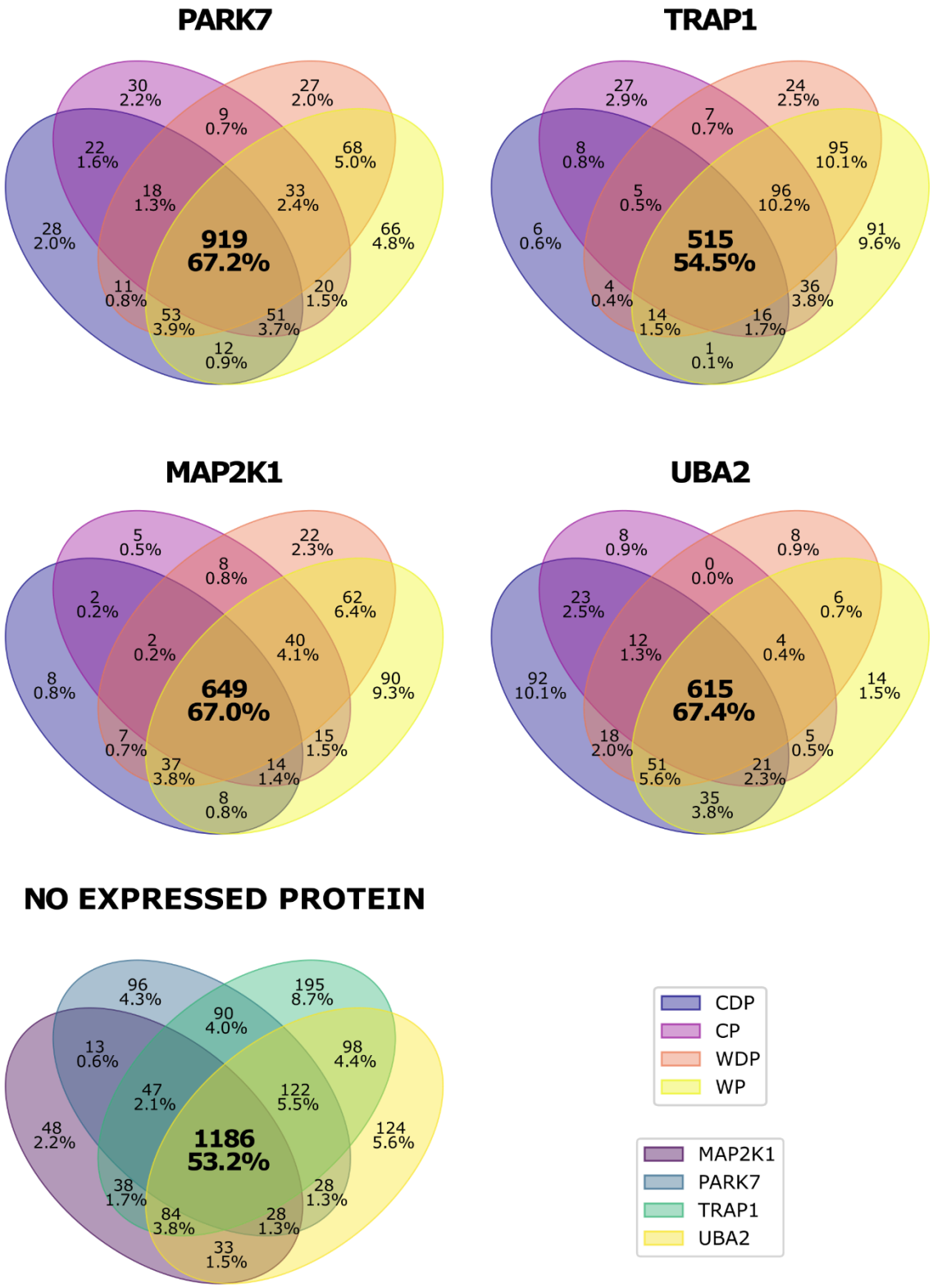

Figure 4.29: *Venn diagram showing similarity of protein sets identified in Co-IP samples. Top four Venn diagrams stained with the same colourmap represent conditions, wherein the same*

protein of interest (POI) was expressed. The last diagram, «no expressed protein», represents protein sets corresponding to CD conditions from experiments with different POIs, wherein POI itself was not expressed. C indicates HEK293 HyPer-DAO-NES (cyto) cell line, D – presence of D-Alanine (2mM), P – expression of POI in cells, W – wild type HEK293 cells.

4.10.3 TRAP1

We identified only two proteins, which significantly varied interaction with TRAP1 under oxidative stress: α- and β-MPP (PMPCA and PMPCB) (Figure 4.30, A) (Table S1). These two proteins form a mitochondrial processing peptidase (MPP), a mitochondria protein complex, which functions as a part of mitochondrial protein import machinery and removes N-terminal mitochondrial targeting sequence (MTS) from preproteins (Braun & Schmitz, 1997). Both of MPP constituents were found in significantly higher amount in CPD samples than in any other samples, which suggests enhanced interaction of MPP with TRAP1 under oxidative stress conditions.

Since TRAP1 is a mitochondrial protein, predominantly localized in the matrix, it synthesizes with MTS and is imported into mitochondria, wherein its MTS should be removed by MPP (Altieri et al., 2012; Felts et al., 2000). To figure out whether enhanced binding of TRAP1 to MPP under oxidative stress conditions is accompanied with increased amount of processed TRAP1, we estimated quantities of peptides corresponding to the mitochondrial targeting sequence of TRAP1 in CPD and CP conditions. We found similar quantities of these peptides in both conditions (Figure 4.31), which suggests that oxidative stress does not affect MPP-mediated cleavage of TRAP1 and most likely TRAP1 mitochondrial import.

4.10.4 PARK7

In our study we found that CPD samples of PARK7 were substantially enriched in several proteins (higher amounts in CPD samples than in other ones) (Figure 4.32). These several proteins were three chaperones: endoplasmic reticulum chaperone BiP (HSPA5/GRP78), heat shock protein 105 kDa (HSPH1) and mitochondrial HSP70 – HSPA9 (GRP75/HSPA9B/mtHSP70/mortalin) (Table S2). Besides abovementioned chaperones, we found that three other chaperones: heat shock protein family A (Hsp70) member 1A (HSPA1A), 1B (HSPA1B) and heat shock cognate 71 kDa protein (HSPA8) were also present in increased amounts in CPD samples of PARK7. However, one can clearly see that three latter chaperones presented in higher amounts not only in CPD, but also in all samples derived from the cyto cell line (CPD, CP and CD), even where the bait protein was not expressed (CD).

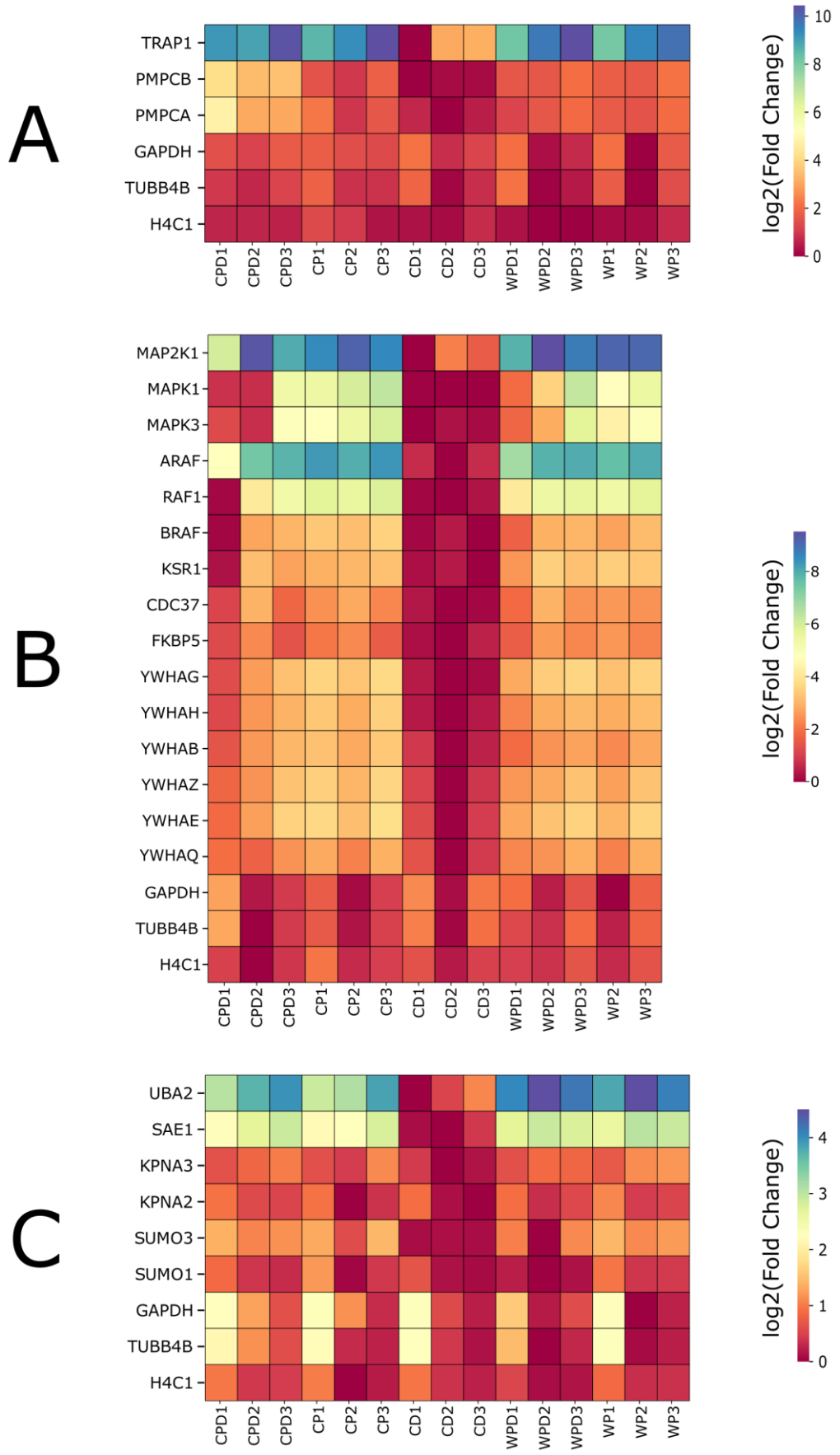

Figure 4.30: *Quantities of some proteins (denoted by gene names) identified in TRAP1 (A), MAP2K1 (B) and UBA2 (C) samples obtained in Co-IP experiment. Protein quantity in each*

sample is represented as a logarithm of protein amount previously normalized to the maximum protein amount in the raw of samples. Designations of conditions were explained earlier (Table 4.6). Numbers behind designations of conditions indicate number of a replicate. The picture was prepared with Alexey Nesterenko.

Statistical factor analysis of all four pulldown-MS experiments showed that these proteins can be considered as non-specifically bound to beads under oxidative conditions (Table S5). As an evident example of such non-specific hits MOB2 protein can be mention (Figure 4.32). Nevertheless, the difference between CPD and CP/CD samples was obvious that may indicate the enhanced interaction of these chaperones with PARK7 under oxidative conditions.

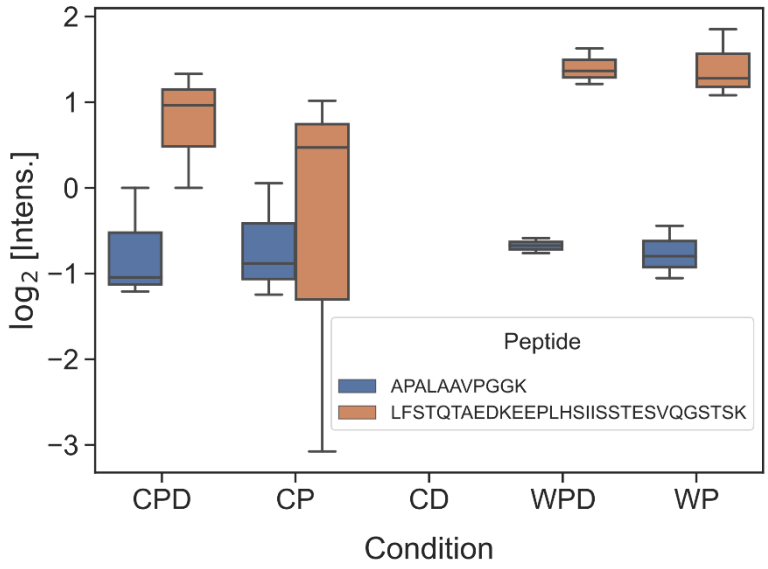

Figure 4.31: *Comparative quantities of two peptides corresponding to the mitochondrial targeting sequence of TRAP1 in different TRAP1 samples derived from cells treated with or without D-Alanine.*

Since some chaperones appeared to be able to non-specifically bind to the agarose resin especially in response to oxidative stress (e.g., HSPA1A and 1B, Table S5), we estimated amounts of chaperones identified in PARK7 samples in TRAP1 samples as well (Figure 4.32). One can see that protein interaction patterns of PARK7 and TRAP1 were different and particularly, in contrary to PARK7, there were no differences in amounts of HSPA5 and HSPH1 between TRAP1 samples. Furthermore, similar to PARK7, amounts of HSPA1A and 1B were increased in CPD, CP and CD samples of TRAP1, however, unlike PARK7, there were no differences in amounts of these chaperones between CPD and CP/CD TRAP1 samples. Obtained Co-IP results suggest that changes of

thermostability observed for PARK7 can be explained by changed pattern of its interactions with chaperone proteins.

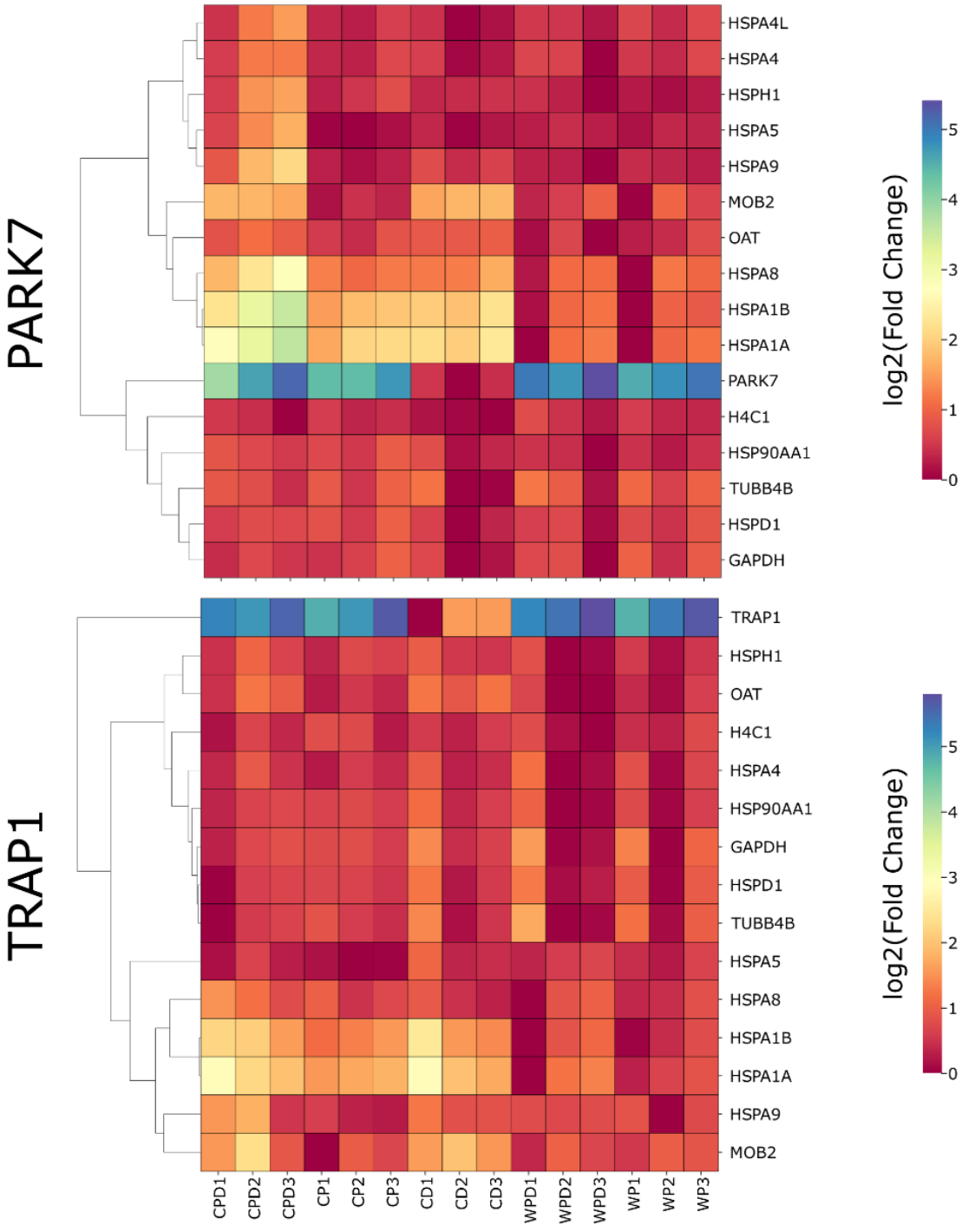

Figure 4.32: *Comparative analysis of chaperone representation in PARK7 (top) and TRAP1 (bottom) samples. Protein quantity in each sample is represented as a logarithm of protein amount previously normalized to the maximum protein amount in the raw of samples. Designations of conditions were explained earlier (Table 4.6). Numbers behind designations of conditions indicate number of a replicate. The picture was prepared by Alexey Nesterenko.*

4.10.5 MAP2K1

RAF/MEK/ERK (MAPK) signalling pathway is a well-known cascade of protein kinases that regulates various cellular processes: proliferation, survival, differentiation etc., (Roberts & Der, 2007). MEK represents a kinase of the middle tier, it is activated by RAF kinase and in turn activates ERK. MEK functions as a stable heterodimer of MEK1 (referred hereinafter as MAP2K1) and MEK2 (MAP2K2), which are different despite high degree of sequence similarity (Caunt et al., 2015).

As a result of Co-IP experiment performed with cells transiently overexpressing MAP2K1, a dual specificity mitogen-activated protein kinase kinase 1 as a bait protein, we identified a group of proteins known to interact with MAP2K1 (Figure 4.30, B). Among these proteins were upstream: ARAF, BRAF, RAF1 (CRAF) and downstream: ERK2 (MAPK1), ERK1 (MAPK3) kinases and adapter proteins: KSR1 and various 14-3-3 proteins (YWHAG, YWHAB, YWHAH, YWHAZ, YWHAE, YWHAQ) participating in the RAF/MEK/ERK pathway (Caunt et al., 2015; Obsilova & Obsil, 2020). Co-IP samples derived from cells, in which MAP2K1-FLAG was expressed, contained all of abovementioned RAF/MEK/ERK pathway-related proteins in significantly higher amounts than samples derived from cells, in which MAP2K1-FLAG was not expressed (Table S3). These data suggest that MAP2K1 indeed binds to aforementioned proteins. However, amounts of most of identified protein interactors did not differ between MAP2K1-FLAG containing samples. This may be explained by insensitivity of interactions of these proteins with MAP2K1 to oxidative stress. Nevertheless, for three proteins (RAF1, MAPK3 and MAPK1), we found statistically significant differences between conditions. This may indicate that binding of these proteins to MAP2K1 decreases in response to oxidative stress, however, considering substantial variation between CPD replicates (Figure 4.30, B), further experimental validations are required to prove this assumption.

Since interactome of MAP2K1 perhaps does not change in response to cytosolic H_2O_2 generation, we tried to find out the reason for decreased thermostability, which MAP2K1 revealed in TPP, by examination of differences in amounts of individual MAP2K1 peptides between TPP samples derived from the same cell line, but treated with and without D-Ala. Since we did not consider modified peptides in the search step of raw MS data analysis, a difference in amount of the same peptide of a protein between two samples may reflect alterations in a status of post-translational modifications of amino acids in that peptide. Only one of MAP2K1 peptides was identified in a substantially lower

amount (around two times) in samples derived from the nuclei and the cyto cell lines after treatment with D-Ala (Figure 4.33). This peptide contained T286 – one of twelve putative phosphorylation sites in human MAP2K1 (S72, S212, S218, S222, S231, T286, T292, S298, Y300, S385, T386 and T388) (Kinoshita et al., 2016). Thus, the observed decrease in amount of the peptide containing T286 can be explained by the increased phosphorylation of T286 under oxidative stress condition that in turn could have led to the observed decrease of MAP2K1 thermostability. T286 in MAP2K1 is known to be phosphorylated by the key regulator of cell cycle progression – cyclin-dependent kinase 1 (CDK1) (Harding et al., 2003; Rossomando et al., 1994). Phosphorylation of T286 in MAP2K1 by cyclin B-CDK1 leads to decreased phosphorylation (and activation) of ERK during mitosis, a phase of the cell cycle characterized with the highest H_2O_2 level that is required for CDK1 activation (Heo et al., 2020).

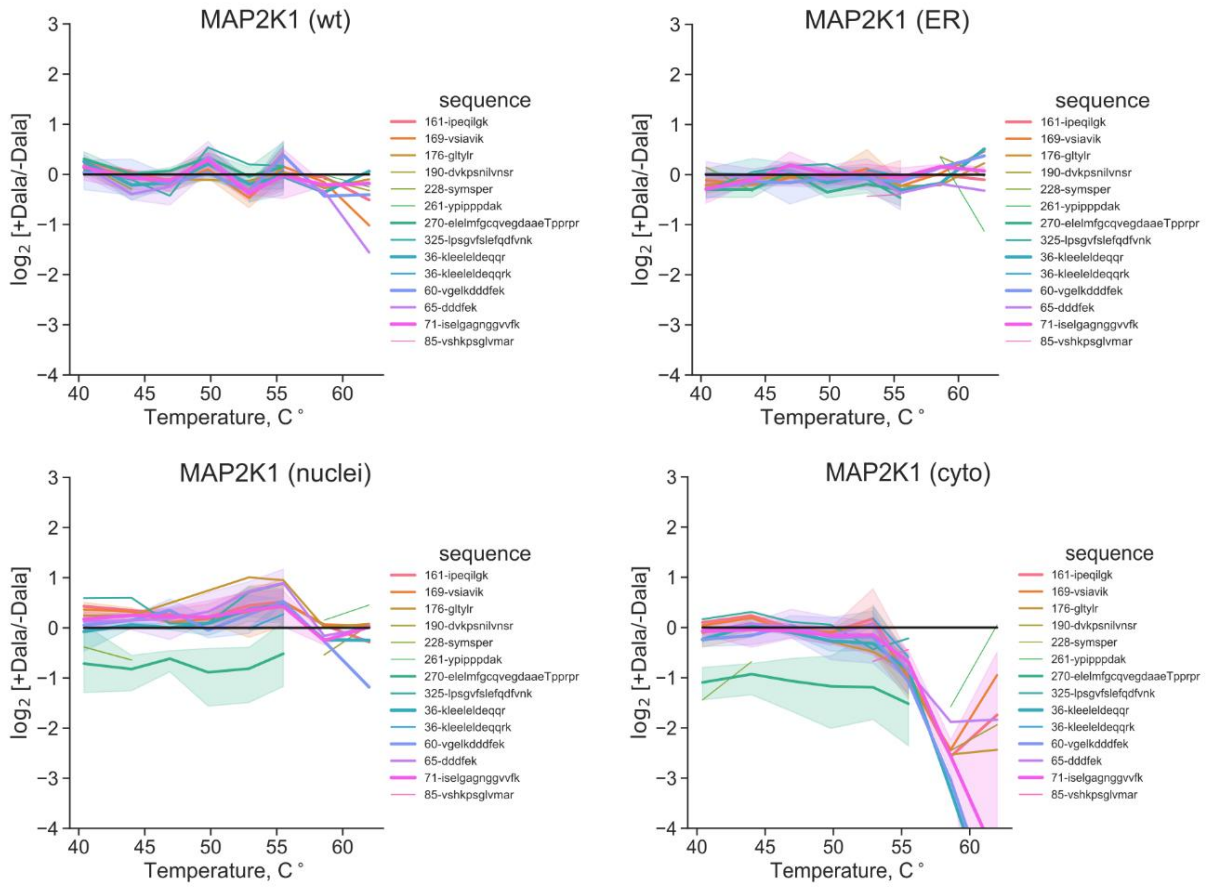

Figure 4.33: *Quantities of MAP2K1-specific peptides detected in TPP samples that were derived from four HEK293 cell lines treated with or without D-Ala and heated at different temperatures. Width of curves corresponds to the contribution of the peptide to protein quantification. Shades around curves represent variation of peptide quantities between different replicates (std). Uppercase letters in peptide sequences denote amino acid residues, which undergo PTMs according to UniProt.*

4.10.6 UBA2

Protein SUMOylation is a post-translational modification mediated by covalent attachment of Small Ubiquitin-like MOdifier (SUMO) proteins to a target protein. As the name suggests, protein SUMOylation strongly resembles ubiquitination and fulfilled with a group of proteins successively acting in the following order: E1 activating enzyme, a heterodimer consisting of SAE1 (AOS1) and UBA2 (SAE2); E2 conjugating enzyme UBC9 (UBE2I); and one of multiple E3 ligases (Stankovic-Valentin & Melchior, 2018). Besides proteins involved in SUMOylation, cells also contain enzymes, which remove SUMOs from target proteins (deSUMOylation), SUMO proteases (isopeptidases). Some participants of protein SUMOylation are known to be regulated by ROS and H_2O_2 particularly. Thus, E1 activating (UBA2) and E2 conjugating (UBC9) enzymes of protein SUMOylation machinery contain catalytic cysteine residues in active sites, which upon oxidation form an intermolecular disulfide bond between E1 and E2 enzymes that leads to inactivation of both enzymes (Bossis & Melchior, 2006). In addition, deSUMOylation enzymes are also known to be redox-regulated, e.g., isopeptidases SENP1, 2 and 3 (Stankovic-Valentin & Melchior, 2018).

As a result of the Co-IP experiment with UBA2-FLAG, we identified several known UBA2 co-interactors (Figure 4.30, C). Among them SAE1, which was substantially overrepresented in UBA2-FLAG samples that is in accordance to the fact that SAE1 and UBA2 form a heterodimer. SUMO2/3 (two isoforms are 95% identical and usually cannot be distinguished) was also found in high amounts, much higher than SUMO1 that can reflect considerable differences in expression level between SUMO1 and SUMO2/3 (total cellular pool of SUMO2/3 was reported to be substantially greater than that of SUMO1) (Saitoh & Hinchey, 2000). For comparison, amounts of some other proteins, namely importin subunit alpha-1 (KPNA2) and importin subunit alpha-4 (KPNA3), which interacts with UBA2 and are involved in the import of UBA2 and its complex with SAE1 (E1 activating enzyme) from the cytosol into the nucleus (Moutty et al., 2011), are also shown, however, interactions of these proteins with UBA2 were not found to be statistically significant (Table S4). Amounts of SAE1 and SUMO2/3 proteins were not found to vary between UBA2 samples of CPD, CP, WPD and WP conditions and these amounts were higher than respective amounts in CD samples, where UBA2-FLAG was not expressed (Figure 4.30, C). These data suggest that interactions of these proteins with UBA2 are not affected by H_2O_2. Unfortunately, we could not identify UBC9, which could be used as a control for evaluation of H_2O_2 effects on UBA2 protein interactome under oxidative stress conditions.

Collectively, present data do not allow to determine the reason for altered UBA2 thermostability identified in TPP.

5 Discussion

Redox processes are extremely important for functioning of individual cells as well as whole organisms in physiology and pathology. Nevertheless, our current understanding of cellular redox processes is far from complete and the role of many cellular proteins, which are involved in these processes, remains elusive. In the current study, we established melanoma and HEK293 cell lines stably expressing proteins for local manipulation of H_2O_2 (HyPer-DAO) and NADPH (iNap-DAAD) in various cellular compartments to investigate how redox disturbances affect cellular function.

5.1 Melanoma

Melanoma is known as the deadliest skin cancer with worldwide incidence steadily increased over the last decades (Cutaneous Melanoma Etiology and Therapy, 2017). Despite substantial advance in treatment and significantly increased survival rate of melanoma patients, new therapies and the improvement of existing ones would be extremely valuable. One way to address this issue is to exploit altered compared to normal cells redox status of cancer (including melanoma) cells. For this reason, we assembled plasmids encoding HyPer-DAO and iNap-DAAD proteins and used these plasmids for production of respective lentiviruses. Produced lentiviruses were then used for infection of three different melanoma cell lines: WM3734, 1205Lu and WM88.

5.1.1 Protein mistargeting in stable cell lines

Among seventeen engineered melanoma cell lines stably expressing HyPer-DAO and iNap-DAAD proteins in the mitochondrial matrix, the nucleus and the cytosol, only three melanoma cell lines expressing iNap-DAAD in the nucleus (2NLS-iNap1-P2A-3NLS-FLAG-DAAD) showed visible mistargeting. In these cell lines, the fluorescent signal in addition to the nucleus was also detected in the cytosol (Figure 4.3-4.5). The reason for this partially cytosolic localization of the signal is likely the presence of only two nuclear localization sequences (2NLS) fused to iNap1 that is obviously not enough to exclusively localize the protein in the nucleus. The observed iNap mistargeting can be reduced via establishing a new cell lines, which can be produced using newly assembled plasmids coding iNap fused to three (or more) instead of two NLS. Nevertheless, this issue is not crucial, since in contrast to DAAD iNap was required only for detection, but not for induction of NADPH level alterations. Meanwhile, DAAD has 3NLS and thus one can assume that it should be properly localized. Yet, since iNap and DAAD are separate proteins, correct cellular localization of DAAD protein should be

verified in each cell line by immunocytochemistry using anti-FLAG antibodies in the future.

5.1.2 Response of stable cell lines to D-Alanine

We started *in vitro* characterization of produced melanoma cell lines with finding a concentration of D-Alanine (D-Ala) required for H_2O_2 generation in WM3734 and 1205Lu stably expressing HyPer-DAO in the cytosol. Addition of D-Ala in the range of low millimolar concentrations to these cell lines revealed that in both cases HyPer was oxidized in response to 2 mM and higher concentrations of D-Ala, and that the cell lines differed in their response to these concentrations.

In case of 1205Lu the obtained results suggested that increase of D-Ala concentration in the range between 2 and 8 mM in cell culture medium led to consistent increase of intracellular level of D-Ala and thus to increased level of H_2O_2 generated by DAO (dose-dependent effect of D-Ala) (Figure 4.7). In contrast to 1205Lu cell line, 4 and 8 mM of D-Ala led to quite similar degree of HyPer oxidation and did not induce its maximal oxidation in the stable WM3734 cell line that is in agreement with limited availability of intracellular D-Ala for DAO (Figure 4.6). As other amino acids D-Ala was reported to enter cells via a set of membrane transporters, many of which are not selective to a particular amino acid and can transport both stereoisomers of amino acids (L and D), reviewed in (Lee et al., 2020). Most likely transporters of WM3734 cells, which are involved in uptake of extracellular D-Ala, have a limited ability to transport D-Ala across the plasma membrane and operate at nearly maximum rate at 4 mM of D-Ala in the culture medium. Meanwhile, respective transporters of 1205Lu cell line seemingly do not have such a restriction. In addition, different $T_{0.5}$ of these cell lines that we observed upon addition of D-Ala may also be at least partially explained by different amino-acid transporters.

Current results indicate that these two melanoma cell lines may have different sets of amino-acid transporters expressed on the cell surface and responsible for D-Ala uptake. Nevertheless, more replicates and higher concentrations of D-Ala, such 16 mM, would allow clarifying this assumption.

5.1.3 Influence of D-Alanine on melanoma cell proliferation

Using Crystal Violet Assay (CVA) in the current study, we found that 8 mM of D-Ala led to proliferation arrest and cell death of WM3734 and 1205Lu melanoma cell lines expressing HyPer-DAO in the cytosol and the nucleus. Since our task was not to kill cells, but instead to figure out how increased H_2O_2, level affects melanoma cell aggressiveness (migration, invasiveness etc.), we plan to

examine the effect of lower concentrations of D-Ala, primarily 2 and 4 mM, on stable melanoma cells in the future.

We also studied the influence of L-Ala on melanoma cell growth, however, did not find (in most of cases) substantial difference from untreated cells (incubated without supplements). Thus, in further experiments with these melanoma cell lines we will use untreated cells as a control.

Despite influence of D-Ala (8 mM) on proliferation and viability of stable WM3734 and 1205Lu melanoma cell lines expressing HyPer-DAO in the cytosol and the nucleus, D-Ala was also found to inhibit growth rate of original (wt) WM3734 and 1205Lu cell lines. Inhibitory effect of D-Ala can be explained by competition of D-Ala with L-amino acids in cell medium for transporters and therefore decreased uptake of L-amino acids by cells in the presence of D-Ala. Furthermore, in accordance to the previous results obtained by addition of different concentrations of D-Ala to WM3734 and 1205Lu expressing HyPer-DAO in the cytosol, we found that inhibitory effect of D-Ala on wt WM3734 and 1205Lu cell lines was different. This difference can be similarly explained by different sets of amino acid transporters represented on the cell surface.

5.2 HEK293

Redox processes are important for functioning of not only cancerous cells, but non-malignant cells as well and thus in addition to melanoma cell lines we employed HEK293 cell line as a cell model for studying redox processes. The strategy for studying redox processes in HEK293 was quite similar to the one used for studying melanoma cells. We assembled additional plasmids encoding HyPer-DAO fused to sequences for protein targeting to different cellular compartments, including peroxisomes, mitochondria- (outer mitochondrial membrane, mitochondrial intermembrane space and the mitochondrial matrix) and ER-related (membrane (cytosolic side) and lumen) compartments, as well as the plasma membrane (cytosolic side). Plasmids encoding proteins, which properly localized in intended cellular compartments and did not display mistargeting to other compartments, were utilized together with previously made plasmids encoding HyPer-DAO fused to signals for targeting to the nucleus and the cytosol, for production of lentiviruses and further for establishing of stable HEK293 cell lines.

5.2.1 Cellular mistargeting of HyPer-DAO proteins

Despite HyPer-DAO protein was properly localized in many of the cellular compartments selected for expression, its localization in some certain cases was not satisfactory.

5.2.1.1 Peroxisomes

Peroxisomal proteins are synthesized in the cytosol and many of them have special localization signal, peroxisomal targeting sequence (PTS), which is required for their import into peroxisomes (Hasan et al., 2013). One of the PTS types, PTS1, representing a C-terminal tripeptide (SKL), which interacts with cytosolic protein PEX5, which in turn is involved in recruiting of PTS1-containg proteins to peroxisomal membrane for further peroxisomal import (Hasan et al., 2013). Due to small size of the signal, it is reasonable to assume that in some cases, depending on the protein sequence, PTS1 can be less accessible for binding by PEX5 and thus the peroxisomal targeting can be compromised (Brocard & Hartig, 2006). Furthermore, the preceding amino acids in a protein sequence are also known to affect cargo-recognition suggesting that PTS1 should be considered as a longer sequence than just a tripeptide (Brocard & Hartig, 2006; Chowdhary et al., 2012). Seemingly, this might be the reason for strong cytosolic background that we observed in cells transfected with HyPer-DAO-PTS1 (Figure 4.11, left). The presence of the longer linker between DAO and the PTS1 in the protein, indeed, allowed to significantly decrease the observed fluorescent signal in the cytosol of cells transiently expressing HyPer-DAO-PTS1 (longer linker) (Figure 4.11, middle). Nevertheless, the stable cell line expressing the same protein with longer linker had increased fluorescent background in the cytosol, however, not that strong compared to HyPer-DAO-PTS1 (Figure 4.11, right). Considering the fact that peroxisomal proteins are synthesized in the cytosol, it is not surprising that we failed to get rid of the protein in the cytosol completely. Obviously, it was not enough to only change the length of the linker and this issue requires more complex approach to address. One strategy for solving this problem was proposed by Fransen group (Lismont et al., 2019). They established a system for selective and controlled generation of H_2O_2 inside peroxisomes of HEK293 cells. To achieve that, they engineered cells in the way to regulate expression of human DAO by addition or removal of doxycycline (inducible DAO expression). Furthermore, DAO was fused to destabilization domain (DD) to be able to send DAO to proteasomal degradation upon Shield1 removal. Shield1 is a high-affinity ligand of DD, which upon binding to the latter, protects the protein with DD from degradation. The rationale behind the approach was to allow cells to accumulate the protein in the cytosol and peroxisomes via addition of both doxycycline and Shield1 to the culture medium and then to remove both compounds to preserve DAO only in peroxisomes (Lismont et al., 2019). This system might have been useful for the current study, nevertheless, it requires additional efforts and time to establish and it is more complex, thus we postponed its implementation for the future.

5.2.1.2 ER-membrane

HyPer-DAO was also not properly localized on the ER-membrane. Despite the transient transfection of HeLa cells with the respective plasmid encoding HyPer-DAO-Sec61B did not reveal any problems, stable expression of the chimeric protein in HEK293 cells led to the visible distortion of the cell structures that prevented the usage of this cell line in any further experiments (Figure 4.12). Seemingly, the observed cell formations represent tightly stacked membrane arrays termed organized smooth ER (OSER) structures (Snapp et al., 2003). OSER structures can take different forms, including whorls, karmellae (stacks of packed cisternae, which surround part of the nucleus), open loops etc., and occur due to binding interactions between proteins on apposing membranes. These binding interactions often becomes possible between overexpressed proteins, which reside in the ER-membrane and have cytosolic domains, capable of dimerization in an antiparallel orientation. In the case of HyPer-DAO-Sec61B, it is plausible that DAO, which forms a stable head-to-tail homodimer, can be at least partially responsible for the formation of the observed structures (Pollegioni et al., 2007). Furthermore, considering that using gel-filtration chromatography HyPer oligomerization state in concentrated samples was previously evaluated as a mixture of dimers and monomers, it is possible that being overexpressed on the ER-membrane HyPer is prone to dimerization and thus along with DAO contributes to OSER formation (Markvicheva et al., 2011). Moreover, high expression level of YFP fused to Sec61B, the protein that we used for targeting HyPer-DAO to the ER-membrane, was also shown to induce OSER formation (Snapp et al., 2003).

OSER occurs due to overexpression of protein, which is prone to dimerization, thus there are several possible options of how to optimize current protein expression system. Since DAO is a crucial part of the H_2O_2-generating system and cannot be replaced or removed, the main strategy for the optimization could be to reduce the expression level of the protein in cells. This task can be accomplished e.g., via changing the plasmid promoter. In addition, HyPer can also be changed for another, monomeric and bright (to compensate decreased protein expression) fluorescent protein, in order to be able at least to estimate the localization of the protein using fluorescence microscopy.

5.2.2 Response of stable cell lines to D-Alanine

In comparison to the original study (Matlashov et al., 2014) and our results obtained using melanoma cell lines, in experiments with HEK293 cell lines stably expressing HyPer-DAO in the nucleus and the cytosol we found that substantially lower concentrations of D-Ala were required for DAO stimulation and H_2O_2

generation. Furthermore, we also found out that addition of D-Ala to stable HEK293 cells led to full (or almost full) HyPer oxidation much faster compared to melanoma cell lines. We assume the reason for such differences between HEK293 and melanoma cell lines is different media that were used for experiments. For experiments with HEK293 cells we utilized DPBS (supplemented only with Ca^{2+}/Mg^{2+} and glucose), which is much poorer medium than cell culture media, such as MEM, that was utilized for the original study and our experiments with stable melanoma cell lines. DPBS does not contain any amino acids, which can compete with added D-Ala for cellular uptake, in comparison to cell culture media, where L-amino acids are present in millimolar range (e.g., concentration of L-Ala in MEM is equal to 1 mM, (Sigma, cat num. M0643, M1018)). Thus, higher influx rate of D-Ala into the cell, even at lower concentrations, due to lack of L-amino acids in DPBS, is a possible reason for the obtained results with HEK293 cells.

5.3 Thermal Proteome Profiling

5.3.1 Common comparison of stable cell lines

Since proteome of melanoma cell lines is more complex and less studied compared to the one of more routinely used eukaryotic cell lines, we primarily focused on the study of the response of HEK293 cells proteome to localized intracellular H_2O_2 generation. With engineered HEK293 cell lines stably expressing HyPer-DAO-NES, HyPer-DAO-3NLS and TagBFP-DAO-KDEL we performed Thermal Proteome Profiling (TPP) to identify proteins involved in cellular response to H_2O_2 generated in the cytosol, the nucleus and the ER-lumen, respectively. We confidently identified more than five thousand cellular proteins, a number that is comparable to results of other TPP studies (Becher et al., 2018). Among these thousands of proteins, several hundreds were identified as hits based on significantly changed abundance/stability in response to induced H_2O_2 generation in at least one of the cellular compartments. The largest number of hits were identified upon H_2O_2 generation in the cytosol and the least one – in the ER-lumen.

The ER-lumen is known to have oxidizing environment (Malinouski et al., 2011) and thus its proteins may be less susceptible to further oxidation, e.g., induced by H_2O_2. Many proteins residing in the ER-lumen have disulfide bonds, which in comparison to free cysteine residues, do not undergo additional oxidation. In addition, the smaller number of cellular proteins, which responded to H_2O_2 generated in the ER-lumen, could be due to incorrect or deficient folding

of DAO and therefore failure of the ER-lumen to produce sufficient amounts of H_2O_2 upon addition of D-Ala. The limited availability of D-Ala to the ER-lumen, e.g., due to the failure of D-Ala to compete with L-amino acids for the transporters in the ER-membrane, may also underlie small amount of H_2O_2 generated in the ER-lumen upon DAO stimulation. Nevertheless, considering facts that D-Ala is able to pass the plasma membrane of HEK293 cells (was able to induce cellular H_2O_2 generation in our study) and membrane transporters initially originate in the ER on their way to the cell surface, this assumption does not seem to be true. Finally, differences in expression level of DAO between stable cell lines that were identified based on MS data can also explain our observations.

The number of identified hit proteins were substantially higher upon H_2O_2 generation in cell lines overexpressing DAO in the cytosol and the nucleus (in comparison to the ER, Table 4.1). The additional difference between the cyto and the nuclei cell lines can be explained by lower expression level of DAO (HyPer-DAO) in the nuclei cell line, e.g., due to less copy number of HyPer-DAO gene inserted into the cell genome and thus by a lower level of H_2O_2, which is produced upon DAO stimulation. Additional data, such as a more reducing nuclear Trx1 pool (Jones & Go, 2010), the capability of cytosolic Trx1 to translocate into the nucleus upon various kinds of stress and thus further enhance the nuclear Trx1 pool (Hirota et al., 1999) and restricted ability of H_2O_2 generated by nuclear DAO to diffuse into the cytosol in response to D-Ala addition (Mishina et al., 2019), may reflect the fact that the nucleus is better protected against oxidative stress than the cytosol (Jones & Go, 2010) and thus more efficiently counteracts H_2O_2 accumulation and its diffusion to other cellular compartments, including the cytosol.

Nevertheless, the ability of H_2O_2 to migrate from the compartment, where it was produced to surrounding cellular compartments, e.g., from the cytosol to the nucleus and vice versa, most likely underlies our observation that many cellular proteins similarly altered abundance/stability in response to H_2O_2 generated in the nucleus and the cytosol (Mishina et al., 2019). Furthermore, considering the fact that many proteins are able to shuttle between the cytosol and the nucleus, we cannot rule out that protein nuclear-cytosolic shuttling can also contribute to the observed similarities between two cell lines.

5.3.2 TPP and oxidative stress induced protein aggregation

The underlying principle of TPP is denaturation and aggregation of proteins in a sample upon heat treatment with following removal of aggregated proteins. Meanwhile oxidative stress itself is also able to lead to protein aggregation (van

Dam & Dansen, 2020). Thus, it is reasonable to emphasize how oxidative stress-induced protein aggregation can affect results of TPP experiment.

It is a long-known fact that oxidative stress accompany protein aggregation in various pathology and diseases, including Parkinson's and Alzheimer's disease, amyotrophic lateral sclerosis, cataract, etc. (Lévy et al., 2019; Michalska et al., 2020). However, it is not established yet if protein aggregation is a cause or a consequence of oxidative stress. Current data suggest that there is a positive feedback loop in which oxidative stress stimulates protein aggregation and vice versa (Lévy et al., 2019 ; van Dam & Dansen, 2020). In support of this hypothesis, some proteins have been shown to be able to undergo redox-regulated aggregation. One of such proteins is $p16^{INK4A}$ – a tumour suppressor regulating cell cycle, and which upon a cysteine oxidation undergo reversible aggregation (Göbl et al., 2020). Among other examples are tryptophan hydroxylase 2 (TPH2), an enzyme involved in serotonin synthesis; visinin-like protein-1 (VSNL1), a neuronal calcium sensor and others (van Dam & Dansen, 2020).

Despite these proteins were not found among hits or candidates in our results (most of mentioned proteins are cell type specific), one can assume that, since removal of protein aggregates from a sample is reflected on a protein amount in soluble fraction, TPP in general should allow finding molecular events such as protein aggregation that makes TPP a suitable candidate for investigation of cell response to oxidative stress.

5.4 Gene ontology enrichment analysis

Based on similarities of abundance/stability changes we grouped hit and candidate proteins into clusters and performed gene ontology enrichment analysis. The analysis revealed that many of obtained clusters were enriched in components of various protein complexes, such as ribosome subunits, RNA-polymerase, MCM complex etc., involved in diverse cellular processes. Connection of some of these protein complexes, such as ribosome, with oxidative stress was reported previously, whereas the role of others, e.g., THO complex, for cellular adaptation to oxidative stress is studied much poorer and requires further investigations. In following sections, we discuss connection of these complexes to oxidative stress in more details.

5.4.1 Protein synthesis

Consistent with our results are reports that protein synthesis (mRNA translation) is a crucial target of different kinds of cellular stress, including

oxidative stress evoked by H_2O_2 (Clemens, 2001; Grant, 2011). It is known that H_2O_2 can modulate mRNA translation at multiple levels, including initiation, elongation and termination (Grant, 2011; Shenton et al., 2006). Due to inhibition of translation initiation, treatment of cells with H_2O_2 leads to evident shift from polysomes (multiple ribosomes actively translating a single mRNA) to monosomes (80S ribosomes) (Shenton et al., 2006). This shift may underlie the observed increase in abundance of ribosomal proteins that we discovered. Furthermore, it was shown recently that H_2O_2 originated from dysfunctional mitochondria is able to directly oxidize conserved redox-sensitive cysteines in ribosomal proteins and attenuate global protein synthesis in yeast (Topf et al., 2018). This oxidation was found to be sufficient to weaken protein synthesis, and the attenuation – to have a reversible nature. One possible explanation for decreased protein synthesis under stress conditions is that translation is a highly energy-demanding process, which may deplete cellular resources available for fighting oxidative stress consequences (Grant, 2011). Furthermore, ROS are known to evoke accumulation of mutations in nucleic acids, including mRNA molecules, and thus via suspending protein synthesis during oxidative stress cells can avoid production of aberrant proteins in error-prone conditions (Shenton et al., 2006).

5.4.2 SKI complex

Regarding the role of SKI complex in oxidative stress, it was shown that non-stop decay (NSD) substrates accumulate upon yeast exposure to H_2O_2, and that yeast mutants lacking any of three components of the SKI complex are very sensitive to H_2O_2, supposedly because of the translation of aberrant mRNAs and production of abnormal proteins (Jamar et al., 2017). Since NSD was demonstrated to exist in mammalian cells (Saito et al., 2013), one can assume that SKI complex may participate in elimination of NSD substrates accumulating under oxidative stress in mammalian cells as well.

5.4.3 THO complex

THO and TREX complexes are poorly studied in a context of oxidative stress, however, there are evidences in support of the importance of their components, such as THOC1 and THOC5, for cellular response to such conditions (Alqawlaq et al., 2021; Griaud et al., 2013). In one of the studies, authors showed that under glutamate-induced oxidative challenge, astrocyte conditioned media supported neuronal viability via PI3K-signaling (Alqawlaq et al., 2021). Authors

identified several proteins that increased interaction with PI3K under these conditions, among which were THOC1 and ZC3H14. Nevertheless, considering the shortage of available data regarding the relationship between these proteins and oxidative stress, it is complicated to provide any explanations for the obtained results. One can presume the discovered concerted decrease in abundance (score) of these proteins was due to their altered binding to mRNA molecules that in turn resulted in ZC3H14 protein and THO complex solubility change, however, this assumption has to be experimentally validated.

5.4.4 RNA polymerase II

Despite RNA polymerase II (Pol II) has been extensively studied, and there are researches devoted to investigation of operation of Pol II under oxidative stress condition, the full understanding of underlying mechanisms is still missing. Apparently, similarly to effects of oxidative stress on other processes, its impact on transcription significantly varies depending on the duration and intensity of exposure. For instance, nuclear extracts derived from HeLa S3 cells treated with 10 mM H_2O_2 for 15 min showed no transcriptional activity on undamaged DNA template *in vitro* indicating possibility for direct repression of transcription apparatus via protein oxidation in response to oxidative stress of high intensity (Heine et al., 2008). Meanwhile, authors of another study showed that treatment of HeLa cells with 0.3 mM H_2O_2 for 10 min results in global Pol II promoter-proximal pausing that was concluded to be a consequence of suppressed aberrant transcriptional termination and unaffected initiation (Nilson et al., 2017). This results in the higher occupation of promoters and enhancers by Pol II and respective depletion of its soluble (free) form. Thus, stabilization of DNA-bound, paused Pol II at promoters and enhancers may underlie the observed increase in thermostability of Pol II components, which the cluster 9 is enriched in (Figure 4.24, C). This assumption is in accordance to the results obtained by Savitski group, who showed that DNA-binding leads to increase of Pol II thermostability (Becher et al., 2018).

5.4.5 MCM complex

Sensitivity of replicating DNA to oxidation is known, however, mechanisms connecting replication and cellular redox homeostasis remain largely unexplored. Notwithstanding, a subunit of MCM complex, MCM3, was identified as a substrate for KEAP1 – a redox-sensitive regulator of proteasomal degradation of NRF2 (a master regulator of cellular response to oxidative stress discussed

previously) (Mulvaney et al., 2016). Authors reported that MCM3 undergoes KEAP1-dependent ubiquitination, which, however, does not lead to proteasomal degradation of MCM3. Furthermore, KEAP1-dependent ubiquitination emerged to be insensitive to various factors, including ROS mimetics and thus its physiological significance was not elucidated (Mulvaney et al., 2016). Authors of another study showed that MCM3 and NRF2 bind to KEAP1 in competitive manner due to identical KEAP1-binding motifs and also demonstrated that MCM3 protein level modulates KEAP1-NRF2 pathway sensitivity to xenobiotic stress (Tamberg et al., 2018). However, whether KEAP1-MCM3 interaction has impact on regulation of DNA replication under oxidative stress conditions still remains unclear. Nevertheless, given multiplicity of PTMs that proteins of MCM complex can undergo (Li & Xu, 2019), and the ability of oxidative stress to affect pattern of protein PTMs (e.g., due to inactivation of protein phosphatases), it is reasonable to assume that other, KEAP1-independent molecular mechanisms, may underlie altered thermostability of MCM complex (Figure 4.24, D).

5.5 Co-immunoprecipitation

One of our experimental approaches was to examine if the altered thermostability of several proteins identified as hits in the TPP experiment was due to altered protein interactions. Using co-immunoprecipitation (Co-IP) we examined protein interactomes of four proteins: TRAP1, PARK7, MAP2K1 and UBA2 under normal and oxidative stress conditions induced by the generation of H_2O_2 in the cytosol of HEK293 cells.

5.5.1 TRAP1

Only two proteins were found to change (enhance) binding to TRAP1 upon H_2O_2 generation in the cytosol of HEK293 cells. These proteins form mitochondrial processing peptidase (MPP) involved in removal of N-terminal targeting peptide from preproteins upon their import into the mitochondrial matrix. Considering the function of MPP we supposed that enhanced interaction of TRAP1 with MPP should lead to increased fraction of TRAP1 without targeting peptide, however, by comparing amounts of peptides corresponding to the N-terminal signal of TRAP1 between samples, we did not find any differences. Given the cytoprotective role of TRAP1 in maintenance of mitochondrial integrity (Altieri et al., 2012), it is tempting to speculate that via enhanced binding to MPP in mitochondria, processed TRAP1 may modulate MPP activity and thus participate in regulation of protein import into the mitochondrial matrix under

oxidative stress conditions, which are known to induce aberrant protein accumulation. Nevertheless, we also cannot rule out the possibility that interaction between these proteins (directly or indirectly modified in response to oxidative stress) is established during lysis, when mitochondrial MPP complex meets unprocessed (due to overexpression), most likely cytosolic TRAP1, that, however, for some reason does not lead to TRAP1 processing.

5.5.2 PARK7

We found that under oxidative stress conditions PARK7 substantially changes interactions with its binding partners. Many of these interactions were reported previously. Interactions of PARK7 with HSPA4 and HSPA5 were found by Co-IP experiment in liver samples of rats with streptozotocin-induced type 1 diabetes mellitus (Chaudhari et al., 2015). In a Co-IP experiment performed with HCT116 cell line transiently overexpressing FLAG-tagged PARK7 as a bait protein and treated with TNFSF10, authors identified an interaction of N-terminally arginylated HSPA5 with oxidized PARK7 required for autophagic disposal of misfolded proteins originating under oxidative stress (Lee et al., 2018). HSPA5 as an interacting protein of PARK7 was also identified by other groups (Eltoweissy et al., 2016). Association and colocalization of HSPA9 (mtHSP70) with PARK7 were observed in HEK293T cells and moreover found to be significantly induced by treatment of cells with 100 μM of H_2O_2 for 4 h (Li et al., 2005). In accordance to this study another group also reported low level of interaction between PARK7 and HSPA9 under normal conditions, which was observed to substantially augment together with mitochondrial translocation of PARK7 in resveratrol pretreated H9c2 cardiomyocytes undergoing hypoxia-reperfusion (Zhou et al., 2020). Accordingly, it was reported that the oxidation-induced formation of C106-SO_2H (cysteine sulfenic acid) leads to the mitochondrial localization (OMM) of PARK7 and increased cell viability (not observed for C106A PARK7 mutant) (Canet-Avilé et al., 2004). In addition, PARK7 was identified as a component of the IP3R-GRP75-VDAC complex, which contributes to the formation of functional mitochondria-ER contacts (MERCs) and the transport of calcium ions between these two organelles (Basso et al., 2020; Liu et al., 2019). Given the long-known mutual interconnection of ROS and calcium, including the ability of calcium to modulate mitochondrial ROS production (Görlach et al., 2015), it is tempting to speculate that PARK7 can also regulate calcium transport between these two organelles under oxidative stress and thus affect mitochondrial ROS generation. In the same Co-IP experiment performed with HCT116 cell line, wherein HSPA5 was found as a co-

interactor of PARK7 under oxidative stress, authors also reported that several other chaperones: HSPA1A, HSPA8 and hsp90α family class A member 1 (HSP90AA1) enhanced interactions with PARK7 as well (Lee et al., 2018). Results provided by authors of the study partly correspond to our results, although we have not identified differences in amounts of HSP90AA1 chaperone between any of PARK7 samples.

Collectively, these data suggest that PARK7 might possibly change thermostability due to altering binding partners under oxidative stress. Nevertheless, since Cys106 in PARK7 is known to be redox-sensitive (Wilson, 2011), we cannot exclude that some oxidative modifications of this residue together with formed interactions may have cooperative effect on altered thermostability of PARK7.

5.6 TPP database

Co-IP is just one type of the experiments out of many that can be used to identify the reason for altered protein thermostability in TPP experiments. Considering the fact that the reasons for altered thermostability of an individual protein can be various, e.g., occurrence of post translational modifications, (un)binding of low-molecular weight ligands, etc., creation of an online database with our TPP results will allow researchers interested in redox biology to answer their own scientific questions by using suitable experimental methods. Furthermore, our TPP results database can be used for comparison with existing databases, wherein high-throughput methods were utilized for studying effects of redox alterations on cell physiology. There have been multiple system researches devoted to investigation of effects of redox disturbances on the cell response. Among them we selected several ones with relatively high proteome coverage for further discussion. Despite differences in utilized techniques, cell models and ways of initiated redox disturbances, results of these studies display similarities both between each other and with our study.

In one of these studies, (Saei et al., 2020) authors used several proteomic methods: TR-TPP, FITExP (Functional Identification of Target by Expression Proteomics) and redox proteomics for identification of protein targets of auranofin in three cell lines: A375, RKO and HCT116. Auranofin is known to target thioredoxin reductase 1 (TrxR1, TXNRD1), which plays an important role in cellular antioxidant defence. TXNRD1 was found to be slightly, nevertheless reproducibly, stabilized (in TR-TPP) upon cell treatment with auranofin, and at least one Cys-containing peptide of TXNRD1 was substantially oxidized (in redox proteomics). Despite another initiation way of redox disturbances, we also identified TXNRD1 as a significantly stabilized protein in all three produced

HEK293 cell lines. Besides TXNRD1, another top protein identified based on the results of all three proteomic methods was the Nuclear factor NF-kappa-B p100 subunit (NFKB2). In addition to upregulation of NFKB2 protein level in two of three cell lines (FITExP), NFKB2 was also found to be substantially oxidized and stabilized in response to cell treatment with auranofin. In our study NFKB2 was not identified in several MS runs that did not enable to estimate entire protein melting curves, while available data did not reveal significant protein stability changes. These results may indicate the involvement of NFKB2 in auranofin-specific cell response. Similar to NFKB2, another auranofin top protein target, CHORDC1 (Cysteine and histidine-rich domain-containing protein 1), was also upregulated in two of three cell lines and was found to undergo oxidation, however, not stabilization. Our TPP results also did not indicate stabilization of CHORDC1 upon H_2O_2 generation in any of three cell lines. Connection of protein thermostability to oxidation was shown by authors for Prx5 (PRDX5). Cys100 of PRDX5 was found to become less oxidized and the protein less stable upon auranofin treatment. Similarly, the protein was significantly stabilized in the cyto and the nuclei cell lines in our study. Perhaps decreased stability of PRDX5 identified in our study also reflects reduction of the same cysteine. Authors also analyzed the pathways, which most significantly affected proteins are involved in, and revealed enrichment of «oxidoreductase», «response to reactive oxygen species», «nucleotide phosphate-binding region: FAD», «mRNA processing» and «mRNA splicing, via spliceosome» among others. Furthermore, significantly modified peptides from redox proteomics mapped to the following KEGG pathways: «ribosome», «DNA replication», «cell cycle», «metabolic pathways», «glycolysis/gluconeogenesis», «adherens junction», «focal adhesion», «ribonucleoprotein complex», etc. Related GO terms were also found to be overrepresented among significantly affected proteins identified in our study (Figures 4.23 and 4.25) suggesting that cellular response to auranofin can at least partially be similar to the response to intracellular H_2O_2 generation.

Authors of another study (van der Reest et al., 2018) used a devised variant of redox proteomics, SICyLIA (see «1.7.4.1 Redox proteomics» section), to profile protein oxidation in chronic and acute oxidative stress models – fumarate hydratase (FH)-deficient ($Fh1^{-/-}$) mouse kidney epithelial cells and $Fh1^{fl/fl}$ cells treated with rather non-physiological amount of 0.5 mM H_2O_2 for 15 min, respectively. Among oxidised proteins under acute stress conditions authors identified known redox-sensitive proteins, such PTEN, PARK7 and GAPDH. In our study we did not identify PTEN, while GAPDH was not found to be significantly stabilized. GOEA (Gene Ontology Enrichment Analysis) implemented for proteins with significantly modified peptides demonstrated that besides proteins related to stress and ROS response, metabolic and mitochondrial proteins (mostly constituents of ETC) were overrepresented under acute oxidative

stress. Authors experimentally demonstrated that oxidation of GAPDH and the mitochondrial proteins led to physiological adaptations due to enhanced production of reducing equivalents (NADPH) in pentose phosphate pathway to fight against oxidants and inhibition of mitochondrial respiration to decrease generation of endogenous ROS, respectively. Nevertheless, alike GAPDH, these mitochondrial proteins did not undergo stabilization in our study. This may be explained by either these proteins are not involved in cellular response to endogenous H_2O_2 generation in HEK293 cells or by their oxidation is not accompanied by abundance/stability change. Similarly, GOEA of data derived from chronic stress model demonstrated that among significantly modified peptides were overrepresented those ones that correspond to metabolic proteins and proteins involved in redox homeostasis. Nevertheless, metabolic proteins significantly modified in response to acute and chronic oxidative stress were quite different. Among the small fraction of shared metabolic proteins, including ALDH18A1, FASN, MTAP, P4HB, PLA2G4A, etc., none were found to be stabilized in our study. Compared to metabolic proteins, proteins corresponding to redox homeostasis displayed greater overlap between two stress models, yet, among shared proteins: ERP44, P4HB, PDIA4, PDIA6, TXNDC5, PRDX5, only the latter altered stability in our study.

In another systemic research, authors used an alternative redox proteomics technique, QTRP (see «1.7.4.1 Redox proteomics» section), for proteome-wide cysteine reactivity profiling (Fu et al., 2017). The method was applied to four human cell lines: A431, HEK293, HepG2 and U2OS upon treatment with a range of H_2O_2 concentrations: 0.02, 0.05, 0.2, 0.5, 2.0, 5.0 mM for 10 min. It was found out that tested cell lines have only a small set of shared H_2O_2-sensitive proteins among which, in addition to known antioxidant enzymes, such as Prx and Trx family members, metabolic proteins (including ALDH5A1, BCAT2, GAPDH and PKM2) were identified. These results indicate that redox-sensitive cysteines in key metabolic proteins are conserved and thus important for cells. In our study though, changes of these proteins (besides not identified PKM2) were found to be non-significant. Despite the fact that some H_2O_2-sensitive cysteines (in antioxidant and metabolic proteins) are shared between the cell lines, the vast majority of them were found to be cell-specific. Based on this finding the authors presumed that conserved redox-sensitive cysteines in antioxidant and metabolic proteins unite with a larger set of redox-sensitive cysteines in the cell to form a cell type-specific H_2O_2-sensitive redoxome. Overall the authors identified different numbers of redox-sensitive cysteines between the cell lines with highest number in U2OS (and lowest in HEK293) that correlates with low reducing capacity of U2OS cells and thus may explain susceptibility of U2OS cells to oxidative stress. Nevertheless, catalytic cysteine of PRDX5 was discovered to be H_2O_2-sensitive only in HEK293 cells (PRDX5 was found to stabilized in our study

as well, see above) suggesting that in addition to intrinsic thiol reactivity and antioxidant capacity other factors determine cell redoxome.

Collectively, we believe that our TPP database will be very useful for future research projects. In this regard, the TPP database alone as well as in combination with existing databases has the potential to broaden our knowledge of how redox alterations affect cellular function in physiology and pathology.

Conclusions and outlook

In the current study we attempted to investigate cellular response to compartmentalized redox alterations. For this purpose, we assembled various plasmids encoding HyPer-DAO and iNap-DAAD proteins fused to sequences for targeting to various cellular compartments and using these plasmids engineered a variety of stable melanoma and HEK293 cell lines. We started *in vitro* characterization of produced melanoma cell lines expressing HyPer-DAO, nevertheless, most of created cell lines remained uncharacterized. In addition to *in vivo* characterization of the derived stable melanoma cell lines, we plan to work on these tasks in the future.

To identify proteins, which are involved in cellular response to compartmentalized H_2O_2 generation, we applied Thermal Proteome Profiling (TPP) – a high-throughput proteomic method that is based on identification of alterations in protein thermostability to three stable HEK293 cell lines expressing HyPer/TagBFP-DAO in the cytosol, the nucleus and the ER-lumen. As a result, we found that cellular response to H_2O_2 generated in the cytosol and the nucleus, was quite similar and differed from the cellular response to H_2O_2 generated in the ER-lumen. Furthermore, we also found that the number of identified proteins, which changed their abundance/stability in response to H_2O_2 production in these compartments was also different, with highest number in the cytosol and the lowest in the ER-lumen. Moreover, we generated a database from the obtained TPP results, which will be available in an online form.

To validate several hit and candidate proteins identified as a result of the TPP experiment we performed co-immunoprecipitation (Co-IP) and registered confident interactome changes in two of four cases (TRAP1 and PARK7) that implies that the reason for alteration of protein thermostability can be various. Another protein, MAP2K1, possibly does not change binding partners under oxidative stress conditions (further validations are required), however, we assume that its altered thermostability may reflect emergence of PTMs, most likely phosphorylation at Thr286. Nevertheless, the results of Co-IP/MS should be considered with caution, since despite all abovementioned, the Co-IP results require further validation by other means, e.g., classical biochemistry methods, such as SDS-PAGE and WB.

Taken together, we demonstrated that cellular response to H_2O_2 is extremely complex and multifaceted and implicates proteins required for diverse cellular processes, ranging from elimination of H_2O_2 to transcription, translation and replication. Accordingly, this study paves the way for future investigations and deeper understanding of the complex cellular redox biology.

References

1. Akita H, Doi K, Kawarabayasi Y, Ohshima T. Creation of a thermostable $NADP^+$-dependent D-amino acid dehydrogenase from Ureibacillus thermosphaericus strain A1 meso-diaminopimelate dehydrogenase by site-directed mutagenesis. Biotechnol Lett. 2012 Sep;34(9):1693-9. doi: 10.1007/s10529-012-0952-1. Epub 2012 May 22. Erratum in: Biotechnol Lett. 2012 Sep;34(9):1701-2. PMID: 22618239.
2. Akita H, Seto T, Ohshima T, Sakuraba H. Structural insight into the thermostable NADP(+)-dependent meso-diaminopimelate dehydrogenase from Ureibacillus thermosphaericus. Acta Crystallogr D Biol Crystallogr. 2015 May;71(Pt 5):1136-46. doi: 10.1107/S1399004715003673. Epub 2015 Apr 24. PMID: 25945579.
3. Alexandrov LB, Nik-Zainal S, Wedge DC, Aparicio SA, Behjati S, Biankin AV, Bignell GR, Bolli N, Borg A, Børresen-Dale AL, Boyault S, Burkhardt B, Butler AP, Caldas C, Davies HR, Desmedt C, Eils R, Eyfjörd JE, Foekens JA, Greaves M, Hosoda F, Hutter B, Ilicic T, Imbeaud S, Imielinski M, Jäger N, Jones DT, Jones D, Knappskog S, Kool M, Lakhani SR, López-Otín C, Martin S, Munshi NC, Nakamura H, Northcott PA, Pajic M, Papaemmanuil E, Paradiso A, Pearson JV, Puente XS, Raine K, Ramakrishna M, Richardson AL, Richter J, Rosenstiel P, Schlesner M, Schumacher TN, Span PN, Teague JW, Totoki Y, Tutt AN, Valdés-Mas R, van Buuren MM, van 't Veer L, Vincent-Salomon A, Waddell N, Yates LR; Australian Pancreatic Cancer Genome Initiative; ICGC Breast Cancer Consortium; ICGC MMML-Seq Consortium; ICGC PedBrain, Zucman-Rossi J, Futreal PA, McDermott U, Lichter P, Meyerson M, Grimmond SM, Siebert R, Campo E, Shibata T, Pfister SM, Campbell PJ, Stratton MR. Signatures of mutational processes in human cancer. Nature. 2013 Aug 22;500(7463):415-21. doi: 10.1038/nature12477. Epub 2013 Aug 14. Erratum in: Nature. 2013 Oct 10;502(7470):258. Imielinsk, Marcin [corrected to Imielinski, Marcin]. PMID: 23945592; PMCID: PMC3776390.
4. Alqawlaq S, Livne-Bar I, Williams D, D'Ercole J, Leung SW, Chan D, Tuccitto A, Datti A, Wrana JL, Corbett AH, Schmitt-Ulms G, Sivak JM. An endogenous PI3K interactome promoting astrocyte-mediated neuroprotection identifies a novel association with RNA-binding protein ZC3H14. J Biol Chem. 2021 Jan-Jun;296:100118. doi: 10.1074/jbc.RA120.015389. Epub 2020 Dec 3. PMID: 33234594; PMCID: PMC7948738.
5. Altieri DC, Stein GS, Lian JB, Languino LR. TRAP-1, the mitochondrial Hsp90. Biochim Biophys Acta. 2012 Mar;1823(3):767-73. doi: 10.1016/j.bbamcr.2011.08.007. Epub 2011 Aug 22. PMID: 21878357; PMCID: PMC3263322.
6. Antonenkov VD, Grunau S, Ohlmeier S, Hiltunen JK. Peroxisomes are oxidative organelles. Antioxid Redox Signal. 2010 Aug 15;13(4):525-37. doi: 10.1089/ars.2009.2996. PMID: 19958170.
7. Ashburner M, Ball CA, Blake JA, Botstein D, Butler H, Cherry JM, Davis AP, Dolinski K, Dwight SS, Eppig JT, Harris MA, Hill DP, Issel-Tarver L, Kasarskis A, Lewis S, Matese JC, Richardson JE, Ringwald M, Rubin GM, Sherlock G. Gene ontology: tool for the unification of biology. The Gene Ontology Consortium. Nat Genet. 2000 May;25(1):25-9. doi: 10.1038/75556. PMID: 10802651; PMCID: PMC3037419.
8. Avagliano A, Fiume G, Pelagalli A, Sanità G, Ruocco MR, Montagnani S, Arcucci A. Metabolic Plasticity of Melanoma Cells and Their Crosstalk With Tumor Microenvironment. Front Oncol. 2020 May 22;10:722. doi: 10.3389/fonc.2020.00722. PMID: 32528879; PMCID: PMC7256186.

9. Bak DW, Weerapana E. Cysteine-mediated redox signalling in the mitochondria. Mol Biosyst. 2015 Mar;11(3):678-97. doi: 10.1039/c4mb00571f. Epub 2014 Dec 18. PMID: 25519845.
10. Basso V, Marchesan E, Ziviani E. A trio has turned into a quartet: DJ-1 interacts with the IP3R-Grp75-VDAC complex to control ER-mitochondria interaction. Cell Calcium. 2020 May;87:102186. doi: 10.1016/j.ceca.2020.102186. Epub 2020 Feb 24. PMID: 32120195.
11. Bates, D., Mächler, M., Bolker, B. M., & Walker, S. C. (2015). Fitting linear mixed-effects models using lme4. *Journal of Statistical Software, 67*(1). https://doi.org/10.18637/jss.v067.i01
12. Becher I, Andrés-Pons A, Romanov N, Stein F, Schramm M, Baudin F, Helm D, Kurzawa N, Mateus A, Mackmull MT, Typas A, Müller CW, Bork P, Beck M, Savitski MM. Pervasive Protein Thermal Stability Variation during the Cell Cycle. Cell. 2018 May 31;173(6):1495-1507.e18. doi: 10.1016/j.cell.2018.03.053. Epub 2018 Apr 26. PMID: 29706546; PMCID: PMC5998384.
13. Becher I, Werner T, Doce C, Zaal EA, Tögel I, Khan CA, Rueger A, Muelbaier M, Salzer E, Berkers CR, Fitzpatrick PF, Bantscheff M, Savitski MM. Thermal profiling reveals phenylalanine hydroxylase as an off-target of panobinostat. Nat Chem Biol. 2016 Nov;12(11):908-910. doi: 10.1038/nchembio.2185. Epub 2016 Sep 26. PMID: 27669419.
14. Belousov VV, Fradkov AF, Lukyanov KA, Staroverov DB, Shakhbazov KS, Terskikh AV, Lukyanov S. Genetically encoded fluorescent indicator for intracellular hydrogen peroxide. Nat Methods. 2006 Apr;3(4):281-6. doi: 10.1038/nmeth866. PMID: 16554833.
15. Bertolotti M, Bestetti S, García-Manteiga JM, Medraño-Fernandez I, Dal Mas A, Malosio ML, Sitia R. Tyrosine kinase signal modulation: a matter of H2O2 membrane permeability? Antioxid Redox Signal. 2013 Nov 1;19(13):1447-51. doi: 10.1089/ars.2013.5330. Epub 2013 Sep 18. PMID: 23541115; PMCID: PMC3797449.
16. Bestetti S, Galli M, Sorrentino I, Pinton P, Rimessi A, Sitia R, Medraño-Fernandez I. Human aquaporin-11 guarantees efficient transport of H_2O_2 across the endoplasmic reticulum membrane. Redox Biol. 2020 Jan;28:101326. doi: 10.1016/j.redox.2019.101326. Epub 2019 Sep 12. PMID: 31546170; PMCID: PMC6812059.
17. Bestetti S, Medraño-Fernandez I, Galli M, Ghitti M, Bienert GP, Musco G, Orsi A, Rubartelli A, Sitia R. A persulfidation-based mechanism controls aquaporin-8 conductance. Sci Adv. 2018 May 2;4(5):eaar5770. doi: 10.1126/sciadv.aar5770. PMID: 29732408; PMCID: PMC5931763.
18. Beyer HM, Gonschorek P, Samodelov SL, Meier M, Weber W, Zurbriggen MD. AQUA Cloning: A Versatile and Simple Enzyme-Free Cloning Approach. PLoS One. 2015 Sep 11;10(9):e0137652. doi: 10.1371/journal.pone.0137652. PMID: 26360249; PMCID: PMC4567319.
19. Bhardwaj R, Hediger MA, Demaurex N. Redox modulation of STIM-ORAI signaling. Cell Calcium. 2016 Aug;60(2):142-52. doi: 10.1016/j.ceca.2016.03.006. Epub 2016 Mar 19. PMID: 27041216.
20. Bienert GP, Schjoerring JK, Jahn TP. Membrane transport of hydrogen peroxide. Biochim Biophys Acta. 2006 Aug;1758(8):994-1003. doi: 10.1016/j.bbamem.2006.02.015. Epub 2006 Mar 10. PMID: 16566894.
21. Bilan DS, Belousov VV. HyPer Family Probes: State of the Art. Antioxid Redox Signal. 2016 May 1;24(13):731-51. doi: 10.1089/ars.2015.6586. Epub 2016 Jan 11. PMID: 26607375.

22. Bilan DS, Pase L, Joosen L, Gorokhovatsky AY, Ermakova YG, Gadella TW, Grabher C, Schultz C, Lukyanov S, Belousov VV. HyPer-3: a genetically encoded H(2)O(2) probe with improved performance for ratiometric and fluorescence lifetime imaging. ACS Chem Biol. 2013 Mar 15;8(3):535-42. doi: 10.1021/cb300625g. Epub 2013 Jan 7. PMID: 23256573.
23. Birk J, Meyer M, Aller I, Hansen HG, Odermatt A, Dick TP, Meyer AJ, Appenzeller-Herzog C. Endoplasmic reticulum: reduced and oxidized glutathione revisited. J Cell Sci. 2013 Apr 1;126(Pt 7):1604-17. doi: 10.1242/jcs.117218. Epub 2013 Feb 19. PMID: 23424194.
24. Bisevac JP, Djukic M, Stanojevic I, Stevanovic I, Mijuskovic Z, Djuric A, Gobeljic B, Banovic T, Vojvodic D. Association Between Oxidative Stress and Melanoma Progression. J Med Biochem. 2018 Jan 1;37(1):12-20. doi: 10.1515/jomb-2017-0040. PMID: 30581337; PMCID: PMC6294103.
25. Bohovych I, Dietz JV, Swenson S, Zahayko N, Khalimonchuk O. Redox Regulation of the Mitochondrial Quality Control Protease Oma1. Antioxid Redox Signal. 2019 Aug 20;31(6):429-443. doi: 10.1089/ars.2018.7642. Epub 2019 Jun 18. PMID: 31044600; PMCID: PMC6653804.
26. Bossis G, Melchior F. Regulation of SUMOylation by reversible oxidation of SUMO conjugating enzymes. Mol Cell. 2006 Feb 3;21(3):349-57. doi: 10.1016/j.molcel.2005.12.019. PMID: 16455490.
27. Boveris A, Oshino N, Chance B. The cellular production of hydrogen peroxide. Biochem J. 1972 Jul;128(3):617-30. doi: 10.1042/bj1280617. PMID: 4404507; PMCID: PMC1173814.
28. Bracalente C, Ibañez IL, Berenstein A, Notcovich C, Cerda MB, Klamt F, Chernomoretz A, Durán H. Reprogramming human A375 amelanotic melanoma cells by catalase overexpression: Upregulation of antioxidant genes correlates with regression of melanoma malignancy and with malignant progression when downregulated. Oncotarget. 2016 Jul 5;7(27):41154-41171. doi: 10.18632/oncotarget.9273. PMID: 27206673; PMCID: PMC5173049.
29. Braun HP, Schmitz UK. The mitochondrial processing peptidase. Int J Biochem Cell Biol. 1997 Aug-Sep;29(8-9):1043-5. doi: 10.1016/s1357-2725(97)00032-0. PMID: 9415998.
30. Brieger K, Schiavone S, Miller FJ Jr, Krause KH. Reactive oxygen species: from health to disease. Swiss Med Wkly. 2012 Aug 17;142:w13659. doi: 10.4414/smw.2012.13659. PMID: 22903797.
31. Brigelius-Flohé R, Maiorino M. Glutathione peroxidases. Biochim Biophys Acta. 2013 May;1830(5):3289-303. doi: 10.1016/j.bbagen.2012.11.020. Epub 2012 Nov 29. PMID: 23201771.
32. Brocard C, Hartig A. Peroxisome targeting signal 1: is it really a simple tripeptide? Biochim Biophys Acta. 2006 Dec;1763(12):1565-73. doi: 10.1016/j.bbamcr.2006.08.022. Epub 2006 Aug 24. PMID: 17007944.
33. Buday K, Conrad M. Emerging roles for non-selenium containing ER-resident glutathione peroxidases in cell signaling and disease. Biol Chem. 2020 Oct 22;402(3):271-287. doi: 10.1515/hsz-2020-0286. PMID: 33055310.
34. Bulina ME, Chudakov DM, Britanova OV, Yanushevich YG, Staroverov DB, Chepurnykh TV, Merzlyak EM, Shkrob MA, Lukyanov S, Lukyanov KA. A genetically encoded photosensitizer. Nat Biotechnol. 2006 Jan;24(1):95-9. doi: 10.1038/nbt1175. Epub 2005 Dec 20. PMID: 16369538.

35. Cadet J, Douki T, Ravanat JL. Oxidatively generated damage to cellular DNA by UVB and UVA radiation. Photochem Photobiol. 2015 Jan-Feb;91(1):140-55. doi: 10.1111/php.12368. Epub 2014 Nov 27. PMID: 25327445.
36. Canet-Avilés RM, Wilson MA, Miller DW, Ahmad R, McLendon C, Bandyopadhyay S, Baptista MJ, Ringe D, Petsko GA, Cookson MR. The Parkinson's disease protein DJ-1 is neuroprotective due to cysteine-sulfinic acid-driven mitochondrial localization. Proc Natl Acad Sci U S A. 2004 Jun 15;101(24):9103-8. doi: 10.1073/pnas.0402959101. Epub 2004 Jun 4. PMID: 15181200; PMCID: PMC428480.
37. Carbon, S., Douglass, E., Good, B. M., Unni, D. R., Harris, N. L., Mungall, C. J., Basu, S., Chisholm, R. L., Dodson, R. J., Hartline, E., Fey, P., Thomas, P. D., Albou, L. P., Ebert, D., Kesling, M. J., Mi, H., Muruganujan, A., Huang, X., Mushayahama, T., … Elser, J. (2021). The Gene Ontology resource: Enriching a GOld mine. *Nucleic Acids Research*, *49*(D1), D325–D334. https://doi.org/10.1093/nar/gkaa1113
38. Carmona M, de Cubas L, Bautista E, Moral-Blanch M, Medraño-Fernández I, Sitia R, Boronat S, Ayté J, Hidalgo E. Monitoring cytosolic H_2O_2 fluctuations arising from altered plasma membrane gradients or from mitochondrial activity. Nat Commun. 2019 Oct 4;10(1):4526. doi: 10.1038/s41467-019-12475-0. PMID: 31586057; PMCID: PMC6778086.
39. Caunt CJ, Sale MJ, Smith PD, Cook SJ. MEK1 and MEK2 inhibitors and cancer therapy: the long and winding road. Nat Rev Cancer. 2015 Oct;15(10):577-92. doi: 10.1038/nrc4000. PMID: 26399658.
40. Chaudhari HN, Kim SW, Yun JW. Gender-dimorphic regulation of DJ1 and its interactions with metabolic proteins in streptozotocin-induced diabetic rats. J Cell Mol Med. 2015 May;19(5):996-1009. doi: 10.1111/jcmm.12490. Epub 2015 Feb 27. PMID: 25726699; PMCID: PMC4420602.
41. Chen J, Li L, Chin LS. Parkinson disease protein DJ-1 converts from a zymogen to a protease by carboxyl-terminal cleavage. Hum Mol Genet. 2010 Jun 15;19(12):2395-408. doi: 10.1093/hmg/ddq113. Epub 2010 Mar 18. PMID: 20304780; PMCID: PMC2876885.
42. Chen H, Zheng Z, Kim KY, Jin X, Roh MR, Jin Z. Hypermethylation and downregulation of glutathione peroxidase 3 are related to pathogenesis of melanoma. Oncol Rep. 2016 Nov;36(5):2737-2744. doi: 10.3892/or.2016.5071. Epub 2016 Sep 5. PMID: 27600457.
43. Cho KJ, Seo JM, Kim JH. Bioactive lipoxygenase metabolites stimulation of NADPH oxidases and reactive oxygen species. Mol Cells. 2011 Jul;32(1):1-5. doi: 10.1007/s10059-011-1021-7. Epub 2011 Mar 18. PMID: 21424583; PMCID: PMC3887656.
44. Chouchani ET, Pell VR, James AM, Work LM, Saeb-Parsy K, Frezza C, Krieg T, Murphy MP. A Unifying Mechanism for Mitochondrial Superoxide Production during Ischemia-Reperfusion Injury. Cell Metab. 2016 Feb 9;23(2):254-63. doi: 10.1016/j.cmet.2015.12.009. Epub 2016 Jan 14. PMID: 26777689.
45. Chowdhary G, Kataya AR, Lingner T, Reumann S. Non-canonical peroxisome targeting signals: identification of novel PTS1 tripeptides and characterization of enhancer elements by computational permutation analysis. BMC Plant Biol. 2012 Aug 11;12:142. doi: 10.1186/1471-2229-12-142. PMID: 22882975; PMCID: PMC3487989.
46. Chung HS, Wang SB, Venkatraman V, Murray CI, Van Eyk JE. Cysteine oxidative posttranslational modifications: emerging regulation in the cardiovascular system. Circ Res. 2013 Jan 18;112(2):382-92. doi: 10.1161/CIRCRESAHA.112.268680. PMID: 23329793; PMCID: PMC4340704.
47. Church SL, Grant JW, Ridnour LA, Oberley LW, Swanson PE, Meltzer PS, Trent JM. Increased manganese superoxide dismutase expression suppresses the malignant

phenotype of human melanoma cells. Proc Natl Acad Sci U S A. 1993 Apr 1;90(7):3113-7. doi: 10.1073/pnas.90.7.3113. PMID: 8464931; PMCID: PMC46247.
48. Clemens MJ. Initiation factor eIF2 alpha phosphorylation in stress responses and apoptosis. Prog Mol Subcell Biol. 2001;27:57-89. doi: 10.1007/978-3-662-09889-9_3. PMID: 11575161.
49. Cox AG, Winterbourn CC, Hampton MB. Mitochondrial peroxiredoxin involvement in antioxidant defence and redox signalling. Biochem J. 2009 Dec 23;425(2):313-25. doi: 10.1042/BJ20091541. PMID: 20025614.
50. Cracan V, Titov DV, Shen H, Grabarek Z, Mootha VK. A genetically encoded tool for manipulation of $NADP^+$/NADPH in living cells. Nat Chem Biol. 2017 Oct;13(10):1088-1095. doi: 10.1038/nchembio.2454. Epub 2017 Aug 7. PMID: 28805804; PMCID: PMC5605434.
51. Cutaneous Melanoma: Etiology and Therapy [Internet]. Brisbane (AU): Codon Publications; Ward WH, Farma JM, editors. 2017 Dec 21. Available from: https://www.ncbi.nlm.nih.gov/books/NBK481860/ doi: 10.15586/codon.cutaneousmelanoma.2017
52. Damsky WE, Rosenbaum LE, Bosenberg M. Decoding melanoma metastasis. Cancers (Basel). 2010 Dec 30;3(1):126-63. doi: 10.3390/cancers3010126. PMID: 24212610; PMCID: PMC3756353.
53. da Veiga Leprevost F, Haynes SE, Avtonomov DM, Chang HY, Shanmugam AK, Mellacheruvu D, Kong AT, Nesvizhskii AI. Philosopher: a versatile toolkit for shotgun proteomics data analysis. Nat Methods. 2020 Sep;17(9):869-870. doi: 10.1038/s41592-020-0912-y. PMID: 32669682; PMCID: PMC7509848.
54. Davis LE, Shalin SC, Tackett AJ. Current state of melanoma diagnosis and treatment. Cancer Biol Ther. 2019;20(11):1366-1379. doi: 10.1080/15384047.2019.1640032. Epub 2019 Aug 1. PMID: 31366280; PMCID: PMC6804807.
55. Day NJ, Gaffrey MJ, Qian WJ. Stoichiometric Thiol Redox Proteomics for Quantifying Cellular Responses to Perturbations. Antioxidants (Basel). 2021 Mar 23;10(3):499. doi: 10.3390/antiox10030499. PMID: 33807006; PMCID: PMC8004825.
56. de Mochel NS, Seronello S, Wang SH, Ito C, Zheng JX, Liang TJ, Lambeth JD, Choi J. Hepatocyte NAD(P)H oxidases as an endogenous source of reactive oxygen species during hepatitis C virus infection. Hepatology. 2010 Jul;52(1):47-59. doi: 10.1002/hep.23671. PMID: 20578128; PMCID: PMC3141587.
57. Dickson-Murray E, Nedara K, Modjtahedi N, Tokatlidis K. The Mia40/CHCHD4 Oxidative Folding System: Redox Regulation and Signaling in the Mitochondrial Intermembrane Space. Antioxidants (Basel). 2021 Apr 12;10(4):592. doi: 10.3390/antiox10040592. PMID: 33921425; PMCID: PMC8069373.
58. Edmondson DE. Hydrogen peroxide produced by mitochondrial monoamine oxidase catalysis: biological implications. Curr Pharm Des. 2014;20(2):155-60. doi: 10.2174/13816128113190990406. PMID: 23701542.
59. Eltoweissy M, Dihazi GH, Müller GA, Asif AR, Dihazi H. Protein DJ-1 and its anti-oxidative stress function play an important role in renal cell mediated response to profibrotic agents. Mol Biosyst. 2016 May 24;12(6):1842-59. doi: 10.1039/c5mb00887e. PMID: 27109140.
60. Ermakova YG, Bilan DS, Matlashov ME, Mishina NM, Markvicheva KN, Subach OM, Subach FV, Bogeski I, Hoth M, Enikolopov G, Belousov VV. Red fluorescent genetically encoded indicator for intracellular hydrogen peroxide. Nat Commun. 2014 Oct 21;5:5222. doi: 10.1038/ncomms6222. PMID: 25330925; PMCID: PMC4553041.

61. Farhood B, Najafi M, Salehi E, Hashemi Goradel N, Nashtaei MS, Khanlarkhani N, Mortezaee K. Disruption of the redox balance with either oxidative or anti-oxidative overloading as a promising target for cancer therapy. J Cell Biochem. 2019 Jan;120(1):71-76. doi: 10.1002/jcb.27594. Epub 2018 Sep 11. PMID: 30203529.
62. Felts SJ, Owen BA, Nguyen P, Trepel J, Donner DB, Toft DO. The hsp90-related protein TRAP1 is a mitochondrial protein with distinct functional properties. J Biol Chem. 2000 Feb 4;275(5):3305-12. doi: 10.1074/jbc.275.5.3305. PMID: 10652318.
63. Flaherty KT, Infante JR, Daud A, Gonzalez R, Kefford RF, Sosman J, Hamid O, Schuchter L, Cebon J, Ibrahim N, Kudchadkar R, Burris HA 3rd, Falchook G, Algazi A, Lewis K, Long GV, Puzanov I, Lebowitz P, Singh A, Little S, Sun P, Allred A, Ouellet D, Kim KB, Patel K, Weber J. Combined BRAF and MEK inhibition in melanoma with BRAF V600 mutations. N Engl J Med. 2012 Nov 1;367(18):1694-703. doi: 10.1056/NEJMoa1210093. Epub 2012 Sep 29. PMID: 23020132; PMCID: PMC3549295.
64. Forman HJ, Zhang H, Rinna A. Glutathione: overview of its protective roles, measurement, and biosynthesis. Mol Aspects Med. 2009 Feb-Apr;30(1-2):1-12. doi: 10.1016/j.mam.2008.08.006. Epub 2008 Aug 30. PMID: 18796312; PMCID: PMC2696075.
65. Franken H, Mathieson T, Childs D, Sweetman GM, Werner T, Tögel I, Doce C, Gade S, Bantscheff M, Drewes G, Reinhard FB, Huber W, Savitski MM. Thermal proteome profiling for unbiased identification of direct and indirect drug targets using multiplexed quantitative mass spectrometry. Nat Protoc. 2015 Oct;10(10):1567-93. doi: 10.1038/nprot.2015.101. Epub 2015 Sep 17. PMID: 26379230.
66. Fransen M, Lismont C. Peroxisomes and Cellular Oxidant/Antioxidant Balance: Protein Redox Modifications and Impact on Inter-organelle Communication. Subcell Biochem. 2018;89:435-461. doi: 10.1007/978-981-13-2233-4_19. PMID: 30378035.
67. Fransen M, Lismont C. Redox Signaling from and to Peroxisomes: Progress, Challenges, and Prospects. Antioxid Redox Signal. 2019 Jan 1;30(1):95-112. doi: 10.1089/ars.2018.7515. Epub 2018 Mar 22. PMID: 29433327.
68. Fu L, Liu K, Sun M, Tian C, Sun R, Morales Betanzos C, Tallman KA, Porter NA, Yang Y, Guo D, Liebler DC, Yang J. Systematic and Quantitative Assessment of Hydrogen Peroxide Reactivity With Cysteines Across Human Proteomes. Mol Cell Proteomics. 2017 Oct;16(10):1815-1828. doi: 10.1074/mcp.RA117.000108. Epub 2017 Aug 21. PMID: 28827280; PMCID: PMC5629266.
69. Fu L, Li Z, Liu K, Tian C, He J, He J, He F, Xu P, Yang J. A quantitative thiol reactivity profiling platform to analyze redox and electrophile reactive cysteine proteomes. Nat Protoc. 2020 Sep;15(9):2891-2919. doi: 10.1038/s41596-020-0352-2. Epub 2020 Jul 20. PMID: 32690958.
70. García-Giménez JL, Òlaso G, Hake SB, Bönisch C, Wiedemann SM, Markovic J, Dasí F, Gimeno A, Pérez-Quilis C, Palacios O, Capdevila M, Viña J, Pallardó FV. Histone h3 glutathionylation in proliferating mammalian cells destabilizes nucleosomal structure. Antioxid Redox Signal. 2013 Oct 20;19(12):1305-20. doi: 10.1089/ars.2012.5021. Epub 2013 May 21. PMID: 23541030; PMCID: PMC3791047.
71. Gao Y, Zhao Z, Meng X, Chen H, Fu G. Migration and invasion in B16-F10 mouse melanoma cells are regulated by Nrf2 inhibition during treatment with ionizing radiation. Oncol Lett. 2018 Aug;16(2):1959-1966. doi: 10.3892/ol.2018.8799. Epub 2018 May 24. PMID: 30008889; PMCID: PMC6036499.
72. Gebhart V, Reiß K, Kollau A, Mayer B, Gorren ACF. Site and mechanism of uncoupling of nitric-oxide synthase: Uncoupling by monomerization and other misconceptions. Nitric

Oxide. 2019 Aug 1;89:14-21. doi: 10.1016/j.niox.2019.04.007. Epub 2019 Apr 22. PMID: 31022534.
73. Genchi G. An overview on D-amino acids. Amino Acids. 2017 Sep;49(9):1521-1533. doi: 10.1007/s00726-017-2459-5. Epub 2017 Jul 5. PMID: 28681245.
74. Giannoni E, Taddei ML, Chiarugi P. Src redox regulation: again in the front line. Free Radic Biol Med. 2010 Aug 15;49(4):516-27. doi: 10.1016/j.freeradbiomed.2010.04.025. Epub 2010 Apr 29. PMID: 20434540.
75. Gibhardt CS, Cappello S, Bhardwaj R, Schober R, Kirsch SA, Bonilla Del Rio Z, Gahbauer S, Bochicchio A, Sumanska M, Ickes C, Stejerean-Todoran I, Mitkovski M, Alansary D, Zhang X, Revazian A, Fahrner M, Lunz V, Frischauf I, Luo T, Ezerina D, Messens J, Belousov VV, Hoth M, Böckmann RA, Hediger MA, Schindl R, Bogeski I. Oxidative Stress-Induced STIM2 Cysteine Modifications Suppress Store-Operated Calcium Entry. Cell Rep. 2020 Oct 20;33(3):108292. doi: 10.1016/j.celrep.2020.108292. PMID: 33086068.
76. Göbl C, Morris VK, van Dam L, Visscher M, Polderman PE, Hartlmüller C, de Ruiter H, Hora M, Liesinger L, Birner-Gruenberger R, Vos HR, Reif B, Madl T, Dansen TB. Cysteine oxidation triggers amyloid fibril formation of the tumor suppressor p16INK4A. Redox Biol. 2020 Jan;28:101316. doi: 10.1016/j.redox.2019.101316. Epub 2019 Sep 3. PMID: 31539802; PMCID: PMC6812003.
77. Görlach A, Bertram K, Hudecova S, Krizanova O. Calcium and ROS: A mutual interplay. Redox Biol. 2015 Dec;6:260-271. doi: 10.1016/j.redox.2015.08.010. Epub 2015 Aug 11. PMID: 26296072; PMCID: PMC4556774.
78. Go YM, Ziegler TR, Johnson JM, Gu L, Hansen JM, Jones DP. Selective protection of nuclear thioredoxin-1 and glutathione redox systems against oxidation during glucose and glutamine deficiency in human colonic epithelial cells. Free Radic Biol Med. 2007 Feb 1;42(3):363-70. doi: 10.1016/j.freeradbiomed.2006.11.005. Epub 2006 Nov 10. PMID: 17210449; PMCID: PMC1800831.
79. Govindarajan B, Sligh JE, Vincent BJ, Li M, Canter JA, Nickoloff BJ, Rodenburg RJ, Smeitink JA, Oberley L, Zhang Y, Slingerland J, Arnold RS, Lambeth JD, Cohen C, Hilenski L, Griendling K, Martínez-Diez M, Cuezva JM, Arbiser JL. Overexpression of Akt converts radial growth melanoma to vertical growth melanoma. J Clin Invest. 2007 Mar;117(3):719-29. doi: 10.1172/JCI30102. Epub 2007 Feb 22. PMID: 17318262; PMCID: PMC1797605.
80. Grant CM. Regulation of translation by hydrogen peroxide. Antioxid Redox Signal. 2011 Jul 1;15(1):191-203. doi: 10.1089/ars.2010.3699. Epub 2011 Apr 10. PMID: 21126188.
81. Griaud F, Pierce A, Gonzalez Sanchez MB, Scott M, Abraham SA, Holyoake TL, Tran DD, Tamura T, Whetton AD. A pathway from leukemogenic oncogenes and stem cell chemokines to RNA processing via THOC5. Leukemia. 2013 Apr;27(4):932-40. doi: 10.1038/leu.2012.283. Epub 2012 Oct 3. PMID: 23032722.
82. Griess B, Tom E, Domann F, Teoh-Fitzgerald M. Extracellular superoxide dismutase and its role in cancer. Free Radic Biol Med. 2017 Nov;112:464-479. doi: 10.1016/j.freeradbiomed.2017.08.013. Epub 2017 Aug 24. PMID: 28842347; PMCID: PMC5685559.
83. Guida M, Maraldi T, Beretti F, Follo MY, Manzoli L, De Pol A. Nuclear Nox4-derived reactive oxygen species in myelodysplastic syndromes. Biomed Res Int. 2014;2014:456937. doi: 10.1155/2014/456937. Epub 2014 Feb 26. PMID: 24719867; PMCID: PMC3955662.

84. Guo J, Nguyen AY, Dai Z, Su D, Gaffrey MJ, Moore RJ, Jacobs JM, Monroe ME, Smith RD, Koppenaal DW, Pakrasi HB, Qian WJ. Proteome-wide light/dark modulation of thiol oxidation in cyanobacteria revealed by quantitative site-specific redox proteomics. Mol Cell Proteomics. 2014 Dec;13(12):3270-85. doi: 10.1074/mcp.M114.041160. Epub 2014 Aug 12. PMID: 25118246; PMCID: PMC4256482.
85. Guo S, Chen X. The human Nox4: gene, structure, physiological function and pathological significance. J Drug Target. 2015 Dec;23(10):888-96. doi: 10.3109/1061186X.2015.1036276. Epub 2015 May 7. PMID: 25950600.
86. Gupta V, Carroll KS. Sulfenic acid chemistry, detection and cellular lifetime. Biochim Biophys Acta. 2014 Feb;1840(2):847-75. doi: 10.1016/j.bbagen.2013.05.040. Epub 2013 Jun 6. PMID: 23748139; PMCID: PMC4184475.
87. Gutscher M, Sobotta MC, Wabnitz GH, Ballikaya S, Meyer AJ, Samstag Y, Dick TP. Proximity-based protein thiol oxidation by H2O2-scavenging peroxidases. J Biol Chem. 2009 Nov 13;284(46):31532-40. doi: 10.1074/jbc.M109.059246. Epub 2009 Sep 15. PMID: 19755417; PMCID: PMC2797222.
88. Guttmann RP, Ghoshal S. Thiol-protease oxidation in age-related neuropathology. Free Radic Biol Med. 2011 Jul 15;51(2):282-8. doi: 10.1016/j.freeradbiomed.2011.04.017. Epub 2011 Apr 14. PMID: 21565267.
89. Halbach F, Reichelt P, Rode M, Conti E. The yeast ski complex: crystal structure and RNA channeling to the exosome complex. Cell. 2013 Aug 15;154(4):814-26. doi: 10.1016/j.cell.2013.07.017. PMID: 23953113.
90. Hansen JM, Moriarty-Craige S, Jones DP. Nuclear and cytoplasmic peroxiredoxin-1 differentially regulate NF-kappaB activities. Free Radic Biol Med. 2007 Jul 15;43(2):282-8. doi: 10.1016/j.freeradbiomed.2007.04.029. Epub 2007 Apr 29. PMID: 17603937; PMCID: PMC2096473.
91. Harding A, Giles N, Burgess A, Hancock JF, Gabrielli BG. Mechanism of mitosis-specific activation of MEK1. J Biol Chem. 2003 May 9;278(19):16747-54. doi: 10.1074/jbc.M301015200. Epub 2003 Feb 27. PMID: 12609978.
92. Hasan S, Platta HW, Erdmann R. Import of proteins into the peroxisomal matrix. Front Physiol. 2013 Sep 24;4:261. doi: 10.3389/fphys.2013.00261. PMID: 24069002; PMCID: PMC3781343.
93. Haskew-Layton RE, Payappilly JB, Smirnova NA, Ma TC, Chan KK, Murphy TH, Guo H, Langley B, Sultana R, Butterfield DA, Santagata S, Alldred MJ, Gazaryan IG, Bell GW, Ginsberg SD, Ratan RR. Controlled enzymatic production of astrocytic hydrogen peroxide protects neurons from oxidative stress via an Nrf2-independent pathway. Proc Natl Acad Sci U S A. 2010 Oct 5;107(40):17385-90. doi: 10.1073/pnas.1003996107. Epub 2010 Sep 20. PMID: 20855618; PMCID: PMC2951414.
94. Hauptmann N, Grimsby J, Shih JC, Cadenas E. The metabolism of tyramine by monoamine oxidase A/B causes oxidative damage to mitochondrial DNA. Arch Biochem Biophys. 1996 Nov 15;335(2):295-304. doi: 10.1006/abbi.1996.0510. PMID: 8914926.
95. Heath CG, Viphakone N, Wilson SA. The role of TREX in gene expression and disease. Biochem J. 2016 Oct 1;473(19):2911-35. doi: 10.1042/BCJ20160010. PMID: 27679854; PMCID: PMC5095910.
96. Heckman KL, Pease LR. Gene splicing and mutagenesis by PCR-driven overlap extension. Nat Protoc. 2007;2(4):924-32. doi: 10.1038/nprot.2007.132. PMID: 17446874.
97. Heine GF, Horwitz AA, Parvin JD. Multiple mechanisms contribute to inhibit transcription in response to DNA damage. J Biol Chem. 2008 Apr 11;283(15):9555-61. doi: 10.1074/jbc.M707700200. Epub 2008 Feb 15. PMID: 18281289; PMCID: PMC2442283.

98. Heo J. Redox control of GTPases: from molecular mechanisms to functional significance in health and disease. Antioxid Redox Signal. 2011 Feb 15;14(4):689-724. doi: 10.1089/ars.2009.2984. Epub 2010 Oct 25. PMID: 20649471.
99. Heo S, Kim S, Kang D. The Role of Hydrogen Peroxide and Peroxiredoxins throughout the Cell Cycle. Antioxidants (Basel). 2020 Mar 26;9(4):280. doi: 10.3390/antiox9040280. PMID: 32224940; PMCID: PMC7222192.
100. Hirota K, Murata M, Sachi Y, Nakamura H, Takeuchi J, Mori K, Yodoi J. Distinct roles of thioredoxin in the cytoplasm and in the nucleus. A two-step mechanism of redox regulation of transcription factor NF-kappaB. J Biol Chem. 1999 Sep 24;274(39):27891-7. doi: 10.1074/jbc.274.39.27891. PMID: 10488136.
101. Ho YS, Xiong Y, Ma W, Spector A, Ho DS. Mice lacking catalase develop normally but show differential sensitivity to oxidant tissue injury. J Biol Chem. 2004 Jul 30;279(31):32804-12. doi: 10.1074/jbc.M404800200. Epub 2004 Jun 3. PMID: 15178682.
102. Huang H, Haar Petersen M, Ibañez-Vea M, Lassen PS, Larsen MR, Palmisano G. Simultaneous Enrichment of Cysteine-containing Peptides and Phosphopeptides Using a Cysteine-specific Phosphonate Adaptable Tag (CysPAT) in Combination with titanium dioxide (TiO2) Chromatography. Mol Cell Proteomics. 2016 Oct;15(10):3282-3296. doi: 10.1074/mcp.M115.054551. Epub 2016 Jun 8. PMID: 27281782; PMCID: PMC5054350.
103. Huber W, von Heydebreck A, Sültmann H, Poustka A, Vingron M. Variance stabilization applied to microarray data calibration and to the quantification of differential expression. Bioinformatics. 2002;18 Suppl 1:S96-104. doi: 10.1093/bioinformatics/18.suppl_1.s96. PMID: 12169536.
104. Hughes JR, Roberts N, McGowan S, Hay D, Giannoulatou E, Lynch M, De Gobbi M, Taylor S, Gibbons R, Higgs DR. Analysis of hundreds of cis-regulatory landscapes at high resolution in a single, high-throughput experiment. Nat Genet. 2014 Feb;46(2):205-12. doi: 10.1038/ng.2871. Epub 2014 Jan 12. PMID: 24413732.
105. Hulstaert N, Shofstahl J, Sachsenberg T, Walzer M, Barsnes H, Martens L, Perez-Riverol Y. ThermoRawFileParser: Modular, Scalable, and Cross-Platform RAW File Conversion. J Proteome Res. 2020 Jan 3;19(1):537-542. doi: 10.1021/acs.jproteome.9b00328. Epub 2019 Dec 6. PMID: 31755270; PMCID: PMC7116465.
106. Imai H, Nakagawa Y. Biological significance of phospholipid hydroperoxide glutathione peroxidase (PHGPx, GPx4) in mammalian cells. Free Radic Biol Med. 2003 Jan 15;34(2):145-69. doi: 10.1016/s0891-5849(02)01197-8. PMID: 12521597.
107. Imlay JA. Cellular defenses against superoxide and hydrogen peroxide. Annu Rev Biochem. 2008;77:755-76. doi: 10.1146/annurev.biochem.77.061606.161055. PMID: 18173371; PMCID: PMC3057177.
108. Jamar NH, Kritsiligkou P, Grant CM. The non-stop decay mRNA surveillance pathway is required for oxidative stress tolerance. Nucleic Acids Res. 2017 Jun 20;45(11):6881-6893. doi: 10.1093/nar/gkx306. PMID: 28472342; PMCID: PMC5499853.
109. Jessen C, Kreß JKC, Baluapuri A, Hufnagel A, Schmitz W, Kneitz S, Roth S, Marquardt A, Appenzeller S, Ade CP, Glutsch V, Wobser M, Friedmann-Angeli JP, Mosteo L, Goding CR, Schilling B, Geissinger E, Wolf E, Meierjohann S. The transcription factor NRF2 enhances melanoma malignancy by blocking differentiation and inducing COX2 expression. Oncogene. 2020 Oct;39(44):6841-6855. doi: 10.1038/s41388-020-01477-8. Epub 2020 Sep 25. Erratum in: Oncogene. 2021 Feb;40(7):1391. PMID: 32978520; PMCID: PMC7605435.

110. Ježek J, Cooper KF, Strich R. Reactive Oxygen Species and Mitochondrial Dynamics: The Yin and Yang of Mitochondrial Dysfunction and Cancer Progression. Antioxidants (Basel). 2018 Jan 16;7(1):13. doi: 10.3390/antiox7010013. PMID: 29337889; PMCID: PMC5789323.
111. Ježek P, Jabůrek M, Porter RK. Uncoupling mechanism and redox regulation of mitochondrial uncoupling protein 1 (UCP1). Biochim Biophys Acta Bioenerg. 2019 Mar 1;1860(3):259-269. doi: 10.1016/j.bbabio.2018.11.007. Epub 2018 Nov 8. PMID: 30414927.
112. Jimeno S, Aguilera A. The THO complex as a key mRNP biogenesis factor in development and cell differentiation. J Biol. 2010;9(1):6. doi: 10.1186/jbiol217. Epub 2010 Jan 28. PMID: 20236444; PMCID: PMC2871528.
113. Jones DP, Go YM. Redox compartmentalization and cellular stress. Diabetes Obes Metab. 2010 Oct;12 Suppl 2(Suppl 2):116-25. doi: 10.1111/j.1463-1326.2010.01266.x. PMID: 21029308; PMCID: PMC3052693.
114. Joseph SK, Booth DM, Young MP, Hajnóczky G. Redox regulation of ER and mitochondrial Ca^{2+} signaling in cell survival and death. Cell Calcium. 2019 May;79:89-97. doi: 10.1016/j.ceca.2019.02.006. Epub 2019 Feb 16. PMID: 30889512; PMCID: PMC8409742.
115. Kakihana T, Nagata K, Sitia R. Peroxides and peroxidases in the endoplasmic reticulum: integrating redox homeostasis and oxidative folding. Antioxid Redox Signal. 2012 Apr 15;16(8):763-71. doi: 10.1089/ars.2011.4238. Epub 2012 Jan 25. PMID: 22146055.
116. Kang DH, Lee DJ, Lee KW, Park YS, Lee JY, Lee SH, Koh YJ, Koh GY, Choi C, Yu DY, Kim J, Kang SW. Peroxiredoxin II is an essential antioxidant enzyme that prevents the oxidative inactivation of VEGF receptor-2 in vascular endothelial cells. Mol Cell. 2011 Nov 18;44(4):545-58. doi: 10.1016/j.molcel.2011.08.040. PMID: 22099303.
117. Karpievitch YV, Dabney AR, Smith RD. Normalization and missing value imputation for label-free LC-MS analysis. BMC Bioinformatics. 2012;13 Suppl 16(Suppl 16):S5. doi: 10.1186/1471-2105-13-S16-S5. Epub 2012 Nov 5. PMID: 23176322; PMCID: PMC3489534.
118. Katane M, Kawata T, Nakayama K, Saitoh Y, Kaneko Y, Matsuda S, Saitoh Y, Miyamoto T, Sekine M, Homma H. Characterization of the enzymatic and structural properties of human D-aspartate oxidase and comparison with those of the rat and mouse enzymes. Biol Pharm Bull. 2015;38(2):298-305. doi: 10.1248/bpb.b14-00690. PMID: 25747990.
119. Katane M, Saitoh Y, Seida Y, Sekine M, Furuchi T, Homma H. Comparative characterization of three D-aspartate oxidases and one D-amino acid oxidase from Caenorhabditis elegans. Chem Biodivers. 2010 Jun;7(6):1424-34. doi: 10.1002/cbdv.200900294. PMID: 20564561.
120. Kelly SM, Leung SW, Pak C, Banerjee A, Moberg KH, Corbett AH. A conserved role for the zinc finger polyadenosine RNA binding protein, ZC3H14, in control of poly(A) tail length. RNA. 2014 May;20(5):681-8. doi: 10.1261/rna.043984.113. Epub 2014 Mar 26. PMID: 24671764; PMCID: PMC3988569.
121. Kim EK, Jang M, Song MJ, Kim D, Kim Y, Jang HH. Redox-Mediated Mechanism of Chemoresistance in Cancer Cells. Antioxidants (Basel). 2019 Oct 10;8(10):471. doi: 10.3390/antiox8100471. PMID: 31658599; PMCID: PMC6826977.
122. Kim YM, Youn SW, Sudhahar V, Das A, Chandhri R, Cuervo Grajal H, Kweon J, Leanhart S, He L, Toth PT, Kitajewski J, Rehman J, Yoon Y, Cho J, Fukai T, Ushio-Fukai M. Redox Regulation of Mitochondrial Fission Protein Drp1 by Protein Disulfide

Isomerase Limits Endothelial Senescence. Cell Rep. 2018 Jun 19;23(12):3565-3578. doi: 10.1016/j.celrep.2018.05.054. PMID: 29924999; PMCID: PMC6324937.
123. Kinoshita E, Kinoshita-Kikuta E, Kubota Y, Takekawa M, Koike T. A Phos-tag SDS-PAGE method that effectively uses phosphoproteomic data for profiling the phosphorylation dynamics of MEK1. Proteomics. 2016 Jul;16(13):1825-36. doi: 10.1002/pmic.201500494. Epub 2016 Jun 8. PMID: 27169363.
124. Klopfenstein DV, Zhang L, Pedersen BS, Ramírez F, Warwick Vesztrocy A, Naldi A, Mungall CJ, Yunes JM, Botvinnik O, Weigel M, Dampier W, Dessimoz C, Flick P, Tang H. GOATOOLS: A Python library for Gene Ontology analyses. Sci Rep. 2018 Jul 18;8(1):10872. doi: 10.1038/s41598-018-28948-z. PMID: 30022098; PMCID: PMC6052049.
125. Knoops B, Goemaere J, Van der Eecken V, Declercq JP. Peroxiredoxin 5: structure, mechanism, and function of the mammalian atypical 2-Cys peroxiredoxin. Antioxid Redox Signal. 2011 Aug 1;15(3):817-29. doi: 10.1089/ars.2010.3584. Epub 2011 Apr 20. PMID: 20977338.
126. Kodali VK, Thorpe C. Oxidative protein folding and the Quiescin-sulfhydryl oxidase family of flavoproteins. Antioxid Redox Signal. 2010 Oct;13(8):1217-30. doi: 10.1089/ars.2010.3098. PMID: 20136510; PMCID: PMC2959182.
127. Kong AT, Leprevost FV, Avtonomov DM, Mellacheruvu D, Nesvizhskii AI. MSFragger: ultrafast and comprehensive peptide identification in mass spectrometry-based proteomics. Nat Methods. 2017 May;14(5):513-520. doi: 10.1038/nmeth.4256. Epub 2017 Apr 10. PMID: 28394336; PMCID: PMC5409104.
128. Konno T, Melo EP, Chambers JE, Avezov E. Intracellular Sources of ROS/H_2O_2 in Health and Neurodegeneration: Spotlight on Endoplasmic Reticulum. Cells. 2021 Jan 25;10(2):233. doi: 10.3390/cells10020233. PMID: 33504070; PMCID: PMC7912550.
129. Kostyuk AI, Demidovich AD, Kotova DA, Belousov VV, Bilan DS. Circularly Permuted Fluorescent Protein-Based Indicators: History, Principles, and Classification. Int J Mol Sci. 2019 Aug 27;20(17):4200. doi: 10.3390/ijms20174200. PMID: 31461959; PMCID: PMC6747460.
130. Kudryavtseva AV, Krasnov GS, Dmitriev AA, Alekseev BY, Kardymon OL, Sadritdinova AF, Fedorova MS, Pokrovsky AV, Melnikova NV, Kaprin AD, Moskalev AA, Snezhkina AV. Mitochondrial dysfunction and oxidative stress in aging and cancer. Oncotarget. 2016 Jul 19;7(29):44879-44905. doi: 10.18632/oncotarget.9821. PMID: 27270647; PMCID: PMC5216692.
131. Lambeth JD. NOX enzymes and the biology of reactive oxygen. Nat Rev Immunol. 2004 Mar;4(3):181-9. doi: 10.1038/nri1312. PMID: 15039755.
132. Lee CJ, Qiu TA, Sweedler JV. d-Alanine: Distribution, origin, physiological relevance, and implications in disease. Biochim Biophys Acta Proteins Proteom. 2020 Nov;1868(11):140482. doi: 10.1016/j.bbapap.2020.140482. Epub 2020 Jul 5. PMID: 32640293.
133. Lee DH, Kim D, Kim ST, Jeong S, Kim JL, Shim SM, Heo AJ, Song X, Guo ZS, Bartlett DL, Oh SC, Lee J, Saito Y, Kim BY, Kwon YT, Lee YJ. PARK7 modulates autophagic proteolysis through binding to the N-terminally arginylated form of the molecular chaperone HSPA5. Autophagy. 2018;14(11):1870-1885. doi: 10.1080/15548627.2018.1491212. Epub 2018 Jul 23. PMID: 29976090; PMCID: PMC6152518.

134. Lefaki M, Papaevgeniou N, Chondrogianni N. Redox regulation of proteasome function. Redox Biol. 2017 Oct;13:452-458. doi: 10.1016/j.redox.2017.07.005. Epub 2017 Jul 6. PMID: 28715730; PMCID: PMC5512181.
135. Leichert LI, Gehrke F, Gudiseva HV, Blackwell T, Ilbert M, Walker AK, Strahler JR, Andrews PC, Jakob U. Quantifying changes in the thiol redox proteome upon oxidative stress in vivo. Proc Natl Acad Sci U S A. 2008 Jun 17;105(24):8197-202. doi: 10.1073/pnas.0707723105. Epub 2008 Feb 14. PMID: 18287020; PMCID: PMC2448814.
136. Lennicke C, Rahn J, Lichtenfels R, Wessjohann LA, Seliger B. Hydrogen peroxide - production, fate and role in redox signaling of tumor cells. Cell Commun Signal. 2015 Sep 14;13:39. doi: 10.1186/s12964-015-0118-6. PMID: 26369938; PMCID: PMC4570748.
137. Lévy E, El Banna N, Baïlle D, Heneman-Masurel A, Truchet S, Rezaei H, Huang ME, Béringue V, Martin D, Vernis L. Causative Links between Protein Aggregation and Oxidative Stress: A Review. Int J Mol Sci. 2019 Aug 9;20(16):3896. doi: 10.3390/ijms20163896. PMID: 31405050; PMCID: PMC6719959.
138. Li Z, Xu X. Post-Translational Modifications of the Mini-Chromosome Maintenance Proteins in DNA Replication. Genes (Basel). 2019 Apr 30;10(5):331. doi: 10.3390/genes10050331. PMID: 31052337; PMCID: PMC6563057.
139. Li HM, Niki T, Taira T, Iguchi-Ariga SM, Ariga H. Association of DJ-1 with chaperones and enhanced association and colocalization with mitochondrial Hsp70 by oxidative stress. Free Radic Res. 2005 Oct;39(10):1091-9. doi: 10.1080/10715760500260348. PMID: 16298734.
140. Lismont C, Nordgren M, Brees C, Knoops B, Van Veldhoven PP, Fransen M. Peroxisomes as Modulators of Cellular Protein Thiol Oxidation: A New Model System. Antioxid Redox Signal. 2019 Jan 1;30(1):22-39. doi: 10.1089/ars.2017.6997. Epub 2017 Jul 14. PMID: 28594286.
141. Liu F, Gomez Garcia AM, Meyskens FL Jr. NADPH oxidase 1 overexpression enhances invasion via matrix metalloproteinase-2 and epithelial-mesenchymal transition in melanoma cells. J Invest Dermatol. 2012 Aug;132(8):2033-41. doi: 10.1038/jid.2012.119. Epub 2012 Apr 19. PMID: 22513785.
142. Liu Y, Ma X, Fujioka H, Liu J, Chen S, Zhu X. DJ-1 regulates the integrity and function of ER-mitochondria association through interaction with IP3R3-Grp75-VDAC1. Proc Natl Acad Sci U S A. 2019 Dec 10;116(50):25322-25328. doi: 10.1073/pnas.1906565116. Epub 2019 Nov 25. PMID: 31767755; PMCID: PMC6911199.
143. Liu-Smith F, Dellinger R, Meyskens FL Jr. Updates of reactive oxygen species in melanoma etiology and progression. Arch Biochem Biophys. 2014 Dec 1;563:51-5. doi: 10.1016/j.abb.2014.04.007. Epub 2014 Apr 26. PMID: 24780245; PMCID: PMC4209333.
144. Lokaj K, Meierjohann S, Schütz C, Teutschbein J, Schartl M, Sickmann A. Quantitative differential proteome analysis in an animal model for human melanoma. J Proteome Res. 2009 Apr;8(4):1818-27. doi: 10.1021/pr800578a. PMID: 19249851.
145. Lu J, Holmgren A. Selenoproteins. J Biol Chem. 2009 Jan 9;284(2):723-7. doi: 10.1074/jbc.R800045200. Epub 2008 Aug 29. PMID: 18757362.
146. Lu J, Holmgren A. The thioredoxin antioxidant system. Free Radic Biol Med. 2014 Jan;66:75-87. doi: 10.1016/j.freeradbiomed.2013.07.036. Epub 2013 Jul 27. PMID: 23899494.
147. Lu J, Holmgren A. The thioredoxin superfamily in oxidative protein folding. Antioxid Redox Signal. 2014 Jul 20;21(3):457-70. doi: 10.1089/ars.2014.5849. Epub 2014 Mar 6. PMID: 24483600.

148. Luke JJ, Flaherty KT, Ribas A, Long GV. Targeted agents and immunotherapies: optimizing outcomes in melanoma. Nat Rev Clin Oncol. 2017 Aug;14(8):463-482. doi: 10.1038/nrclinonc.2017.43. Epub 2017 Apr 4. PMID: 28374786.
149. Lukosz M, Jakob S, Büchner N, Zschauer TC, Altschmied J, Haendeler J. Nuclear redox signaling. Antioxid Redox Signal. 2010 Mar 15;12(6):713-42. doi: 10.1089/ars.2009.2609. PMID: 19737086.
150. Lu SC. Regulation of glutathione synthesis. Mol Aspects Med. 2009 Feb-Apr;30(1-2):42-59. doi: 10.1016/j.mam.2008.05.005. Epub 2008 Jun 14. PMID: 18601945; PMCID: PMC2704241.
151. Makino Y, Yoshikawa N, Okamoto K, Hirota K, Yodoi J, Makino I, Tanaka H. Direct association with thioredoxin allows redox regulation of glucocorticoid receptor function. J Biol Chem. 1999 Jan 29;274(5):3182-8. doi: 10.1074/jbc.274.5.3182. PMID: 9915858.
152. Malinouski M, Zhou Y, Belousov VV, Hatfield DL, Gladyshev VN. Hydrogen peroxide probes directed to different cellular compartments. PLoS One. 2011 Jan 21;6(1):e14564. doi: 10.1371/journal.pone.0014564. PMID: 21283738; PMCID: PMC3024970.
153. Marfatia KA, Crafton EB, Green DM, Corbett AH. Domain analysis of the Saccharomyces cerevisiae heterogeneous nuclear ribonucleoprotein, Nab2p. Dissecting the requirements for Nab2p-facilitated poly(A) RNA export. J Biol Chem. 2003 Feb 28;278(9):6731-40. doi: 10.1074/jbc.M207571200. Epub 2002 Dec 19. PMID: 12496292.
154. Marinho HS, Real C, Cyrne L, Soares H, Antunes F. Hydrogen peroxide sensing, signaling and regulation of transcription factors. Redox Biol. 2014 Feb 23;2:535-62. doi: 10.1016/j.redox.2014.02.006. PMID: 24634836; PMCID: PMC3953959.
155. Markvicheva KN, Bilan DS, Mishina NM, Gorokhovatsky AY, Vinokurov LM, Lukyanov S, Belousov VV. A genetically encoded sensor for H2O2 with expanded dynamic range. Bioorg Med Chem. 2011 Feb 1;19(3):1079-84. doi: 10.1016/j.bmc.2010.07.014. Epub 2010 Aug 5. PMID: 20692175.
156. Masgras I, Sanchez-Martin C, Colombo G, Rasola A. The Chaperone TRAP1 As a Modulator of the Mitochondrial Adaptations in Cancer Cells. Front Oncol. 2017 Mar 29;7:58. doi: 10.3389/fonc.2017.00058. PMID: 28405578; PMCID: PMC5370238.
157. Mateus A, Hevler J, Bobonis J, Kurzawa N, Shah M, Mitosch K, Goemans CV, Helm D, Stein F, Typas A, Savitski MM. The functional proteome landscape of Escherichia coli. Nature. 2020 Dec;588(7838):473-478. doi: 10.1038/s41586-020-3002-5. Epub 2020 Dec 9. PMID: 33299184.
158. Mateus A, Kurzawa N, Becher I, Sridharan S, Helm D, Stein F, Typas A, Savitski MM. Thermal proteome profiling for interrogating protein interactions. Mol Syst Biol. 2020 Mar;16(3):e9232. doi: 10.15252/msb.20199232. PMID: 32133759; PMCID: PMC7057112.
159. Mateus A, Määttä TA, Savitski MM. Thermal proteome profiling: unbiased assessment of protein state through heat-induced stability changes. Proteome Sci. 2017 Jun 24;15:13. doi: 10.1186/s12953-017-0122-4. PMID: 28652855; PMCID: PMC5482948.
160. Matlashov ME, Belousov VV, Enikolopov G. How much H(2)O(2) is produced by recombinant D-amino acid oxidase in mammalian cells? Antioxid Redox Signal. 2014 Mar 1;20(7):1039-44. doi: 10.1089/ars.2013.5618. Epub 2013 Oct 23. PMID: 24020354; PMCID: PMC3928830.
161. Matsui R, Ferran B, Oh A, Croteau D, Shao D, Han J, Pimentel DR, Bachschmid MM. Redox Regulation *via* Glutaredoxin-1 and Protein *S*-Glutathionylation. Antioxid Redox Signal. 2020 Apr 1;32(10):677-700. doi: 10.1089/ars.2019.7963. Epub 2020 Jan 23. PMID: 31813265; PMCID: PMC7047114.

162. Mehmeti I, Lortz S, Lenzen S. The H2O2-sensitive HyPer protein targeted to the endoplasmic reticulum as a mirror of the oxidizing thiol-disulfide milieu. Free Radic Biol Med. 2012 Oct 1;53(7):1451-8. doi: 10.1016/j.freeradbiomed.2012.08.010. Epub 2012 Aug 10. PMID: 22921589.
163. Melo FH, Mologhoni F, Morais AS, Toricelli M, Mouro MG, Higa EM, Lopes JD, Jasiulionis MG. Endothelial nitric oxide synthase uncoupling as a key mediator of melanocyte malignant transformation associated with sustained stress conditions. Free Radic Biol Med. 2011 May 15;50(10):1263-73. doi: 10.1016/j.freeradbiomed.2011.02.022. Epub 2011 Mar 15. PMID: 21362470.
164. Mencke P, Boussaad I, Romano CD, Kitami T, Linster CL, Krüger R. The Role of DJ-1 in Cellular Metabolism and Pathophysiological Implications for Parkinson's Disease. Cells. 2021 Feb 7;10(2):347. doi: 10.3390/cells10020347. PMID: 33562311; PMCID: PMC7915027.
165. Mermelekas G, Makridakis M, Koeck T, Vlahou A. Redox proteomics: from residue modifications to putative biomarker identification by gel- and LC-MS-based approaches. Expert Rev Proteomics. 2013 Dec;10(6):537-49. doi: 10.1586/14789450.2013.855611. PMID: 24206227.
166. Meyskens FL Jr, McNulty SE, Buckmeier JA, Tohidian NB, Spillane TJ, Kahlon RS, Gonzalez RI. Aberrant redox regulation in human metastatic melanoma cells compared to normal melanocytes. Free Radic Biol Med. 2001 Sep 15;31(6):799-808. doi: 10.1016/s0891-5849(01)00650-5. PMID: 11557318.
167. Michalska P, León R. When It Comes to an End: Oxidative Stress Crosstalk with Protein Aggregation and Neuroinflammation Induce Neurodegeneration. Antioxidants (Basel). 2020 Aug 12;9(8):740. doi: 10.3390/antiox9080740. PMID: 32806679; PMCID: PMC7463521.
168. Miller AJ, Mihm MC Jr. Melanoma. N Engl J Med. 2006 Jul 6;355(1):51-65. doi: 10.1056/NEJMra052166. PMID: 16822996.
169. Mimura K, Kua LF, Shimasaki N, Shiraishi K, Nakajima S, Siang LK, Shabbir A, So J, Yong WP, Kono K. Upregulation of thioredoxin-1 in activated human NK cells confers increased tolerance to oxidative stress. Cancer Immunol Immunother. 2017 May;66(5):605-613. doi: 10.1007/s00262-017-1969-z. Epub 2017 Feb 21. PMID: 28224212.
170. Miriyala S, Holley AK, St Clair DK. Mitochondrial superoxide dismutase--signals of distinction. Anticancer Agents Med Chem. 2011 Feb;11(2):181-90. doi: 10.2174/187152011795255920. PMID: 21355846; PMCID: PMC3427752.
171. Miseta A, Csutora P. Relationship between the occurrence of cysteine in proteins and the complexity of organisms. Mol Biol Evol. 2000 Aug;17(8):1232-9. doi: 10.1093/oxfordjournals.molbev.a026406. PMID: 10908643.
172. Mishina NM, Bogdanova YA, Ermakova YG, Panova AS, Kotova DA, Bilan DS, Steinhorn B, Arnér ESJ, Michel T, Belousov VV. Which Antioxidant System Shapes Intracellular H_2O_2 Gradients? Antioxid Redox Signal. 2019 Sep 20;31(9):664-670. doi: 10.1089/ars.2018.7697. Epub 2019 Apr 24. PMID: 30864831; PMCID: PMC6657290.
173. Mishina NM, Tyurin-Kuzmin PA, Markvicheva KN, Vorotnikov AV, Tkachuk VA, Laketa V, Schultz C, Lukyanov S, Belousov VV. Does cellular hydrogen peroxide diffuse or act locally? Antioxid Redox Signal. 2011 Jan 1;14(1):1-7. doi: 10.1089/ars.2010.3539. Epub 2010 Oct 12. PMID: 20690882.
174. Mishra M, Jiang H, Wu L, Chawsheen HA, Wei Q. The sulfiredoxin-peroxiredoxin (Srx-Prx) axis in cell signal transduction and cancer development. Cancer Lett. 2015 Oct

1;366(2):150-9. doi: 10.1016/j.canlet.2015.07.002. Epub 2015 Jul 10. PMID: 26170166; PMCID: PMC4532351.

175. Mishra, R., Patel, H., Yuan, L., & Garrett, J. (2018). Role of Reactive Oxygen Species and Targeted Therapy in Metastatic Melanoma. *Cancer Research Frontiers, 4*(1), 101–130. https://doi.org/10.17980/2018.101

176. Moloney JN, Cotter TG. ROS signalling in the biology of cancer. Semin Cell Dev Biol. 2018 Aug;80:50-64. doi: 10.1016/j.semcdb.2017.05.023. Epub 2017 Jun 3. PMID: 28587975.

177. Morgan B, Van Laer K, Owusu TN, Ezeriņa D, Pastor-Flores D, Amponsah PS, Tursch A, Dick TP. Real-time monitoring of basal H2O2 levels with peroxiredoxin-based probes. Nat Chem Biol. 2016 Jun;12(6):437-43. doi: 10.1038/nchembio.2067. Epub 2016 Apr 18. PMID: 27089028.

178. Morris KJ, Corbett AH. The polyadenosine RNA-binding protein ZC3H14 interacts with the THO complex and coordinately regulates the processing of neuronal transcripts. Nucleic Acids Res. 2018 Jul 27;46(13):6561-6575. doi: 10.1093/nar/gky446. PMID: 29912477; PMCID: PMC6061872.

179. Moutty MC, Sakin V, Melchior F. Importin α/β mediates nuclear import of individual SUMO E1 subunits and of the holo-enzyme. Mol Biol Cell. 2011 Mar 1;22(5):652-60. doi: 10.1091/mbc.E10-05-0461. Epub 2011 Jan 5. PMID: 21209321; PMCID: PMC3046061.

180. Mulvaney KM, Matson JP, Siesser PF, Tamir TY, Goldfarb D, Jacobs TM, Cloer EW, Harrison JS, Vaziri C, Cook JG, Major MB. Identification and Characterization of MCM3 as a Kelch-like ECH-associated Protein 1 (KEAP1) Substrate. J Biol Chem. 2016 Nov 4;291(45):23719-23733. doi: 10.1074/jbc.M116.729418. Epub 2016 Sep 12. PMID: 27621311; PMCID: PMC5095425.

181. Murphy MP. How mitochondria produce reactive oxygen species. Biochem J. 2009 Jan 1;417(1):1-13. doi: 10.1042/BJ20081386. PMID: 19061483; PMCID: PMC2605959.

182. Nagy P. Kinetics and mechanisms of thiol-disulfide exchange covering direct substitution and thiol oxidation-mediated pathways. Antioxid Redox Signal. 2013 May 1;18(13):1623-41. doi: 10.1089/ars.2012.4973. Epub 2013 Jan 9. PMID: 23075118; PMCID: PMC3613173.

183. Nasti TH, Timares L. MC1R, eumelanin and pheomelanin: their role in determining the susceptibility to skin cancer. Photochem Photobiol. 2015 Jan-Feb;91(1):188-200. doi: 10.1111/php.12335. Epub 2014 Nov 7. PMID: 25155575; PMCID: PMC4299862.

184. Nauser T, Steinmann D, Grassi G, Koppenol WH. Why selenocysteine replaces cysteine in thioredoxin reductase: a radical hypothesis. Biochemistry. 2014 Aug 5;53(30):5017-22. doi: 10.1021/bi5003376. Epub 2014 Jul 16. PMID: 24999795.

185. Niethammer P, Grabher C, Look AT, Mitchison TJ. A tissue-scale gradient of hydrogen peroxide mediates rapid wound detection in zebrafish. Nature. 2009 Jun 18;459(7249):996-9. doi: 10.1038/nature08119. Epub 2009 Jun 3. PMID: 19494811; PMCID: PMC2803098.

186. Nilson KA, Lawson CK, Mullen NJ, Ball CB, Spector BM, Meier JL, Price DH. Oxidative stress rapidly stabilizes promoter-proximal paused Pol II across the human genome. Nucleic Acids Res. 2017 Nov 2;45(19):11088-11105. doi: 10.1093/nar/gkx724. PMID: 28977633; PMCID: PMC5737879.

187. Niu Y, DesMarais TL, Tong Z, Yao Y, Costa M. Oxidative stress alters global histone modification and DNA methylation. Free Radic Biol Med. 2015 May;82:22-8. doi: 10.1016/j.freeradbiomed.2015.01.028. Epub 2015 Feb 3. PMID: 25656994; PMCID: PMC4464695.

188. Nott A, Watson PM, Robinson JD, Crepaldi L, Riccio A. S-Nitrosylation of histone deacetylase 2 induces chromatin remodelling in neurons. Nature. 2008 Sep 18;455(7211):411-5. doi: 10.1038/nature07238. Epub 2008 Aug 27. PMID: 18754010.
189. Nulton-Persson AC, Starke DW, Mieyal JJ, Szweda LI. Reversible inactivation of alpha-ketoglutarate dehydrogenase in response to alterations in the mitochondrial glutathione status. Biochemistry. 2003 Apr 15;42(14):4235-42. doi: 10.1021/bi027370f. PMID: 12680778.
190. Obsilova V, Obsil T. The 14-3-3 Proteins as Important Allosteric Regulators of Protein Kinases. Int J Mol Sci. 2020 Nov 21;21(22):8824. doi: 10.3390/ijms21228824. PMID: 33233473; PMCID: PMC7700312.
191. Ogata FT, Branco V, Vale FF, Coppo L. Glutaredoxin: Discovery, redox defense and much more. Redox Biol. 2021 Jul;43:101975. doi: 10.1016/j.redox.2021.101975. Epub 2021 Apr 20. PMID: 33932870; PMCID: PMC8102999.
192. Okado-Matsumoto A, Fridovich I. Subcellular distribution of superoxide dismutases (SOD) in rat liver: Cu,Zn-SOD in mitochondria. J Biol Chem. 2001 Oct 19;276(42):38388-93. doi: 10.1074/jbc.M105395200. Epub 2001 Aug 15. PMID: 11507097.
193. Okumoto K, El Shermely M, Natsui M, Kosako H, Natsuyama R, Marutani T, Fujiki Y. The peroxisome counteracts oxidative stresses by suppressing catalase import via Pex14 phosphorylation. Elife. 2020 Aug 24;9:e55896. doi: 10.7554/eLife.55896. PMID: 32831175; PMCID: PMC7498260.
194. Pak VV, Ezeriņa D, Lyublinskaya OG, Pedre B, Tyurin-Kuzmin PA, Mishina NM, Thauvin M, Young D, Wahni K, Martínez Gache SA, Demidovich AD, Ermakova YG, Maslova YD, Shokhina AG, Eroglu E, Bilan DS, Bogeski I, Michel T, Vriz S, Messens J, Belousov VV. Ultrasensitive Genetically Encoded Indicator for Hydrogen Peroxide Identifies Roles for the Oxidant in Cell Migration and Mitochondrial Function. Cell Metab. 2020 Mar 3;31(3):642-653.e6. doi: 10.1016/j.cmet.2020.02.003. PMID: 32130885; PMCID: PMC7088435.
195. Park J, Lee S, Lee S, Kang SW. 2-cys peroxiredoxins: emerging hubs determining redox dependency of Mammalian signaling networks. Int J Cell Biol. 2014;2014:715867. doi: 10.1155/2014/715867. Epub 2014 Feb 4. PMID: 24672551; PMCID: PMC3932224.
196. Parker MW, Botchan MR, Berger JM. Mechanisms and regulation of DNA replication initiation in eukaryotes. Crit Rev Biochem Mol Biol. 2017 Apr;52(2):107-144. doi: 10.1080/10409238.2016.1274717. Epub 2017 Jan 17. PMID: 28094588; PMCID: PMC5545932.
197. Passarelli A, Mannavola F, Stucci LS, Tucci M, Silvestris F. Immune system and melanoma biology: a balance between immunosurveillance and immune escape. Oncotarget. 2017 Oct 31;8(62):106132-106142. doi: 10.18632/oncotarget.22190. PMID: 29285320; PMCID: PMC5739707.
198. Pedregosa, F., Varoquaux, Ga"el, Gramfort, A., Michel, V., Thirion, B., Grisel, O., … others. (2011). Scikit-learn: Machine learning in Python. Journal of Machine Learning Research, 12(Oct), 2825–2830.
199. Peng D, Belkhiri A, Hu T, Chaturvedi R, Asim M, Wilson KT, Zaika A, El-Rifai W. Glutathione peroxidase 7 protects against oxidative DNA damage in oesophageal cells. Gut. 2012 Sep;61(9):1250-60. doi: 10.1136/gutjnl-2011-301078. Epub 2011 Dec 9. PMID: 22157330; PMCID: PMC3419307.
200. Perillo B, Di Donato M, Pezone A, Di Zazzo E, Giovannelli P, Galasso G, Castoria G, Migliaccio A. ROS in cancer therapy: the bright side of the moon. Exp Mol Med. 2020

Feb;52(2):192-203. doi: 10.1038/s12276-020-0384-2. Epub 2020 Feb 14. PMID: 32060354; PMCID: PMC7062874.
201. Peskin AV, Pace PE, Behring JB, Paton LN, Soethoudt M, Bachschmid MM, Winterbourn CC. Glutathionylation of the Active Site Cysteines of Peroxiredoxin 2 and Recycling by Glutaredoxin. J Biol Chem. 2016 Feb 5;291(6):3053-62. doi: 10.1074/jbc.M115.692798. Epub 2015 Nov 24. PMID: 26601956; PMCID: PMC4742766.
202. Pfanner N, Warscheid B, Wiedemann N. Mitochondrial proteins: from biogenesis to functional networks. Nat Rev Mol Cell Biol. 2019 May;20(5):267-284. doi: 10.1038/s41580-018-0092-0. Erratum in: Nat Rev Mol Cell Biol. 2021 May;22(5):367. PMID: 30626975; PMCID: PMC6684368.
203. Pizzimenti S, Ribero S, Cucci MA, Grattarola M, Monge C, Dianzani C, Barrera G, Muzio G. Oxidative Stress-Related Mechanisms in Melanoma and in the Acquired Resistance to Targeted Therapies. Antioxidants (Basel). 2021 Dec 3;10(12):1942. doi: 10.3390/antiox10121942. PMID: 34943045; PMCID: PMC8750393.
204. Platta HW, Erdmann R. The peroxisomal protein import machinery. FEBS Lett. 2007 Jun 19;581(15):2811-9. doi: 10.1016/j.febslet.2007.04.001. Epub 2007 Apr 9. PMID: 17445803.
205. Pollegioni L, Piubelli L, Sacchi S, Pilone MS, Molla G. Physiological functions of D-amino acid oxidases: from yeast to humans. Cell Mol Life Sci. 2007 Jun;64(11):1373-94. doi: 10.1007/s00018-007-6558-4. PMID: 17396222.
206. Poole LB, Hall A, Nelson KJ. Overview of peroxiredoxins in oxidant defense and redox regulation. Curr Protoc Toxicol. 2011 Aug;Chapter 7:Unit7.9. doi: 10.1002/0471140856.tx0709s49. PMID: 21818754; PMCID: PMC3156475.
207. Porporato PE, Payen VL, Pérez-Escuredo J, De Saedeleer CJ, Danhier P, Copetti T, Dhup S, Tardy M, Vazeille T, Bouzin C, Feron O, Michiels C, Gallez B, Sonveaux P. A mitochondrial switch promotes tumor metastasis. Cell Rep. 2014 Aug 7;8(3):754-66. doi: 10.1016/j.celrep.2014.06.043. Epub 2014 Jul 24. PMID: 25066121.
208. Quirós PM, Langer T, López-Otín C. New roles for mitochondrial proteases in health, ageing and disease. Nat Rev Mol Cell Biol. 2015 Jun;16(6):345-59. doi: 10.1038/nrm3984. Epub 2015 May 13. PMID: 25970558.
209. Raman D, Pervaiz S. Redox inhibition of protein phosphatase PP2A: Potential implications in oncogenesis and its progression. Redox Biol. 2019 Oct;27:101105. doi: 10.1016/j.redox.2019.101105. Epub 2019 Jan 14. PMID: 30686777; PMCID: PMC6859563.
210. Ramming T, Hansen HG, Nagata K, Ellgaard L, Appenzeller-Herzog C. GPx8 peroxidase prevents leakage of H2O2 from the endoplasmic reticulum. Free Radic Biol Med. 2014 May;70:106-16. doi: 10.1016/j.freeradbiomed.2014.01.018. Epub 2014 Feb 22. PMID: 24566470.
211. Ren X, Zou L, Zhang X, Branco V, Wang J, Carvalho C, Holmgren A, Lu J. Redox Signaling Mediated by Thioredoxin and Glutathione Systems in the Central Nervous System. Antioxid Redox Signal. 2017 Nov 1;27(13):989-1010. doi: 10.1089/ars.2016.6925. Epub 2017 May 18. PMID: 28443683; PMCID: PMC5649126.
212. Rezende F, Brandes RP, Schröder K. Detection of Hydrogen Peroxide with Fluorescent Dyes. Antioxid Redox Signal. 2018 Aug 20;29(6):585-602. doi: 10.1089/ars.2017.7401. Epub 2017 Dec 13. PMID: 29054131.
213. Rhee SG, Kil IS. Multiple Functions and Regulation of Mammalian Peroxiredoxins. Annu Rev Biochem. 2017 Jun 20;86:749-775. doi: 10.1146/annurev-biochem-060815-014431. Epub 2017 Feb 2. PMID: 28226215.

214. Rhee SG, Woo HA, Kil IS, Bae SH. Peroxiredoxin functions as a peroxidase and a regulator and sensor of local peroxides. J Biol Chem. 2012 Feb 10;287(7):4403-10. doi: 10.1074/jbc.R111.283432. Epub 2011 Dec 6. PMID: 22147704; PMCID: PMC3281607.
215. Ribeiro-Pereira C, Moraes JA, Souza Mde J, Laurindo FR, Arruda MA, Barja-Fidalgo C. Redox modulation of FAK controls melanoma survival--role of NOX4. PLoS One. 2014 Jun 9;9(6):e99481. doi: 10.1371/journal.pone.0099481. PMID: 24911159; PMCID: PMC4050056.
216. Richarme G, Mihoub M, Dairou J, Bui LC, Leger T, Lamouri A. Parkinsonism-associated protein DJ-1/Park7 is a major protein deglycase that repairs methylglyoxal- and glyoxal-glycated cysteine, arginine, and lysine residues. J Biol Chem. 2015 Jan 16;290(3):1885-97. doi: 10.1074/jbc.M114.597815. Epub 2014 Nov 21. PMID: 25416785; PMCID: PMC4340429.
217. Riddick DS, Ding X, Wolf CR, Porter TD, Pandey AV, Zhang QY, Gu J, Finn RD, Ronseaux S, McLaughlin LA, Henderson CJ, Zou L, Flück CE. NADPH-cytochrome P450 oxidoreductase: roles in physiology, pharmacology, and toxicology. Drug Metab Dispos. 2013 Jan;41(1):12-23. doi: 10.1124/dmd.112.048991. Epub 2012 Oct 19. PMID: 23086197; PMCID: PMC3533425.
218. Ritchie ME, Phipson B, Wu D, Hu Y, Law CW, Shi W, Smyth GK. limma powers differential expression analyses for RNA-sequencing and microarray studies. Nucleic Acids Res. 2015 Apr 20;43(7):e47. doi: 10.1093/nar/gkv007. Epub 2015 Jan 20. PMID: 25605792; PMCID: PMC4402510.
219. Roberts PJ, Der CJ. Targeting the Raf-MEK-ERK mitogen-activated protein kinase cascade for the treatment of cancer. Oncogene. 2007 May 14;26(22):3291-310. doi: 10.1038/sj.onc.1210422. PMID: 17496923.
220. Rojo de la Vega M, Chapman E, Zhang DD. NRF2 and the Hallmarks of Cancer. Cancer Cell. 2018 Jul 9;34(1):21-43. doi: 10.1016/j.ccell.2018.03.022. Epub 2018 May 3. PMID: 29731393; PMCID: PMC6039250.
221. Roscoe JM, Sevier CS. Pathways for Sensing and Responding to Hydrogen Peroxide at the Endoplasmic Reticulum. Cells. 2020 Oct 18;9(10):2314. doi: 10.3390/cells9102314. PMID: 33080949; PMCID: PMC7603117.
222. Rossomando AJ, Dent P, Sturgill TW, Marshak DR. Mitogen-activated protein kinase kinase 1 (MKK1) is negatively regulated by threonine phosphorylation. Mol Cell Biol. 1994 Mar;14(3):1594-602. doi: 10.1128/mcb.14.3.1594-1602.1994. PMID: 8114697; PMCID: PMC358518.
223. Saei AA, Gullberg H, Sabatier P, Beusch CM, Johansson K, Lundgren B, Arvidsson PI, Arnér ESJ, Zubarev RA. Comprehensive chemical proteomics for target deconvolution of the redox active drug auranofin. Redox Biol. 2020 May;32:101491. doi: 10.1016/j.redox.2020.101491. Epub 2020 Mar 3. PMID: 32199331; PMCID: PMC7082630.
224. Saitoh H, Hinchey J. Functional heterogeneity of small ubiquitin-related protein modifiers SUMO-1 versus SUMO-2/3. J Biol Chem. 2000 Mar 3;275(9):6252-8. doi: 10.1074/jbc.275.9.6252. PMID: 10692421.
225. Saito S, Hosoda N, Hoshino S. The Hbs1-Dom34 protein complex functions in non-stop mRNA decay in mammalian cells. J Biol Chem. 2013 Jun 14;288(24):17832-43. doi: 10.1074/jbc.M112.448977. Epub 2013 May 10. PMID: 23667253; PMCID: PMC3682582.

226. Sakauchi C, Wakatsuki H, Ichijo H, Hattori K. Pleiotropic properties of ASK1. Biochim Biophys Acta Gen Subj. 2017 Jan;1861(1 Pt A):3030-3038. doi: 10.1016/j.bbagen.2016.09.028. Epub 2016 Sep 30. PMID: 27693599.
227. Salmeen A, Andersen JN, Myers MP, Meng TC, Hinks JA, Tonks NK, Barford D. Redox regulation of protein tyrosine phosphatase 1B involves a sulphenyl-amide intermediate. Nature. 2003 Jun 12;423(6941):769-73. doi: 10.1038/nature01680. PMID: 12802338.
228. Sarkisyan KS, Zlobovskaya OA, Gorbachev DA, Bozhanova NG, Sharonov GV, Staroverov DB, Egorov ES, Ryabova AV, Solntsev KM, Mishin AS, Lukyanov KA. KillerOrange, a Genetically Encoded Photosensitizer Activated by Blue and Green Light. PLoS One. 2015 Dec 17;10(12):e0145287. doi: 10.1371/journal.pone.0145287. PMID: 26679300; PMCID: PMC4683004.
229. Savitski MM, Reinhard FB, Franken H, Werner T, Savitski MF, Eberhard D, Martinez Molina D, Jafari R, Dovega RB, Klaeger S, Kuster B, Nordlund P, Bantscheff M, Drewes G. Tracking cancer drugs in living cells by thermal profiling of the proteome. Science. 2014 Oct 3;346(6205):1255784. doi: 10.1126/science.1255784. Epub 2014 Oct 2. PMID: 25278616.
230. Schadendorf D, Fisher DE, Garbe C, Gershenwald JE, Grob JJ, Halpern A, Herlyn M, Marchetti MA, McArthur G, Ribas A, Roesch A, Hauschild A. Melanoma. Nat Rev Dis Primers. 2015 Apr 23;1:15003. doi: 10.1038/nrdp.2015.3. PMID: 27188223.
231. Schimmel M, Bauer G. Proapoptotic and redox state-related signaling of reactive oxygen species generated by transformed fibroblasts. Oncogene. 2002 Aug 29;21(38):5886-96. doi: 10.1038/sj.onc.1205740. PMID: 12185588.
232. Schneider CA, Rasband WS, Eliceiri KW. NIH Image to ImageJ: 25 years of image analysis. Nat Methods. 2012 Jul;9(7):671-5. doi: 10.1038/nmeth.2089. PMID: 22930834; PMCID: PMC5554542.
233. Schwertassek U, Haque A, Krishnan N, Greiner R, Weingarten L, Dick TP, Tonks NK. Reactivation of oxidized PTP1B and PTEN by thioredoxin 1. FEBS J. 2014 Aug;281(16):3545-58. doi: 10.1111/febs.12898. Epub 2014 Jul 23. PMID: 24976139; PMCID: PMC4162488.
234. Seabold, S., & Perktold, J. (2010). Statsmodels: Econometric and Statistical Modeling with Python. In *PROC. OF THE 9th PYTHON IN SCIENCE CONF*. http://statsmodels.sourceforge.net/
235. Shcherbik N, Pestov DG. The Impact of Oxidative Stress on Ribosomes: From Injury to Regulation. Cells. 2019 Nov 2;8(11):1379. doi: 10.3390/cells8111379. PMID: 31684095; PMCID: PMC6912279.
236. Shenton D, Smirnova JB, Selley JN, Carroll K, Hubbard SJ, Pavitt GD, Ashe MP, Grant CM. Global translational responses to oxidative stress impact upon multiple levels of protein synthesis. J Biol Chem. 2006 Sep 29;281(39):29011-21. doi: 10.1074/jbc.M601545200. Epub 2006 Jul 18. PMID: 16849329.
237. Shi Y, Carroll KS. Activity-Based Sensing for Site-Specific Proteomic Analysis of Cysteine Oxidation. Acc Chem Res. 2020 Jan 21;53(1):20-31. doi: 10.1021/acs.accounts.9b00562. Epub 2019 Dec 23. PMID: 31869209; PMCID: PMC7061859.
238. Sies H. Hydrogen peroxide as a central redox signaling molecule in physiological oxidative stress: Oxidative eustress. Redox Biol. 2017 Apr;11:613-619. doi: 10.1016/j.redox.2016.12.035. Epub 2017 Jan 5. PMID: 28110218; PMCID: PMC5256672.

239. Sims RJ 3rd, Mandal SS, Reinberg D. Recent highlights of RNA-polymerase-II-mediated transcription. Curr Opin Cell Biol. 2004 Jun;16(3):263-71. doi: 10.1016/j.ceb.2004.04.004. PMID: 15145350.
240. Singh RR, Reindl KM. Glutathione S-Transferases in Cancer. Antioxidants (Basel). 2021 Apr 29;10(5):701. doi: 10.3390/antiox10050701. PMID: 33946704; PMCID: PMC8146591.
241. Smith JK, Patil CN, Patlolla S, Gunter BW, Booz GW, Duhé RJ. Identification of a redox-sensitive switch within the JAK2 catalytic domain. Free Radic Biol Med. 2012 Mar 15;52(6):1101-10. doi: 10.1016/j.freeradbiomed.2011.12.025. Epub 2012 Jan 15. PMID: 22281400; PMCID: PMC3319112.
242. Snapp EL, Hegde RS, Francolini M, Lombardo F, Colombo S, Pedrazzini E, Borgese N, Lippincott-Schwartz J. Formation of stacked ER cisternae by low affinity protein interactions. J Cell Biol. 2003 Oct 27;163(2):257-69. doi: 10.1083/jcb.200306020. PMID: 14581454; PMCID: PMC2173526.
243. Sobotta MC, Liou W, Stöcker S, Talwar D, Oehler M, Ruppert T, Scharf AN, Dick TP. Peroxiredoxin-2 and STAT3 form a redox relay for H2O2 signaling. Nat Chem Biol. 2015 Jan;11(1):64-70. doi: 10.1038/nchembio.1695. Epub 2014 Nov 24. PMID: 25402766.
244. Soucek S, Zeng Y, Bellur DL, Bergkessel M, Morris KJ, Deng Q, Duong D, Seyfried NT, Guthrie C, Staley JP, Fasken MB, Corbett AH. The Evolutionarily-conserved Polyadenosine RNA Binding Protein, Nab2, Cooperates with Splicing Machinery to Regulate the Fate of pre-mRNA. Mol Cell Biol. 2016 Nov;36(21):2697-2714. doi: 10.1128/MCB.00402-16. Epub 2016 Aug 15. PMID: 27528618; PMCID: PMC5064217.
245. Srinivas US, Tan BWQ, Vellayappan BA, Jeyasekharan AD. ROS and the DNA damage response in cancer. Redox Biol. 2019 Jul;25:101084. doi: 10.1016/j.redox.2018.101084. Epub 2018 Dec 21. PMID: 30612957; PMCID: PMC6859528.
246. Stankovic-Valentin N, Melchior F. Control of SUMO and Ubiquitin by ROS: Signaling and disease implications. Mol Aspects Med. 2018 Oct;63:3-17. doi: 10.1016/j.mam.2018.07.002. Epub 2018 Aug 4. PMID: 30059710.
247. Strimmer, K. (2008). fdrtool: A versatile R package for estimating local and tail area-based false discovery rates. *Bioinformatics*, *24*(12), 1461–1462. https://doi.org/10.1093/bioinformatics/btn209.
248. Su F, Bradley WD, Wang Q, Yang H, Xu L, Higgins B, Kolinsky K, Packman K, Kim MJ, Trunzer K, Lee RJ, Schostack K, Carter J, Albert T, Germer S, Rosinski J, Martin M, Simcox ME, Lestini B, Heimbrook D, Bollag G. Resistance to selective BRAF inhibition can be mediated by modest upstream pathway activation. Cancer Res. 2012 Feb 15;72(4):969-78. doi: 10.1158/0008-5472.CAN-11-1875. Epub 2011 Dec 28. PMID: 22205714.
249. Supek F, Bošnjak M, Škunca N, Šmuc T. REVIGO summarizes and visualizes long lists of gene ontology terms. PLoS One. 2011;6(7):e21800. doi: 10.1371/journal.pone.0021800. Epub 2011 Jul 18. PMID: 21789182; PMCID: PMC3138752.
250. Swann Matassa, D., Arzeni, D., Landriscina, M., & Esposito, F. (2014). ER stress protection in cancer cells: the multifaceted role of the heat shock protein TRAP1. *Endoplasmic Reticulum Stress in Diseases*, *1*(1). https://doi.org/10.2478/ersc-2014-0003.
251. Szatrowski TP, Nathan CF. Production of large amounts of hydrogen peroxide by human tumor cells. Cancer Res. 1991 Feb 1;51(3):794-8. PMID: 1846317.

252. Takahashi S. D-Aspartate oxidase: distribution, functions, properties, and biotechnological applications. Appl Microbiol Biotechnol. 2020 Apr;104(7):2883-2895. doi: 10.1007/s00253-020-10439-9. Epub 2020 Feb 11. PMID: 32043187.
253. Tamberg N, Tahk S, Koit S, Kristjuhan K, Kasvandik S, Kristjuhan A, Ilves I. Keap1-MCM3 interaction is a potential coordinator of molecular machineries of antioxidant response and genomic DNA replication in metazoa. Sci Rep. 2018 Aug 14;8(1):12136. doi: 10.1038/s41598-018-30562-y. PMID: 30108253; PMCID: PMC6092318.
254. Tan CSH, Go KD, Bisteau X, Dai L, Yong CH, Prabhu N, Ozturk MB, Lim YT, Sreekumar L, Lengqvist J, Tergaonkar V, Kaldis P, Sobota RM, Nordlund P. Thermal proximity coaggregation for system-wide profiling of protein complex dynamics in cells. Science. 2018 Mar 9;359(6380):1170-1177. doi: 10.1126/science.aan0346. Epub 2018 Feb 8. PMID: 29439025.
255. Tao R, Zhao Y, Chu H, Wang A, Zhu J, Chen X, Zou Y, Shi M, Liu R, Su N, Du J, Zhou HM, Zhu L, Qian X, Liu H, Loscalzo J, Yang Y. Genetically encoded fluorescent sensors reveal dynamic regulation of NADPH metabolism. Nat Methods. 2017 Jul;14(7):720-728. doi: 10.1038/nmeth.4306. Epub 2017 Jun 5. PMID: 28581494; PMCID: PMC5555402.
256. Topf U, Suppanz I, Samluk L, Wrobel L, Böser A, Sakowska P, Knapp B, Pietrzyk MK, Chacinska A, Warscheid B. Quantitative proteomics identifies redox switches for global translation modulation by mitochondrially produced reactive oxygen species. Nat Commun. 2018 Jan 22;9(1):324. doi: 10.1038/s41467-017-02694-8. PMID: 29358734; PMCID: PMC5778013.
257. Toussaint O, Medrano EE, von Zglinicki T. Cellular and molecular mechanisms of stress-induced premature senescence (SIPS) of human diploid fibroblasts and melanocytes. Exp Gerontol. 2000 Oct;35(8):927-45. doi: 10.1016/s0531-5565(00)00180-7. PMID: 11121681.
258. Ushioda R, Nagata K. Redox-Mediated Regulatory Mechanisms of Endoplasmic Reticulum Homeostasis. Cold Spring Harb Perspect Biol. 2019 May 1;11(5):a033910. doi: 10.1101/cshperspect.a033910. PMID: 30396882; PMCID: PMC6496348.
259. van Bergen LA, Roos G, De Proft F. From thiol to sulfonic acid: modeling the oxidation pathway of protein thiols by hydrogen peroxide. J Phys Chem A. 2014 Aug 7;118(31):6078-84. doi: 10.1021/jp5018339. Epub 2014 Jul 29. PMID: 25036614.
260. van Dam L, Dansen TB. Cross-talk between redox signalling and protein aggregation. Biochem Soc Trans. 2020 Apr 29;48(2):379-397. doi: 10.1042/BST20190054. PMID: 32311028; PMCID: PMC7200635.
261. van der Reest J, Lilla S, Zheng L, Zanivan S, Gottlieb E. Proteome-wide analysis of cysteine oxidation reveals metabolic sensitivity to redox stress. Nat Commun. 2018 Apr 20;9(1):1581. doi: 10.1038/s41467-018-04003-3. PMID: 29679077; PMCID: PMC5910380.
262. van Hoof A, Frischmeyer PA, Dietz HC, Parker R. Exosome-mediated recognition and degradation of mRNAs lacking a termination codon. Science. 2002 Mar 22;295(5563):2262-4. doi: 10.1126/science.1067272. PMID: 11910110.
263. Watson WH, Jones DP. Oxidation of nuclear thioredoxin during oxidative stress. FEBS Lett. 2003 May 22;543(1-3):144-7. doi: 10.1016/s0014-5793(03)00430-7. PMID: 12753922.
264. Wilson MA. The role of cysteine oxidation in DJ-1 function and dysfunction. Antioxid Redox Signal. 2011 Jul 1;15(1):111-22. doi: 10.1089/ars.2010.3481. Epub 2011 Jan 14. PMID: 20812780; PMCID: PMC3110098.

265. Winterbourn, Christine. (2012). Biological Chemistry of Reactive Oxygen Species. 10.1002/9781119953678.rad077.
266. Winterbourn CC. The biological chemistry of hydrogen peroxide. Methods Enzymol. 2013;528:3-25. doi: 10.1016/B978-0-12-405881-1.00001-X. PMID: 23849856.
267. Wittgen HG, van Kempen LC. Reactive oxygen species in melanoma and its therapeutic implications. Melanoma Res. 2007 Dec;17(6):400-9. doi: 10.1097/CMR.0b013e3282f1d312. PMID: 17992124.
268. Wong HS, Dighe PA, Mezera V, Monternier PA, Brand MD. Production of superoxide and hydrogen peroxide from specific mitochondrial sites under different bioenergetic conditions. J Biol Chem. 2017 Oct 13;292(41):16804-16809. doi: 10.1074/jbc.R117.789271. Epub 2017 Aug 24. PMID: 28842493; PMCID: PMC5641882.
269. Woo HA, Yim SH, Shin DH, Kang D, Yu DY, Rhee SG. Inactivation of peroxiredoxin I by phosphorylation allows localized H(2)O(2) accumulation for cell signaling. Cell. 2010 Feb 19;140(4):517-28. doi: 10.1016/j.cell.2010.01.009. PMID: 20178744.
270. Woolley JF, Corcoran A, Groeger G, Landry WD, Cotter TG. Redox-regulated growth factor survival signaling. Antioxid Redox Signal. 2013 Nov 20;19(15):1815-27. doi: 10.1089/ars.2012.5028. Epub 2013 Jan 15. PMID: 23198948.
271. Wu S, Lu H, Bai Y. Nrf2 in cancers: A double-edged sword. Cancer Med. 2019 May;8(5):2252-2267. doi: 10.1002/cam4.2101. Epub 2019 Mar 30. PMID: 30929309; PMCID: PMC6536957.
272. Xavier, C., Liu, X., Liu, Y., & Wu, H. (2018). The Important Functions of GSH-Dependent Enzyme Glutaredoxin 2 (Grx2). In *Glutathione in Health and Disease*. InTech. https://doi.org/10.5772/intechopen.78653.
273. Xian D, Lai R, Song J, Xiong X, Zhong J. Emerging Perspective: Role of Increased ROS and Redox Imbalance in Skin Carcinogenesis. Oxid Med Cell Longev. 2019 Sep 16;2019:8127362. doi: 10.1155/2019/8127362. PMID: 31636809; PMCID: PMC6766104.
274. Xiao H, Jedrychowski MP, Schweppe DK, Huttlin EL, Yu Q, Heppner DE, Li J, Long J, Mills EL, Szpyt J, He Z, Du G, Garrity R, Reddy A, Vaites LP, Paulo JA, Zhang T, Gray NS, Gygi SP, Chouchani ET. A Quantitative Tissue-Specific Landscape of Protein Redox Regulation during Aging. Cell. 2020 Mar 5;180(5):968-983.e24. doi: 10.1016/j.cell.2020.02.012. Epub 2020 Feb 27. PMID: 32109415; PMCID: PMC8164166.
275. Yamamoto M, Kensler TW, Motohashi H. The KEAP1-NRF2 System: a Thiol-Based Sensor-Effector Apparatus for Maintaining Redox Homeostasis. Physiol Rev. 2018 Jul 1;98(3):1169-1203. doi: 10.1152/physrev.00023.2017. PMID: 29717933.
276. Yamaura M, Mitsushita J, Furuta S, Kiniwa Y, Ashida A, Goto Y, Shang WH, Kubodera M, Kato M, Takata M, Saida T, Kamata T. NADPH oxidase 4 contributes to transformation phenotype of melanoma cells by regulating G2-M cell cycle progression. Cancer Res. 2009 Mar 15;69(6):2647-54. doi: 10.1158/0008-5472.CAN-08-3745. Epub 2009 Mar 10. PMID: 19276355.
277. Yoboue ED, Sitia R, Simmen T. Redox crosstalk at endoplasmic reticulum (ER) membrane contact sites (MCS) uses toxic waste to deliver messages. Cell Death Dis. 2018 Feb 28;9(3):331. doi: 10.1038/s41419-017-0033-4. PMID: 29491367; PMCID: PMC5832433.
278. Yu F, Haynes SE, Nesvizhskii AI. IonQuant Enables Accurate and Sensitive Label-Free Quantification With FDR-Controlled Match-Between-Runs. Mol Cell Proteomics. 2021;20:100077. doi: 10.1016/j.mcpro.2021.100077. Epub 2021 Apr 2. PMID: 33813065; PMCID: PMC8131922.

279. Zarkovic N. Roles and Functions of ROS and RNS in Cellular Physiology and Pathology. Cells. 2020 Mar 21;9(3):767. doi: 10.3390/cells9030767. PMID: 32245147; PMCID: PMC7140712.
280. Zeeshan HM, Lee GH, Kim HR, Chae HJ. Endoplasmic Reticulum Stress and Associated ROS. Int J Mol Sci. 2016 Mar 2;17(3):327. doi: 10.3390/ijms17030327. PMID: 26950115; PMCID: PMC4813189.
281. Zhang J, Tripathi DN, Jing J, Alexander A, Kim J, Powell RT, Dere R, Tait-Mulder J, Lee JH, Paull TT, Pandita RK, Charaka VK, Pandita TK, Kastan MB, Walker CL. ATM functions at the peroxisome to induce pexophagy in response to ROS. Nat Cell Biol. 2015 Oct;17(10):1259-1269. doi: 10.1038/ncb3230. Epub 2015 Sep 7. PMID: 26344566; PMCID: PMC4589490.
282. Zhang X, Smits AH, van Tilburg GB, Ovaa H, Huber W, Vermeulen M. Proteome-wide identification of ubiquitin interactions using UbIA-MS. Nat Protoc. 2018 Mar;13(3):530-550. doi: 10.1038/nprot.2017.147. Epub 2018 Feb 15. PMID: 29446774.
283. Zhao RZ, Jiang S, Zhang L, Yu ZB. Mitochondrial electron transport chain, ROS generation and uncoupling (Review). Int J Mol Med. 2019 Jul;44(1):3-15. doi: 10.3892/ijmm.2019.4188. Epub 2019 May 8. PMID: 31115493; PMCID: PMC6559295.
284. Zhao Y, Hu Q, Cheng F, Su N, Wang A, Zou Y, Hu H, Chen X, Zhou HM, Huang X, Yang K, Zhu Q, Wang X, Yi J, Zhu L, Qian X, Chen L, Tang Y, Loscalzo J, Yang Y. SoNar, a Highly Responsive NAD+/NADH Sensor, Allows High-Throughput Metabolic Screening of Anti-tumor Agents. Cell Metab. 2015 May 5;21(5):777-89. doi: 10.1016/j.cmet.2015.04.009. PMID: 25955212; PMCID: PMC4427571.
285. Zhou L, Yang K, Randall Wickett R, Zhang Y. Dermal fibroblasts induce cell cycle arrest and block epithelial-mesenchymal transition to inhibit the early stage melanoma development. Cancer Med. 2016 Jul;5(7):1566-79. doi: 10.1002/cam4.707. Epub 2016 Apr 6. PMID: 27061029; PMCID: PMC4944884.
286. Zhou TT, Wang XY, Huang J, Deng YZ, Qiu LJ, Liu HY, Xu XW, Ma ZX, Tang L, Chen HP. Mitochondrial Translocation of DJ-1 Is Mediated by Grp75: Implication in Cardioprotection of Resveratrol Against Hypoxia/Reoxygenation-Induced Oxidative Stress. J Cardiovasc Pharmacol. 2020 Apr;75(4):305-313. doi: 10.1097/FJC.0000000000000805. PMID: 32040033.
287. Zinder JC, Lima CD. Targeting RNA for processing or destruction by the eukaryotic RNA exosome and its cofactors. Genes Dev. 2017 Jan 15;31(2):88-100. doi: 10.1101/gad.294769.116. PMID: 28202538; PMCID: PMC5322736.
288. Zissimopoulos S, Lai FA. Redox regulation of the ryanodine receptor/calcium release channel. Biochem Soc Trans. 2006 Nov;34(Pt 5):919-21. doi: 10.1042/BST0340919. PMID: 17052227.

Appendix

Supplementary Tables

Table S1: *The influence of* ***TRAP1-FLAG*** *(A) and oxidative stress (B) on protein quantities in samples derived in Co-IP experiment. Regression model and meaning of R_{poi}/R_{ox} are described in «Analysis of Co-IP/MS data» subsection of «Methods». With yellow background we highlight first unconfident row, with gray — other unconfident rows. In subtable B, with pink we additionally highlight background genes, which are confident in Table S5, and with red font colour – confident genes in both A and B subtables.*

A. Influence of presence of POI protein				
UniProt ID	**Gene**	***R_{poi}***	***t* value**	**qval**
Q12931^{+FLAG}	TRAP1	5.05	19.6	1.99E-14
O75439	PMPCB	2.22	8.62	1.99E-14
Q10713	PMPCA	2.1	8.15	1.99E-14
P11142	HSPA8	1.33	5.17	5.44E-06
O14744	PRMT5	0.96	3.73	4.22E-02
P38646	HSPA9	0.96	3.71	4.65E-02
A0A0G2JIW1	HSPA1B	0.93	3.62	6.59E-02
P0DMV8	HSPA1A	0.91	3.53	9.83E-02
Q14257	RCN2	0.83	3.23	2.86E-01
P02768	ALB	0.81	3.15	3.58E-01
B. Influence of oxidative stress				
UniProt ID	**Gene**	***R_{ox}***	***t* value**	**qval**
A0A0G2JIW1	HSPA1B	1.74	8.13	1.99E-14
HyPerDAO	HyPerDAO	2.66	12.41	1.99E-14
P0DMV8	HSPA1A	1.84	8.58	1.99E-14
Q10713	PMPCA	1.41	6.59	8.45E-12
O75439	PMPCB	1.41	6.56	1.10E-11
Q70IA6	MOB2	1.38	6.45	3.71E-11
P09382	LGALS1	1.29	6.03	2.53E-09
P38646	HSPA9	1.19	5.57	1.85E-07
P11142	HSPA8	1.07	5.00	1.95E-05
P04259	KRT6B	-0.41	-1.89	2.12E-05
Q9H7C9	AAMDC	1.06	4.94	2.93E-05
P04181	OAT	1.03	4.81	7.52E-05
P02533	KRT14	-0.36	-1.68	9.23E-05

P54886	ALDH18A1	1.00	4.65	2.09E-04
O43290	SART1	0.98	4.59	3.01E-04
Q9H773	DCTPP1	0.86	4.00	1.17E-02
Q00403	GTF2B	0.84	3.94	1.60E-02
P13647	KRT5	-0.16	-0.74	2.61E-02
Q04760	GLO1	-0.13	-0.63	4.48E-02
P04264	KRT1	-0.12	-0.57	5.64E-02
Q92598	HSPH1	0.77	3.61	6.85E-02
Q9Y2H1	STK38L	0.77	3.61	6.90E-02
Q8WWY3	PRPF31	0.77	3.61	7.01E-02

Table S2: *The influence of* ***PARK7-FLAG*** *(A) and oxidative stress (B) on protein quantities in samples derived in Co-IP experiment. Regression model and meaning of Rpoi/Rox are described in «Analysis of Co-IP/MS data» subsection of «Methods». With yellow background we highlight first unconfident row, with gray — other unconfident rows. In subtable B, with pink we additionally highlight background genes, which are confident in Table S5, and with red font colour – confident genes in both A and B subtables.*

A. Influence of presence of POI protein				
UniProt ID	**Gene**	R_{poi}	***t* value**	**qval**
Q99497^{+FLAG}	PARK7	4.58	20.79	3.20E-14
P02769	ALB	1.29	5.85	8.90E-05
P0DMV8	HSPA1A	1.28	5.8	1.07E-04
A0A0G2JIW1	HSPA1B	1.27	5.75	1.36E-04
P11021	HSPA5	1.25	5.65	1.97E-04
P38646	HSPA9	1.23	5.57	2.84E-04
P11142	HSPA8	1.19	5.42	5.44E-04
P63313	TMSB10	1.16	5.26	1.06E-03
P84090	ERH	1.06	4.8	6.48E-03
Q92598	HSPH1	0.95	4.32	3.21E-02
P0CG47	UBB	0.94	4.27	3.73E-02
P34932	HSPA4	0.92	4.16	5.26E-02
O95757	HSPA4L	0.9	4.09	6.62E-02
P14174	MIF	0.84	3.81	1.45E-01
P06733	ENO1	0.8	3.63	2.25E-01
B. Influence of oxidative stress				
UniProt ID	**Gene**	R_{ox}	***t* value**	**qval**

P0DMV8	HSPA1A	2.13	11.69	3.20E-14
A0A0G2JIW1	HSPA1B	2.07	11.35	3.20E-14
HyPerDAO	HyPerDAO	1.84	10.09	3.20E-14
P11142	HSPA8	1.49	8.15	1.19E-10
P38646	HSPA9	1.38	7.58	5.47E-09
Q70IA6	MOB2	1.28	7.04	1.54E-07
P11021	HSPA5	1.07	5.85	8.84E-05
O00159	MYO1C	0.97	5.31	8.56E-04
Q92598	HSPH1	0.9	4.95	3.67E-03
O75531	BANF1	-0.59	-3.22	6.09E-03
P09382	LGALS1	0.87	4.74	7.93E-03
P84090	ERH	0.84	4.62	1.23E-02
P02769	ALB	0.79	4.33	3.19E-02
A0A0B4J2D5	GATD3B	-0.48	-2.65	3.86E-02
P51649	ALDH5A1	-0.42	-2.31	1.09E-01
P24666	ACP1	-0.42	-2.31	1.11E-01
Q9ULV4	CORO1C	-0.42	-2.29	1.16E-01
Q13526	PIN1	-0.41	-2.26	1.27E-01

Table S3: *The influence of* ***MAP2K1-FLAG*** *(A) and oxidative stress (B) on protein quantities in samples derived in Co-IP experiment. Regression model and meaning of* R_{poi}/R_{ox} *are described in «Analysis of Co-IP/MS data» subsection of «Methods». With yellow background we highlight first unconfident row, with gray — other unconfident rows. In subtable B, with pink we additionally highlight background genes, which are confident in Table S5, and with red font colour – confident genes in both A and B subtables.*

A. Influence of presence of POI protein				
UniProt ID	**Gene**	R_{poi}	***t* value**	**qval**
Q02750^{+FLAG}	MAP2K1	4.07	17.47	1.09E-13
P10398	ARAF	3.75	16.10	1.09E-13
P04049	RAF1	2.13	9.12	8.38E-09
P28482	MAPK1	1.61	6.91	8.03E-04
P61981	YWHAG	1.53	6.58	3.19E-03
P62258	YWHAE	1.53	6.54	3.73E-03
P63104	YWHAZ	1.43	6.13	1.86E-02
Q04917	YWHAH	1.43	6.12	1.98E-02
P31946	YWHAB	1.41	6.04	2.66E-02

P27361	MAPK3	1.39	5.98	3.29E-02
P15056	BRAF	1.39	5.96	3.53E-02
Q16543	CDC37	1.32	5.68	8.92E-02
Q8IVT5	KSR1	1.21	5.19	3.28E-01
P27348	YWHAQ	1.05	4.53	7.68E-01
Q13451	FKBP5	0.95	4.08	9.10E-01
P14174	MIF	0.80	3.44	9.74E-01
B. Influence of oxidative stress				
UniProt ID	**Gene**	***R*$_{ox}$**	***t* value**	**qval**
HyPerDAO	HyPerDAO	2.31	11.79	1.09E-13
A0A0G2JIW1	HSPA1B	1.53	7.79	1.30E-05
P28482	MAPK1	-0.95	-4.85	1.98E-05
P0DMV8	HSPA1A	1.45	7.38	9.61E-05
P27361	MAPK3	-0.76	-3.86	1.86E-03
P04181	OAT	1.29	6.6	2.92E-03
P04049	RAF1	-0.71	-3.63	4.77E-03
P54886	ALDH18A1	1.21	6.17	1.59E-02
P38646	HSPA9	1.06	5.39	2.06E-01
Q70IA6	MOB2	1	5.12	3.75E-01
Q9H773	DCTPP1	0.99	5.06	4.23E-01
P11142	HSPA8	0.96	4.91	5.31E-01

Table S4: *The influence of* ***UBA2-FLAG*** *(A) and oxidative stress (B) on protein quantities in samples derived in Co-IP experiment. Regression model and meaning of R_{poi}/R_{ox} are described in «Analysis of Co-IP/MS data» subsection of «Methods». With yellow background we highlight first unconfident row, with gray — other unconfident rows. In subtable B, with pink we additionally highlight background genes, which are confident in Table S5, and with red font colour – confident genes in both A and B subtables.*

A. Influence of presence of POI protein				
UniProt ID	**Gene**	***R*$_{poi}$**	***t* value**	**qval**
Q9UBT2^{+FLAG}	UBA2	3.27	11.57	2.88E-14
Q9UBE0	SAE1	2.56	9.05	2.88E-14
A8MUA9	SUMO3	1.29	4.55	8.56E-09
O00505	KPNA3	0.58	2.04	2.65E-01
P0CG47	UBB	0.57	2	2.96E-01
P35908	KRT2	0.56	1.96	3.23E-01

P04406	GAPDH	0.55	1.93	3.42E-01
B. Influence of oxidative stress				
UniProt ID	**Gene**	R_{ox}	***t* value**	**qval**
HyPerDAO	HyPerDAO	1.8	7.61	2.88E-14
P04181	OAT	1.08	4.56	7.28E-09
A0A0G2JIW1	HSPA1B	0.99	4.19	2.93E-07
P0DMV8	HSPA1A	0.92	3.88	4.91E-06
Q70IA6	MOB2	0.91	3.85	6.33E-06
Q9UHB6	LIMA1	-0.65	-2.77	1.13E-05
P54886	ALDH18A1	0.85	3.59	4.82E-05
P0DP23	CALM1	0.82	3.47	1.26E-04
Q16643	DBN1	-0.53	-2.23	7.14E-04
Q9ULV4	CORO1C	-0.46	-1.94	4.51E-03
P14923	JUP	-0.45	-1.92	5.08E-03
Q9HCK1	ZDBF2	-0.44	-1.87	6.71E-03
P09382	LGALS1	0.68	2.87	7.00E-03
A0A1B0GTW1	TJP2	-0.43	-1.83	8.62E-03
Q8N5W9	RFLNB	-0.42	-1.78	1.10E-02
P12277	CKB	0.65	2.77	1.21E-02
Q14692	BMS1	-0.4	-1.7	1.73E-02
Q9Y3D9	MRPS23	-0.38	-1.61	2.79E-02
Q8IWZ8	SUGP1	-0.36	-1.54	3.89E-02
P80723	BASP1	0.59	2.5	4.95E-02
Q5JXI8	FHL1	0.59	2.49	5.21E-02
Q8IUE6	H2AC21	-0.34	-1.44	6.30E-02
Q92598	HSPH1	0.55	2.35	9.64E-02
P15924	DSP	-0.31	-1.33	1.00E-01
P38646	HSPA9	0,55	2,32	1.04E-01

Table S5: *The influence of oxidative stress on protein quantities in all four Co-IP experiments. The meaning of R_{ox} and regression model are described in «Analysis of Co-IP/MS data» subsection of «Methods». With yellow we highlight first unconfident row, with gray — other unconfident rows.*

UniProt ID	**Gene**	R_{ox}	***t* value**	**qval**
A0A0G2JIW1	HSPA1B	1.59	16.52	7.07E-15

UniProt ID	Gene	R_{ox}	*t* value	qval
HyPerDAO	HyPerDAO	2.27	23.56	7.07E-15
P0DMV8	HSPA1A	1.59	16.57	7.07E-15
Q70IA6	MOB2	1.44	14.93	7.07E-15
P04181	OAT	1.25	12.98	6.03E-14
P54886	ALDH18A1	1.24	12.86	1.65E-13
P09382	LGALS1	1.15	12.01	1.23E-10
Q9H7C9	AAMDC	1.15	11.99	1.44E-10
P38646	HSPA9	1.11	11.5	4.70E-09
Q9H773	DCTPP1	0.94	9.83	8.07E-05
P11142	HSPA8	0.94	9.82	8.42E-05
Q92598	HSPH1	0.89	9.3	9.71E-04
O75688	PPM1B	0.87	9.08	2.44E-03
P84090	ERH	0.86	8.91	4.69E-03
P80723	BASP1	0.85	8.85	5.80E-03
Q9Y2W1	THRAP3	0.83	8.65	1.16E-02
Q9UH99	SUN2	0.82	8.54	1.62E-02
P0DP23	CALM1	0.81	8.44	2.22E-02
Q9Y2H1	STK38L	0.78	8.14	5.60E-02
P13797	PLS3	0.77	8.03	7.45E-02
O00268	TAF4	0.77	7.97	8.74E-02
P12277	CKB	0.76	7.87	1.12E-01

Acknowledgements

First of all, I would like to thanks Prof. Dr. Ivan Bogeski and Prof. Dr. Vsevolod Belousov for the great opportunity to work in their labs on this exciting project, here in Göttingen. Thanks for their scientific guidance, freedom and versatile help.

I would like also to express my sincere gratitude to my thesis committee members Prof. Dr. Blanche Schwappach and Prof. Dr. med. Wolfram-Hubertus Zimmermann for their helpful scientific advice, understanding and support during my thesis.

Additionally, I would like to thank Prof. Dr. med. Dörthe M. Katschinski, Prof. Dr. Silvio Rizzoli and PD Dr. Antje Ebert who kindly agreed to be members of my examination board.

Many thanks to Dr. Anke Zieseniss for her help with biosafety issues regarding lentivirus production.

Special acknowledgement to Mikhail Savitski (EMBL, Heidelberg) and members of his team, PhD Isabelle Becher, who helped me to perform Thermal Proteome Profiling experiment and to PhD Frank Stein for the analysis of obtained data.

Additional thanks to Prof. Dr. Joris Messens (Vrije Universiteit Brussel) for the provided opportunity to work in his lab on co-immunoprecipitation experiment in VUB, Brussels, as well as Dr. Daria Ezerina and Ting Luo for their valuable advice.

Huge thanks to Alexey Nesterenko for versatile help in statistical analysis.

Finally, to my sister and mom whose support is impossible to describe in any words.